PROFESSIONAL ENGINEERING DOCTORATE

Detecting and Correcting Calculated Fluid Density Errors in Coriolis Meters Due to Ambient Air Temperature Changes

Lindsay, Gordon

Award date:
2020

Awarding institution:
Coventry University
TÜV SÜD National Engineering Laboratory

Detecting and Correcting Calculated Fluid Density Errors in Coriolis Meters Due to Ambient Air Temperature Changes

By

Gordon Stewart Lindsay

September 2019

In collaboration with

National Engineering Laboratory

A thesis submitted in partial fulfilment of the University's requirements for the degree of Doctor of Engineering.

Certificate of Ethical Approval

Applicant:

Gordon Lindsay

Project Title:

Compensating for air temperature effects on Coriolis Flow Meter Density Calculation

This is to certify that the above named applicant has completed the Coventry University Ethical Approval process and their project has been confirmed and approved as Low Risk

Date of approval:

27 August 2019

Project Reference Number:

P93962

Dedication

For my family.
Past, present and yet to come.

Abstract

Coriolis-based sensing technology is widely used within the oil and gas industry for measuring mass flow rate, density and temperature of fluids within pipelines. It is common for Coriolis mass flow meters to be installed within environments that are subject to variations in ambient temperatures due to factors such as direct sunlight and third-party equipment (pumps and heat exchangers). To date, however, little research has been conducted to quantify the extent of errors that can be induced by such conditions.

Through experimentation and data analysis conducted at the United Kingdom's national standard for fluid flow and density measurement (NEL), this work investigates how the thermomechanical effects induced in Coriolis flow meters by variation in ambient air temperature affects the error in the calculated fluid density value output by the technology.

The results reveal that a common measurement problem exists in multiple Coriolis meter designs with respect to the technology's ability to determine fluid density in conditions where there is a significant differential between the process fluid present within the device and the ambient air temperature. This work has also shown that the fluid properties will affect the extent of the measurement error.

In addition, a new correction model was developed in this work which is capable of determining meter error due to the combined effects of fluid properties, ambient temperature and fluid temperature. This thesis shows through experimentation and data analysis that when the solution is implemented on two distinct models of Coriolis meter, the devices are capable of live correcting for the errors observed.

Acknowledgements

Trips to Coventry with my fellow EngD colleagues these past four years have been great fun. So, thank you Chris Mills, Craig Marshall, Zak Latif and David Millington, I'll always look back on this time fondly, as well as question why it took us over a year to decide to get the train instead of drive.

I am very grateful for the advice and support from my director of studies Prof. James Brusey and my second supervisor Dr Seyed Shariatipour, whose collective experience in academic writing and experimentation have assisted in producing a thesis of which I am immensely proud of. A special thank you as well to my external supervisor Prof. Manus Henry of the University of Oxford for taking an interest in this project after a conference poster session and going on to advise on Coriolis matters, papers and beyond.

During the ten years in which I have been employed by NEL, I have acquired a wealth of knowledge and experience from every person I have worked with. In particular, I am extremely grateful to Graeme Ryan and Brendan Robson for inviting me to join their team all those years ago, a role that has given me the necessary knowledge and experience for undertaking a project of this complexity, while having a job that I genuinely enjoy coming to work for every day. The enthusiasm for this project of Dr Norman Glen (industrial supervisor for this thesis) and John Hay went above and beyond on a number of occasions. I had a great time running these experiments in NEL's density standards lab and will be forever grateful for your advice and the extra pair of hands that were always on offer. Thank you also to Neil Bowman, Bobby Anderson, Scott Churchill, David Addison, Richard Harvey, Les Wales and Bob Belshaw for their assistance and advice during the rig specification, fluid transfers and sample analysis. Dr Behzad Nobakht's insights in the field of data science were very much appreciated and provided me with a new perspective on how data can be visualised. Lastly thank you to Dr Brian Millington and Dr Martin Hanton for developing and supporting the Engineering Doctorate programme at TÜV SÜD National Engineering Laboratory.

Collaborating with a Coriolis meter manufacturer allowed this project to delve deeper into the science and engineering involved throughout the experimentation and data analysis phases. Thank you to Rheonik's managing director Uwe Hettrich and head of systems engineering Mahdi Taheri for being so willing to participate and for engaging in many data analytics discussions over Skype.

The love and support of my Mum and Dad throughout my life is the reason I have found myself in a position where undertaking this project was an option. So thank you for the midnight 'Higher Physics' past paper sessions, triple checked plans and cinema trips, which led to nerdy chats with my brother Andrew, instilling a mindset essential to an engineer.

Thank you Kirsty for being the most wonderful wife and best friend, and thank you for reading this thesis more times than anyone else ever will. The smiles from you and our son Adam (who was born midway through this venture) are all I need in life.

Publication Output

Journal Papers: -

Profiling and Trending of Coriolis Meter Secondary Process Value Drift Due to Ambient Temperature Fluctuations – Flow Measurement and Instrumentation, 2018, Vol 59, Pgs 225-232

Coriolis Meter Density Errors Induced by Ambient Air and Fluid Temperature Differentials – Flow Measurement and Instrumentation, expected in 2020, (Under editorial review at the time of writing)

Conference Papers: -

Detecting and Correcting for Coriolis Meter Calculated Fluid Density Drift Due to Ambient Temperature Variation – North Sea Flow Measurement Workshop, Aberdeen, Scotland, 2018

Coriolis Density Error – Targeting Ambient Temperature Fluctuation and the Development of a new Temperature Compensation Model – North Sea Flow Measurement Workshop, Tønsberg, Norway 2019

Posters: -

Flow Measurement Institute (FMI) Conference, Coventry, 2016
North Sea Flow Measurement Workshop, St Andrews, 2016
Coventry University Engineering Faculty Research Symposium, 2017
Coventry University Engineering Faculty Research Symposium, 2018
North Sea Flow Measurement Workshop, Aberdeen, 2018
Coventry University Engineering Faculty Research Symposium, 2019
Advanced Multiphase Research Facility Launch Event, NEL, East Kilbride, 2019

Presentations: -

North Sea Flow Measurement Workshop (Young Engineers Session), St Andrews, 2016

Flow Measurement Institute (FMI) Conference, Coventry, 2017

TÜV SÜD National Engineering Laboratory Technical Forum, 2018

North Sea Flow Measurement Workshop, Aberdeen, 2018

Oil and Gas Focus Group, Aberdeen, December 2018

Oil and Gas Focus Group, Aberdeen, February 2019

Oil and Gas Focus Group Norwich, May 2019

Society of Petroleum Engineering Offshore Europe Conference, Aberdeen 2019

North Sea Flow Measurement Workshop, Tønsberg, October 2019

Table of Contents

List of Figures

List of Tables

Nomenclature

Symbols	Description	Units
$\boldsymbol{A}$	Cross-sectional area	m^2
$\boldsymbol{a_i}$	NEL – Water reference density calculation, coefficient	–
$\boldsymbol{A_{id}}$	Internal cross-sectional area of flow tube	m^2
$\boldsymbol{a_r}$	Centripetal acceleration	m/s^2
$\boldsymbol{a_t}$	Transverse acceleration	m/s^2
$\boldsymbol{C}$	Mechanical stiffness	kg/s^2
$\boldsymbol{E}$	Young's modulus	N/m^2
$\boldsymbol{f_{rf}}$	Resonant frequency	Hz
$\boldsymbol{f_{20}}$	Rheonik/NEL – Sensor frequency at ambient conditions (20°C)	Hz
$\boldsymbol{F}$	Force	$N = m.kg/s^2$
$\boldsymbol{F_{C\ Inlet}}$	Coriolis force experienced at inlet	$N = m.kg/s^2$
$\boldsymbol{F_{C\ Outlet}}$	Coriolis force experienced at outlet	$N = m.kg/s^2$
$\boldsymbol{K_R}$	Conversion factor	$kg/s\ /s$
$\boldsymbol{K_x}$	Density calibration factor	–
$\boldsymbol{L_O}$	Original Length	m
$\boldsymbol{L_n}$	New Length	m
$\boldsymbol{M}$	Gradient for linear density fit (Manufacturer B – Density Mode 2)	–
$\boldsymbol{m}$	Mass	kg
$\boldsymbol{m_f}$	Mass of fluid within Coriolis tubes	kg
$\boldsymbol{m_{tb}}$	Mass of Coriolis tubes	kg
$\boldsymbol{M_{comp}}$	Rheonik – Temperature compensated mass flow rate	kg/s
$\boldsymbol{M_{uncomp}}$	Rheonik – Raw mass flow rate (uncorrected)	kg/s
$\boldsymbol{m(i)}$	NEL – Water reference density calculation, temperature exponent	–
$\boldsymbol{n(i)}$	NEL – Water reference density calculation, pressure exponent	–
$\boldsymbol{N}$	Number of samples	–
$\boldsymbol{N_c}$	Number of cycles	–
$\boldsymbol{P}$	Fixed point with respect to r in generalised theoretical Coriolis flow description	–

Symbols	Description	Units
p_1	Rheonik – The Lower specification limit period value (air)	s
p_2	Rheonik - The Upper specification limit period value (water)	s
p_n	Rheonik – The actual harmonic period of the Coriolis meter	s
p_{n-comp}	Rheonik – Temperature compensated harmonic period of the Coriolis meter	s
q_m	Mass Flow Rate	kg/s
r	Known distance in generalised theoretical Coriolis flow description	m
r_{XY}	Correlation coefficient relating to two variables (X and Y)	$-$
S_{01}	Rheonik – Mass Flow calculation - Torsion bar temperature sensor temperature compensation coefficient	$-$
S_{10}	Rheonik - Mass Flow calculation - Tube temperature sensor temperature compensation coefficient	$-$
sin_A	Sinusoidal motion at device inlet (note - can be measured as deformation, velocity or acceleration)	m, m/s or m/s^2
sin_B	Sinusoidal motion at device outlet (note - can be measured as deformation, velocity or acceleration)	m, m/s or m/s^2
sin_D	Driving Sinusoidal function at device centre (note - can be measured as deformation, velocity or acceleration)	m, m/s or m/s^2
S_{XY}	Covariance value relating to two variables (X and Y)	$-$
T_A	Low Temperature Reference value (Manufacturer B – Density Mode 2)	$°C$
T_B	High Temperature Reference value (Manufacturer B – Density Mode 2)	$°C$
t_d	Time delay	s
T_1	Rheonik – Tube temperature sensor reading	$°C$
T_2	Rheonik – Torsion bar temperature sensor reading	$°C$
T_{1Ref}	Rheonik - Initial calibration reference value for tube temperature sensor (Mass flow calculation)	$°C$
T_{2Ref}	Rheonik – Initial calibration reference value for torsion bar temperature sensor (Mass flow calculation)	$°C$
$T_{1Ref(Dens)}$	Rheonik - Initial calibration reference value for tube temperature sensor (Density calculation)	$°C$

Symbols	Description	Units
$T_{2Ref(Dens)}$	Rheonik – Initial calibration reference value for torsion bar temperature sensor (Density calculation)	$°C$
T_{rf}	Period of oscillating Coriolis tube	s
t_W	Time window (gated signal)	s
U_{00}	Rheonik - Density calculation - Temperature compensation factor (value of 1 deactivates live transmitter compensation)	$-$
U_{10}	Rheonik - Density calculation - Tube temperature sensor temperature compensation coefficient	$-$
U_{01}	Rheonik - Density calculation - Torsion bar temperature sensor temperature compensation coefficient	$-$
v	Velocity	m/s
V_f	Volume of fluid within Coriolis tubes	m^3
X	Rheonik/NEL – Fluid specific density correction coefficient	$-$
X_i	Individual sample element value for variable X	$Specific\ to\ units$
$\bar{X}$	Mean of sample element values for variable X	$Specific\ to\ units$
Y_i	Individual sample element value for variable Y	$Specific\ to\ units$
$\bar{Y}$	Mean of sample element values for variable Y	$Specific\ to\ units$
α	Oil reference density calculation - Slope	-
ΔT_1	Rheonik - Difference between measured T_1 and $T_{1,Ref}$ ($\Delta T_1 = T_1 - T_{1,Ref}$)	$°C$
ΔT_2	Rheonik - Difference between measured T_2 and $T_{2,Ref}$ ($\Delta T_2 = T_2 - T_{2,Ref}$)	$°C$
$\Delta T_{1(Dens)}$	Rheonik - Difference between measured T_1 and $T_{1,Ref(Dens)}$ ($\Delta T_1 = T_1 - T_{1,Ref(Dens)}$)	$°C$
$\Delta T_{2(Dens)}$	Rheonik - Difference between measured T_2 and $T_{2,Ref(Dens)}$ ($\Delta T_2 = T_2 - T_{2,Ref(Dens)}$)	$°C$
$\Delta T_{1,2}$	Rheonik/NEL – The difference between the live tube and Torsion bar sensor readings ($\Delta T_{1,2} = T_1 - T_2$)	$°C$
θ	NEL – Oil reference density calculation, temperature input	$°C$
θ^m	NEL – Water reference density calculation - Temperature input	$°C$
π^n	NEL – Water reference density calculation, Pressure input	MPa

Symbols	Description	Units
$\boldsymbol{\delta F_C}$	Coriolis Force	$N = m.kg/s^2$
$\boldsymbol{\delta m_f}$	Mass of flowing fluid	kg
$\boldsymbol{\delta m_{tb}}$	Mass of Coriolis flow tube	kg
$\boldsymbol{\delta x}$	Variable length at any point on a Coriolis meter flow tube	m
$\boldsymbol{\rho}$	Density	kg/m^3
$\boldsymbol{\rho_C}$	Known density at "high temperature" reference value (Manufacturer B – Density Mode 2)	kg/m^3
$\boldsymbol{\rho_D}$	Known density at "low temperature" (Manufacturer B – Density Mode 2)	kg/m^3
$\boldsymbol{\rho_f}$	Density of fluid	kg/m^3
$\boldsymbol{\rho_{ref}}$	Fluid Density at reference calibration conditions	kg/m^3
$\boldsymbol{\rho_t}$	NEL - Oil fluid density (Temperature corrected)	kg/m^3
$\boldsymbol{\rho_1}$	Rheonik - Lower Specification Limit density (The air density at the highest temperature in the measured range)	kg/m^3
$\boldsymbol{\rho_2}$	Rheonik - Upper Specification Limit density (The water density at the lowest temperature in the measured range)	kg/m^3
$\boldsymbol{\rho_{20}}$	NEL - Oil reference density calculation (Oil fluid density at 20°C)	kg/m^3
$\boldsymbol{\sigma}$	Standard Deviation	$Specific\ to\ units$
$\boldsymbol{\omega}$	Angular velocity	rad/s

Abbreviation	Description
BP-ANN	Backpropogation-Artificial Neural Network
BS	British Standard
CCS	Carbon Capture and Storage
CFD	Computational Fluid Dynamics
CO2	Carbon dioxide
DAQ	Data Acquisition
DDS	Direct Digital Synthesizer
FEM	Finite Element Method
GVF	Gas Volume Fraction
I.D.	Inner diameter
MEMS	Micro Electro Mechanical System

Abbreviation	Description
NEL	TÜV SÜD National Engineering Laboratory – UK national standard for fluid flow and density measurement
O.D.	Outer diameter
P(n)	Pump and unique numerical identifier
PCI	Peripheral Component Interconnect
PI	Pressure Indicator
PT	Pressure Transmitter
PT100	100 ohm Platinum resistance thermometer (See RTD)
RTD	Resistive Temperature Detector
SEVA	Self-Validating Sensors
SG	Specific Gravity
tb	Coriolis flow meter tube
TC	Thermocouple
TT	Temperature Transmitter
V(n)	Valve and unique numerical identifier
UK	United Kingdom
UKAS	United Kingdom Accreditation Service

Communication Protocol	Description
GPIB/IEEE-488	General Purpose Interface Bus enabling parallel communication between multiple data acquisition units and logging master computers
MXI-4	Master/Follower communications protocol over a fiber optic data link cable. Supported by 'National Instruments'. Allows for extension of computer motherboard capabilities by way of Peripheral Component Interconnect (PCI) standard technology
OPC	Open Platform Communications. Allows for the free flow of data between multiple digital fieldbus protocols by way of a server/client setup.
RS485	Serial Communications Protocol allowing for data exchange via Modbus protocol.

Chapter 1

1 Introduction

1.1 **Objectives**

In addition to their primary function of calculating mass flow, Coriolis mass flow meters are also capable of calculating fluid density. This can be advantageous when designing flow measurement systems as this 'two measurements in one device' concept can reduce facility space requirements as well as equipment and ongoing maintenance costs by removing the need to purchase and install a dedicated in-line densitometer device. While manufacturers provide associated error specifications for Coriolis meter density output, there is an increasing interest from end-users in ensuring that the technology is capable of correctly calculating fluid density in environmental conditions that are representative of field conditions. Variables such as changes in ambient air temperatures, fluid properties, fluid flow rates and fluid pressures are likely to be experienced in many industrial environments. While considerable research has been undertaken with respect to quantifying fluid pressure effects on the density output performance, there is a gap in knowledge with respect to the potential effects of ambient air temperature. From the author's own experience in designing and commissioning flow facilities for the UK's national standard for flow and density measurement, it has been observed during past projects that the reported fluid density from a Coriolis meter drifted from the expected value under controlled fluid temperature, pressure and flow rate conditions. The key variable unaccounted for was the fluctuating ambient air temperature condition created by wider facility construction activity.

The aim of this thesis is therefore to develop a deep understanding of how ambient air temperature changes can affect the extent of measurement error in the density value output by Coriolis flow meters and resolve the source of error using an automatic correction that can be applied live within the device transmitter. The solution should be practical and applicable to industry standard devices and their associated components.

At present there is a lack of definitive scientific and experimental data available relating to Coriolis meter output error under these conditions.

The project had the following objectives:

- Obtain high resolution data that profiles the response of commercially available Coriolis meters density output in a fluctuating ambient air temperature environment through targeted experimentation.
- Through data analysis, determine the extent of density calculation error as well as any other key process value drift due to ambient temperature.
- Present initial data sets to meter manufacturers and form a research partnership. In doing so, gain full access to patented meter internal correction algorithms and mechanical specifications.
- With manufacturer level access to meter design and operation specifications, obtain a comprehensive data set through experimentation with respect to ambient temperature fluctuations that highlights potential inefficiencies in existing temperature correction techniques currently implemented by the manufacturer with respect to differing fluid properties.
- Through analysis of the data obtained, develop a new automated method to allow the meter to self-determine and apply the appropriate temperature correction measures for fluid density calculation, ultimately improving the uncertainty of the process value in industrial installations and therefore the uncertainty of any flow measurement system that relies upon the value.

1.2 Outline

The format of the thesis is as follows: -

Chapter 1 establishes the aim, objectives and research questions that the thesis will answer.

Chapter 2 provides an overview of the Coriolis meter operating principles which are relevant to the thesis. A comprehensive literature review of previous works and their resulting influence on the thesis' experimental direction is provided.

Chapter 3 details the research facility and data infrastructure which forms the basis of the experimental methods described in all subsequent chapters.

Chapter 4 details experiments and results which explore the density calculation performance of two commercially available types of Coriolis meter within a changing ambient air temperature environment. The results were published in the journal of Flow Measurement and Instrumentation [1].

Chapter 5 describes further experiments conducted as part of a research partnership with a Coriolis manufacturer. The chapter describes how the results were used to develop a new method for live ambient temperature correction. The results are under final editorial review with the journal of Flow Measurement and Instrumentation [2] and appear the 2018 North Sea Flow Measurement Workshop proceedings [3].

Chapter 6 describes the experiments and results used to establish whether the new correction method can be transferred to a prototype design of Coriolis meter, provided by the research partner. The results were presented at the 2019 North Sea Flow Measurement Workshop [4].

Chapter 7 provides the overall research conclusions and suggests potential directions for furthering the discoveries of the thesis.

1.3 Hypothesis and Research Questions

Changes in the ambient air temperature surrounding a Coriolis flow meter are the cause of increased errors present in the fluid density value output by the device.

The thesis will answer the following research questions: -

1. Does an increased differential with respect to air and fluid temperature surrounding Coriolis flow meters induce errors in the data output by the device?

2. Can errors that are induced by air and fluid temperature differentials be isolated and compensated for via mathematical and electronic means?

3. Are the compensation methods developed as part of this thesis transferable to differing models of Coriolis flow meter?

Chapter 2

2 Background

Within the field of fluid flow measurement, Coriolis flow meters have become a widely adopted technology used to measure mass flow of a fluid through a pipeline as well as determine the density of the fluid present within its internals. The Coriolis force was first described by Gustave-Gaspard Coriolis in 1832 [5], where the concept of an inertia force acting on a moving body in a rotating frame of reference was first described. From the mid-20th century onwards, patent applications for technology designed to harness and exploit these forces with respect to metering fluid flow emerged. Each patent and associated manufacturer continued to build upon the technology with respect to geometry, electronic sensors and transmitters to the point where today the technology conforms to a largely generic operating specification with variations in geometry, sensor placement and transmitter complexity differing between the specific manufacturers.

This chapter will summarise the key developments in Coriolis flow metering technology, describe the principles of device operation with respect to its present-day form, describe known sources of error with respect to device performance, highlight gaps in knowledge with respect to ambient temperature effects and finally outline a methodology which this thesis adopts to answer the research questions outlined in chapter 1.

2.1 **Evolution of Coriolis force-based metering technology**

A patent published in 1952 [6] describes a rotational based device in which an impeller is driven to a constant rotation by a motor, which then interacts with a fluid that is fed through an inlet, over the impeller and expelled through an outlet port. A secondary rotor is then used to measure the resulting force imparted by the accelerated flow of liquid due to the impeller from which a mass flow rate can be inferred. A patent filed by Pearson [7] in 1953, details designs for a curved flow tube device that can be driven to rotate or oscillate. Reference is also made to using electrical transducers to determine the extent of oscillation and by extension the mass flow rate. The induction of an

oscillation on the flow tube as opposed to utilising a fully rotational system ensures a more efficient and practical implementation of the theory while still observing the same Coriolis effects, a concept which is taken on in all further design variations. A patent filed by Wiley et al. in 1963 [8] describes two variations in the design for a straight tube Coriolis flow meter. The first of which being a single tube design with an open end that outputs to a vessel, the second being a single tube design, with continuous flow into downstream pipework, with flexible flow input and output sections. For both designs the tubes are oscillated to a resonant frequency. An electromagnetic pick up is the method by which the amplitude of oscillation is detected with the difference in driving force required to oscillate the inlet and outlet sections indicating the mass flow rate through the system, specifically the amount of torque required to maintain tube oscillation at a constant frequency and amplitude.

A further development of this concept is described by Sipin [9], [10] for both straight and bent tube designs. Specific reference is made to two methods of tube oscillation, a mechanical motor/cam setup and an electromagnetic drive mechanism. Strain gauges and magnetic pickups are described for use in determining the tube deflection force at both the inlet and outlets as a means of calculating mass flow rate. The use of a dual U-tube configuration to reduce the amount of force required to provide oscillation is described in a patent submitted in 1978 by Cox and Gonzalez [11]. The device's ability to infer fluid density based on the oscillation power requirements at fixed resonant frequency of the flow tubes is embraced in future design iterations, ultimately becoming the secondary output of Coriolis flow meter technology.

The use of time difference between the inlet and outlet of a single U-shaped Coriolis flow meter was described in a patent submitted in 1980 by Smith [12]. Smith describes a method for calculating mass flow by accounting for the stiffness of the flow tube as well as the pipe length downstream of the device, with the governing factor being the measured time difference in meter oscillation frequency between the inlet and outlet legs of the device.

By using the time delay on the oscillation of the pipe due to mass flow as opposed to phase shift and measured force, Smith overcame the dependency on drive frequency of oscillation. Reference is also made to the determination of a density factor that can be

used to infer fluid density, which is also dependent on the spring constant as the total mass subjected to oscillation.

Smith and Cage further built upon the use of twin U-tube designed Coriolis meters in a patent filed on behalf of Micromotion [13]. A dual tube parallel flow is described, with reference made to the limitation in Coriolis meter size and potential pressure drops. Simply put for a single tube Coriolis meter, the greater the fluid quantity one wishes to measure, the greater the mass of flow tubes and associated pressure drops and manufacturing costs. The use of a dual tube configuration allows for smaller diameter tubes to be used while allowing for greater quantities of fluid to pass and therefore reducing the stated disadvantages of single tube devices. The use of thinner tubes is also stated to enable a more sensitive Coriolis device to be constructed.

This section has highlighted the key step changes in Coriolis mass flow meter design during the 20th century that have resulted in the general form in which the device exists in present day. Extensive reviews focusing on the incremental development of Coriolis mass flow technology have been conducted by Baker [14] and Wang and Baker [15].

2.2 Present Day Coriolis Meter Design Standards

The developments described in section 2.1 resulted in multiple device manufacturers converging on the same key principles of operation. To that effect standards have been agreed and published in ISO 10790 [16]. The key information pertaining to standardised principles of operation and device design are summarised within this section.

The technology exploits the forces generated when a fluid present within a rotating body moves relative to the body in a direction that is either towards or away from the center of rotation. Figure 2-1 demonstrates such an interaction.

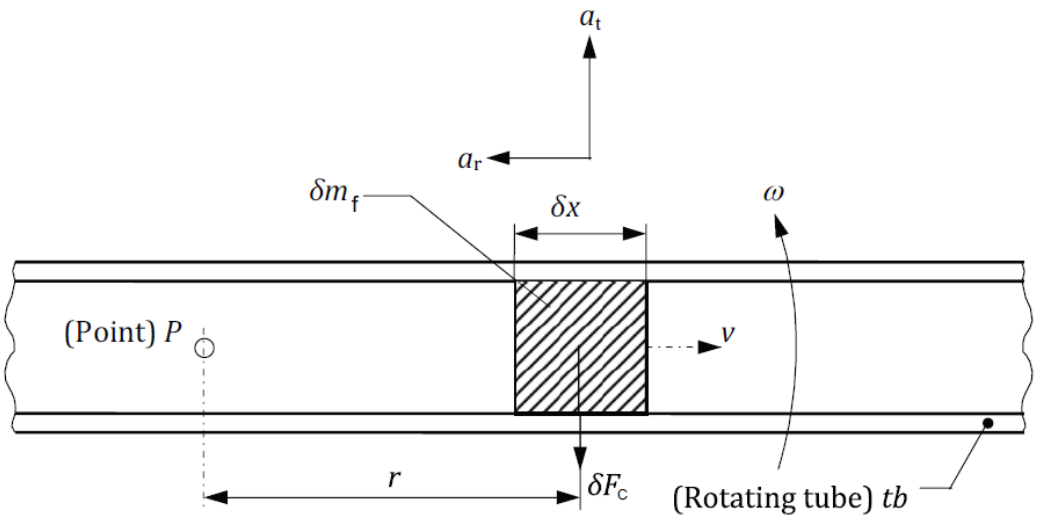

Figure 2-1 Coriolis forces with respect to pipe geometry

Figure 2-1 shows that when a particle of mass δm_f moves with a constant velocity v, a known distance r, with respect to a fixed point P, within a rotating tube tb, that has an angular velocity ω, the particle will experience a two-component acceleration: -

1. Centripetal acceleration a_r directed towards point P
2. Transverse acceleration a_t at right angles to a_r

Where

$$a_r = r\omega^2 \quad (1)$$

$$a_t = 2v\omega \quad (2)$$

The resulting Coriolis force δF_C from the particle is therefore defined as the product of the angular velocity ω, particle velocity v, and particle mass δm_f, as expressed in Equation 3 below.

$$\boldsymbol{\delta F_C = 2\omega v \delta m_f} \quad (1)$$

With respect to Figure 2-1 this means that in order to impart a transverse Coriolis acceleration in the direction of a_t, the magnitude of the required force is equal to the Coriolis force, which is calculated by Equation 3.

When one then considers a flowing fluid and its associated density ρ, Equation 3 can therefore be modified to account for the cross-sectional area A_{id} of the inner flow tube, and any length along the rotating tube to produce Equation 4 below.

$$\boldsymbol{\delta F_C = 2\omega v \rho A_{id} \delta x} \quad (2)$$

Mass flow rate is the product of the velocity, fluid density and cross-sectional area as expressed by Equation 5 below

$$\boldsymbol{q_m = v \rho A_{id}} \quad (3)$$

Therefore, the transverse Coriolis force can be expressed as the product of angular velocity, mass flow rate and specific length as shown in Equation 6 below

$$\boldsymbol{\delta F_C = 2\omega q_m \delta x} \quad (4)$$

For practical application within a real-world engineering environment, ISO 10790 [16] defines the use of an oscillatory system as opposed to a rotational system to generate these Coriolis forces. Figure 2-2 shows the generic forms of potential meter shapes and component configurations that have been adopted by various manufacturers throughout the years to achieve this.

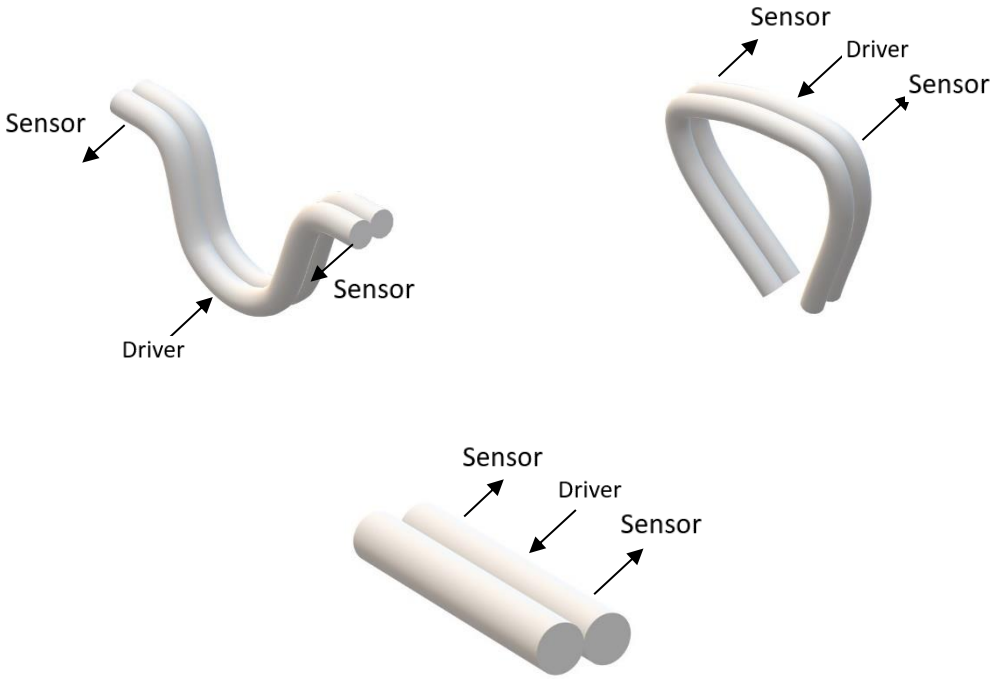

Figure 2-2 Typical design variants of Coriolis meter with annotations indicating oscillation driver and phase shift sensor locations

It is noteworthy that differing end-user requirements and installation locations can typically lead to the selection of either a straight tube or bent tube Coriolis meter. For example, a straight tube Coriolis meter may be selected for hygiene critical applications as they are easier to clean. Whereas a bent tube Coriolis meter will allow for greater quantities of fluid to pass as well as reduce the pressure drop imposed by the device on the flow system.

The physics behind the operation of these devices as defined by the British standard [16] is shown in Figures 2-3 to 2-6.

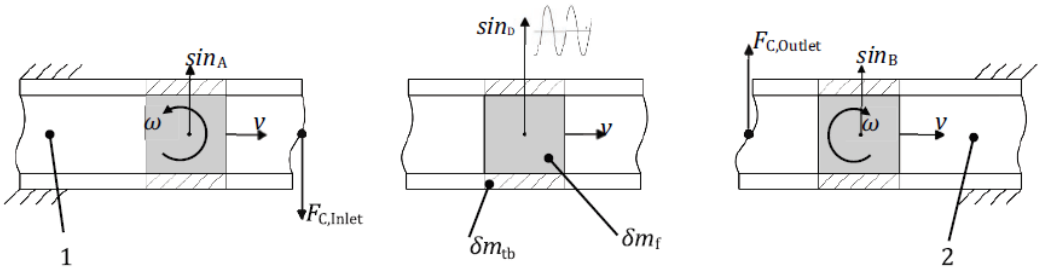

Figure 2-3 Individual Coriolis forces (Location 1 = Tube Inlet, Location 2 = Tube Outlet)

Figure 2-3 shows that for either a bent or straight tube system, the driver mechanism, which is typically an electromagnetic arrangement consisting of a coil and magnet, is located on the center of the structure. The driver excites the flow tube into continuous vibration in a sinusoidal manner by pushing and pulling the tube into oscillation. Therefore, the motion of both the flow tube (δm_{tb}) and the fluid present within the flow tube (δm_{mf}) are effectively coupled. The driving sinusoidal wave is represented by sin_D in Figure 2-3. The resulting Coriolis forces at the inlet ($F_{C\ Inlet}$), and outlet ($F_{C\ Outlet}$), of the device are generated by the velocity (v) and rotation (ω) of the fluid flowing through the device. This force is detected by the inlet and outlet sensors, which are also electromagnetically based. A voltage of a given amplitude is generated depending on the distance between the coil and the magnet, where the distance is a function of the magnitude of the Coriolis force being exerted on the inlet or outlet section of the flow tube. A simplified diagram of this concept is shown below in Figure 2-4.

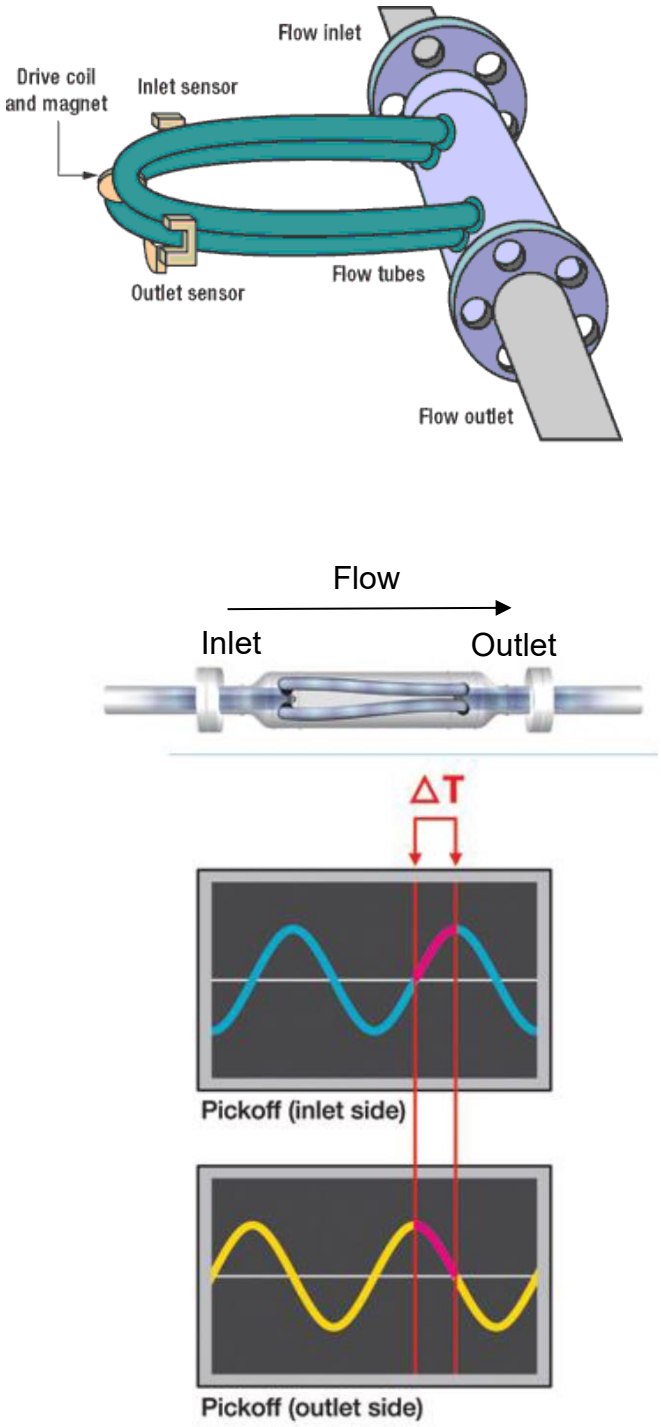

Figure 2-4 Simplified diagram of Coriolis meter components, operation and resulting wave form and analysis.

Figure 2-5 shows that for conditions where there is no flow through the Coriolis flow tube, the measured sinusoidal waveforms at both the inlet and the outlet of the flowmeter will be in phase.

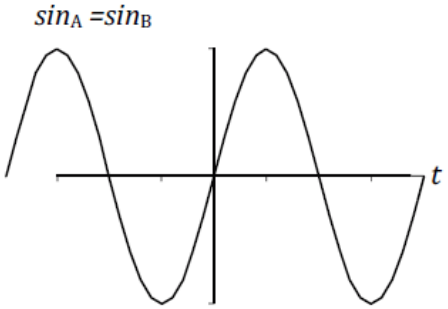

Figure 2-5 Expected waveform from both inlet and outlet transducers under no flow conditions

When fluid begins to flow through the oscillating tubes, the Coriolis force is now present at the inlet and outlet sensing mechanisms of the device. Due to the opposite rotational components of the system, the Coriolis forces present at both the inlet and the outlet oppose each other. The resulting effect on the sinusoidal waveforms detected by the inlet and outlet sensors (sin_A and sin_B) is that they are now out of phase as shown in Figure 2-6. Mass flow rate is therefore determined by the multiplication of the time delay between the inlet and outlet sine waves (t_d) and a meter specific conversion factor as shown in Equation 7.

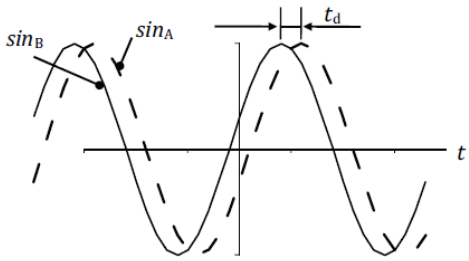

Figure 2-6 Phase shift imparted by Coriolis forces due to fluid flow through Coriolis flowmeter

$$\boldsymbol{q_m = K_R \,.\, t_d} \qquad (5)$$

Where

- K_R is conversion factor programmed within the transmitter (determined at reference conditions)
- t_d is time delay

Since a Coriolis meter relies upon the oscillation of the flow tubes at their respective resonant frequency, it is also possible to use the device as an in-line densitometer. The physical properties relating to stiffness will vary between the manufacturers of the device due to differing materials and manufacturing techniques. The resonant frequency (f_{rf}) for a Coriolis mass flow meter is reliant on the spring constant (C) and total mass (m), as the defined in the ISO standard [16] as follows

$$\boldsymbol{f_{rf} = (1/2\pi) \,.\, (C/m)^{1/2}} \quad (6)$$

The total mass is defined as the mass of the oscillation tube combined with the mass of fluid within the flow tubes

$$\boldsymbol{m = m_{tb} + m_f} \quad (7)$$

The mass of fluid is the product of the actual density and volume of the fluid within the flow tubes

$$\boldsymbol{m_f = (\rho_f).(V_f)} \quad (8)$$

where

- f_{rf} is the resonant frequency
- C is the mechanical stiffness/spring constant
- m is the total mass
- m_{tb} is the mass of the oscillating tube(s)
- m_f is the mass of fluid within the oscillating tubes(s)
- V_f is the volume of fluid within the oscillating tubes(s)
- ρ_f is the density of the fluid

To calculate the density of the fluid present within the flow tubes, the resulting resonant frequency (f_{rf}) and respective fluid (m_f) and tube mass (m_{tb}) values can be used in equations 11 to 14.

$$\boldsymbol{\rho_f = \left\{ \frac{C}{\left[V_f \left(2\pi f_{rf}\right)^2\right]} \right\} - m_{tb}/m_f} \quad (9)$$

Fluid density (ρ_f) can also be determined with knowledge of the specific fluid properties and process conditions the meter is likely to experience during service. Therefore, applying fluid density coefficients (K) which can be determined during a calibration performed either by the meter manufacturer or the end-user once in service, fluid density (ρ_f) can be calculated with respect to the resonant frequency (f_{rf}) as shown in Equation 12.

$$\boldsymbol{\rho_f = K_1 + \frac{K_2}{(f_{rf})^2}} \quad (10)$$

It should be noted that the relevance of the (K) coefficients with respect to the validity of a given calibration are influenced by temperature. Therefore, at present the ISO standard [16] states that should an end-user be operating with fluids at temperatures above or below ambient (20°C) then a "special density calibration" to account for these conditions may be required.

However, this assumes constant temperature conditions throughout the period of service and does not account for the potential for the fluid temperature to fluctuate drastically out with these conditions, nor does it account for the potential for the surrounding ambient air temperatures to vary.

If the tube oscillating period is known, then resonant frequency (f_{rf}) can be determined

$$\boldsymbol{f_{rf} = \frac{1}{T_{rf}}} \quad (11)$$

Alternatively, for a gated measurement where measurement is triggered for a specific time window, the resonant frequency (f_{rf}) can be determined by the number of cycles divided by the time window.

$$\boldsymbol{f_{rf} = \frac{N_c}{t_W}} \quad (12)$$

Where

- T_{rf} is oscillating tube period
- N_c is the number of cycles
- t_W is the time window of measurement (gated)

It is also possible to determine the specific gravity of fluids by utilising the determined fluid density at process conditions and the known calibrated reference value of fluid density. This is calculated by Equation 15 below:

$$\boldsymbol{SG} = \frac{(\boldsymbol{\rho_f})}{(\boldsymbol{\rho_{ref}})} \qquad (13)$$

Due to the sensitivity of the K_x coefficients with respect to temperature and pressure, an uncertainty is stated per Coriolis device as to its ability to correctly determine fluid density. This stated uncertainty should be with respect to reference conditions, specified by the manufacturer of the device.

The Coriolis meters described in the chapters that follow were manufactured in accordance with the standards described herein. It is noteworthy that there have been attempts to modify the design of Coriolis meters to make use of fiber optic technology, specifically fiber bragg gratings. Wade and Dandridge [17] describe a Coriolis flow meter where the standard electromagnetic transducers were replaced by fiber optics sensors. This concept was further built upon by Zhao et al. [18]. However, at present, to the authors knowledge, electromagnetic sensors are still used as the primary phase shift detection mechanism.

2.3 Errors Resulting from Process Parameters

In general, the use of Coriolis flow meters between the late 1980s and present day has continued to increase in multiple industrial sectors. Arguably the primary reason for this is the technology's proven ability to calculate mass flow rate [19] which, as a unit of measurement, is independent of variables such as temperature, pressure and density. For fiscal purposes, this provides a means of metering valuable fluids such as oil and gas in custody transfer scenarios between operators and vendors in environments where such effects are prevalent. There are, however, practical limitations with respect to manufacturing a physical device [16] that can perform independently of such parameters due to the inherent variations in material properties used in device construction. Specifically, the elastic properties of the flow measurement tube are a critical consideration. Youngs modulus (E) [20] provides a numerical constant to allow these physical effects to be quantified by describing the properties of a solid undergoing tension or compression. It is the quotient of the corresponding longitudinal stress and strain on the material as described in Equation 16.

$$E = \frac{FL_O}{A(L_n - L_O)} \quad \textbf{(16)}$$

Where

- E is Young's modulus
- F is the applied force at each end of the material
- L_O is the original length of the material
- L_n is the new length of the material due to tension or compression
- A is the cross-sectional area of the material

The following sections within this chapter therefore detail theoretical and experimental bodies of work that have been undertaken to establish the limitations of the technology as well as enable the continued improvement of the technology due to evolution of the surrounding practices of instrumentation and control, neural networks, intelligent diagnostics and software modelling. While this thesis' focus is the effect of ambient temperature on meter performance, the previous research discussed herein influenced the experiment designs discussed later in chapter 3.

2.3.1 Pressure

Due to Coriolis technology's reliance on the principles of Young's modulus [20], variations in fluid pressure within the flow tubes will alter the performance of the device by changing the rigidity of the flow tubes and therefore effecting their sensitivity to Coriolis forces. The effect of pressure on Coriolis meters has been researched by a number of laboratories over the years.

Theoretical predictions with respect to potential fluid pressure effects as well as manufacturer specific effects were first described in 1994 by Keita [21]. Under such increased pressures (greater than 15 bar), Coriolis meters will produce greater uncertainties in data outputs than quoted by the manufacturer as experimentally demonstrated by Cascetta [22]. A laboratory inter-comparison exercise also demonstrated that two differing Coriolis meter flow measurement outputs were affected by variations in fluid pressure, therefore highlighting the potential for a wider technology problem as opposed to a manufacturer specific design flaw [23]. An experimental program comparing the performance of two Coriolis meters manufactured by the same vendor but of different generations (1990 and 1996) compared device performance at pressures of 26, 28 and 30 bar. The results showed that the mass flow rate on the newer generation showed considerable performance improvement on mass flow determination over the older generation (-0.5% vs -3.5%) respectively [24]. Wang and Hussain [25] undertook a theoretical and experimental investigation, studying linear damping techniques to account for pressure effects. Such effects are inherently manufacturer specific. This is due to differing construction materials and techniques as well as meter dimensions and geometries. However, all manufacturers attempt to compensate for this by programming correction algorithms within the meter electronics.

It should be noted that commercially available Coriolis meters do not contain an internal pressure measurement capability. On specific models it is possible to connect an external pressure transmitter installed locally to the meter, therefore allowing for live compensation of pressure effects [26]. Alternatively, some Coriolis flow meters have the capability to allow end users to enter a fixed constant pressure correction [27]. However, such a system assumes a constant process pressure, which may not be the case for specific applications. In 2014 [28], NEL undertook a joint industry research project with the

participation of three Coriolis meter manufacturers in an effort to characterise the differences between manufacturers at high pressures (40 bar). While the participating manufacturers remain anonymous, the report highlights that mass flow rate errors ranging from 0.17% to 1.23% were induced due to the increase in pressure. The following year (2015), NEL commissioned a new liquid flow facility, designed to test flow metering technologies at elevated temperatures and pressures (90 Bar, 80°C). This facility was used in research by Mills in 2018 [29] where pressure effects on Coriolis accuracy were investigated. Mills highlighted that as the pressure increases, the rigidity of the Coriolis flow tubes increases, causing a decrease in the device's ability to measure Coriolis force and therefore report an incorrect mass flow rate value. Errors of -1.7% were observed at 40 bar for one manufacturer with -0.5% error at 60 bar for a different manufacturer, highlighting a manufacturer dependence. Mills published further work in this field in 2019 [30], where the uniformity of pressure effects on three identical Coriolis meters was investigated across a pressure range of 5 to 80 bar. The experimental results demonstrated a consistent and linear pressure effect across the three meters, culminating in a -0.6% mass flow error at 80 bar. With an applied pressure compensation coefficient, this error was reduced to within -0.04%.

The use of bespoke micro sensors to detect pressure effects in microfabricated Coriolis transmitters has recently been demonstrated [31], [32], [33]. However, it would appear that the technology in its current form is only applicable to the non-circular tube structure inherent in microcoriolis design, a niche field which has seen continued growth over the years by making use of silicon wafer fabricated Coriolis meters to measure microfluidic flow and fluid density [34], [35], [36], [37]. The deformation of the non-circular section of the flow channel is measured to infer frequency, phase shift and pressure by identifying the modes of operation and offset due to pressure respectively. Therefore, implementation in larger scale meters requires further research.

In summary, if process pressure varies considerably, dynamic compensation within Coriolis meters would improve measurement accuracy. However, incorporating this within meter designs as they currently stand would significantly increase their cost and complexity. Therefore, at present, calibrating meters at known operating conditions is the optimal solution.

2.3.2 Fluid Temperature

Due to the fact that a temperature sensor is fitted to Coriolis meters as standard [38], [26], there can be an assumption from end users that this eliminates potential temperature induced errors. However, it should be noted that the sensor itself is not in direct contact with the fluid and is in fact mounted on the outer wall of the flow tubes. There is therefore a potential lag in temperature measurement in applications where the process fluid temperature is fluctuating rapidly. Depending on the manufacturer, more than one temperature sensor may be installed to determine the temperature profile across the meter body. The effectiveness of Coriolis fluid temperature compensation has been researched over the years by the following works.

In Cryogenic conditions, errors of 2% were observed when a Coriolis meter was calibrated at cryogenic conditions (-193°C). However, when the meter's manufacturer specific internal correction coefficients were adjusted to account for the deviation from factory calibration conditions it is noted that the reported errors were reduced by $\pm$0.2% [39]. These findings were followed up with a theoretical and experimental analysis of potential correction methods to take into account material properties when operating conditions deviate from factory calibration conditions [40]. Tschabold et al. [27] note that exposure to elevated temperatures causes a structural change in the measuring tube therefore effecting Young's modulus principles and introducing additional stresses into the oscillation mechanism, causing a shift in the meter's resonant frequency. A joint industry research project carried out by NEL in 2014 [41], where a total of seven Coriolis meters of differing sizes and manufacturers were tested, found variations in fluid temperature to be a contributing factor to meter mass flow error. However, the extent of error variation differed between manufacturers across a ranging from 0.05% to 0.16%. The report advises that meters be calibrated at their operating conditions or at a range of potential temperatures that are likely to be encountered during operation. Temperature variation was also a parameter discussed by Mills [29], whereby a Coriolis meter was exposed to fluid temperatures of 20°C, 40°C and 60°C, causing respective mass flow rate errors of +0.1%, +1% and +2%. The program also zeroed the meter at each fluid temperature and in doing so was able to demonstrate that errors could be restricted to +0.1%.

The overall effects of fluid temperature on the principles of device operation are similar to those of pressure described in section 2.3.1. However, the presence of a temperature sensor does in theory allow for dynamic compensation of associated effects on meter performance. The research discussed in this section has highlighted that techniques developed by manufacturers which are currently employed have limitations when the device is operated out with its base calibration conditions. There is therefore a need to further develop the temperature compensation techniques to allow them to be more robust in such conditions. As with pressure, the current recommendation is to calibrate the device at operating conditions, however in a system where the fluid temperature is likely to vary, the validity of such a calibration also varies.

2.3.3 Fluid Properties

Research focusing on multiple Coriolis meter manufacturers performance in slurry flow was conducted by Heywood and Mehta [42]. The work highlights that the calibration coefficients generated by the manufacturers using water as the baseline fluid does not produce accurate results when process fluid properties deviate. They recommended that Coriolis meters should be calibrated using fluids of properties comparable to those seen in service. However, Fyrippi and Escudier [43] demonstrated through experimentation in 2004 that Coriolis flow meters were not affected by Non-Newtonian flow.

Research into fluid property effects carried out by Miller and Belshaw [44] investigated Coriolis meter performance using four distinct fluids. The authors demonstrated that for the low viscosity fluids (Kerosene at 1-3 cSt and Gasoil at 4-10 cSt), the mass flow rate reporting capabilities of the meters tested were close to the manufacturers specifications (within ±0.1% mass flow error), however for high viscosity fluids (Velocite at 10 – 30 cSt and Primol at 40 – 300 cSt) the meters were shown to underestimate flow rate with a maximum error of -1.5% observed at 5 kg/s and -0.7% at 70 kg/s.

The research summarised in this section continues the observations of sections 2.3.1 and 2.3.2. Deviations from initial factory calibration conditions have been shown to affect performance. In this instance the cause is deviation from the properties of water, the value of which is typically used in baseline meter calibration. In theory, dynamic compensation of such effects is possible given the meter's ability to determine fluid

density from the resonant frequency. The challenge in such an endeavour is isolating the effects of temperature and pressure on tube resonant frequency and developing correlations between the individual effects. Such a process also yields results that are manufacturer and even model specific.

2.3.4 Multiphase flow

The research and experimentation described to this point in the thesis has been relevant to single phase gas or liquid flow. However, when multiple fluid phases are present within the same flow regime, the response and accuracy of Coriolis meter mass flow and density outputs are affected. Coriolis meters are however still commonly used in this field as a means of metering single phase fluid flow rates before they are combined to form multiphase flow. In addition, the density value is used to determine water in oil and oil in water contamination on the outlet legs of fluid separator units as well as within single phase reference sections of flow facilities. While the focus of this thesis is primarily the effect of ambient air changes in single phase fluid processes, it is important to note the wider industry applications of the device and its limitations, which were discovered by the works discussed in this section.

Such limitations were demonstrated by Skea [45], [46] where errors due to the presence of gas fractions of 6% and 9% were shown to produce mass flow errors of up to 9%. Skea notes that beyond a gas fraction of 9% the Coriolis meter experiences instability in the flow tube oscillation mechanism and therefore errors of ±40% can be observed. It should be noted that for both of Skea's papers, the results from the meters tested are shown to be volumetric (litres per second), therefore the meter's ability to correctly measure both fluid temperature and density has been assumed in the results presented. However, since neither paper specifically states that either process parameter was logged during data collection, no further conclusions can be drawn in this regard.

A neural network can be trained to correct for two-phase related mass flow errors by focusing on key parameters such as density (or resonant frequency of the flow tube), damping, sensor balance, raw and corrected sensor signals, apparent flow rate and temperature as demonstrated in research conducted by Liu et al. [47]. The authors note

that due to the differing Coriolis meter designs between manufacturers, the results are restricted to a specific make, model and size.

Bubble size in multiphase conditions has an effect on meter accuracy. Seeger [48] presented data demonstrating that as the diameter increases from 0.04mm to 0.16mm, the corresponding mass flow error can range from -0.5% to -11%. Seeger does however note that the effects will differ between meter geometries. Similarly, changes in fluid inhomogeneity and compressibility can cause errors as stated by Gylsing [49]. The theoretical model presented by the author is shown to account for a "relaxation" in both parameters and specifically targets the prediction of potential errors resulting in using a calibration obtained for non-aerated flow conditions in aerated flow conditions.

Multiphase flow can cause the flow tube oscillation mechanism to stall and therefore render the device incapable of measuring flow or density. It has been shown by Yeung et al. [50], that by implementing a new digital feedback model within the meter transmitter, operation and flow rate measurement in two phase flow can be improved. Specifically, tests were conducted on two differing sizes of Coriolis meter (one inch and two inch) under three differing phase combinations, (oil and water, air and oil, air and water). It was shown that the new correction algorithms were capable of suppressing flow measurement errors due to the presence of gas to within 2% at GVFs up to 30%. Further research has also demonstrated potential for error corrections in two phase flows with respect to meter orientation, meter geometries and differing phase viscosities, the theoretical and experimental results of which were published by Yeung, Henry et al. [51], [52], [53]. In addition, Henry et al. [54], [55] researched Coriolis technology performance in three phase flow describing experimental work where a water cut meter and additional secondary instrumentation were used in combination with a Coriolis meter as a method of determining individual phase flow measurements. This highlights the potential for innovation using Coriolis technology, and also demonstrates an industrial interest in adopting the technology is due to its versatility as a multi-parameter fluid measurement device.

Particle entrainment is also considered to be an additional phase within the fluid flow, the presence of which reduces the data quality output by the meter with errors of 25%

demonstrated for sand-water mixtures due to the decoupling of the entrained particles and fluid within the Coriolis meter. Basse [56], [57].

The homogeneity of the multiphase mixtures passing through the meter can affect the magnitude of mass flow error output by the technology as demonstrated by O'Donnel and Harvey [58], [59]. Their experimentation on differing Coriolis meter sizes, geometries and manufacturers demonstrated mass flow errors and density errors as a result of two and three phase flow across a range of water cut and gas volume fractions (GVF). For example, 20% GVF conditions produced mass flow errors ranging from -20% to -40%. Both experimental setups determined that multiphase flow at low velocities produced the largest errors in meter output. Research in this field continues with Tombs et al. [60] and Li et al. [61] focusing on model development and validation through experimentation with regards to high viscosity two phase flow and complex signal processing for two phase flow. The development and testing of a new generation of Coriolis meter developed by Krohne was described by Kunze et al. [62], where it was shown that as a result of new fast signal processing techniques using a direct digital synthesizer (DDS), the meter was capable of accurate mass flow and density measurement in a range entrained gas flow GVFs. During a theoretical and experimental study to assess the performance of Coriolis technology in two phase CO_2 flows, Wang et al. [63] demonstrated the viability of using a BP-ANN (Backpropogation-Artificial Neural Network) to correct any resulting mass flow rate errors by detecting and utilising erroneous mass flow rate and fluid density outputs.

Multiphase flow has been extensively researched, with future work planning to encompass the effect of higher pressure and temperatures. While this thesis does not investigate multiphase flow, the observations from the research described in this section are of relevance to the research questions. The recurring theme of meter specificity with respect to error compensation techniques and meter intelligence continues the themes highlighted in the preceding sections. The need for a meter specific understanding with respect variables likely to be encountered in service is key to developing dynamic compensation methods to correct for density calculation errors.

2.3.5 Zero Drift and Adjustment

Sources of zero drift include tube construction materials, symmetry imperfection in flow tube design, fluid properties and connecting pipe works as confirmed by approximation models developed by Keita in 1989 [64]. It is however possible to perform online zero drift correction via modelling solutions designed to specifically target these variables as demonstrated by Storm et al. [65]. More recent research in this field specifically cite temperature effects on the meter body as a potential cause of zero drift, [66], [67] (discussed further in section 2.4). Non-uniform damping and non-uniform mass distribution on the meter body has also been experimentally shown to cause zero drift by Enz et al. [68]. To reduce measurement errors, online zero drift correction should be carried out with little or no data lag within the meter transmitter. To that end, theory and simulations for detecting and correcting zero drift per scan cycle have been detailed by Röck and Koschmieder [69]. In addition, changes in external parameters such as the length of supporting pipelines as well as vibrations incurred from 3rd party components can cause zero drift as demonstrated by Yaushev [70].

Whereas preceding sections have highlighted the potential for errors due to deviating from factory conditions, the works discussed in this section have demonstrated the potential for errors due to a deviation from installation and setup conditions, highlighting the need and continued interest from industry and end users of the technology in improving upon the built-in intelligence of the meter.

2.3.6 Pulsating Flow

The cyclic nature of the pulsating flow combined with flow velocity variation can produce flow conditions which affect the physics of operation of multiple flow measurement technologies. The history and challenges associated with measuring flow where pulsations are present in the system is highlighted by Mottram [71]. At the time of writing Mottram postulates that pulsations are unlikely to affect the operation of Coriolis meters. However, Vetter and Notzon [72] describe potential real-world effects through mathematical analysis of potential pulse sources as well as experimentation, specifically highlighting that when pulsations match the operating resonant frequency of a Coriolis meter, measurement errors will occur. Cheesewright and Clark [73] build upon this observation by developing new modal decomposition techniques by analysing steady flow and pulsating flow through a Coriolis meter mathematically. The authors note that meter manufacturers were not willing to provide details of device operation and such knowledge would have assisted in the verification of the results.

Flow pulsations induced by a diaphragm pump have been shown to induce unwanted vibrations in the measuring tube of Coriolis meters and can cause two distinct effects. The first being to simply excite additional components of motion (internal vibrations) in the measuring tube, the second being to produce motions in the meter that are the sum or difference of the pulsation frequency and the drive frequency [74].

Finite element analysis can be used to further our understanding of meter operation and the influence of specific parameters as demonstrated by Belhadj et al [75]. Specifically, four distinct geometries were modeled and validated against previous experimental data [74]. Further experimentation was conducted by Cheesewright et al. [76] to investigate flow pulsations effects on eight Coriolis flow meters (from five manufacturers) where the flow pulsation frequencies induced were lower than the drive frequency. Perturbation modelling and analysis can also be used to implement prediction of pulsation effects and apply corrections to meter output [77].

Pulsations induced by manufacturing imperfections in the Coriolis flow metering tube have shown to induce shaking forces, which in turn effects meter accuracy. Svete et al. [78] were able to demonstrate these effects both experimentally and through

mathematical modelling. However, the authors note that the meter used in testing was a prototype unit not commercially available and the effects observed may not be representative of real-world effects.

This section has highlighted the need to sample multiple manufacturers when developing experimentation to target a specific effect. The research discussed also highlights the importance of designing a bespoke facility to target a single parameter. The proprietary information that was denied to [73] is not uncommon and is a clear roadblock and an underlying limitation in the majority of the work described in this chapter.

2.3.7 Compressibility

Finite element method (FEM) and computation fluid dynamics (CFD) are techniques that can be used to determine potential mechanical and fluid compressibility effects on Coriolis flow meters. However, until recently, the availability of hardware and software to enable realistic modelling to the low uncertainties required to make effective corrections to meter outputs has been slow to emerge. Early in the Coriolis meter's commercial availability, Keita [21] outlined that no consideration had been given to the potential effects of fluid compressibility on meter performance and describes modelling approaches to account for fluid compressibility effects on the surrounding mechanical structure of the flow tubes. The author states that fluid compressibility may cause the meter factor to reduce and postulates this will produce negatively biased errors on the mass flow rate reported by the meter. However, at the time of writing (1994), the author notes that the available software packages were not capable of modelling the complex interactions of parameters such as fluid flow and Coriolis flow tube oscillation simultaneously. It is noteworthy that errors observed in software models of Coriolis meters can in fact be due to computing rounding errors as discussed by Cheesewright et al. [79].

As modelling capabilities have become more reliable and widely available, this has allowed for viable methods to automatically determine compensation factors to emerge. Specifically, a patent filed by Cage and Dragnea [80] detailed fluid compressibility compensation methods which could be implemented in Coriolis electronic transmitter design. The advances in modelling have allowed for a better understanding of how the

manufacturing quality and consistency can affect errors in fluid flow and density measurements output by the technology as detailed. Specifically, the need for symmetry in Coriolis meter flow tube manufacturing was noted in a compressibility effects study conducted by Hemp and Kutin in 2006 [81].

2.3.8 Factors that can cause incorrect density measurement

Targeted research with respect to the performance of the Coriolis meter fluid density determination is at present limited compared to the vast amount of research summarised in sections 2.3.1-2.3.7, which focuses on characterising the mass flow calculation capabilities of Coriolis meters. This is not unexpected since most end-users utilise the device for flow rate reporting. However, it is important to note that multiple industry sectors rely on the density output as a means of determining process fluid composition. As discussed in section 2.3.4, multiphase applications analyse the density output for multiphase flow water cut determination. The importance of the density value is not limited to the oil and gas sector. Food and drink industries also use fluid density measurement as a means of batch quality control, for example determining sugar or alcohol content. In addition, as we continue to move towards clean fuels replacing fossil fuels, the determination of flowing hydrogen and CO_2 densities is becoming increasingly important in emerging infrastructure models.

As industries continue to adopt big data analytical techniques as part of 'Digital Oilfield technologies', the Coriolis meter calculated density value has recently seen an increase in its perceived importance to process systems. Therefore, it is important that the gaps in published work relating to the potential for error in the density value are investigated and understood by both device manufacturers and end-users.

The capabilities and potential advantages of using Coriolis meters in industrial environments to determine process fluid density and viscosity were highlighted by Kalotay in 1999 [82]. However, no mention was made to the potential for error in the associated calculations.

At a density conference hosted at NEL in 1994, several papers were presented that refer to the Coriolis meter's ability to calculate fluid density. Mathews [83] detailed the

potential secondary effects of temperature, pressure flow rate and viscosity for vibrating element liquid and gas densitometers used in the hydrocarbon industry. In particular, the technology's reduced capability to correctly report fluid density due to temperature effects on the flow tube elasticity and dimensions were highlighted. Both Philp [84] and Geach [85] state that the density output from a Coriolis flow meter can be used to directly calculate a volumetric flow rate. While the statements from both authors at the time is true, there is no mention of the potential for incorrect volumetric calculation, should the density value be adversely influenced by external factors.

More recent research has highlighted that the potential for error in fluid density calculation is routed in the fundamental reliance on interpreting the resonant frequency of the measuring tube. While the existing temperature sensor-based compensation methods account for changes due to Young's modulus as a result of fluid temperature, they do not account for potential gradients along the length of the measuring tube. Kolahi et al. [86], [87] provided an alternative method for calculating fluid density based on determining the "actual" tube stiffness by stimulating the tube at two additional frequencies as well as the resonant frequency. The corresponding experimental results are provided by the authors as a validation of the new method. However, despite a focus on describing temperature effects as a source of error in the background literature, the papers instead present an experimental setup where the pressure of a static fluid within a Coriolis meter was incrementally increased. The standard Coriolis density output is shown to contain errors of +7% at a maximum pressure of 50 bar. Under the same conditions, the new model is shown to keep to within +1%. From experience, the 7% error observed is significantly greater than expected. For example, NEL's pressure effect calibrations of their high-pressure Wet Gas facility contain errors of ±0.8% at 60 bar. No further conclusions can be offered as to the cause of this as neither the geometry or size of meter is detailed. The use of a static fluid, while ensuring pressure to be the only parameter to affect tube frequency, does not fully test the applicability of the model in real world scenarios. The authors conclude that the new method can be used to provide the correct tube stiffness without the need for additional sensors, however this statement neglects to highlight the need to alter Coriolis tube excitation mechanisms to obtain the additional frequencies needed to derive "actual" tube stiffness. The authors also state that only one temperature sensor is required on a Coriolis meter to correct for thermal expansion of the tubes, which conflicts with the authors initial statement regarding the

potential for temperature gradients along the tube. The concepts presented in this paper are therefore interesting, however a lack of clarity and detailed experimental validation produced further questions that have ultimately gone unanswered.

Jianxin [88] demonstrated the potential errors in calculated density due to non-uniform distribution of fluid mass within the meter tubes by modelling a simplified cantilever beam with an additional mass component fixed to the end allowing for the effects on tube resonant frequency to be determined. In a similar vain to the work described in section 2.3.1, Huber et al. [89] detail the development and testing of a Micro Electro Mechanical System (MEMS) based Coriolis based sensor at Endress & Hausser. By etching the tube structure into a silicon wafer the technology was demonstrated to determine the density in microfluidic flows of gas and liquids.

The increased interest from industry in pursuing carbon capture and storage (CCS) solutions has highlighted the importance of the density calculation for facilities flow measurement applications [90]. Glen and Hunter [91] discuss the measurement challenges associated with carbon capture and storage applications and reference the use of Coriolis meters as a favorable technology due to their ability to determine fluid properties live. Hardie [92] also references the use of Coriolis meters in CO_2 measurement, stating the technology's ability to measure both fluid temperature and density makes it a preferable choice in this field. Both Glen and Hardie's works are examples that, if extrapolated to assume a wider industry view, show that it is likely that many end-users will or may already be using the density value output from Coriolis technologies simply due to its convenience, i.e. no need for an additional instrument for measuring density. However, as this section demonstrates, while some validation of this process value has taken place in recent years, the data is largely installation and meter manufacturer specific.

Research conducted by Nazeri et al. [93] evaluated the potential for utilising Coriolis technology for monitoring CO_2 flow applications. The authors state that potential pressure and temperature effects on tube stiffness were compensated for by working within the manufacturers stated operating tolerances and internal correction algorithms. Nazeri et al. [94] followed this work up with further experimentation focusing on the performance of the density process value and identified said value as important to

understanding the composition of the CO_2 as well as any impurities within the Carbon Capture and Storage (CCS) applications. The density value was validated against offline sample data generated using lab-based densitometer equipment across a range of pressures and fluid temperatures (therefore generating fluid densities between 9.0 and 197.6 kg/m^3). The experiments, which were conducted at ambient lab conditions, found that the Coriolis meter used in testing output values with an average deviation of 10.7 kg/m^3 less than the expected value. The author suggests that the deviations observed at low fluid densities may have been due to low inertia of the gas mixture present within the flow tubes or due to an offset in the meter calibration factors.

Seifert [95] highlights the industrial use of live fluid density measurement to determine process changes critical to the operation and safety of a facility. Seifert also states that Coriolis flow meters are now capable of measuring fluid density with a maximum uncertainty of +/-0.2% without the need for special calibration. This is a direct reference to a new generation Coriolis based device developed by manufacturer Endress and Hauser known as the Promass Q, [96]. The device, which has been designed with additional emphasis on its use as a densitometer, underwent field trials in a number of facilities including NEL's [97], [98], [99]. The existence of such a device highlights that if industry is to make operational and financial decisions based on Coriolis meter density values, the overall design must reflect this through appropriate compensation techniques and validation of the data. Garcia-Berrocal [100] et al. also reference the advantages using a Coriolis flow meter for custody transfer due to its ability to measure secondary parameters such as temperature and density.

The rise in demand for monitoring the flow and fluid properties of CO_2 has imparted a new importance on the density measurement capabilities of Coriolis meters. However, the limitations of the technology discussed in 2.3.1 – 2.3.7 will also affect the accuracy of fluid density values output by the meter. Since the density value is entirely dependent on the resonant frequency of the tube, variations in manufacturing quality of the measuring tubes and the potential for temperature gradient profiles have been identified as sources of error. Manufacturers have gone as far as creating bespoke Coriolis-based densitometer devices, which have been designed both mechanically and electrically to compensate for known process effects. However, most end-users are likely to use standard Coriolis meters to determine density and may be unaware of the potential for error. There is, therefore,

a gap in the current knowledge base with respect to retrofitting improved correction methods to existing meter designs as well as designing standard meters to have more robust density determination capabilities.

2.3.9 Targeting Individual Coriolis Mass Flow Meter Components

A Coriolis mass flow meter consists of what are generally referred to as primary and secondary components. The flow tubes and associated electromagnetic driver/magnetic sensors are considered to be the primary elements, while the transmitter carries out the secondary functionality of control, signal processing and correction as well as signal output to data acquisition systems. The desired dynamic capabilities to correct for process effects described in preceding sections are realized through the use of said transmitters.

2.3.9.1 Primary Element (Flow Sensor)

The sensor itself will consist of one or more flow tubes that will either be straight or bent, as well as an excitation/oscillation system consisting of coils and magnets for electromagnetic excitation. [38] The phase shift detection mechanism will consist of sensors that will be placed within the inlet and outlet regions of the device. There will be at least one temperature sensor, typically a resistive temperature detector (RTD), which will be mounted on the external wall of the flow tube as a means of determining fluid temperature. Each manufacturer will introduce their own variation on the sensing components depending on the meter size and intended application of the device. These sensing components will typically be housed in a protective casing to isolate the sensing mechanism from potential damage as well as immediate ambient effects. Manufacturers account for variations in metal composition, sensor resolution, meter size through calibration factors which are either programmed internally into the signal processing element of the transmitter or made available to the end user via a calibration certificate or information plate attached to the meter.

2.3.9.2 Secondary Element (Signal Processing)

While the signal processing can be referred to as the secondary component of the flow measurement device [38], this does not mean it is less important with respect to the operation of the meter. It provides the sensor with control capabilities to allow the oscillation of the sensor via the excitation coils and is responsible for the logging and interpretation and subsequent calculation and correction of the phase shift information relating to the mass flow rate.

Since the early 1990s, there has been significant investment in researching and developing intelligent digital signal processing and control algorithms for optimizing the performance of Coriolis meters. Research conducted by Kolahi [101] produced control algorithms centered around the monitoring and control of the Coriolis meters eigenfrequencies, therefore providing potential to expand the limitations of Coriolis flow meters at the time of writing with respect to gas flow measurement. Clarke [102] discussed the potential in using positive feedback non-linear control. The concept of self-validating sensors (SEVA) was first described by Henry et al. [103]. The authors describe the evolution of industry's expectations with respect to sensors and the data they generate. Specifically, the move from a simple signal generator that electrically represents a physical phenomenon to a device that is capable of performing on-line calculations, internal diagnostics and uncertainty evaluation. The authors utilise Coriolis flow metering technology as an example of the application potential of the SEVA concept due to the technology's need for self-control of tube oscillation, process value calculation and the advantage of fault detection. A prototype Coriolis meter imbued with SEVA functionality was demonstrated by Henry [104]. The authors simulated two device failures independently. The failure of the meter's internal fluid temperature sensor and the effect on the associated flow rate and density calculations was simulated. The test demonstrated that the SEVA model is capable of providing diagnostic information and updating said information as the fault continues. For example, immediately after the sensor fails, the device informs the user of the measurement fault via a series of pre-defined health categories and continues to calculate mass flow and density based on the historical temperature values stored on the device before the failure. The failure of one of the two drive coils responsible for maintaining flow tube oscillation was the second simulation. The failure of one drive coil

is not enough to stop the meter from physically operating but it does introduce a measurement error. Therefore, the use of an in-built self-diagnostic system to alert users to such a scenario is demonstrated to avert the continued collection of inaccurate data.

Further work on a second-generation sensor validation is described by Henry et al. in [105] and Henry in [106], where an all-digital transmitter is demonstrated to eliminate the remaining analogue restrictions inherent in [104], such as improved control, measurement precision and internal diagnostics as well as an increased robustness to two-phase conditions. The SEVA model has since been introduced within the British standard, BS 7986 [107], [108]. Clark et al. [109] describes the need for fast response digital transmitters due to the increase in Coriolis meters use in metering high value products in batches as well as fast control of gas turbine engine fuel flow. The authors describe modelling and experimental research that took account of both the SEVA digital transmitter and a second meter supplied by a different manufacturer.

More recently advances in signal processing using digital filters to replace legacy analog components, which can be influenced by temperature, have been discussed by Ruoff et al. [110]. The authors suggest replacing the standard electromagnetic sensors used to determine pipe motion [16] with optical fork light barriers as a means of reducing potential sensor misalignment errors that can occur due to device and material ageing. Hou et al. [111] [112] describe the development of their own digital transmitter with an emphasis on improving flow tube oscillation performance two-phase conditions, however the authors note in [111] that while the transmitter is ultimately able to improve upon the performance of a commercially available flow meter with respect to driving oscillations, the calculated flow rate contains considerable errors. This work was followed up by Zhang et al. [113], where the errors observed by Hou were targeted through further modifications to their transmitter design. It was shown that by mathematically modelling the stable components (average mass flow rate or totalised flow) as well as the fluctuating components of instantaneous flow rate it is possible to correct for two-phase flow errors within the transmitter. The authors note that the response is not linear and therefore only partial correction was possible. Leach et al. [114] describes a prototype transmitter that showcases a new method for fast monitoring referred to as Prism-based. The authors apply this technique to monitor the

short flow pulses (1ms or less) associated with diesel fuel injection. The concept of Prism signal processing is further explained by Henry [115].

The variations in design of digital transmitters described above rely on digital fieldbus technology to transmit and log sensor and processor data as well as provide end-users with access to both the standards outputs associated with Coriolis meters and additional diagnostic parameters, for example drive gain, electromagnetic transducer amplitude etc. This is typically achieved via Modbus protocol due to the address structure however Profibus and Foundation Fieldbus are also available options on commercially available meters. A recent NEL report [116] provided an overview as to the physical layer and network layer difference between the varying network protocols.

Any new technique for dynamically compensating for errors induced by deviating from ideal operating conditions will be built into the transmitter. Therefore, the technique developed must make use of the information that is available within the transmitter via established digital registers. The research summarized in this section has demonstrated the possibilities and models for realizing a system that can self-diagnose, self-correct and inform the user of errors present in meter output.

2.4 Errors Resulting from External Parameters

Unlike the research described in section 2.3, considerably less theoretical and experimental work has been undertaken to provide a quantitative analysis of errors resulting from external parameters such as ambient temperature variation. Considering the industrial environments that Coriolis meters tend to be installed in, this is somewhat surprising. It is clear from section 2.3 that the development of temperature correction algorithms has focused on accounting for fluid temperature. However, since the temperature sensor(s) installed on Coriolis meters are not in direct contact with the fluid and are in fact measuring the outer tube wall temperature, there is potential for the air temperature surrounding the meter to influence the data obtained from the sensor. In particular when there is a differential between the process fluid temperature and the air temperature. This section therefore discusses previous work carried out with the goal of understanding the potential effects to meter output while highlighting the remaining gaps in knowledge to which the research questions of this thesis will answer.

2.4.1 Ambient Temperature Effects

The experimental work carried out by Wang et al. [66] determined that the mass flow rate calculated by the Coriolis meter under test was affected by changing the surrounding ambient temperature conditions of the meter. This paper is one of the few published works that specifically targets ambient temperature effects. The authors simulated such effects by installing a Coriolis meter within an oven to allow the isolation and control of ambient temperature as an experimental parameter. It should be noted however that the tests made use of a single Coriolis meter design and manufacturer. The variations between manufacturers with respect to geometry and correction algorithms discussed in 2.3 are therefore likely to produce differing results. It is also not stated within the paper the method by which fluid was circulated through the device. The data published does indicate a flow measurement, however this is not directly referenced in the text. The temperature of the fluid will impact the operation of the device as discussed in section 2.3.2. The rate of fluid flow will also inherently affect the rate of heat transfer and achievable thermal equilibrium between the air, meter body and fluid. If the fluid is static then full thermal equilibrium within the system will be achieved if given enough time to settle. It is therefore an oversight that there is no mention of fluid temperature within the paper and it would appear based on the published data that fluid flow rate remained constant throughout testing. It is demonstrated that the ambient air temperature changes affect the physical distance between transducers causing changes in the damping of the signal, which ultimately produce the zero-shift observed by the authors. The authors state in the abstract that the purpose of the experiments conducted was to address industry concerns regarding the ambient temperature variations and resulting effect on meter output. However, while the general experimental concept and overall conclusions based on the data available are sound, the paper ultimately raises more questions than it answers. No mention is made regarding the experiments effect on the meter's ability to determine fluid density. The authors observe that the pattern in which the ambient temperature was adjusted had the capability to produce differing sets of data, however the rate of temperature variation was only changed once as part of the test program. It is therefore difficult to draw any definitive conclusions as to the extent of the rate of temperature change effects on the meter.

The research conducted by Enz [117] further explores the concept of sensor physical dimensions effecting results. The mathematical modelling undertaken is primarily focused on compensating for sensor misalignment due to manufacturing errors. In contrast to [66], Enz highlights the value in modelling for more than one manufacturer to account for variations in construction methods. Enz provides a detailed description and mathematical analysis of conditions that can impede the performance of the meter. It is noteworthy that the conditions modelled in this paper are similar to those that are encountered in the experimental work described by Wang [66]. Enz, however, does not make any reference to ambient temperature variations as a cause of sensor misalignment. The abstract highlights from the outset that Enz has "hands-on" experience with the issue highlighting that, while the work carried out was a theoretical simulation, it was designed with knowledge of 'real world' effects. Enz highlights that variations in meter design such as pipe geometry and transducer mounting location have the potential to cause deviations in the reliability of the data.

Ghayesh et al. [118] includes the factor of thermal loading across the pipeline as part of their model to determine phase shift, and states that ambient temperature can affect phase shift results obtained from the electromagnetic sensors. This highlights the importance of maintaining controlled temperature conditions whenever possible. Although not expressly noted, it is indicated throughout the paper that the model is assuming symmetry in the numerical analysis with regards to both temperature rise across the meter and added mass. Imperfections in manufacturing techniques could, however, produce subtle variations in symmetry, which in turn could affect the model produced in this paper. A similar observation was made by Koschmeider and Röck [67] where it was noted that temperature variations across the wall of the pipe effected Young's modulus, which in turn lead to compensation factors being applied to the control scheme. Enz also noted in [68] that by severely increasing the ambient air temperature around the meter flow tube it was demonstrated that this greatly affected the output from the meter. It should be noted that the method by which the ambient temperature was increased only demonstrated extreme temperature rise and may not reflect real time conditions under normal meter operation. This experiment only focused on one flow meter manufacturer, therefore, limiting the wider industrial implications of the results.

In an experimental program carried out by Øiestad et al. [119] to assess the suitability of Coriolis meters for use in a specific metering application, environmental temperature effects were identified as a potential factor in the observed drift in meter k-factor along with other facility/process specific factors. As part of the tests detailed by the authors, three Coriolis meters were installed in series within a calibration laboratory environment and subjected to flowing conditions and ambient air temperature variations. Each meter was individually exposed to an ambient air temperature of approximately 20˚C above fluid temperature and meter k-factor variation assessed to determine the extent of ambient effects. It is not stated as to whether the change in air temperature was achieved in an enclosed environment or simply localized to the meter in an open lab space. The authors state that a blower was used to introduce environmental change by blowing warm air. The work concludes that ambient air temperature caused two out of the three meter's k-factor to drift out with acceptable limits. However, it should be noted that the investigation into ambient effects was part of a larger study into meter performance and as such the resolution of data regarding ambient effects is limited. Varying the ambient air temperature and trending drift over time, for example, may have produced a distinctive meter response profile with respect to air fluctuations that could have been used as an installation and meter data interpretation guide for the specific facility setup in question.

It is noteworthy that Cheesewright et al. [120] undertook experimentation designed simply to build up a knowledge base from which an 'intelligent' meter could be created in line with the SEVA principles described in section 2.3.9.2. Three different manufacturers took part in the program and provided meters of comparable pipe diameter to allow a consistent dataset to be obtained. A patent filled in the U.S [121] demonstrated capabilities of calculating derived fluid temperature based on a 'meter temperature' sensor and an 'ambient temperature' sensor. The existence of such a patent highlights that there is interest within the industry for a method that can accurately discount ambient temperature effects as a source of error in the internal calculations of the meter. However, as previously stated, manufacturers are generally unwilling to disclose the inner workings of their current commercial devices, therefore it cannot be confirmed as to whether the use of such sensor arrangement has been undertaken in current devices.

Outside the field of flow measurement, Apostolyuk [122] and Nesterenko et al. [123] highlighted that for Coriolis vibratory gyroscopes, the influence of environmental temperature shifts can produce angular rate errors in the system due to thermal loading. The author states that temperature sensors can be used to correct for said effects, however for smaller scale devices where temperature measurement is not possible, the author eludes to a statistical based approach to account for temperature induced errors.

The validation of the target meter design detailed in [18] highlights two instances in the experimentation where ambient temperature fluctuations in the laboratory were shown to affect elastic properties of the cantilever design, and therefore negatively bias the fiber optic sensor wavelengths.

Ambient temperature effects on Coriolis meters is a research area with large gaps in published works and general understanding. The works described in this section have each brought a unique experimental or theoretical observation to the field, however at the point of this research project's inception (2015), there had not been a targeted experimental setup that quantified and correlated the key process and ambient parameters which are experienced by the meter in real world installations (fluid temperature, flow rate, fluid properties and pressure).

2.5 Other External Parameters

2.5.1 Electromagnetic Interference

With regards to potential electromagnetic interference causing disturbance in meter output quality, there appears to have been little experimental work that has been designed specifically to look at this area. The reason for this could well be due to end users and researchers relying on the manufacturer quality assurance checks. For example major manufacturers within the European marketplace will adhere to European Directive 2004/108/EC [124] which sets the standard for all products ability to operate unhindered by electromagnetic interference. Therefore, assumptions can be made that all manufacturers quality control procedures adequately check and discount electromagnetic interference as a factor that can affect the quality of measurement. However, due to the fact that the measured flow through the meter relies on the phase shift data produced by the electromechanical transducers at the inlet and outlets of the meter, it is plausible to assume that there is a risk of incorrect data being produced by the meter in unusually high magnetic fields.

Enz [68] experiments included a setup to determine if magnetic damping via eddy currents will effect meter output. By distributing neodymium magnets across the pipe, it was demonstrated that both pipe damping and phase shift were indeed affected. This experimentation could be extended to cover a wider range of manufacturers to observe this effect across industrial applications. It is also noteworthy that a patent was filed in 1995 by Kalotay and Colo [125] that described a Fiber-Optic sensing method that replaced the currently used Electromagnetic actuators for measuring phase shift. One of the reasons stated for this design was to eliminate the potential for electromagnetic interference. If this method were to be adopted by industry, it may be possible to eliminate errors due to manufacturing imperfections with regards to the placing and lifespan of electromagnetic sensors.

2.5.2 Effect of External Vibration

With regards to vibrating motion acting upon the meter, there has been considerable research undertaken in this area. This is an area of great interest in Coriolis

manufacturing due to the mechanics of how the meter operates. Since the operating principle relies on the internals of the meter being vibrated in a controlled manner in order to infer a flow rate, it is vital that external vibrations are not transmitted into the meter structure and in doing so influence the reliability of the measurement data produced by the meter. Depending on the specific characteristics of a given meter, the associated frequency can vary between 100Hz and 1500Hz. Industrial equipment such as pumps, drive units and shaker tables can induce vibrations of a similar frequency and can therefore interfere with the ability of a Coriolis meter to maintain the required vibratory motions.

It has been postulated that zero stability of the meter is not affected as long as the meter is well balanced and decoupled from external vibration effects [126]. This is further explored and confirmed in an experimental program described in a paper by Van de Ridder [127]. The paper highlights the fact that different meter designs (specifically tube configurations) will require different levels of decoupling as well as the fact that external effects (specifically in this case vibration) will affect Coriolis flow meters greatest when they are measuring at the low end of their stated range. Van de Ridder et al. [128] published works on a new feedforward/feedback control model demonstrating a method for improved vibration isolation in Coriolis control algorithms. An interesting point highlighted in by Anklin [126] refers to the Coriolis meter itself being a source of unwanted vibration effects by way of transmitting out into the environment and then reflected in on itself. The paper however does not make mention of how this would affect a second Coriolis meter installed close in proximity. If one were to extend Anklin's theory on this matter it could well be possible for multiple paths of interference between Coriolis meters if they were to be installed in series. Cheesewright [120] reports on a series of experiments concerned with focusing in on multiple external factors than can affect meter calibration integrity. The experimentation detailed provides a good cross-section of the Coriolis meters commercially available as well as ensuring that the meter dimensions were comparable. The results from the experimentation carried out in this paper highlight the importance of sampling multiple meter manufacturers as the results obtained from each do vary. Clark [129] further explores vibration effects and makes reference to the fact multiple meter types and manufacturers were again compared. Smith et al. [36] note that with respect to their MEMs Coriolis device, the technology is not affected by external vibration due to the

high oscillation frequencies employed (20 to 30kHz) by the technology being out with the potential frequency range of plant equipment frequencies.

2.6 Summary of Literature and Resulting Methodology

This chapter has discussed the evolution of Coriolis metering technology into its current form. The potential to induce errors on meter output has been broken down into process parameter and external parameter specific effects, with previous research cited and discussed. It is now clear that, despite being a well-researched and popular variant of flow metering technology, there is a gap in knowledge with respect to how Coriolis metering technology performs under fluctuating ambient temperature conditions. While there are multiple examples of ambient temperature affecting meter performance cited in section 2.4.1, there is a distinct lack of clarity and consistency with respect to targeted research programs to assess and quantify such effects and relate them to the parameters discussed in section 2.3. There is also a gap in knowledge with respect to the technology's ability to calculate fluid density across a range of varying parameters.

To answer the research questions of this project, and fill the gaps in knowledge highlighted herein, a targeted experimental program that quantified and isolated the effects of ambient air temperature fluctuations on Coriolis meter performance was required. The performance of multiple meter manufacturers under such conditions was assessed to determine the variations in effects that are likely to be seen by devices in service throughout industry. In order to fully understand meter performance and develop improved performance under such conditions, access to manufacturer specific information pertaining to internal correction algorithms and mechanical operation was required.

To effectively isolate and control the interaction of the parameters already known to affect meter performance, as well as interpret the extent of unquantified errors induced by ambient temperature, a bespoke fluid flow loop was designed. To quantify fluid temperature effects, the facility included direct contact fluid temperature sensing at multiple points in the loop. To account for potential pressure effects, upstream and downstream pressure measurements were present. The response of fluid density with respect to temperatures ranging from 5 - 55°C was determined through fluid sampling

and analysis using NEL's fluid property laboratory equipment. The resulting density polynomial curves combined with the facility temperature sensors therefore allowed for live determination of fluid properties during data collection and analysis and thus was the 'true reference' from which meter density percentage error was determined.

The test meter itself was installed within an oven to allow controlled variation of ambient temperature, and experienced continuous fluid flow to minimize fluid residency time and the potential for heat transfer between the surrounding air, meter body and fluid internal to the meter. Varying the air temperature within the oven is an effective simulation of potential conditions that may be experienced in real world installations. As examples, air temperature changes can occur due to proximity to third party equipment such as pumps, or natural phenomena such as direct sunlight on meters installed in hot climates. Directly downstream of the test meter an identical 'reference' meter was installed in series but with ambient air kept to a controlled room temperature. The presence of a reference meter allows for a direct comparison of meter performance with the same mass of fluid passing through each, where the only variable is ambient temperature (accounting for unavoidable manufacturing inconsistencies between the two devices). While it is commonplace in meter calibration scenarios for a 'reference meter' to be located upstream of any intentional flow or temperature disturbances, it was decided that for this research program the meter would only serve as a fundamental check between controlled and fluctuating conditions, with the true reference derived from the fluid sample data. Therefore, by situating the reference meter in the downstream location, additional information pertaining to the temperature effects on the fluid incurred by the oven could be observed in the 'reference meter' density and temperature outputs.

The following variables effect on meter performance were individually assessed through repeat points at varying ambient temperatures.

- Fluid Flow Rate
- Fluid Properties
- Fluid Temperature

By adopting the described methodology, one could then ascertain not only the individual process and ambient parameters effect on overall meter performance, but determine at an individual digital meter process value the manner in which the physics of meter operation affected, for example, resonant frequency or meter drive gain power requirements. Previous attempts to ascertain ambient effects such as [66] and [119] have only targeted one or two of these parameters. The data gathered therefore can only infer meter specific results across a narrow band of parameter variation.

In the following chapter, the fluid flow research facility, associated instrumentation and data infrastructure used in all thesis experiments is described.

Chapter 3

3 Test Facility and Data Infrastructure

3.1 **Overview**

This chapter provides an overview of the components of experimental design that remained constant throughout all thesis experimentation. Details are provided on flow loop design, Coriolis meter specification and data acquisition (DAQ) infrastructure.

To understand the effects of fluctuating ambient temperature on Coriolis meters, all associated experimentation and data collection was carried out within a system where all variables could either be controlled or quantified.

As discussed in chapter 2, the effect of fluid temperature on Coriolis flow metering technology has been well documented. Therefore, the test fluid temperature circulated throughout the flow loop was controlled within predefined limits during any experiment in which the variation of fluid temperature was not the focus. Any deviation in fluid temperature that was unavoidable due to parameters beyond the control capabilities of the facility were documented and accounted for via the facility reference instrumentation. To account for and improve upon the experiments conducted by Wang [66], the fluid was not static during any of the data points collected, avoiding thermal equilibrium between the surrounding air, meter body and fluid. This therefore made it feasible to separate and identify the individual component temperature effects on the data output from the meters under test.

To allow for the direct comparison of a meter exposed to a fluctuating ambient temperature environment with respect to a stable environment, the facility build incorporated two identical Coriolis meters. One meter designated as “Test Meter” was installed within a scientific oven. The second meter designated as “Reference Meter” was installed in series, downstream of the test meter but out with the scientific oven, and exposed to the stable ambient air environment of the room in which the flow loop is situated. This arrangement allowed for the same mass of fluid to pass through both

meters and therefore enabled a direct comparison of the meter's measurement abilities under differing ambient conditions. The downstream location of the reference meter allowed for any fluid density or temperature changes due to the presence of the oven to be detected and quantified during data analysis.

3.2 Facility Description

The facility designated as the 'Very Low Flow Loop' located within NEL's single phase calibration laboratory was most suited to the research parameters. The standard facility layout and secondary instrumentation locations are detailed in Figure 3-1

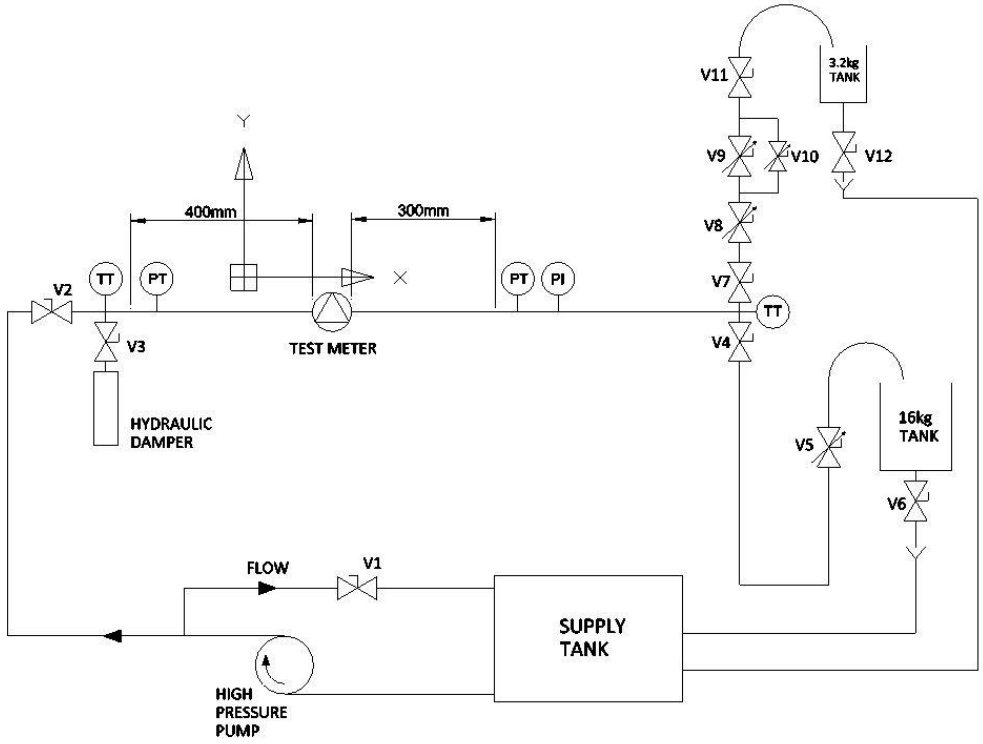

Figure 3-1 Schematic of TUV SUD National Engineering Laboratory's 'Very Low Flow Facility' in standard operating configuration

The operation of the facility is as follows: - Fluid is drawn from the supply tank by a circulation pump, from which point it is discharged to the facility test section. The pump installed in the facility is a positive displacement gear pump with a 240V drive motor that operates under the principle of magnetic drive coupling. The pump is protected by a safety cut off, which allows decoupling from the magnetic drive should it experience unacceptable flow conditions such as a dead-end flow circuit or high upstream fluid

pressure. The facility test section measures at 700 mm long as standard however this can be modified as required.

The facility has two pumps,

- P1 - high range flow
    - Single phase 50Hz, 240 V, 2.15 A
    - 0.25 kw
    - 2850 rev/min
- P2 - low range flow
    - Single phase 50Hz, 240 V, 1.24 A
    - 0.18 kw
    - 2870 rev/min

The downstream piping from the two pumps is constructed using 12 mm (10 mm I.D.) and 8 mm (6 mm I.D.) high-pressure stainless-steel pipework respectively and using Swagelok high pressure compression fittings.

Flow conditions are manually controlled by the facility operator via a bypass valve downstream of the pumps but upstream of the test section. This can be used to return a proportion of the flow to the supply tank as required. A throttle valve installed downstream of the test section provides line throttle control. Isolation valves are located at the inlet and outlet of the test section.

Bourdon tube pressure gauges are used as standard to measure the upstream and downstream pressures during standard facility operation however, for the purposes of this research programme, electrical feedback pressure transducers were installed in said locations to enable live trending of facility pressures during data collection. These sensors were calibrated in NEL's UKAS accredited pressure calibration laboratory to an uncertainty of ±0.25 Bar.

The facility also contains upstream and downstream temperature measurement in the form of custom designed PT100s. These sensors were calibrated in NEL's UKAS accredited temperature calibration laboratory. The measurement uncertainty of each probe was ±0.02°C.

Ambient room temperature is monitored by a k-type thermocouple (standard uncertainty of ±2.2°C) located in the test section area of the flow loop.

The test fluid is stored in a 330 Litre stainless steel supply tank. Six female quick connectors are installed on the side of the tank, two of which provide fluid outlets for the P1 and P2 inlet lines. There are also four fluid return ports, which are used for the bypass and recirculation loops.

The supply tank is equipped with a heating/cooling coil. This is used to control the temperature of the fluid within the tank within the range of 5 to 50°C. The temperature control unit is a Huber CC40 Thermostat Bath.

The capabilities of the facility are summarised in Table 3-1 with further description in Appendix 1.

Table 3-1 'Very Low Flow' Facility Operating Specifications

Pump Loop	Pipe Size (mm)	Flow Range (l/min)	Viscosity Range (cP)	Uncertainty of Measured Mass/Volume (%)
P2	6	0.002 - 0.9	1 - 40	0.05
P1	10	0.2 - 5	1 - 40	0.05

3.3 Test section modifications

To allow for the inclusion of the scientific oven (Gallenkamp – 'Plus II Oven'), the test section was modified by way of rerouting the piping to enter and exit the oven as shown in Figure 3-2. The test meter was installed within the oven and connected to the pipework by way of flange and thread adaptors. All piping internal to the oven was insulated to minimise heat transfer. Figure 3-3 details the meter position, support stands and piping within the oven. A thermocouple was located on each wall as well as at the oven centre point to allow for heat distributions to be mapped during analysis.

Immediately downstream of the oven (0.3 m), an additional 'mid-point' PT100 temperature probe was installed to allow for direct measurement of fluid temperature. The inclusion of this sensor ensured that any heat exchange as a result of flow through the oven and test meter could be quantified during data analysis. The probe is of the same manufacturing batch as the upstream and downstream PT100s (section 3.2) with an uncertainty of ±0.02°C. The 'reference meter' was installed downstream (0.7 m) of the PT100. Due to its proximity to both the test and reference meters, the temperature measurement provided by this sensor was utilised as the true fluid temperature value for all absolute error calculations with respect to Coriolis meter temperature output. It is referred to as "actual fluid temperature" in chapters 4, 5 and 6.

It should be noted that the function of the reference meter was effectively limited to a live check between controlled and fluctuating ambient conditions. Test meter density error was determined using live fluid property data obtained through sample analysis as described in section 3.4 below.

To rule out temperature effects on the meter transmitter performance, the test meter transmitter heads were not installed within the oven. They were located within the temperature-controlled laboratory, with the electrical connection to the meter made via service ports on the oven.

All piping within the oven was insulated to minimise heat transfer between the air temperature, pipes and fluid in locations directly upstream and downstream of the test meter.

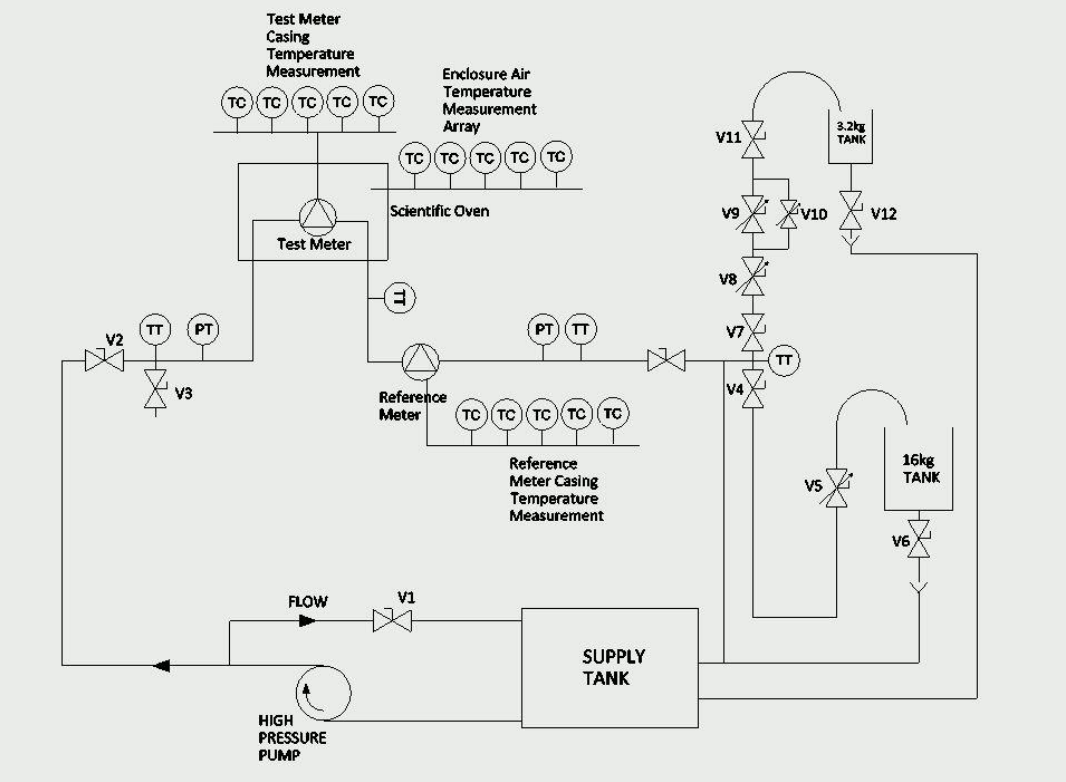

Figure 3-2 Schematic of TUV SUD National Engineering Laboratory's 'Very Low Flow' facility with modifications of the test section to accommodate oven, additional sensors and two test meters

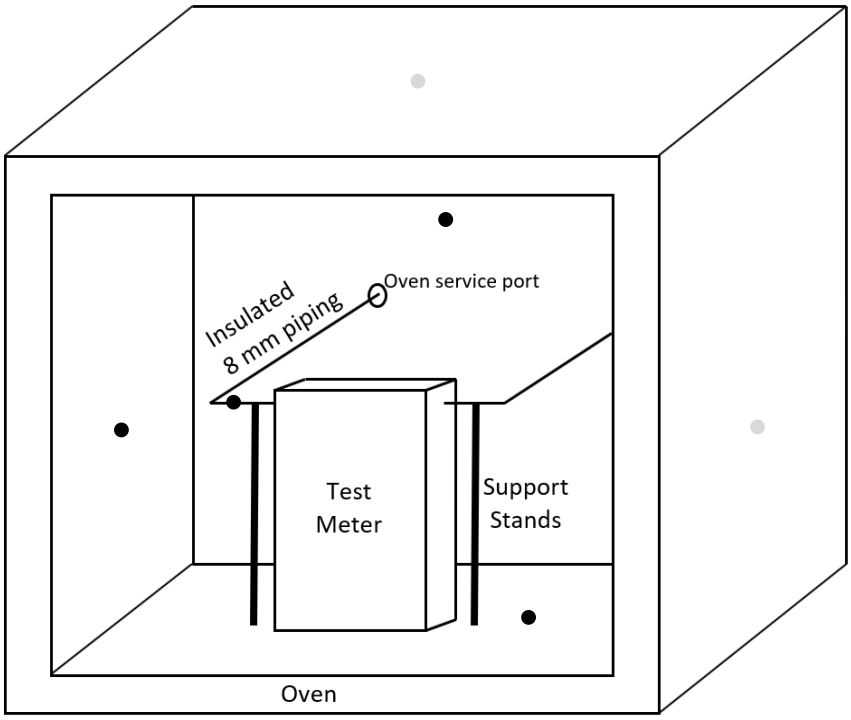

- ● - Thermocouple (TC)

Figure 3-3 Oven and test meter arrangement.

3.4 Fluid Property analysis

For each experiment, a sample of the fluid under test was analysed using an Anton Paar DMA 5000 benchtop densitometer. The stated uncertainty of NEL's fluid density measurement capabilities is ±0.00001 kg/l·

The density of water across a temperature range of 5 - 55°C is calculated at NEL as standard using the following equation as defined by Glen and Johns [130]. The equation makes use of secondary instrumentation inputs to provide live fluid temperature and pressure corrections.

$$\boldsymbol{\rho_{t,p} = 1000 \sum_{i=1}^{13} a\,(i)\theta^{m(i)}\pi^{n(i)}} \quad (17)$$

Where

- $\rho_{t,p}$ is fluid density with respect to temperature and pressure
- θ is the reduced temperature
- π is the reduced pressure
- $a(i)$, $m(i)$ and $n(i)$ are coefficients

The density of Kerosene and Gas Oil across a temperature range of 5 - 55°C is calculated at NEL as standard using Equation 18. As with Equation 17, the equation makes use of secondary instrumentation inputs to provide live temperature corrections.

$$\boldsymbol{\rho_t = \rho_{20}\,[1 + \{\alpha(\theta - 20)\}]} \quad (18)$$

where

- ρ_t is the calculated density with respect to measured temperature
- ρ_{20} is the density at 20°C
- α is the slope/ρ_{20}
- θ is the live fluid temperature
-

The equations and calibration curves generated from the fluid samples were programmed into the Data acquisition (DAQ) software (Appendix 2) allowing for live, true fluid density calculation per system scan cycle. The resulting calculated densities therefore allowed for a direct comparison with the density values output by both the test and reference meters and therefore represented the 'true' value from which the

calculated ‘test’ and ‘reference’ meter density percentage errors (discussed further in chapters 4, 5 and 6) were determined.

3.5 Data Acquisition

In recent years it has become standard for modern Coriolis meter transmitters to make available additional diagnostic information by way of digital fieldbus. This allows end users of the technology to gain access to information that is used internally by the meter to perform corrections, calculations and maintain device operation (e.g. oscillation control power requirements). This level of diagnostic data access was a key component of meter specification allowing for data to be gathered pertaining to device operation and allow for a complete understanding as to how the temperature effects propagate through the meter subsystems and calculations. As such all meters tested had RS485 Modbus capabilities to standardise on digital networking requirements.

Figure 3-4 summarises the digital and analog signal infrastructure which was designed to comply with the thesis methodology (section 2.6). Additional descriptions of the DAQ hardware and software used in this thesis can be found in Appendix 2.

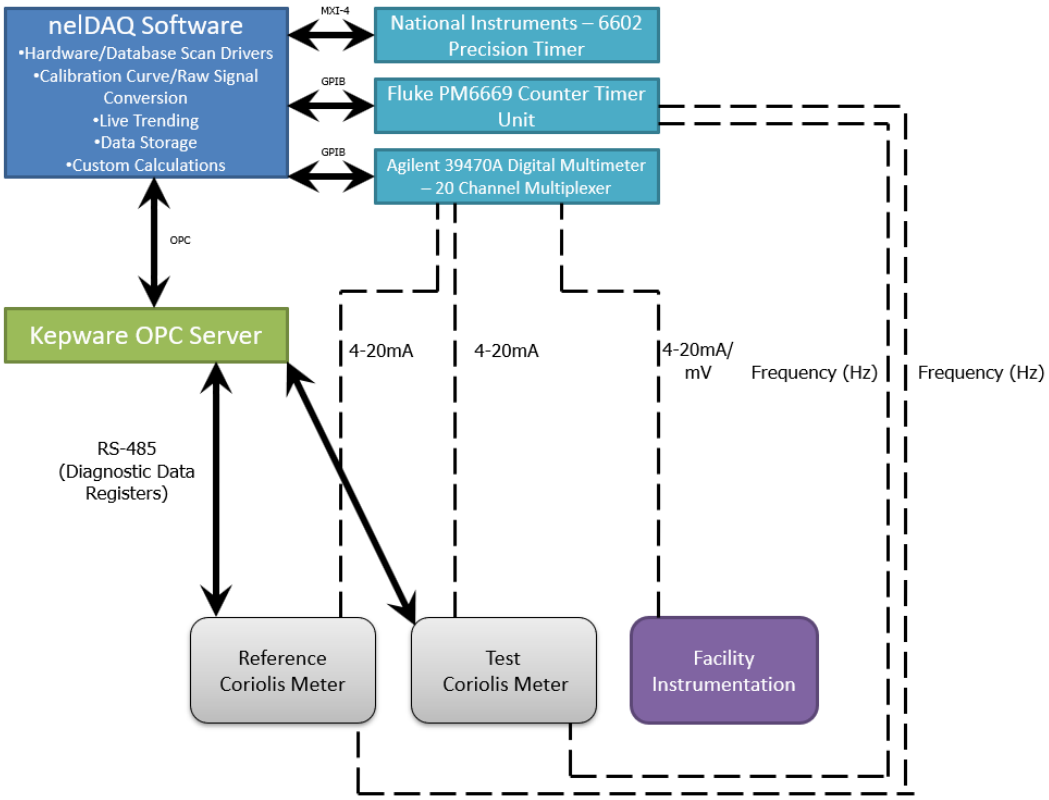

Figure 3-4 Data infrastructure summarising digital communication protocol setup, analog signal routing and well as nelDAQ software build for the duration of thesis experimentation.

For analog signal acquisition, a multiplexer-based system was set up. A Keysight 34970A data acquisition mainframe was used in combination with a Keysight 34901A 20 channel multiplexer. This was linked to the main data acquisition PC by communications protocol IEEE 488.2 (General Purpose Interface Bus). The circuit diagram shown in Figure 3-5 shows the internal circuitry for the multiplexer unit.

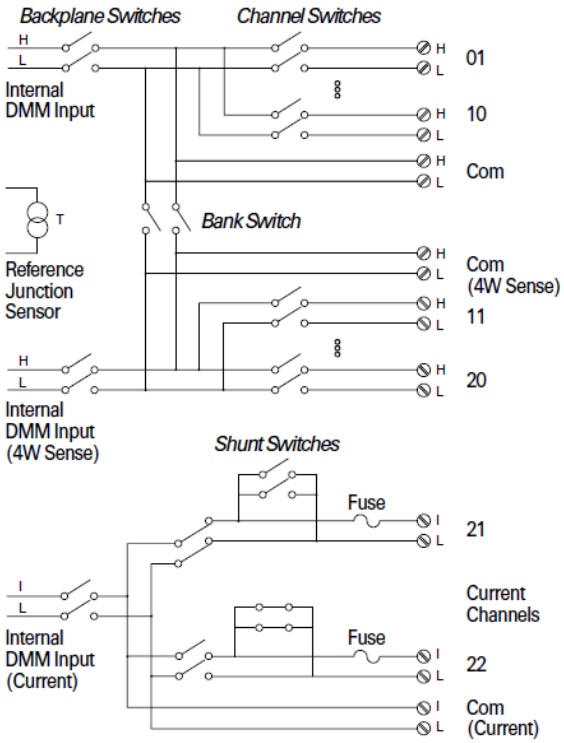

Figure 3-5 Multiplexer switch unit used for logging reference RTDs 4 wire resistance and 4-20mA signals from reference pressure transmitters and Coriolis flow meters [131]

The analog measurements detailed in Table 3-2 were logged using this device.

Table 3-2 Instrument Overview

Measurement Description	Sensor Type/Make	Signal Output
Upstream Temperature (TT)	PT100 (Custom designed by Sensing Devices Ltd)	4 Wire Resistance (Ω)
Ref/Test Meter "Middle" (TT) ('Reference/True' Temperature Value)	PT100 (Custom designed by Sensing Devices Ltd)	4 Wire Resistance (Ω)
Downstream Temperature (TT)	PT100 (Custom designed by Sensing Devices Ltd)	4 Wire Resistance (Ω)
Upstream Pressure (PT)	'Gems' Pressure Transducer	4-20mA
Downstream Pressure (PT)	'Gems' Pressure Transducer	4-20mA
Reference Meter Case Temperature Position 1 (TC)	K-Type Thermocouple	mV
Reference Meter Case Temperature Position 2 (TC)	K-Type Thermocouple	mV
Reference Meter Case Temperature Position 3 (TC)	K-Type Thermocouple	mV
Reference Meter Case Temperature Position 4 (TC)	K-Type Thermocouple	mV
Reference Meter Case Temperature Position 5 (TC)	K-Type Thermocouple	mV
Test Meter Case Temperature Position 1 (TC)	K-Type Thermocouple	mV
Test Meter Case Temperature Position 2 (TC)	K-Type Thermocouple	mV
Test Meter Case Temperature Position 3 (TC)	K-Type Thermocouple	mV
Test Meter Case Temperature Position 4 (TC)	K-Type Thermocouple	mV
Test Meter Case Temperature Position 5 (TC)	K-Type Thermocouple	mV
Oven Centre Position (TC)	K-Type Thermocouple	mV
Oven Upper Wall Position (TC)	K-Type Thermocouple	mV
Oven Lower Wall Position (TC)	K-Type Thermocouple	mV
Oven Left Wall Position (TC)	K-Type Thermocouple	mV
Oven Right Wall Position (TC)	K-Type Thermocouple	mV
Oven Back Wall Position (TC)	K-Type Thermocouple	mV
Room Air Temperature (TC)	K-Type Thermocouple	mV

Motherboard Extension/NI 6602 Chassis.

A National Instruments 1042Q PXI Chassis was employed to provide additional bus connections to the main data acquisition PC and communicated over MXI-4 protocol [132]. This allowed for the installation of a National Instruments PXI 6602 timer module, which was used for precision timing and data synchronisation throughout data collection. A PXI-GPIB module was also installed within the chassis and facilitated the IEEE 488.2 network connections.

The digital communication protocols commonly implemented in commercially available flow meters rely on proprietary drivers to pass data to 3rd party devices [116]. To simplify this process, a generic OPC (Open Platform Communications) server and client was setup and customised to suit the particulars of each device's digital addressing structure. Figure 3-6 shows a top-level overview of this setup.

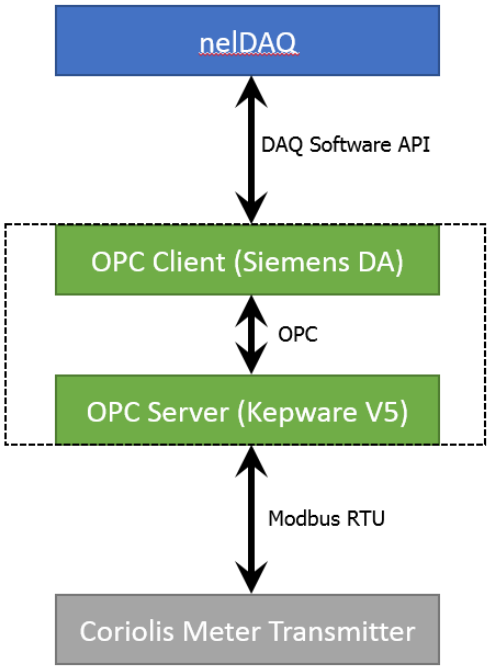

Figure 3-6 Overview of digital fieldbus OPC infrastructure

The OPC server package implemented was Kepware V5, configured for RS485 RTU (remote terminal unit) communications. The client package used was Siemens DA (Data Access). All OPC data was polled as a single data request (summarised in Figure 3-7) from the DAQ software which was called after the analog multiplexing had completed

per scan cycle. Structuring the read/write cycle in this manner ensured minimised scan times.

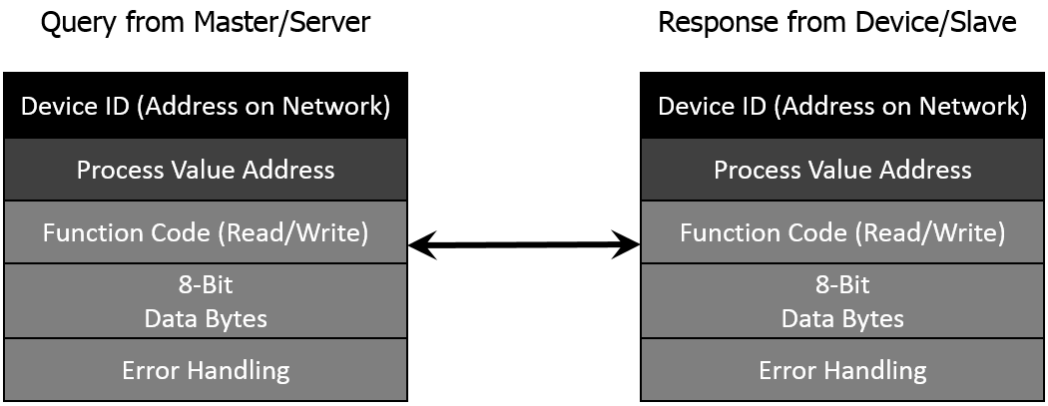

Figure 3-7 Modbus query response cycle for Mater/Slave setup

The sequential nature of the multiplexing system, coupled with the individual channel settling time associated with the internal 34901 module electronics, resulted in a scan cycle time of ~ 4 seconds for the experimentation described later in chapters 4 and 5. This time was later reduced to ~2 seconds (chapter 6) due to the removal of the meter casing thermocouples (table 3-2) that had been deemed surplus to requirements after reviewing the data discussed in chapters 5 and 6. Since this body of work did not investigate fast moving transient/pulsating effects, both scan cycle times were optimal for this research programme and within the recommended Nyquist parameters.

3.6 Coriolis Meter Diagnostic Values

Due to the variances in available process parameters between manufacturers and the specific meter models tested (discussed further in chapters 4, 5 and 6), the digital data logged also varies between meter design. Table 3-3 summarises key digital process values that were available from each manufacturer variant.

Table 3-3 Modbus Digital Process Value Overview

Process Value	Manufacturer A (Ch. 4)	Manufacturer B (Ch. 4)	Rheonik Meter 1 (Ch. 5)	Rheonik Meter 2 (Ch. 6)
Density	x	x	x	x
Mass Flow	x	x	x	x
Volume Flow	x	x	x	x
Tube Temperature	x	x	x	x
Drive Gain	x	x		x
Frequency	x	x	x	x
Period	x		x	x
Flow Velocity		x		
Input Pickup Amplitude	x	x		x
Output Pickup Amplitude	x	x		x
Electronics Temperature	x	x	x	x
Live Zero	x			
Mass Total	x			x
Volume Total	x			
Delta	x			
Input Voltage	x			
Strain 1		x		
Strain 2		x		
2 Phase Detection		x		
Torsion Bar Temperature			x	x
Drive Current				x
Amplifier Value			x	x
Output Control Value				x
Drive Stability				x
Amplifier Stability				x
Amplifier Performance				x

3.6.1 Logging intervals

A standard flow meter calibration or research setup will only log facility and test meter instrumentation values once steady state conditions have been achieved. However, given the nature of the effects targeted by this thesis, all data recorded during experimentation was done as a continuous time series log, lasting up to 10 hours in some instances. In doing so, any gradual transient effects in meter and facility component response was captured and allowed for direct correlation during data analysis.

3.7 **Statistical Analysis**

The data obtained using the setups described in this chapter were statistically analysed to validate any experimental observations relating to correlations between meter output drift and the controlled experimental variables of ambient air temperature, fluid properties and flow rate.

The Pearson correlation test was selected as the standard test to apply to all data sets during data analysis. The resulting correlation coefficient value of the test indicates whether the two variables are positively or negatively correlated. The strength and direction of the correlation is indicated by a value between -1 and +1. The test is mathematically defined as the covariance of two process variables, S_{XY}, divided by the product of the individual process value standard deviations $(\sigma_X \sigma_Y)$.

$$r_{XY} = \frac{S_{XY}}{\sigma_X \sigma_Y} \tag{19}$$

Where covariance, S_{XY}, is the sum of the products of the individual sample element $(X_i \; and \; Y_i)$ difference with respect to the corresponding mean for both process variables $(\bar{X} \; and \; \bar{Y})$ for each data point, divided by the number of data points, N, minus 1.

$$S_{XY} = \frac{\sum_{i=1}^{n}(X_i - \bar{X})(Y_i - \bar{Y})}{N-1} \tag{20}$$

The value obtained from Equation 20 also gives an indication of the direction of correlation as well as the strength. However, the value is not limited between -1 and +1, nor does the result rely on the standard deviations of the two sample process values.

Standard deviation, σ, is defined as the square root of the sum of the sample element, X_i minus the mean of the sample, $\bar{X}$, squared for each data point, divided by the number of data points, N, minus 1.

$$\sigma = \sqrt{\frac{\sum_{i=1}^{N}(X_i - \bar{X})^2}{N-1}} \tag{21}$$

3.8 Summary

This chapter has described the components of the research facility that were deemed critical to ensuring data quality and consistency throughout the experimentation undertaken. Key equations used during data analysis were also described. The use of a facility which is part of the national standard for flow measurement ensures that the equipment and resulting data is of a standard that is fully traceable to individual component calibrations. From the authors experience and by extension the collective experience of NEL in the field of measurement and traceability, a change in any of the setups described in this section would yield different results in the chapters that follow. By expanding the process values logged to include digital diagnostic parameters, the experiments can determine individual meter component response to the temperature differentials tested. If one were to only log the standard analog outputs typically available to end-users, the true effects of temperature would be masked by signal post processing and damping embedded within the meter transmitter firmware.

In the next chapter, the first research question posed by this thesis is addressed through experimentation and results analysis.

Chapter 4

4 Investigating the Effect of Ambient Temperature on Coriolis Meter Performance

4.1 **Experiment Parameters**

Two manufacturers supplied Coriolis flow meters with the following specifications for the experiments described in this chapter:

Meter Type:-

- U – shaped, dual tube Coriolis flow meter.

Sizing and Specifications:-

- 0.5” Coriolis Meter (Manufacturer A)
    - ±0.10% of flow rate
    - ±0.5 kg/m^3
- 1” Coriolis Meter (Manufacturer B)
    - ±0.05% of flow rate
    - ±1 kg/m^3

Communications:-

- Pulse Output
- 4-20mA Output
- RS485 Modbus Output

Both manufacturers stated as a condition for the loan of this equipment that all data produced must be anonymised. As such the specific details relating to manufacturer and model numbers of meter body and transmitters will not appear in this thesis. Henceforth they shall be referred to as Manufacturer A and Manufacturer B.
During this phase, two ovens were used. This was to accommodate the differing dimensions in meter body between Manufacturer A and B. Manufacturer A used a

'Gallenkamp Plus II' oven with an internal volume of 0.08 m^3 henceforth referred to as 'Oven A'. The oven used for manufacturer B was manufactured by 'Astell' (model EBC230) and had an internal volume of 0.7 m^3, henceforth referred to as 'Oven B'.

A reduced test matrix was performed for manufacturer B whereby the meters were subject to only one fluid type, due to limited access to Oven B.
Due to the differences in volume, Ovens A and B had differing rates of temperature change, resulting in differing test matrices between Manufacturers A and B.
There was not a specific need for direct comparison between meter manufacturers as the key objective of phase 1 was to determine whether ambient temperature fluctuations can affect data output from Coriolis flow meters.

Test Matrix:

The following variables were controlled to remain at a constant during testing:-

- Fluid Temperature – Controlled by Facility heat exchanger conditioning circuits
- Room Temperature – Room ventilation and conditioning
- Upstream Pressure – Controlled by facility throttle and bypass valves
- Downstream Pressure - Controlled by facility throttle and bypass valves

The variables adjusted were:-

- Oven internal air temperature
- Rate of air oven air temperature change
- Fluid Flow Rate
- Fluid Properties

Varying the rate of air temperature change was performed to determine the time until thermal equilibrium was achieved between the air and meter body.

Varying the fluid flow rate was performed to target the fluid temperature effect on the meter flow tubes while conversely assessing the flow tube wall temperature effect on fluid temperature.

Under real world process conditions it may be common for fluid flow rate to vary frequently depending on the specifics of the application, and as such any ambient temperature effects are amplified or reduced by variations in fluid flow.

The purpose of changing the fluid during this test program was to allow for the categorisation of potential thermal effects resulting from the differing specific heat capacities of the fluids being metered.

Before data collection commenced, the fluid was circulated for at least 1 hour within the facility to allow for steady state conditions to be achieved. After this time the data acquisition system was started. The chamber door remained opened to allow all test points to begin with an established baseline for both meters at ambient conditions. After a predetermined period, the chamber door was closed and an ambient temperature setpoint was set.

Tables 4-1 and 4-2 summarise the individual test points for manufacturers A and B. Note that due to additional facility time available during Manufacturer A testing, additional test points were logged with the locations of the test and reference meters swapped. This allowed for assessment of meter specificity with respect to any performance drift observed due to the test variables.

Table 4-1 Manufacturer A test matrix

Test No	Fluid	Highest Fluid Flow Rate (kg/hr)	Initial Test Meter Air Temp (˚C)	Final Test Meter Air Temp (˚C)	Rate of Test Meter Air Temp Change (˚C)	Reference Meter Air Temp (˚C)	Fluid Temp Setpoint (˚C)	Test Duration (Hrs)	Comment
1	Gas Oil	130	20	65	2 /15 mins	20	20	8	Initial Positions
2	Gas Oil	130	20	65	5 / 15 mins	20	20	8	Initial Positions
3	Gas Oil	130	20	65	8 / 15 mins	20	20	6	Initial Positions
4	Gas Oil	130	20	65	5 / 15 mins	20	20	8	Swapped Positions
5	Gas Oil	120	20	65	2 /15 mins	20	20	8	Swapped Positions
6	Gas Oil	130	20	65	8 / 15 mins	20	20	6	Swapped Positions
7	Water	130	20	65	2 /15 mins	20	20	8	Initial Positions
8	Water	130	20	65	5 / 15 mins	20	20	8	Initial Positions
9	Water	130	20	65	8 / 15 mins	20	20	6	Initial Positions
10	Water	130	20	65	2 / 30 mins	20	20	9	Initial Positions
11	Water	130	20	65	2 / 30 mins	20	20	9	Swapped Positions
12	Water	130	20	65	2 /15 mins	20	20	8	Swapped Positions
13	Water	130	20	65	5 / 15 mins	20	20	8	Swapped Positions
14	Water	130	20	65	8 / 15 mins	20	20	6	Swapped Positions

Manufacturer A's transmitter provided no interface to allow for interrogation or adjustment of correction algorithms implemented within the device firmware.
The fluid type was changed from gas oil to water mid test matrix for Manufacturer A. The rig was flushed through with water to minimise any contamination from the previous fluid. The storage tank was then filled with the replacement water and was circulated through the flow loop.

In addition, the casing design of Manufacturer A's meter allowed for K-type thermocouples to be fixed in strategic locations on both the reference and test meter as described in Chapter 3. This allowed for a temperature profile across the meter bodies to be determined. Figure 4-1 shows the meter casing thermocouple locations.

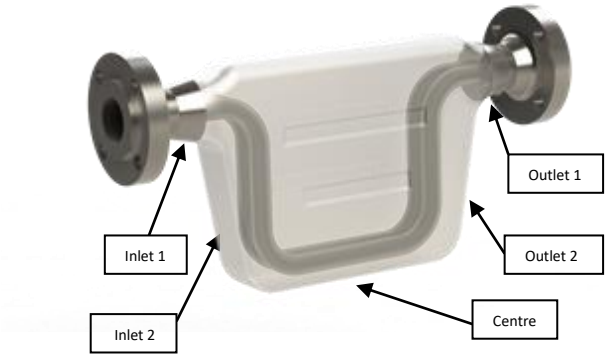

Figure 4-1 Generic Coriolis meter showing locations of additional thermocouples installed on outer casing

Table 4-2 Manufacturer B test matrix

Test No	Fluid	Highest Fluid Flow Rate (kg/hr)	Initial Test Meter Air Temp (˚C)	Final Test Meter Air Temp (˚C)	Rate of Test Meter Air Temp Change (˚C per mins)	Reference Meter Air Temp (˚C)	Fluid Temp Setpoint (˚C)	Test Duration (Hrs)	Comment
1	Kerosene	55	20	65	40 /1 mins	20	20	8	Density Mode 1
2	Kerosene	75	20	65	10 / 60 mins	20	20	4	Density Mode 1
3	Kerosene	75	20	65	10 / 60 mins	20	20	4	Density Mode 2
4	Kerosene	55	20	65	40 / 1 mins	20	20	8	Density Mode 2

Manufacturer B's transmitter allowed for two possible modes of operation for density calculation. To maintain anonymity these modes will be described herein as "Density Mode 1" and "Density Mode 2".
Density Mode 1 was the default setting on the transmitter upon arrival. It did not require any additional information to be programmed before testing commenced. The

density was calculated via the manufacturers patented algorithms and predefined reference values.

Density Mode 2 required the user to input a linear scale representative of the fluid properties passing through the meter. This took the form of a line gradient value based on the fluid density values at two distinct points on the fluid property range with respect to temperature. As shown in Table 4-2, Kerosene was used during Manufacturer B testing. Density values of 807 kg/m^3 for Kerosene at 20˚C and 782 kg/m^3 at 55˚C as determined by NEL's calibration lab were used to calculate a gradient (M) of 0.714, which was in turn programmed into the transmitters of both the reference and test meters. The gradient was calculated as follows: -

$$\boldsymbol{M = \frac{\rho_D - \rho_C}{T_B - T_A}} \qquad (22)$$

where

- T_A = Low Temperature
- T_B = High Temperature
- ρ_C = Density at High Temperature
- ρ_D = Density at Low Temperature

The test Matrix for Manufacturer B accommodated two elevated ambient air temperature tests with Density Mode 1 active. These conditions were then repeated with Density mode 2 active. The difference in meter performance between the two modes was observed.

4.2 Manufacturer A Results

The experimental setup described in section 4.1 was used to obtain the data presented in this section. Section 4.2.1 presents the data resulting from the conditions of test 1 and test 7 detailed in Table 4-1. These data points were chosen as a summary of the observed effects of ambient temperature on Coriolis data across two fluids of differing properties. The remaining test points are summarised in tabular form in section 4.2.5.

4.2.1 Stepped Ambient Air Increases

4.2.1.1 Reference Conditions

Figure 4-2 depicts the flow loop reference measurements pertaining to test meter ambient air temperature and fluid temperature. During testing the actual fluid temperature (as measured by the middle facility PRT – Figure 3-2) for Gas Oil and Water increased by 2.5°C and 0.8°C respectively over a stable trend, therefore when analysing the performance of Coriolis meter outputs in the following sections, any deviations in associated process values are considered to be in error.

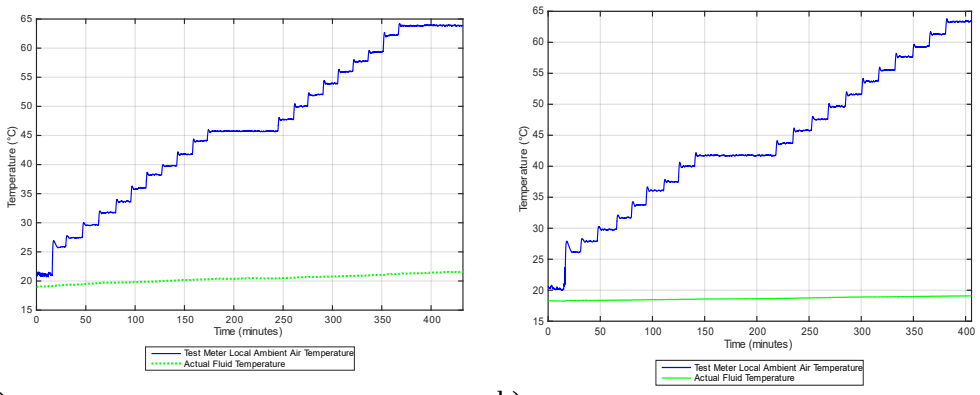

a) b)

Figure 4-2 Measurements of test meter air temperature and fluid temperature a) Test 1 (Gas Oil), b) Test 7 (Water)

For both tests, the room ambient air temperature fluctuated by ±2°C over the course of 7 hours.

4.2.1.2 Reference Fluid Properties

Figure 4-3 contains the calibration data derived from fluid samples for both gas oil and water. The variation in density with respect to fluid temperature is shown across a range of 5°C - 55°C.

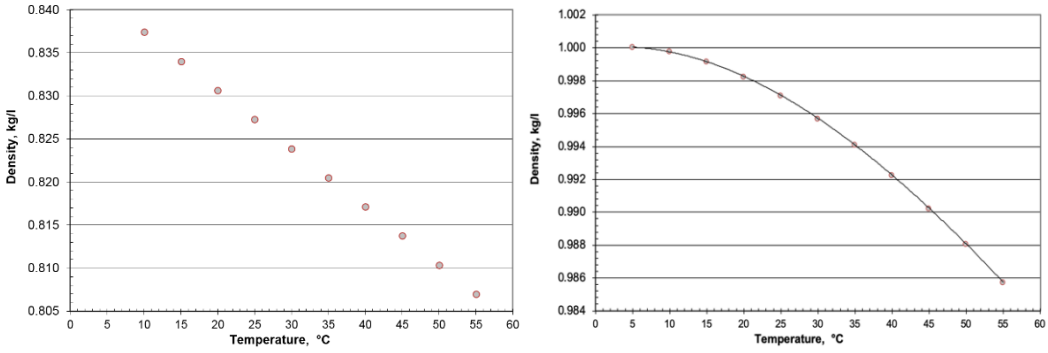

a) b)

Figure 4-3 Fluid density response with respect to temperature. Derived from samples of test fluid used during testing a) Test 1 (Gas Oil), b) Test 7 (Water)

4.2.1.3 Indicated Fluid Temperature Error

The fluid temperature as determined by both test and reference Coriolis meters is depicted in Figure 4-4. Noting the reference conditions described above, there is a clear trend associated with the test meter ambient air heating pattern and the temperatures reported from both meters, with the test meter showing a drift of 6.5°C and 2.5°C for gas oil and water respectively. The reference meter for both tests reported temperature increases of 2.5°C and 0.8°C, which corresponded to the actual fluid temperature (Figure 4-2).

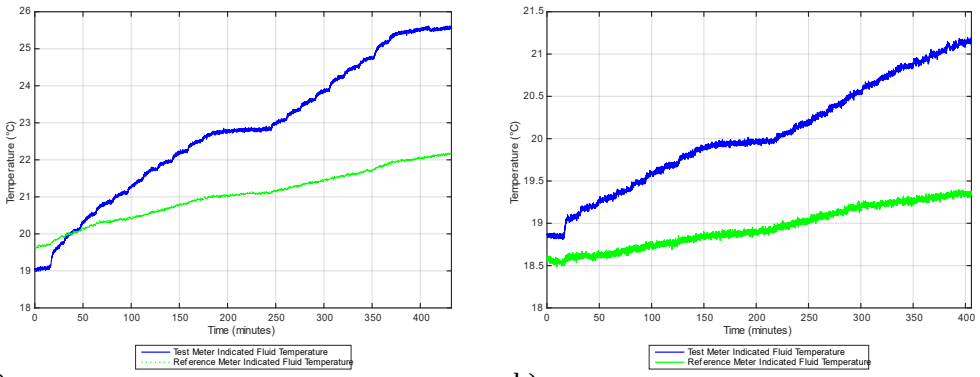

a) b)

Figure 4-4 Test and reference meter indicated fluid temperature output during testing a) Test 1 (Gas Oil), b) Test 7 (Water)

Figure 4-5 details the error in the test meter temperature value with respect to reference the fluid temperature probe. At the maximum ambient temperatures tested, absolute errors of 4.1°C and 2.1°C were present for gas oil and water respectively (noting an initial absolute error offset of 0.6°C in test 7).

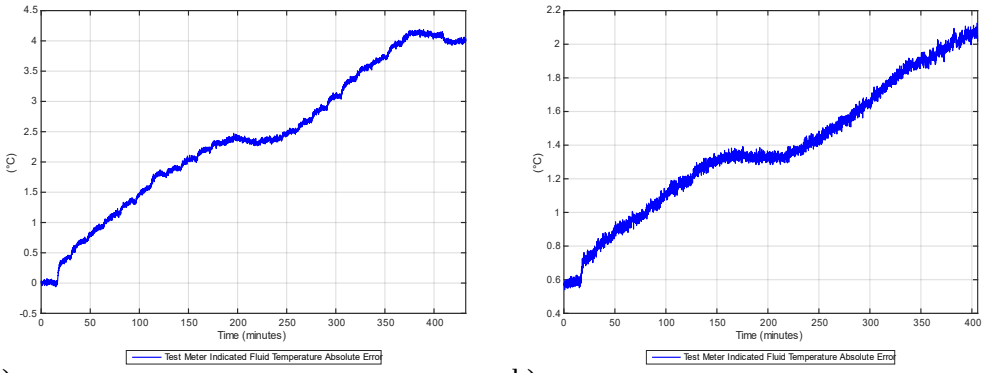

a) b)

Figure 4-5 Test meter fluid temperature measurement absolute error with respect to facility reference RTD a) Test 1 (Gas Oil), b) Test 7 (Water)

Figure 4-6 shows that, while the reference meter contained an absolute temperature error offset of ~0.65°C and ~0.28°C in gas oil and water respectively with respect to the true temperature value, the error remained consistent throughout testing and therefore is in contrast to the trend induced by a changing ambient temperature which was observed in the test meter (Figure 4-5).

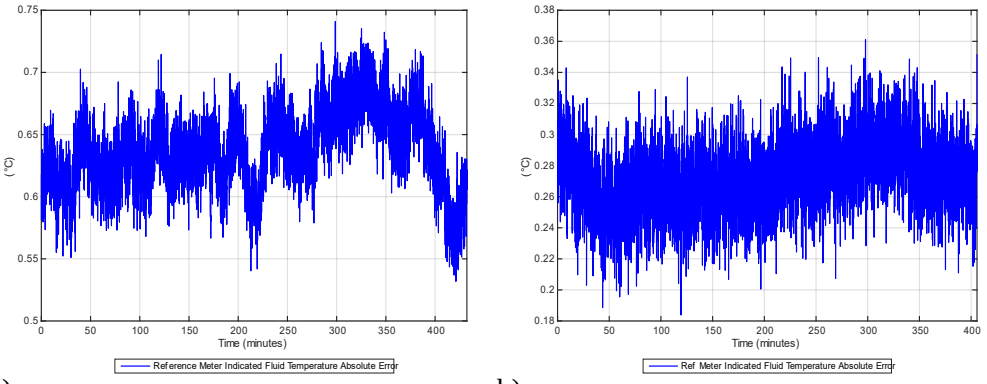

a) b)

Figure 4-6 Reference meter fluid temperature measurement absolute error with respect to facility reference RTD a) Test 1 (Gas Oil), b) Test 7 (Water)

4.2.1.4 Calculated Fluid Density Error

The test and reference meter fluid density calculated values during testing is shown in figure 4-7. There is a clear correlation present in both datasets with respect to the stepped increases in ambient air temperature and the test meter density output when one considers the manufacturer's stated uncertainty is ±0.5 kg/m^3.

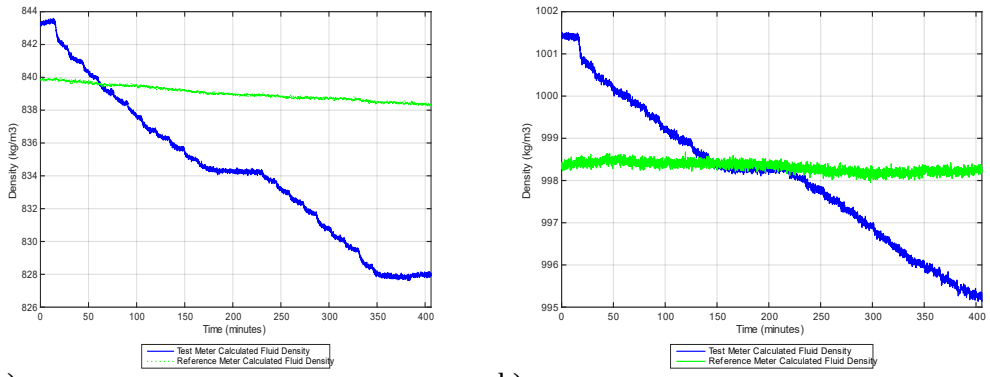

Figure 4-7 Test and reference fluid density calculation output a) Test 1 (Gas Oil), b) Test 7 (Water)

Figure 4-8 shows that errors of -1.7% and -0.6% were present at the maximum ambient air temperatures tested in gas oil and water respectively with respect to NEL's fluid property sample analysis data (Figure 4-3).

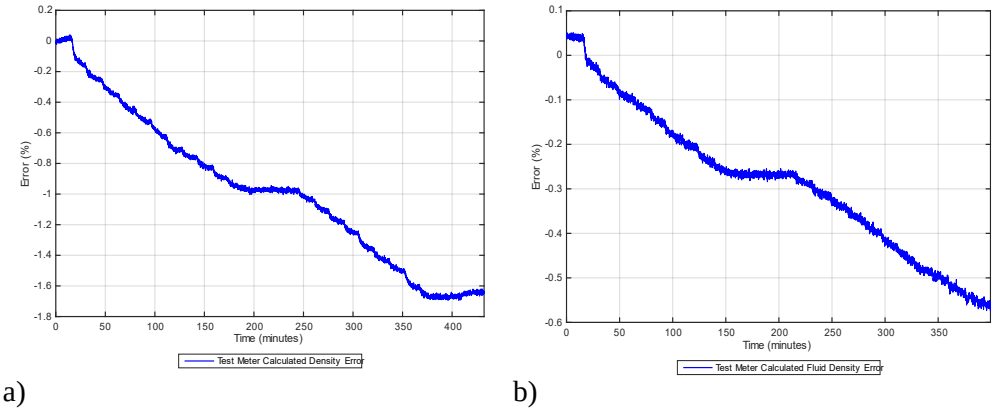

Figure 4-8 Test meter fluid density error a) Test 1 (Gas Oil), b) Test 7 (Water)

Figure 4-9 shows that the reference meter contained errors of +0.04 to 0.01% and +0.01 to -0.04% for water and gas oil respectively and therefore indicates that the drift in reported density from the test meter (Figures 4-7 and 4-8) was induced by the ambient air conditions local to the test meter and not a result of any real fluid property variations.

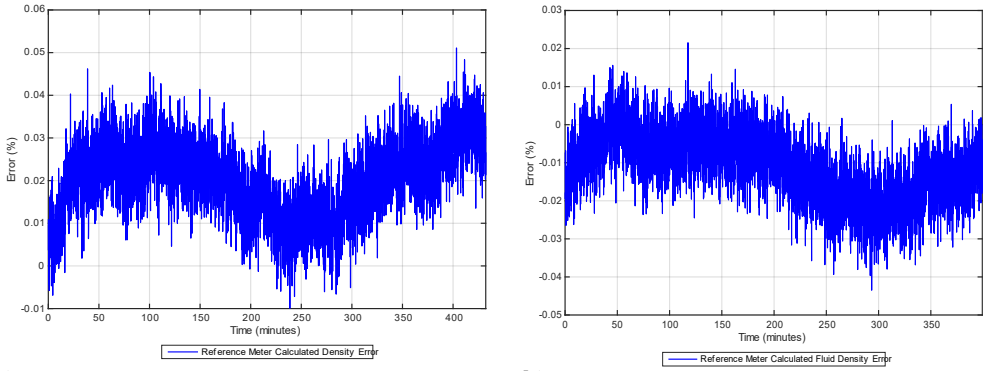

a) b)

Figure 4-9 Reference meter fluid density error a) Test 1 (Gas Oil), b) Test 7 (Water)

4.2.1.5 Mass Flow

While this thesis' focus is with respect to the density calculation, for interest Figure 4-10 shows the mass flow rate error present between the test meter and reference meter during both tests with trends increase from +0.15% to -0.1% for gas oil and 0% to +0.25% for water.

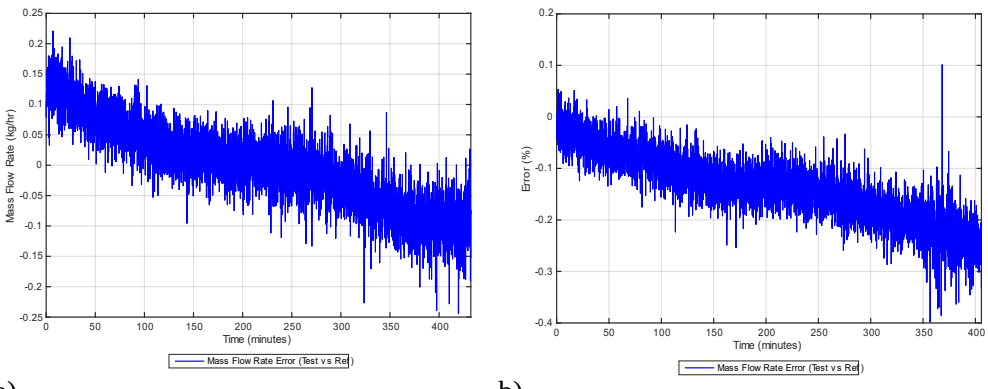

a) b)

Figure 4-10 Test meter error with respect to reference meter a) Test 1 (Gas Oil), b) Test 7 (Water)

A trend with a comparable pattern to the oven air temperature was observed during both tests 1 and 7. This is not unexpected and is an unintentional result of the gradual heat exchange between the oven air, test meter and fluid over the course of the test (Figure 4-2 -'Actual Fluid Temperature' trend) altering the fluid density and viscosity and therefore altering the mass flow rate potential in the system.

4.2.2 Statistical analysis

A Pearson test (Defined in Section 3.7, Equation 19) was used to evaluate the correlation between the individual process parameters. Figure 4-11 details the determined correlation coefficients with respect to the oven ambient air temperature as the primary variable during test 1 (gas oil). The variables presented are defined in table 4-3.

Table 4-3 Definition of test facility and meter generated process values assessed for correlation with test variables

Process Variable	Description
Centre T/C	Meter casing thermocouple. Centre position (Figure 4-1).
Delta T	Meter generated 'diagnostic' value output over modbus. Value used by transmitter to determine mass flow rate due to Coriolis effect at inlet and outlet sensors.
Drive Gain	Meter generated 'diagnostic' value output over modbus. Power requirements to maintain tube oscillation.
Inlet T/C 1	Meter casing thermocouple. Meter inlet position 1 (Figure 4-1).
Inlet T/C 2	Meter casing thermocouple. Meter inlet position 2 (Figure 4-1).
Left Pickoff Amplitude	Meter generated 'diagnostic' value output over modbus. Coriolis phase shift sensor signal amplitude.
Mass Flow Rate	Mass flow rate determined and output by meter.
Meter Density	Fluid density determined and output by meter.
Meter Density Error	Based on % error calculated from Meter Density value and true density determined from fluid sampling process.
Meter Temperature	Fluid temperature determined and output by meter.
Meter Temperature Error	Based on absolute error calculated from Meter Temperature value and true fluid temperature determined from test facility 'Middle' PRT probe.

Process Variable	Description
Outlet T/C 1	Meter casing thermocouple. Meter outlet position 1 (Figure 4-1).
Outlet T/C 2	Meter casing thermocouple. Meter outlet position 2 (Figure 4-1).
Pressure U/S	Upstream pressure reported from test facility pressure transducer.
Pressure D/S	Downstream pressure reported from test facility pressure transducer.
Raw Tube Frequency	Meter generated 'diagnostic' value output over modbus. Live tube frequency value output by meter transmitter.
Right Pickoff Amplitude	Meter generated 'diagnostic' value output over modbus. Coriolis phase shift sensor signal amplitude.
Room Temperature	Room temperature local to reference meter reported by facility K-type thermocouple.
Temperature U/S	Upstream fluid temperature determined from test facility PRT
Temperature D/S	Downstream fluid temperature determined from test facility PRT.
Temperature Middle	Test and reference meter actual fluid temperature determined from test facility PRT
Tube Period	Meter generated 'diagnostic' value output over modbus. Live tube period value output by meter transmitter.
Volumetric Flow Rate	Mass flow rate determined and output by meter.

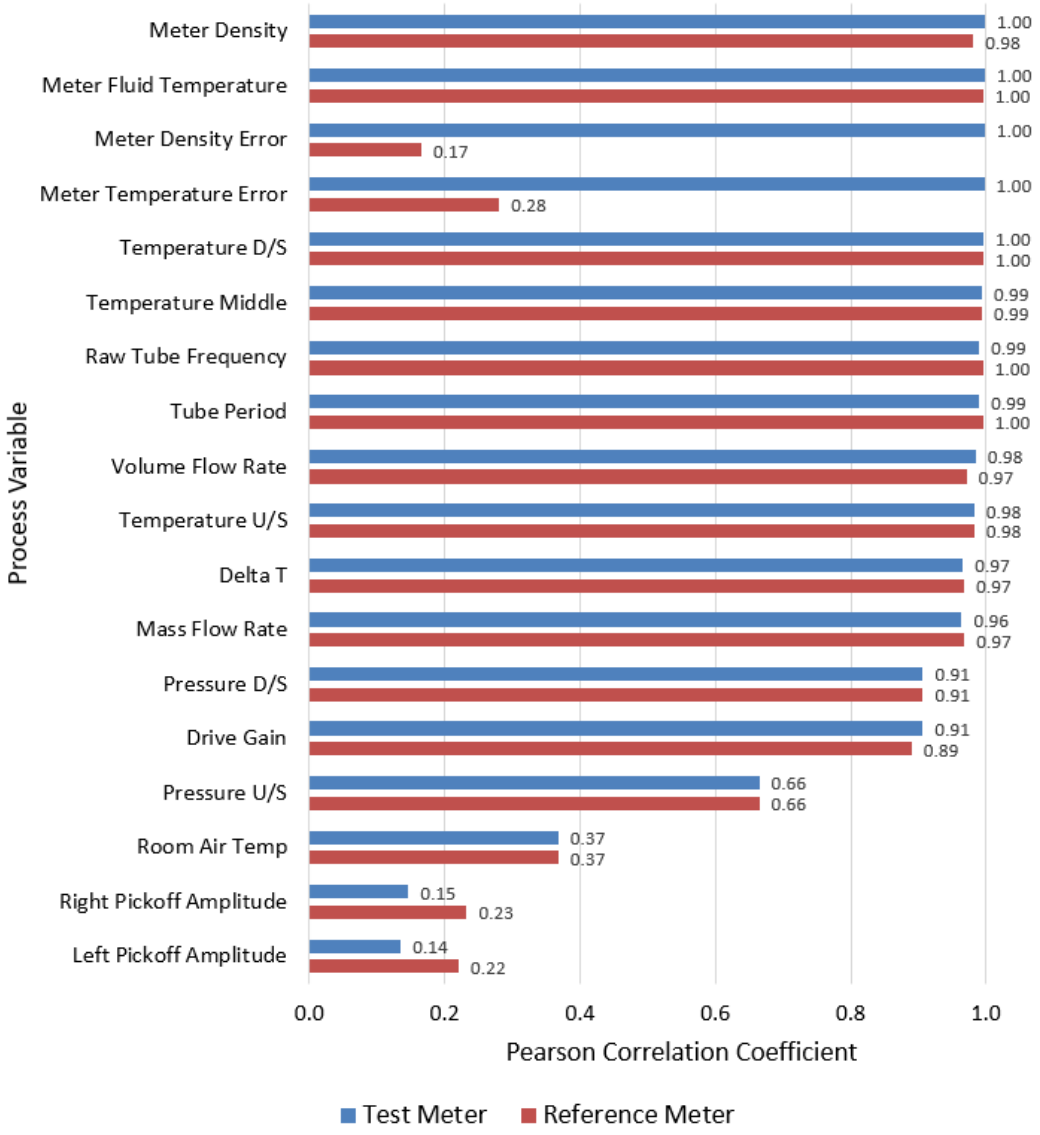

Figure 4-11 Manufacturer A - Test 1 Pearson correlation coefficients for both test and reference meter diagnostic values and facility reference instrumentation values. Coefficients represent correlation with oven air temperature.

The comparison of the 'meter density error' and 'meter temperature error' Pearson coefficients between the reference and test meter showed both meters to have significantly contrasting correlation values. Confirming the experimental observations discussed in section 4.2.1.

The left and right pickoff amplitudes are shown to have the lowest correlation coefficients. Since both parameters are responsible for detecting the phase shift used for mass flow rate calculation, this validates the lesser test meter errors observed in this process parameter during testing and discussed in section 4.2.1.5. Furthermore, the comparable Pearson coefficients between the test and reference meter for mass flow

rate confirm that, while the oven air temperature affected the reported flow rate by altering the actual fluid temperature and hence fluid properties to a minimal extent, there was no difference to the extent of the affects between the meters, hence air temperature does did not induce significant mass flow measurement errors.

The overall saturation of highly correlated Pearson coefficients did not give an indication of the individual parameter importance with respect to the errors measured. Therefore, further statistical analysis was performed using a covariance test (defined in Section 3.7, Equation 20). Figure 4-12 summarises the covariance test results with respect to oven air temperature as the primary variable.

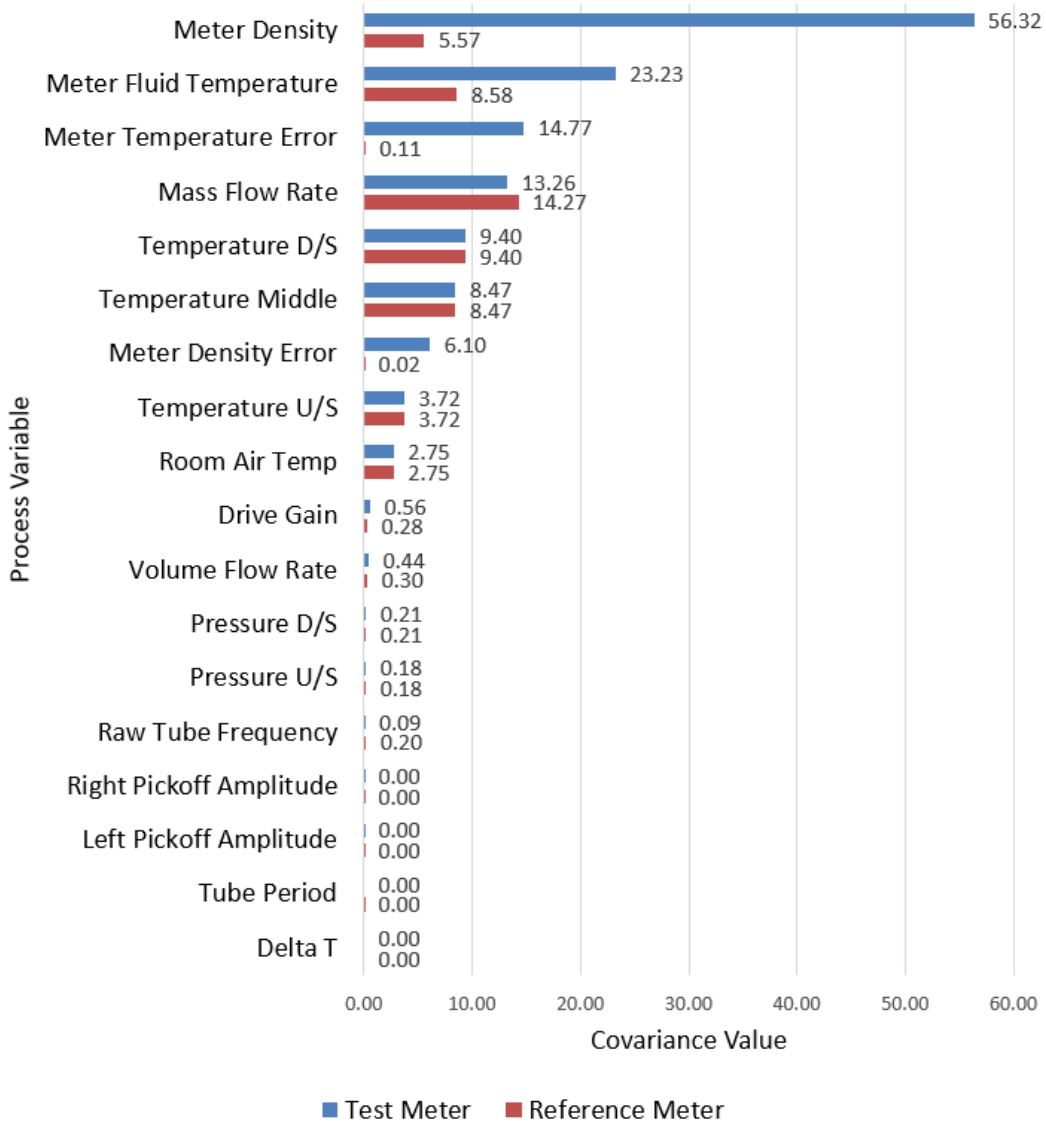

Figure 4-12 Manufacturer A - Test 1 covariance values for both test and reference meter diagnostic values and facility reference instrumentation values. Values represent the impact of oven air temperature on individual process parameters.

The covariance test confirms the observations discussed in section 4.2.1 and further highlights the test meter's potential for error in fluid temperature and density reporting due to a change in surrounding air temperature. 'Meter Density', 'Meter Fluid Temperature', 'Meter Fluid Temperature Error' and 'Meter Density Error' were shown to

have high covariance as well as having the greatest difference between the reference and test meters. It is interesting to note that raw tube frequency was shown to have low covariance. Considering this parameter is used for calculating fluid density, this was an unexpected result. It is known from experience that manufacturers compensate tube frequency values internally and may only output temperature corrected representations of the value. With no access to manufacturer algorithms for Manufacturer A, it cannot be further clarified if this was the cause of low covariance in this instance. The covariance values for multiple parameters associated with mass flow rate calculation and tube oscillation control are comparatively low (drive gain, pickoff amplitude) further confirming the observations of 4.2.1.5.

Further analysis with respect to fluid property dependency was carried out via further covariance testing using the data logged during test 7. Figure 4-13 compares the individual process parameter dependencies with respect to ambient air temperature for gas oil and water.

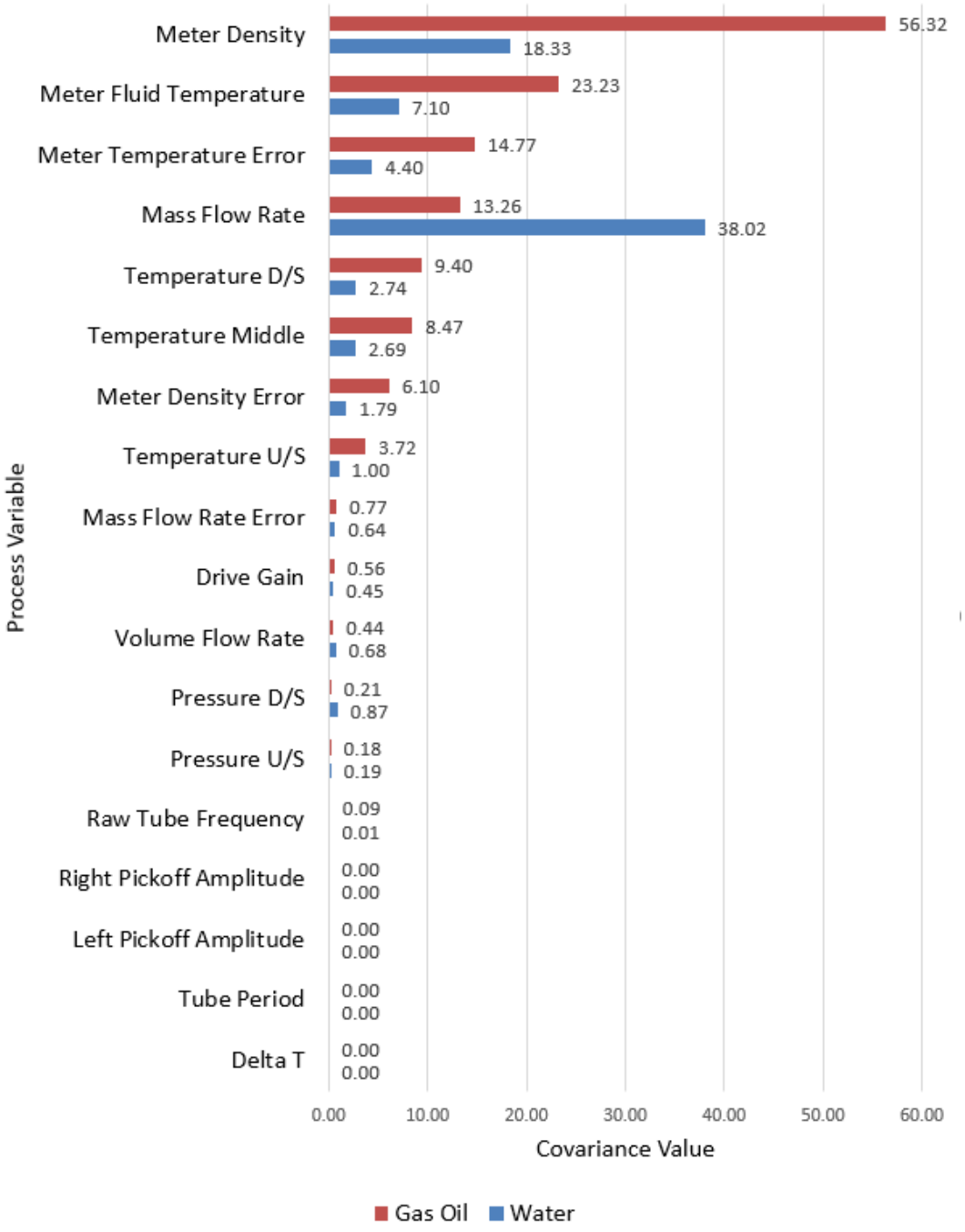

Figure 4-13 Manufacturer A - Test 1 and Test 7 covariance values for the test meter diagnostic values and facility reference instrumentation values. Values highlight the impact of differing fluid properties with respect to the changing oven air temperature.

While test meter fluid temperature, meter temperature error, density and density error were shown to have the highest covariances for both fluids, the covariance test further validates the increased errors observed during experimentation when gas oil was used as the test medium over water. This indicates a fluid property dependency with respect to meter accuracy where all other variables remain constant. It is known that

Manufacturer A validates their products using a water flow facility. It is therefore probable, based on these observations, that the effectiveness of the temperature compensation algorithms utilised by Manufacturer A rely on process conditions similar to those used during device development and factory calibration.

4.2.3 Mass Flow Fluctuation at Elevated Air Temperatures

This test was performed with Gas Oil present as an additional investigation after test 6 was completed and before the facility fluid was switched to water for the commencement of test 7. The purpose of this test was to observe the response of the test meter temperature and density output errors with respect to sudden changes in mass flow at a constant elevated ambient air temperature.

4.2.3.1 Reference Conditions

Figure 4-14 details the reference conditions during the fluctuating flow rate test. After an initial baseline run between 0 and 60 minutes, where both the reference and test meter ambient air temperature were equal, the setpoint for air temperature within the oven was set to 50^{o}C. The facility was then allowed to reach thermal equilibrium over 215 minutes. Once achieved, the flow rate of liquid passing through the meter was reduced by 50% at 275 mins from a value of 130 kg/hr to 65 kg/hr while all other variables were controlled to remain constant.

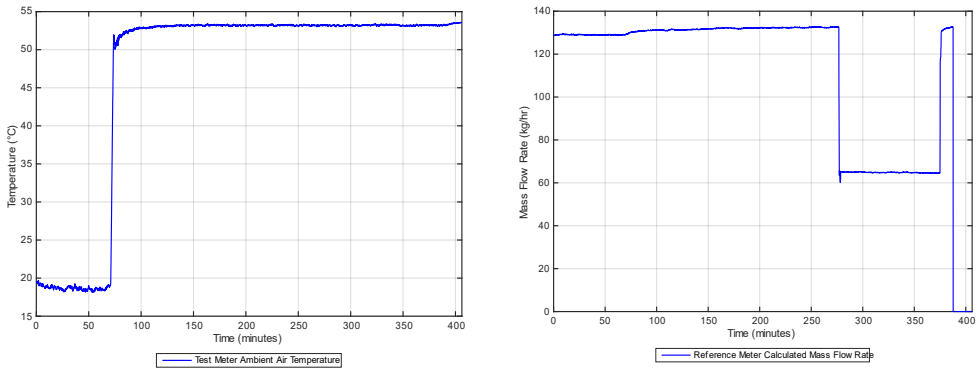

a) b)

Figure 4-14 a) Test meter air temperature - sudden increase from 18°C to 53°C then left to settle b) Mass flow rate Initial value of 130 kg/hr, reduced 65 kg/hr then returned to 130 kg/hr before complete stop

4.2.3.2 Indicated Fluid Temperature Error

At 53°C (test meter ambient air temperature), an absolute error of 4°C was observed on the test meter fluid temperature indication. The reduction of flow rate at 270 minutes caused the error to increase to a value of 5°C. It should be noted that during this time there was also an increase in actual fluid temperature (19.7 – 20.2°C). When the mass flow rate was returned to 100% at 375 minutes, the test meter indicated fluid temperature absolute error returned to 4°C at which point the actual fluid temperature is also shown to return to 19.7°C. When flow was stopped at 380 minutes, Figure 4-15 shows an immediate increase in indicated fluid temperature from the test meter inside the enclosure and begins to converge on the ambient air temperature surrounding the test meter within 30 minutes of stopping the flow rate.

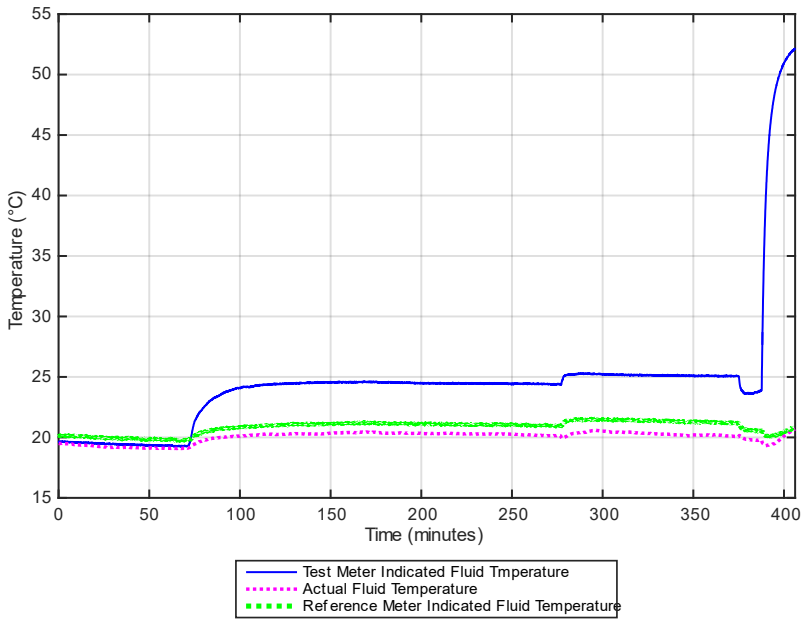

Figure 4-15 Response of test meter and reference meter indicated fluid temperature vs actual fluid temperature due to sudden air temperture increase and fluid flow changes

Figure 4-16 shows the corresponding meter error for both tests with respect to the true fluid temperature.

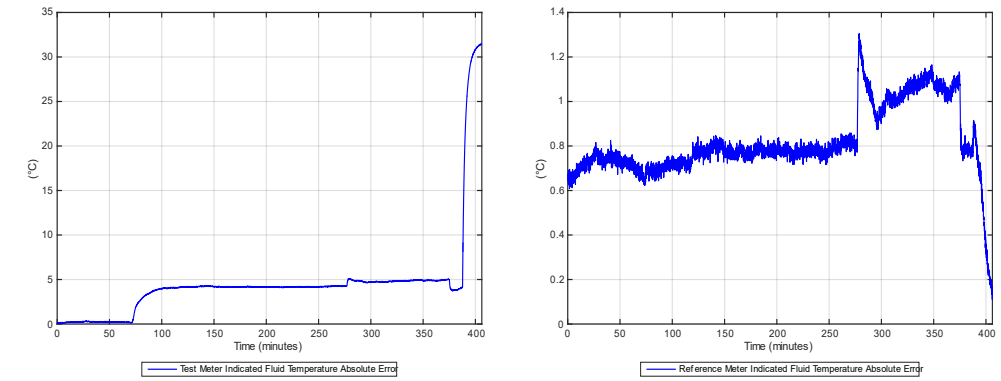

a) b)

Figure 4-16 a) Test meter indicated fluid temperature error b) Reference meter indicated fluid temperature error

4.2.3.3 Meter Casing Temperature Profile

The effects observed in 4.2.2.2 were further analysed by cross referencing with the data logged from the casing thermocouples (Figure 4-1). Figure 4-17 shows the temperature profile of the meter casing as well as the thermal interactions of both the fluid and ambient air and the different sensor locations.

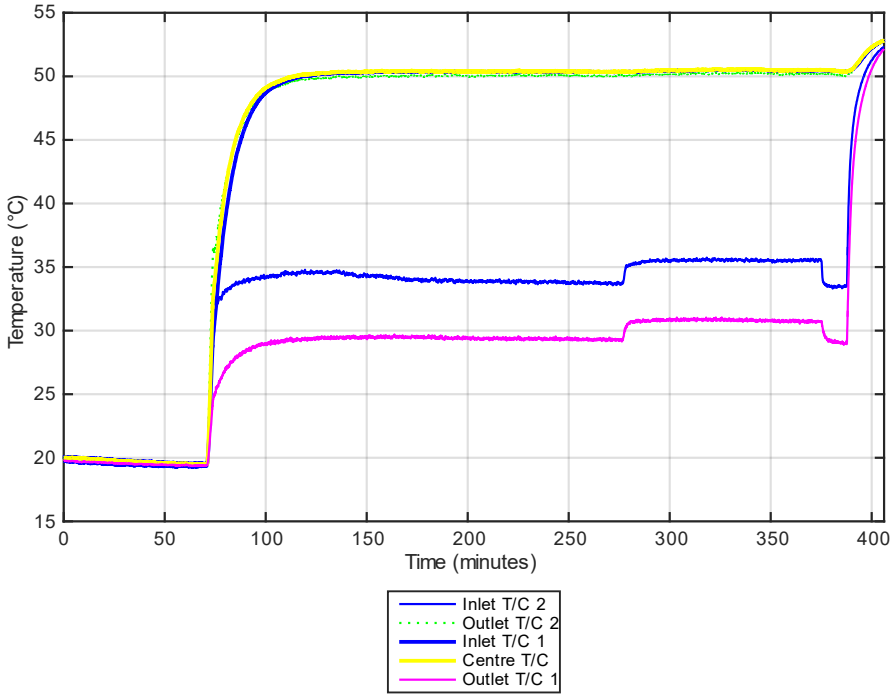

Figure 4-17 Measurements from additional thermocouples attached to meter casing, highlighting reduced temperatures at inlet and output locations due to internal cooling of meter body from fluid. Legend corresponds to thermocouple (T/C) locations annotated on Figure 4-1 and noted in table 3-2.

The thermocouples located at locations Inlet 2, Centre and Outlet 2 follow the trend and value of the ambient air temperature to 53°C. However, while the thermocouples at locations Inlet 1 and Outlet 1 demonstrated an increase in temperature which trended with the ambient air, the final value was limited to 35°C. When the flow rate was reduced, the same trend as observed in Figure 4-15 is observed but at elevated temperatures consistent with the meter casing temperatures at those locations. Due to the reduced metal mass at the weld points between the flow tubes and the pipe flanges, as well as a reduction in meter casing mass at Inlet 1 and Outlet 1 (Figure 4-1), these locations are effectively being cooled by the fluid (22°C) passing through the flow tubes.

4.2.3.4 Calculated Fluid Density Error

The corresponding response of the test meter density value is shown in Figures 4-18 and 4-19. An error of -1.5% was observed at steady state conditions (elevated ambient temperature). When the flow rate was reduced a further drift of 2 kg/m^3 was observed resulting in an error of -1.7%. When the flow rate was returned to 130 kg/hr the density recovered to an error of -1.45%. When the flow was stopped, the test meter density error is shown to increase to -3.3% (Figure-19a).

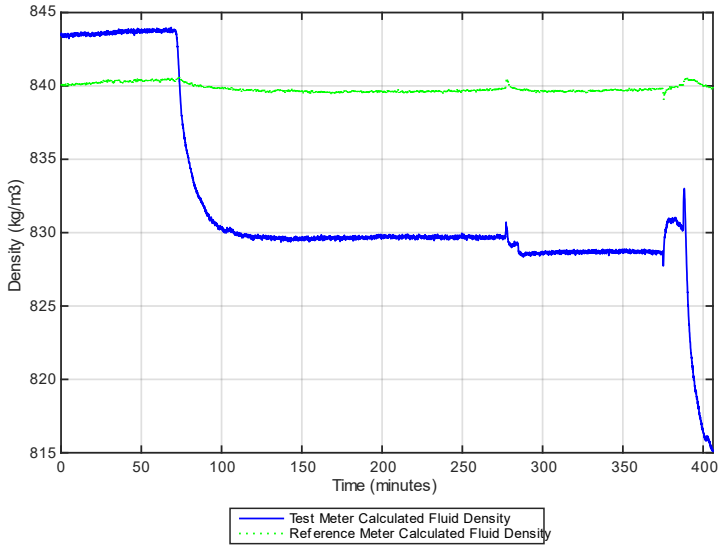

Figure 4-18 Test and reference meter fluid density calculation output during test

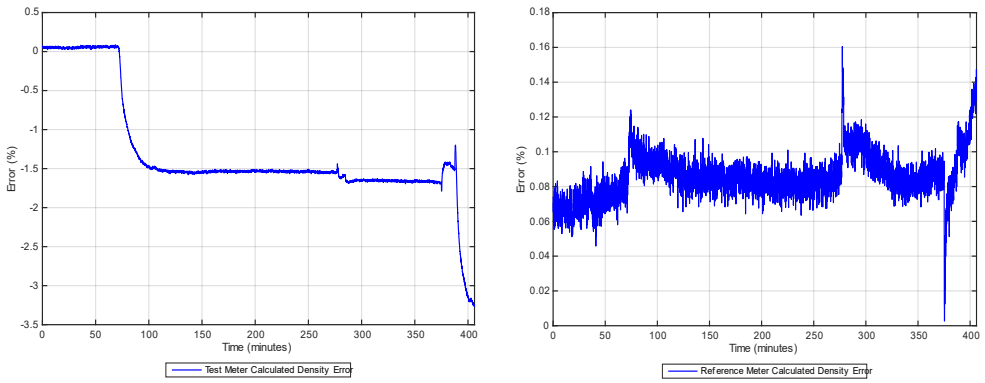

a) b)

Figure 4-19 a) Test meter fluid density error b) Reference meter fluid density error

It is noteworthy that the large errors observed in the test meter temperature and density outputs due to no flow at high ambient air temperatures (380 mins on Figures 4-16 and 4-19) validates this research programme's experimental methods. By ensuring a constant flow rate for all tests, we have ensured that the errors observed are representative of live flowing process conditions. The data in this section has demonstrated that static fluid within the meter will simply absorb heat from the meter body and in doing so, the test meter effectively becomes an isolated fluid container, which will ultimately reach thermal equilibrium.

4.2.4 Statistical analysis

The covariance test results for the test and reference meter process values (defined in table 4-3), with respect to mass flow rate as the primary variable are summarised below in Figure 4-20.

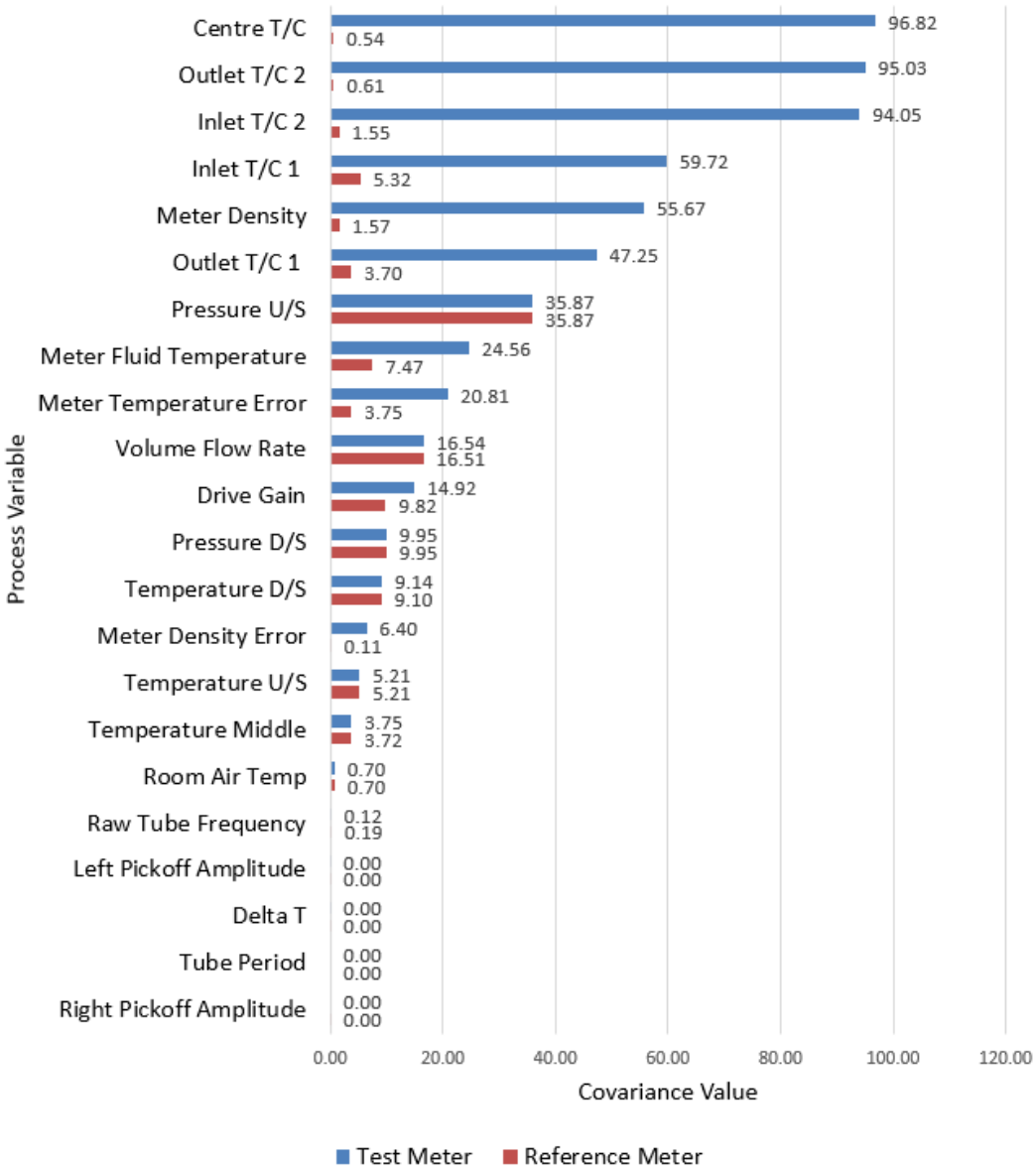

Figure 4-20 Manufacturer A - Covariance values for the test and reference meter diagnostic variables, facility reference instrumentation and meter body thermocouples. Values highlight the impact of a changing fluid flow rate in combination with a high external air/process fluid temperature differential.

The influence of varying the mass flow at elevated air/fluid temperature differentials on test meter's fluid temperature and density reporting capabilities are clear from the covariance data when compared against the corresponding reference meter and therefore validates the errors observed during experimentation (section 4.2.3). Both the inlet and outlet thermocouples (T/C 1) are confirmed to be less influenced by the mass flow rate changes as discussed in 4.2.3.3.

4.2.5 Additional Manufacturer A Results Highlights

The results from the individual test points are detailed in Table 4-4.

Table 4-4 Manufacturer A individual test results summary

Test Point No	Maximum Indicated Fluid Temperature Error (Test) (°C)	Maximum Calculated Fluid Density Error (Test) (%)	Maximum Indicated Fluid Temperature Error (Ref) (°C)	Maximum Calculated Fluid Density Error (Ref) (%)	Mass Flow Error (%)
1	+4.19	-1.69	+0.74	+0.04	+0.22
2	+4.43	-1.75	+0.75	+0.11	+0.18
3	+4.45	-1.82	+0.78	+0.12	+0.29
4	+5.63	-1.38	+0.36	-0.38	-0.26
5	+7.41	-1.33	+0.60	-0.43	+0.39
6	+5.62	-1.30	+0.29	-0.33	+0.36
7	+2.12	-0.57	+0.36	-0.04	+0.40
8	+2.15	-0.59	+0.35	+0.06	+0.32
9	+2.54	-0.57	+0.38	+0.06	+0.30
10	+2.07	-0.54	+0.34	+0.06	+0.32
11	+1.73	-0.42	+0.70	-0.21	-0.17
12	+1.82	-0.47	+0.71	-0.21	-0.18
13	+1.86	-0.49	+0.66	-0.21	-0.17
14	+1.99	-0.41	+0.70	-0.21	-0.15

It was observed that increasing the rate of change in test meter air temperature exaggerates the effect described in section 4.1. For example, in test 3 the full extent of error per temperature increment was not observed as thermal equilibrium was not reached until the final air temperature of 60 was reached. However, it was observed for all tests that the rate of change does not affect the final error (steady state) observed once thermal equilibrium has been achieved.

By swapping meter positions in test points 4 – 6 it was confirmed that, while the specific values of error changed due to differing baseline offsets, the overall trend and extent of

error was common to both meters and as such it is logical to extrapolate that this is a general design fault in manufacturer A's density calculation mechanism.

It was also observed that changing between fluids of differing specific heat capacities had an effect on the error for both the indicated temperature and fluid density process values.

4.3 Manufacturer A Discussion and Conclusions

For both indicated fluid temperature and calculated fluid density, the data output from the test meter showed a clear correlation with the heating pattern of its surrounding ambient air. When the errors, Pearson correlations and covariance values of said parameters are compared across the two fluids tested, there is a notable difference with respect to the extent of the values. The test meter was shown to produce lesser errors in water than in gas oil, highlighting a fluid property (specific heat capacity) dependency with respect to meter performance.

The density responses observed are arguably unexpected if one presumes that the manufacturers of the device utilise the meter's indicated fluid temperature process value to calculate fluid density combined with calibration coefficients that are derived with water as a baseline fluid. However, the extent of the associated errors cannot be explained by a linear correlation with the error in fluid temperature measurement. For example, in test 1, the test Coriolis meter has determined that at 400 minutes (ambient air at 60°C), the fluid temperature has increased by 6.5°C. The reference fluid properties show that such a change in fluid temperature should only cause a decrease in fluid density of 4 kg/m^3. The meter however calculates a decrease of 15 kg/m^3. Since the trials were conducted with no access to manufacturer patents or compensation algorithms, no further conclusion can be drawn as to the nature of the additional error present in the data without further access to proprietary information.

When observed in isolation, the mass flow rate process value did not show a clear correlation with ambient temperature. The gradual increase in fluid flow rate observed during testing can be attributed to the increase in real fluid temperature and the corresponding effect on the test fluid properties.

Varying the rate of air temperature change does not affect the final value steady state error induced at the maximum air temperature tested.

By reducing the flow rate while at stable and elevated ambient air temperatures with respect to the fluid temperature it was shown that the extent of error was further increased. However, by reducing the flow rate, the fluid's residency time within the meter was increased, therefore the results show that the fluid temperature increased due to the fact the meter is effectively acting as a heat exchanger. Stopping fluid flow showed an immediate increase in errors highlighting that, in order to obtain meaningful data in this field of study, it is important to minimise the fluid residency time within the test meter so as to reduce heat transfer between the meter body and fluid as well as allowing the fluid to effectively 'cool' the internals of the meter.

The results of this test programme were peer reviewed and published by the author and supervisory team [1].

4.4 Meter Manufacturer B - Flow Rate Fluctuation Results

This section describes the data resulting from the conditions of test 1 and test 2 detailed in Table 4-2. These data points are presented as a summary of the observed effects of ambient temperature on Coriolis data across two fluids of differing properties. A summary of the errors observed for tests 1 – 4 are detailed in Table 4-6 in section 4.5.5.

4.4.1 Reference Conditions

Figure 4-21 depicts the flow loop reference measurements pertaining to test meter ambient air temperature, fluid temperature and mass flow. During testing, the actual fluid temperature for Kerosene varied between 20.0°C and 22.5°C, therefore when analysing the performance of Coriolis meter outputs in the following sections, any deviations in associated process values are considered to be in error. Note that between 88 and 118 minutes the actual fluid temperature (Figure 4-21 (a)) is shown to decrease when the fluid flow is reduced by 50% (Figure 4-21 (c)).

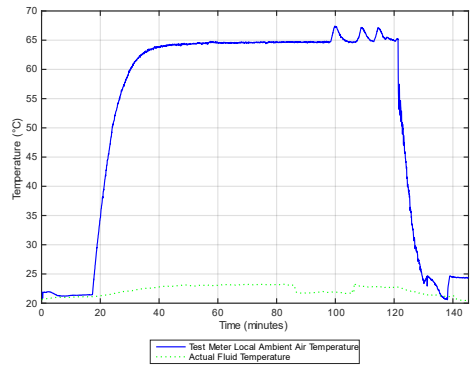

a)

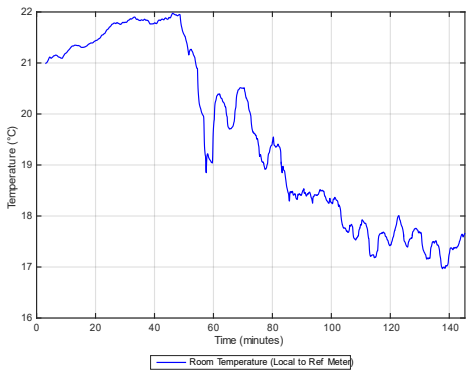

b)

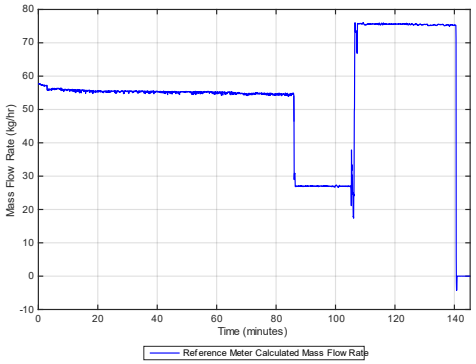

c)

Figure 4-21 Reference conditions during Test 1 a) Test meter air temperature and actual fluid temperature b) Reference meter air temperature c) Mass flow rate changes

4.4.2 Reference Fluid Properties

Figure 4-22 contains the calibration data derived from a fluid sample of the kerosene used during testing. The variation in density with respect to fluid temperature is shown across a range of 10°C - 55°C.

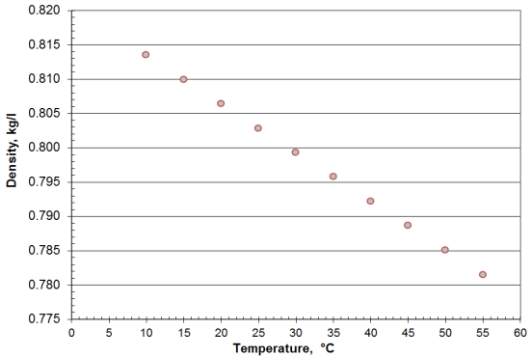

Figure 4-22 Test fluid (Kerosene) sample density response with respect to temperature.

4.4.3 Indicated Fluid Temperature Error

The fluid temperature as determined by both test and reference Coriolis meters is depicted in Figure 4-23. Noting the reference conditions detailed in 4.4.1, there is a clear correlation between the test meter ambient air temperature and resulting drift in flow meter output.

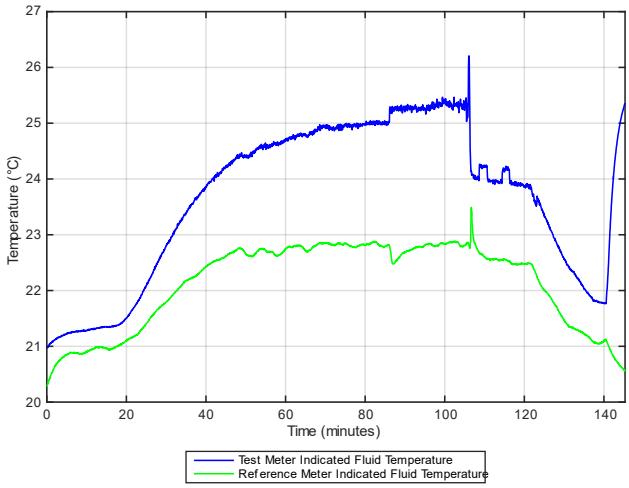

Figure 4-23 Test and reference meter indicated fluid temperature response during test 1

The reduction in fluid flow (Figure 4-21 (c)) at 85 mins induces an immediate further drift in the test meter fluid temperature value. The reference meter does not report such an increase, nor does the actual fluid temperature (Figure 4-21a). It is of particular note that the subtle fluctuations in test meter air temperature, as shown in Figure 4-21a, affects the test meter fluid temperature reading at ~107 mins and again at ~117 mins. During the rapid cooling initiated at ~125 mins, there is an immediate correlation seen in both trends.

Figure 4-24 details the absolute error in meter output with respect to the true fluid temperature as measured by the facility reference PRT. An absolute error of 1.7°C is observed at the initial flow rate. When the flow rate is reduced, the error increases to 3.5°C before reducing to 1°C when the flow rate is increased. The reference showed a ~1°C absolute error during the time period where flow was reduced.

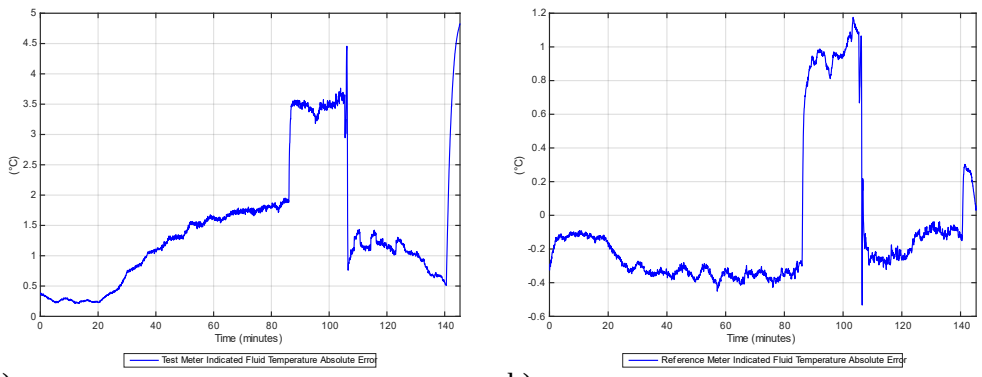

a) b)

Figure 4-24 Test a) and reference b) meter indicated fluid temperature error with respect to facility reference RTDs during test 1

4.4.4 Calculated Fluid Density Error

The test and reference meter fluid density outputs are shown in Figure 4-25. The data trends with the changes in both ambient temperature and mass flow rate. As noted in section 4.4.3, there is even a noticeable effect with respect to the minor fluctuations in air temperature between ~110 and 119 minutes.

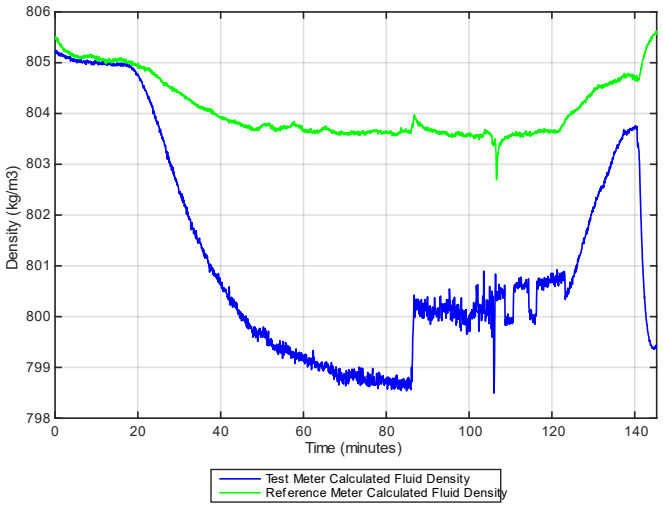

Figure 4-25 Test and reference meter calculated fluid density response to test 1 conditions

Figure 4-26 shows an error of -0.7% was present at 60°C ambient, before the reduction in mass flow. It is interesting to note that when the mass flow was reduced, causing the test meter fluid temperature value error to increase further, the fluid density does not follow the same trend and in fact recovers by +0.1%. When the flow is increased, the density recovers further to a value of -0.45% before experiencing the minor air temperature fluctuations. These experimental results contradict the manufacturer's ±1.0 kg/m^3 uncertainty claim for density measurement.

Figure 4-26 shows that the reference meter contained errors of -0.06% until the mass flow reduction, whereby an error of -0.18% was observed, reducing to -0.1% at the point of mass flow rate increase.

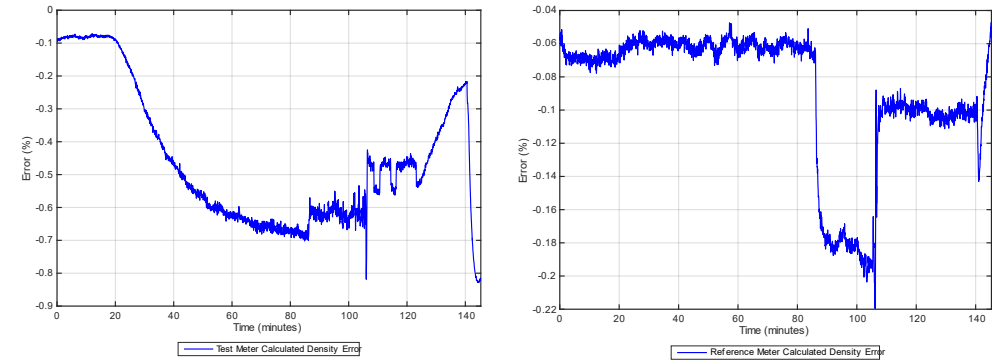

a) b)

Figure 4-26 Test and reference meter calculated fluid density error during test 1

4.4.5 Mass Flow

As with Manufacturer A, it was observed that the temperature compensations used by Manufacturer B were able to compensate for the changing ambient conditions and mass flow rate. Over the course of the test, accounting for the initial offset from the reference meter, the test meter error was shown to increase by 1% overall, with no clear correlation to the heating pattern of ambient air.

4.4.6 Covariance

The process values statistically analysed in this section are detailed below in Table 4-5.

Table 4-5 Description of meter process values statistically analysed for correlations

Process Variable	Description
Drive Gain	Meter generated 'diagnostic' value output over modbus. Power requirements to maintain tube oscillation.
Left Pickoff Amplitude	Meter generated 'diagnostic' value output over modbus. Coriolis phase shift sensor signal amplitude.
Meter Density	Fluid density determined and output by meter.
Meter Density Error	Based on % error calculated from Meter Density value and true density determined from fluid sampling process.

Process Variable	Description
Meter Temperature	Fluid temperature determined and output by meter.
Meter Temperature Error	Based on absolute error calculated from Meter Temperature value and true fluid temperature determined from test facility 'Middle' PRT probe.
Pressure U/S	Upstream pressure reported from test facility pressure transducer.
Pressure D/S	Downstream pressure reported from test facility pressure transducer.
Raw Tube Frequency	Meter generated 'diagnostic' value output over modbus. Live tube frequency value output by meter transmitter.
Right Pickoff Amplitude	Meter generated 'diagnostic' value output over modbus. Coriolis phase shift sensor signal amplitude.
Room Temperature	Room temperature local to reference meter reported by facility K-type thermocouple.
Temperature U/S	Upstream fluid temperature determined from test facility PRT
Temperature D/S	Downstream fluid temperature determined from test facility PRT.
Temperature Middle	Test and reference meter middle fluid temperature determined from test facility PRT

The covariance of the test and reference meter process values with respect to mass flow rate fluctuation is summarised in Figure 4-27.

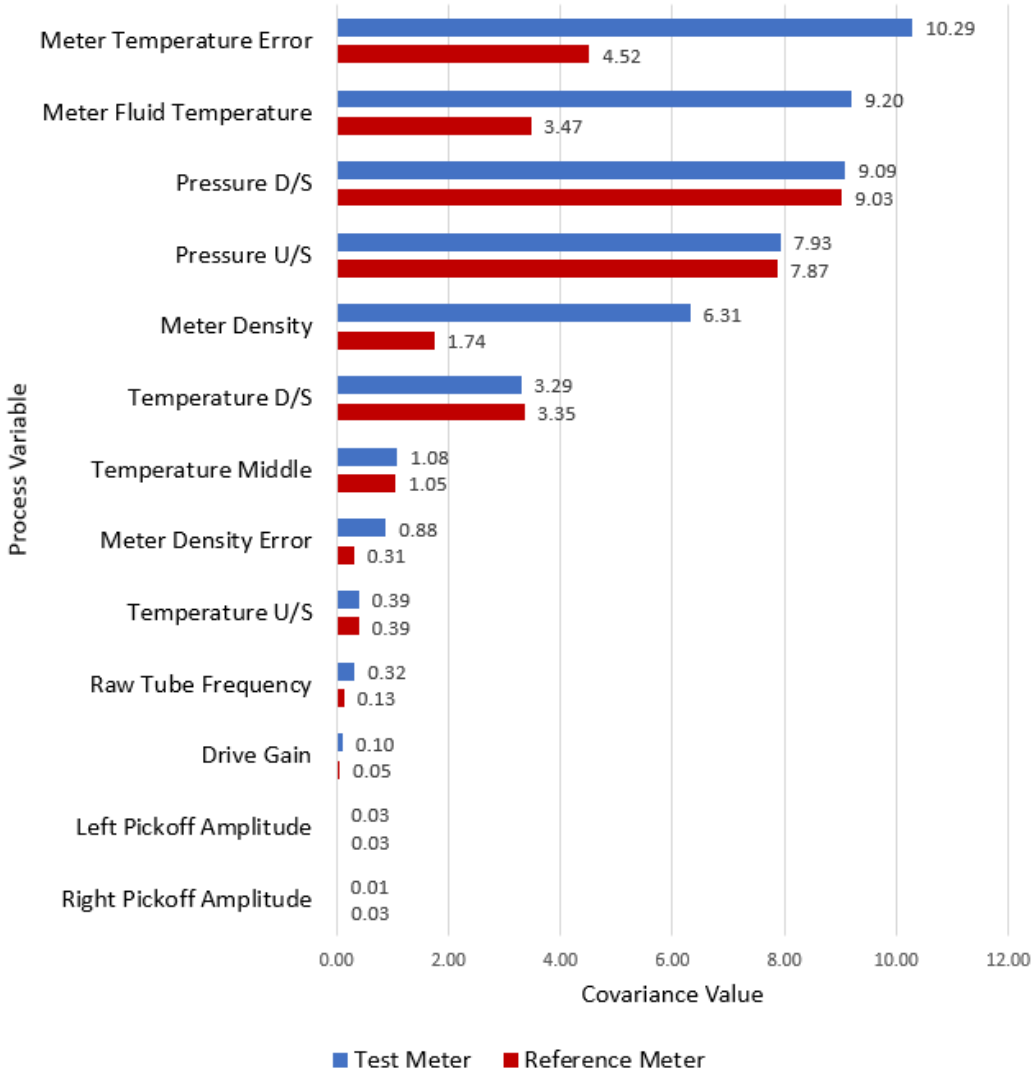

Figure 4-27 Manufacturer B - Test 1 Covariance values for the test and reference meter diagnostic variables, facility reference instrumentation. Values highlight the impact of a changing fluid flow rate in combination with a high external air/process fluid temperature differential.

Manufacturer B shows similar dependencies via the covariance test to Manufacturer A (4.2.4). In this case, however, the test meter temperature error is shown to have the greatest covariance with respect to fluid flow fluctuation at high air/fluid temperature differentials. When compared with the corresponding reference meter covariance values, meter density is shown to be the process value with the greatest divergence between the two meters.

4.5 **Manufacturer B Stepped Air Temperature Results**

4.5.1 Reference Conditions

Figure 4-28 depicts the flow loop reference measurements pertaining to test meter ambient air temperature, fluid temperature and mass flow. During testing the actual fluid temperature for Kerosene increased by 2°C. Due to the cold climate at time of testing (October 2016), the room temperature decreased from 22.5°C to 17°C, therefore the reference meter was exposed to a gradual decrease in its surrounding air temperature.

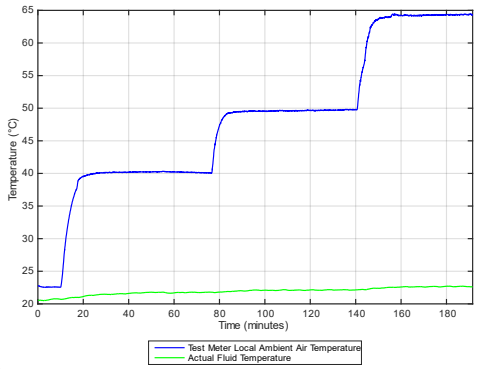

a)

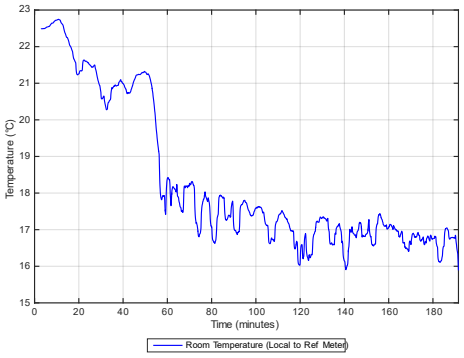

b)

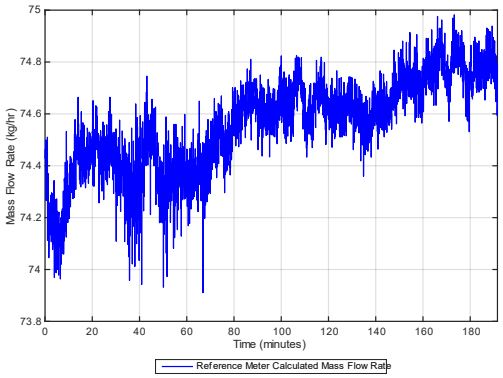

c)

Figure 4-28 Reference conditions for test 3 a) Test meter ambient air temperature and actual fluid temperature, b) Reference meter ambient air temperature c) Mass flow rate (as recorded by the reference meter)

4.5.2 Indicated Fluid Temperature Error

Figure 4-29 shows the fluid temperature as reported by the test and reference meter during testing. The test meter data demonstrates a correlation with the increases in ambient air temperature. The reference meter reported the gradual fluid temperature increase over the course of the test, however it should also be noted that there is a clear correlation with the stepped increase in the test meter air temperature, demonstrating the heat transfer between the test meter body and fluid passing through it.

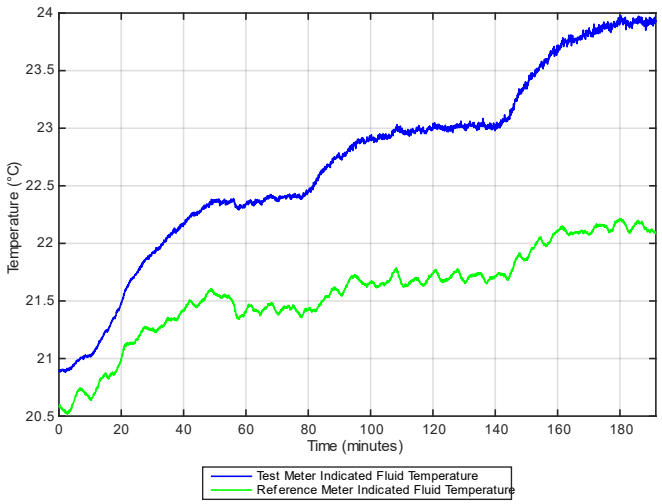

Figure 4-29 Test and reference meter indicated fluid temperature response during test 2

The test meter absolute error was observed to increase by 1°C as shown in Figure 4-30. The reference meter was shown to contain a -0.5°C absolute error by the end of testing. This trend does however correspond with the unexpected drop in room temperature (Figure 4-28b) and therefore shows the sensitivity of this meter type to less extreme temperature differentials between the fluid and surrounding air.

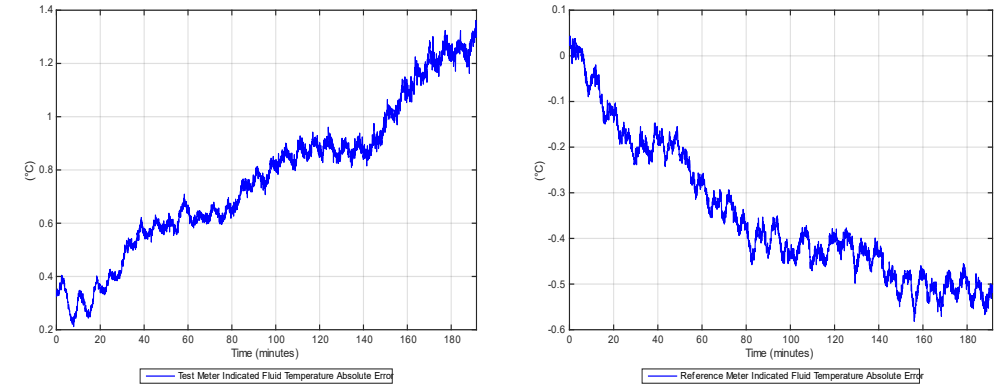

a) b)

Figure 4-30 Test meter (a) and reference meter (b) indicated fluid temperature error during test 2

4.5.3 Calculated Fluid Density Error

Figure 4-31 shows the test and reference meter density values response to the stepped increase in ambient air temperature. The test meter density value was shown to drift by 8 kg/m^3 with the reference meter density reducing by 1 kg/m^3 over the course of the test.

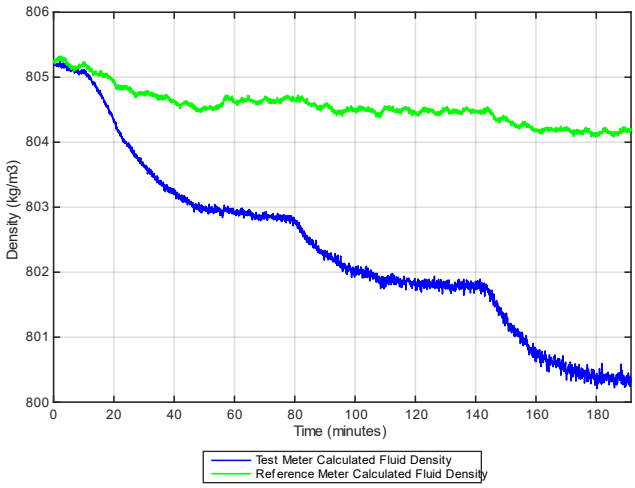

Figure 4-31 Test and reference meter calculated fluid density response during test 2

The corresponding errors with respect to known fluid properties are shown in Figure 4-32. The test meter error was observed to deviate a further -0.6% with respect to the baseline value. The reference meter error deviated a further -0.14%, with an overall trend that corresponded with the unexpected drop in room temperature (Figure 4-28b).

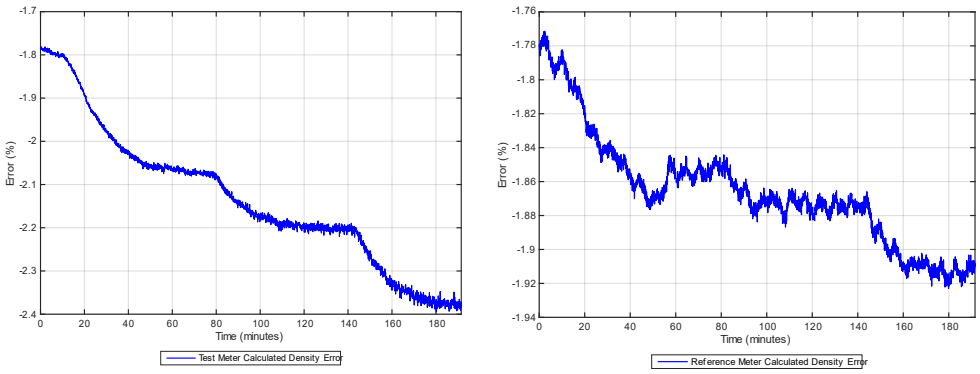

a) b)

Figure 4-32 Test and reference meter calculated density error during test 2

4.5.4 Statistical analysis

The Pearson correlation coefficients for the process values (detailed in table 4-5) observed during test 2 are summarised in Figure 4-33 with respect to oven air temperature as the primary variable.

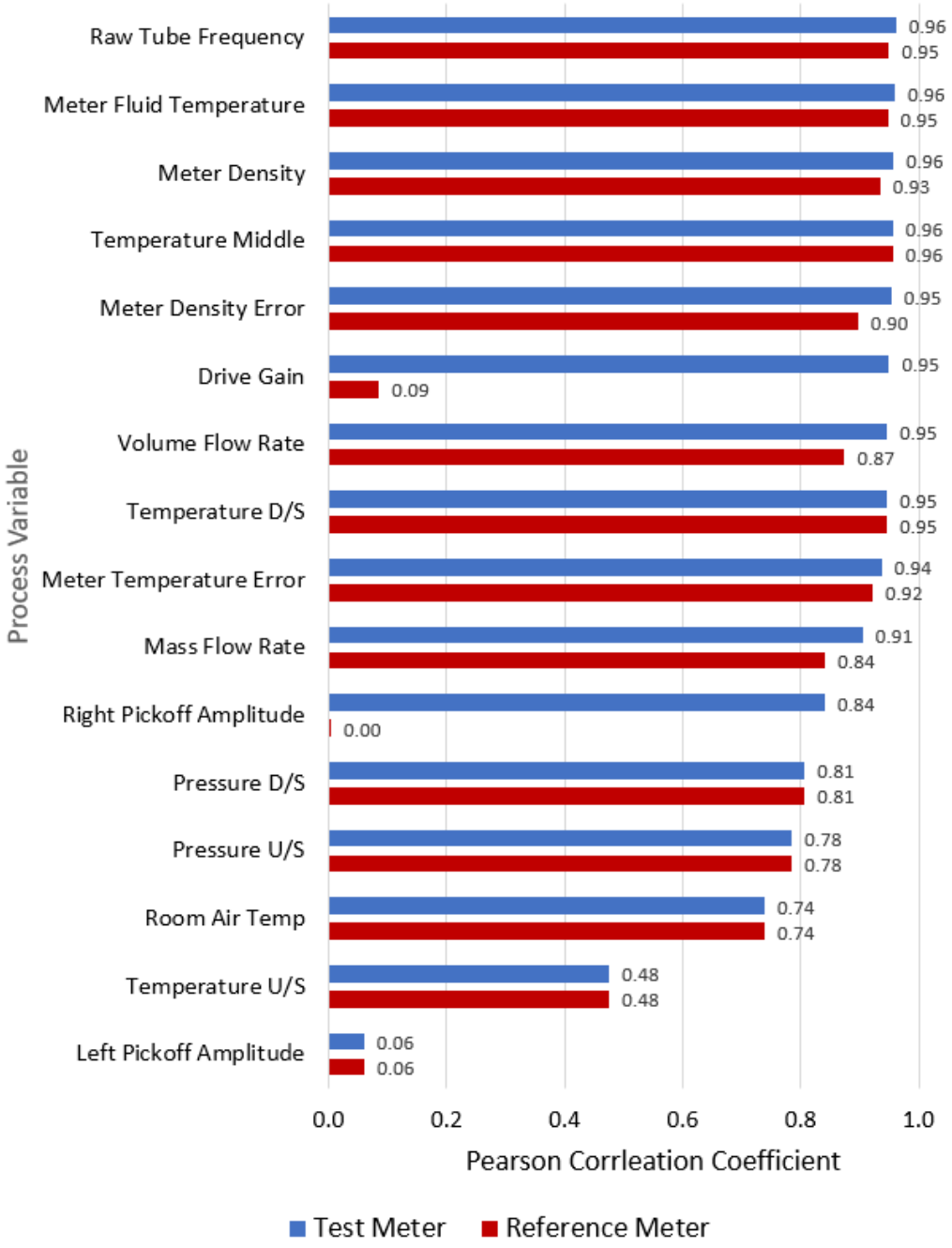

Figure 4-33 Manufacturer B - Test 2 Pearson correlation coefficients for both test and reference meter diagnostic values and facility reference instrumentation values. Coefficients represent correlation with oven air temperature.

As discussed in section 4.2.2, the coefficients associated with this experimental setup are largely saturated due to the heat transfer between the oven and fluid. However, it is noteworthy that for this particular meter the test meter's drive gain value was shown to have a high correlation (0.95) compared to that of the reference meter downstream (0.09). This is a contrasting result to that of manufacturer A as detailed in Figure 4-11. The larger size of manufacturer B's meter (1") compared to manufacturer A (0.5") combined with a difference in meter body construction materials and oscillation energy control parameters are potential explanations for this observed difference. It's also noteworthy that the right pickoff signal amplitude is shown to have a high covariance with oven air temperature whereas the corresponding left pickoff is shown to have a low covariance. This may indicate a weakness in meter construction where the right pickoff sensor may be situated in a location that is vulnerable to air temperature changes.

The corresponding covariance test results are shown in Figure 4-34.

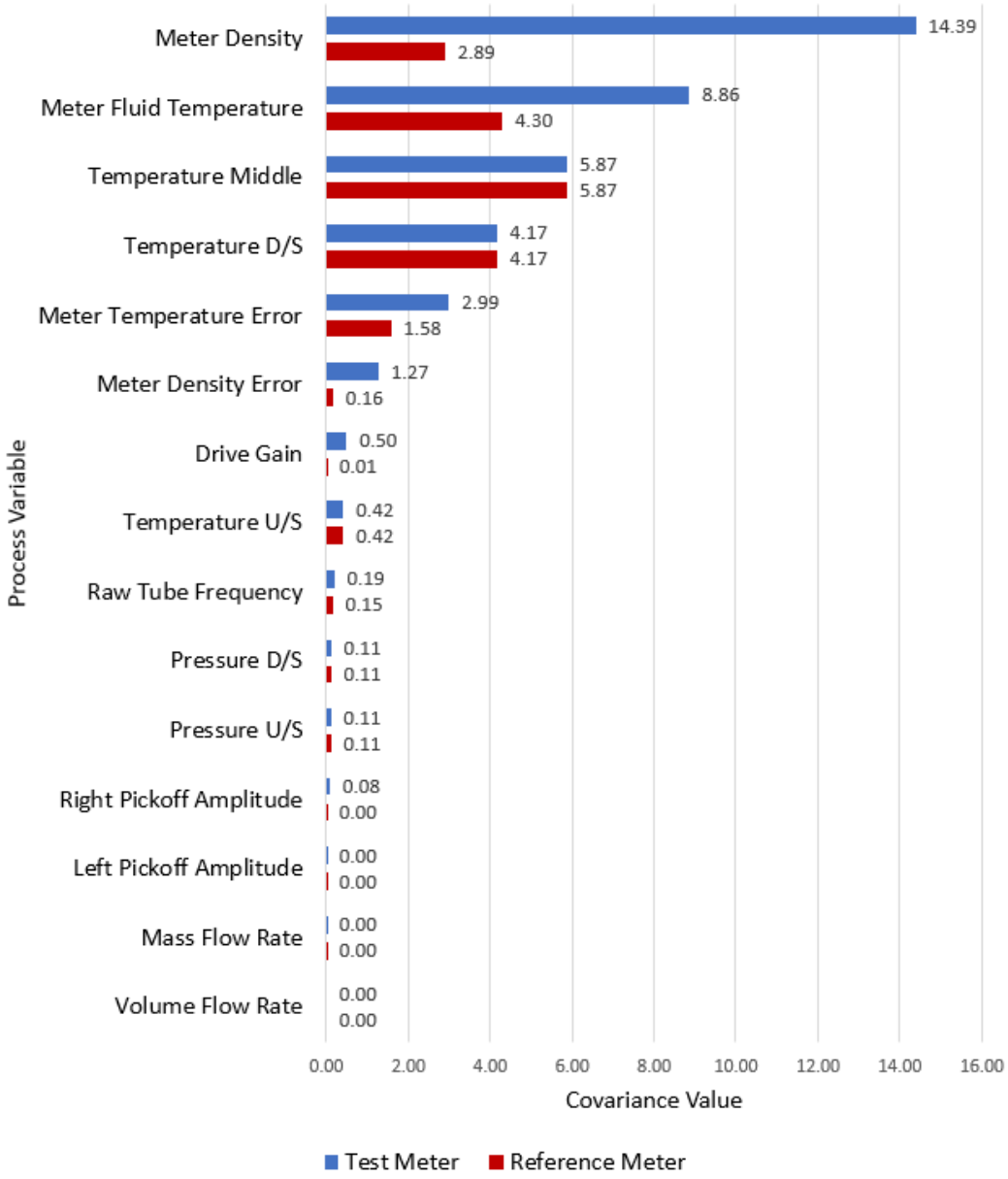

Figure 4-34 Manufacturer B - Test 2 covariance values for both test and reference meter diagnostic values and facility reference instrumentation values. Values represent the impact of oven air temperature on individual process parameters.

The covariance values above confirm the experimental observations. The test meter process values are shown to have a high dependency on oven air temperature. Specifically, the calculated fluid density value, meter temperature error and meter temperature. The middle and downstream facility reference temperature sensors (Figure 3-2, table 4-5) show equal covariance between both the test and reference meters, highlighting that the fluid temperature is indeed influenced by passing through the oven, however this does not imbalance the data. Both reference and test meters are

measuring the same mass of fluid, the temperature of which is governed by the same overriding parameters.

4.5.5 Density Mode Change

The results of the repeat tests (3 and 4) highlighted that changing from Density Mode 1 to Density Mode 2 reduced the errors from -0.81% to -0.21% for the stepped air temperature heating condition and from -0.53% to -0.15% for the fluctuating flow condition. However, there was still a correlation with the ambient air heating pattern present. Table 4-6, summarises the maximum errors observed in both the reference and test meter data.

Table 4-6 Manufacturer B individual test results summary

Test Point No	Maximum Indicated Fluid Temperature Error (Test) (°C)	Maximum Calculated Fluid Density Error (Test) (%)	Maximum Indicated Fluid Temperature Error (Ref) (°C)	Maximum Calculated Fluid Density Error (Ref) (%)	Mass Flow Error (%)
1	+4.45	-0.71	+1.17	-0.18	+11.06
2	+1.36	-0.59	-0.58	-0.14	-1.10
3	+1.80	-0.15	-0.34	+0.20	+1.21
4	+4.83	-0.21	+1.86	+0.23	+4.57

4.6 Manufacturer B Discussion and Conclusions

The results discussed in section 4.5 demonstrate that, like Manufacturer A (section 4.2), the density output is shown to be susceptible to errors that increase as the differential between the fluid temperature and ambient air temperature increases. The error is not dependent on heating pattern (with all other variables remaining constant). The ability to program in a linear fluid property calibration into the transmitter was shown to reduce errors, however errors were still detected and were shown to still increase with ambient air temperature. Density mode 2 is not dynamic in nature and still requires manual adjustment from the end user should the fluid properties deviate from their initial values and associated temperature range.

4.7 **Overall Conclusions**

The results gathered as part of this phase of experimentation have answered the first research question posed in this thesis. Coriolis meter data is affected by ambient air temperature. This has been shown to be true for differing meter manufacturers of differing geometries. The results have shown that the greater the difference between the process fluid temperature within the meter, the greater the error imposed on the data output by the meter. The properties of the fluid were also shown to affect the extent of the error. The process values most affected are the meter's fluid temperature indication and its calculated value of fluid density.

Since the experiments conducted in this phase were done so from an 'end user' perspective, there is little else that can be categorically stated without further access to the full schematics and specifications, which is confidentially held by the manufacturer.

The data proved that there is a problem with the existing temperature compensation methods for density calculation used by manufacturers A and B.

In the next chapter the second research question posed by the thesis is explored. Is it possible to correct for the effects of ambient temperature? The experiments, results, data analysis and proposed solution are detailed.

Chapter 5

5 Temperature Compensation

5.1 Overview

An industrial partnership was formed with Coriolis flow meter manufacturing company Rheonik for the remainder of the project. The key objective going forward into the research phase of this chapter was the development of a new temperature correction model for fluid density calculation where errors do not exceed 2% due to ambient air temperature fluctuation. The facility build described in chapter 3 (using Oven A) was not altered for this research phase. Due to the findings of chapter 4, Rheonik granted access to their propriety knowledge specific to the temperature compensation methods implemented on their Coriolis flow meters as well as the mechanical designs and operation specifications specific to their technology.

5.2 Experiment Parameters

The meter specification was as follows:-

Meter Type:-

- 2 of Omega shaped, dual tube Coriolis flow meter.
- Model RHM04.

Sizing and Specifications:-

- 0.25” Coriolis Meter.
    - ±0.10% of flow rate
    - ±5 kg/m^3

Communications:-

- Transmitter Model RHE16.
- Pulse Output.
- 4-20mA Output.
- RS485 Output.

Custom Features:-

- Removable meter case to allow access to meter internals.
- Ability to access correction factors and reference values stored on meter transmitter.
- Ability to deactivate all temperature compensation methods present on the meter transmitter.

Figures 5-1 to 5-3 show the mechanical and electrical internals of an RHM04 Rheonik Coriolis meter. The key components of the device are highlighted. During normal use, the meter cover shown in Figure 5-3 is fitted as means of both protection and insulation. Therefore, all experimentation was conducted with the cover fitted in order to simulate field use.

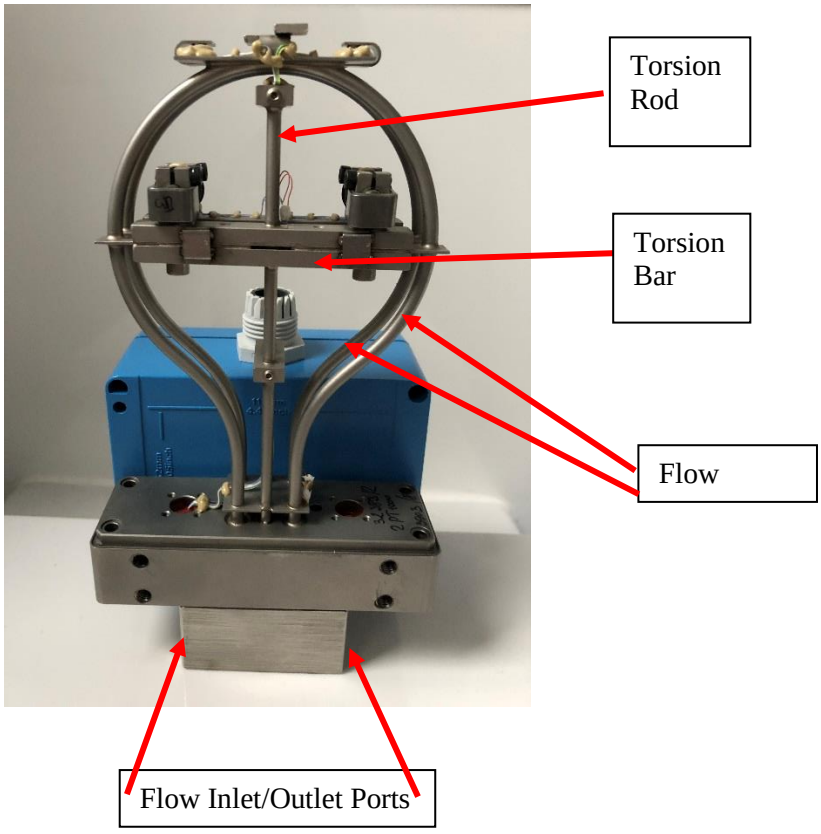

Figure 5-1 Rheonik RHM04 1/4" Coriolis Mass Flow Sensor with key mechanical elements highlighted

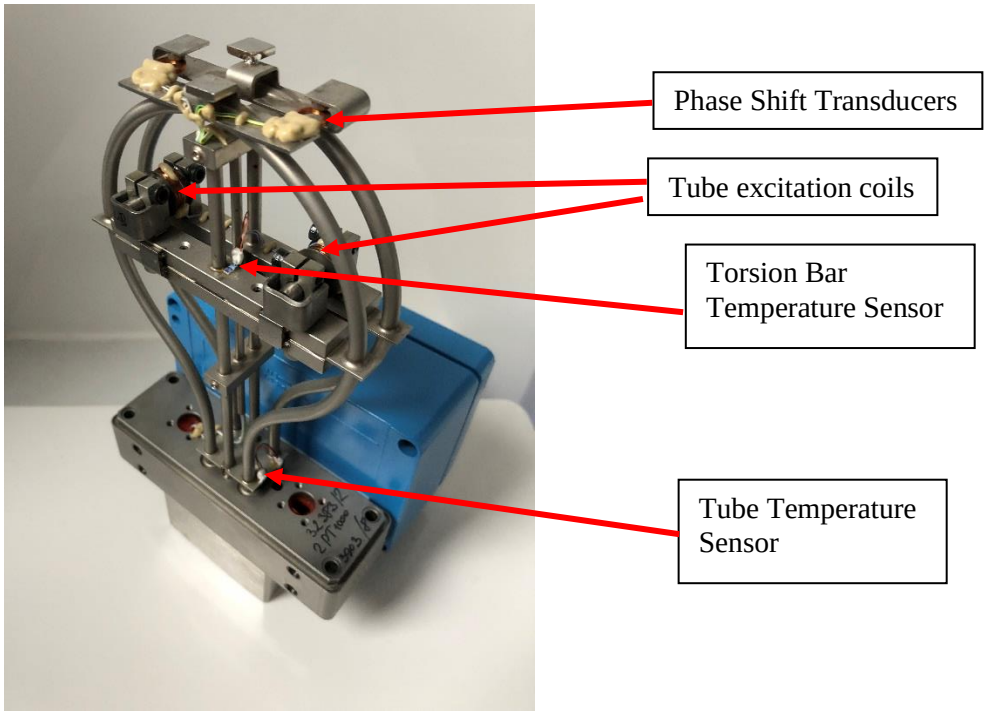

Figure 5-2 Rheonik RHM04 1/4" Coriolis Mass Flow Sensor with sensor and driver elements highlighted

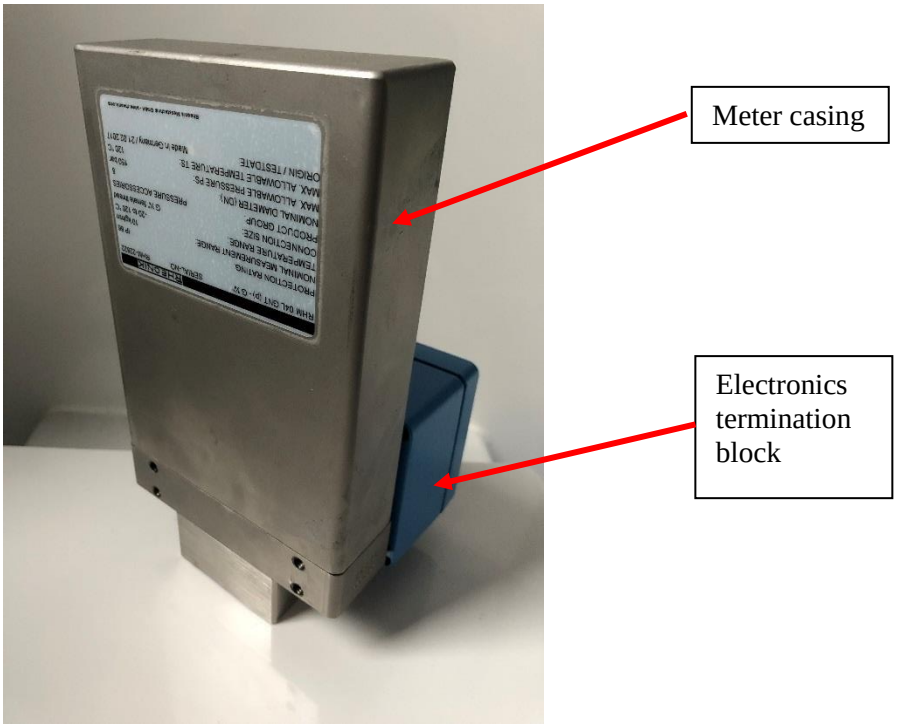

Figure 5-3 Rheonik RHM04 1/4" Coriolis Mass Flow Sensor with protective cover on as per installation during testing

The torsion bar shown in the above figures provides mechanical support to the flow tube oscillation mechanism (induced via the pictured drive coils) with the torsion rod guiding the oscillation movements. It is noteworthy that in installation scenarios where multiple meters of the same specification may be present, it is possible to supress potential cross-talk induced through the individual meter oscillations by changing the total mass of the torsion bar and in doing so modifying the specific meter characteristics.

Figure 5-4 shows the orientation of the Coriolis meter when installed in the liquid flow line.

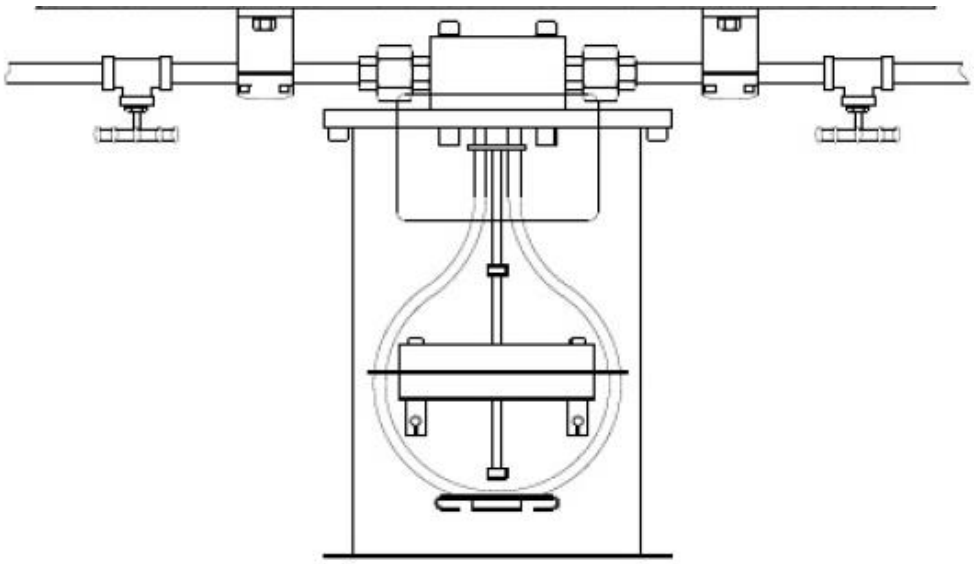

Figure 5-4 Mounting and support diagram for RHM04 as recommended by Rheonik [133]

5.3 Rheonik Temperature Correction Techniques

The correction algorithms currently implemented by Rheonik relate to both 'Mass Flow Rate' and 'Calculated Fluid Density'. Both equations make use of a base set of coefficients, coded into the meter transmitter by the manufacturer during initial factory setup and calibration. The coefficients are derived for fluids with the properties of air and water and their corresponding effects on the resonant frequency of the meter tubes.

Table 5-1 contains the coefficients provided by the manufacturer for both the reference and test meters.

Table 5-1 Manufacturer supplied temperature compensation coefficients for both reference and test meters

	U_{00}	U_{10}	U_{01}	S_{01}	S_{10}	$T_{1\,Ref}$	T_{2Ref}	$\rho_{1\,(air)}$	$\rho_{2\,(water)}$	$P_{1\,(air)}$	$P_{2\,(water)}$	$T_{1Ref(Dens)}$	$T_{2Ref(Dens)}$
Ref	1	-0.000230054	-0.00017958	-0.000275046	-0.00056739	23.56	23.74	1.182	997.5	1.84E-05	1.93E-05	22.83	24.97
Test	1	-0.000185313	-0.00026667	0.00026612	-0.00053438	22.34	22.12	1.2	997.67	1.77E-05	1.86E-05	22.27	21.93

The temperature compensation equation for mass flow is the product of the uncompensated mass flow (M_{uncomp}) initially determined by the meter and the combined products of the temperature differentials relating to both the torsion and tube temperature sensors with respect to the reference conditions and the mass flow calibration coefficients (S_x) noted in table 5-1.

$$\boldsymbol{M_{comp} = M_{uncomp}(1 + S_{10} * \Delta T_1 + S_{01} * \Delta T_2)} \quad (23)$$

where

- T_1 = Tube Temperature
- T_2 = Torsion Bar Temperature
- $T_{1,Ref}$ = Tube Temperature at time of calibration
- $T_{2,Ref}$ = Torsion Bar Temperature at the time of calibration
- ΔT_1 = Difference between T_1 and $T_{1,Ref}$ ($\Delta T_1 = T_1 - T_{2,Ref}$)
- ΔT_2 = Difference between T_2 and $T_{2,Ref}$ ($\Delta T_2 = T_2 - T_{2,Ref}$)

The temperature compensation relies heavily on the calibration factors developed by Rheonik at the point of manufacture. The calculated density is determined using upper and lower limit values for period ($p_1 and\ p_2$) and density values ($\rho_1\ and\ \rho_2$) with the only dynamic variable in the equation being the temperature compensated period value (p^2_{n-comp}).

$$\boldsymbol{\rho = \rho_1 + (\rho_2 - \rho_1) * \frac{p^2_{n-comp} - p^2_1}{p^2_2 - p^2_1}} \quad (24)$$

where

- p_n is the actual harmonic period of RHM
- p_{n-comp} is the temperature compensated harmonic
- ρ_1 is the LSL (Lower Specification Limit) density – for example the air density at the highest temperature in the measured range
- p_1 is the LSL period – at the LSL density
- ρ_2 is the USL (Upper Specification Limit) density – for example the water density at the lowest temperature in the measured range
- p_2 is the USL period – at the USL density

Temperature compensated harmonic period (p^2_{n-comp}) is calculated by taking the individual products of the torsion and tube temperature sensor density calibration coefficients (u_x) with respect to the measured temperature differential between initial factory reference conditions ($\Delta T_{x(Dens)}$).

$$\mathbf{p^2_{n-comp} = p^2_n\left(1 + u_{10} * \Delta T_{1(Dens)} + u_{01} * \Delta T_{2(Dens)}\right)} \quad (25)$$

where

- T_1 is the tube temperature
- T_2 is the torsion bar temperature
- $T_{1,Ref(Dens)}$ is the tube temperature at the time of density calibration
- $T_{2,Ref(Dens)}$ is the torsion bar temperature at the time of density calibration
- $\Delta T_{1(Dens)}$ is the difference between actual T_1 and $T_{1,Ref(Dens)}$ $\left(\Delta T_{1(Dens)} = T_1 - T_{1,Ref(Dens)}\right)$
- $\Delta T_{1(Dens)}$ is the difference between actual T_1 and $T_{1,Ref(Dens)}$ $\left(\Delta T_{1(Dens)} = T_1 - T_{1,Ref(Dens)}\right)$

The correction algorithms were deactivated on both the reference and test meter during data collection so that only the raw process values were logged. The correction algorithms were then applied to the data post testing in the analysis phase. The relevant correction algorithms were applied to each individual instrument scan as opposed to the overall average value to ensure that time series data sets for both raw and corrected value could be analysed.

5.4 **Test Matrix**

The test matrices designed for the experiments discussed in this chapter accounted for the facility performance and temperature settling times that were observed in chapter 4.

Testing was split into two matrices. Matrix 1 shown in Appendix 3 was defined as an extended facility/meter commissioning program. The test and reference meter response with respect to differing rates of ambient temperature change, fluid flow using water as a baseline informed test matrix shown in Table 5-2. The matrix represented a

streamlined experiment run from which a consistent set of parameters could be targeted and directly compared. The resulting data is discussed in the following sections of this chapter.

Table 5-2 Test Matrix 2 - Targeted ambient tests

Test No	Fluid	Highest Fluid Flow Rate (kg/hr)	Lowest Fluid Flow Rate (kg/hr)	Description of Fluid Flow Change	Initial Test Meter Air Temp (˚C)	Final Test Meter Air Temp (˚C)	Rate of Test Meter Air Temp Change (˚C)	Reference Meter Air Temp (˚C)	Fluid Temp Setpoint (˚C)	Test Duration (Hrs)	Comment
1	Water	230	230	N/A	20	60	10 / 60 mins	20	20	8	Standardised test air temperature increase
2	Kerosene	230	230	N/A	20	60	10 / 60 mins	20	20	8	Standardised test air temperature increase
3	Gas Oil	230	230	N/A	20	60	10 / 60 mins	20	20	8	Standardised test air temperature increase

5.5 **Results**

5.5.1 Reference Conditions

Figure 5-5 shows the facility reference conditions during test 1 – 3 respectively. The fluid temperature is shown to remain stable during the periods of sudden air temperature increase. During testing the fluid temperature increased by 1°C, 0.8°C and 4°C for water, kerosene and gas oil respectively.

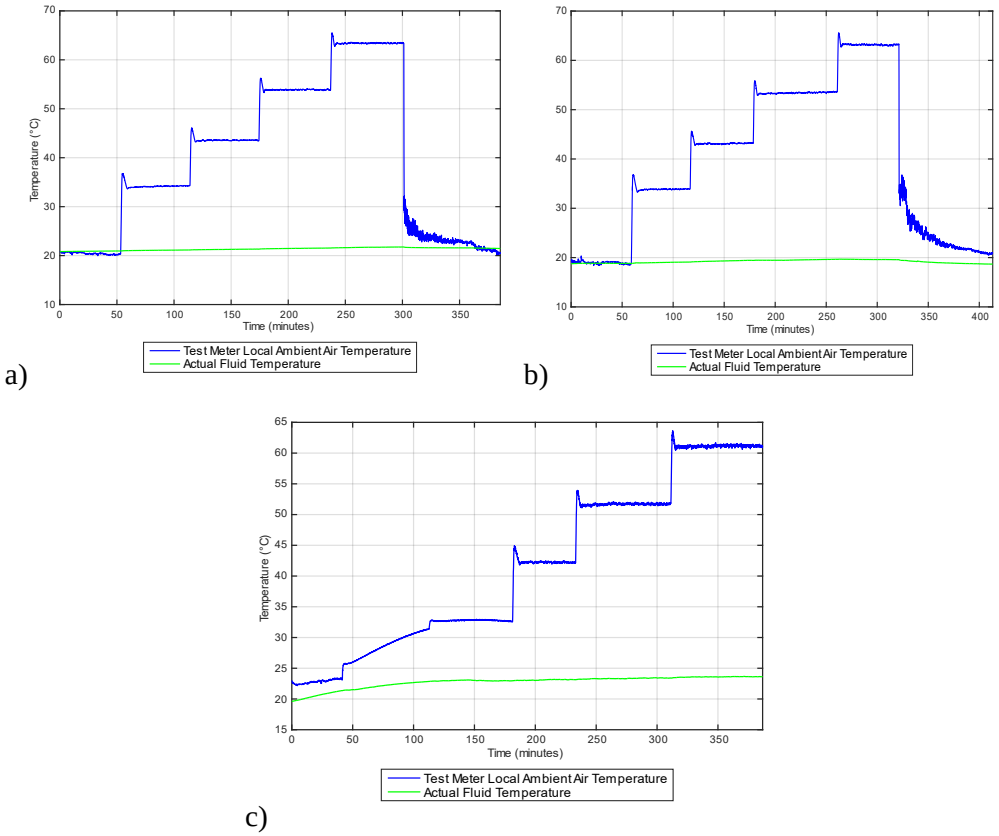

Figure 5-5 Reference measurements of test meter ambient air temperature and fluid temperature. a) Test 1 (Water) b) Test 2 (Kerosene) c) Test 3 (Gas Oil)

During test 3 (gas oil), the control of both the test meter air temperature and fluid temperature was not as efficient as with tests 1 and 2. Figure 5-5c shows that, between 50 and 120 mins, the air temperature increased gradually as opposed to the desired sudden step change as shown during the rest of the test. However, this loss of temperature control provided an insight into the response of the Coriolis meters in a non-ideal scenario, which informed later testing in this thesis (Chapter 6).

5.5.2 Fluid Properties

Figure 5-6 details the properties of the water, kerosene and Gas Oil used in tests 1-3 between 5°C to 55°C. The calibration data was generated from direct fluid samples and analysis in NEL's fluid property laboratory. As in chapter 4, this data was used in combination with the facility reference PRT to determine the meter density errors per scan cycle as shown in 5.5.3.

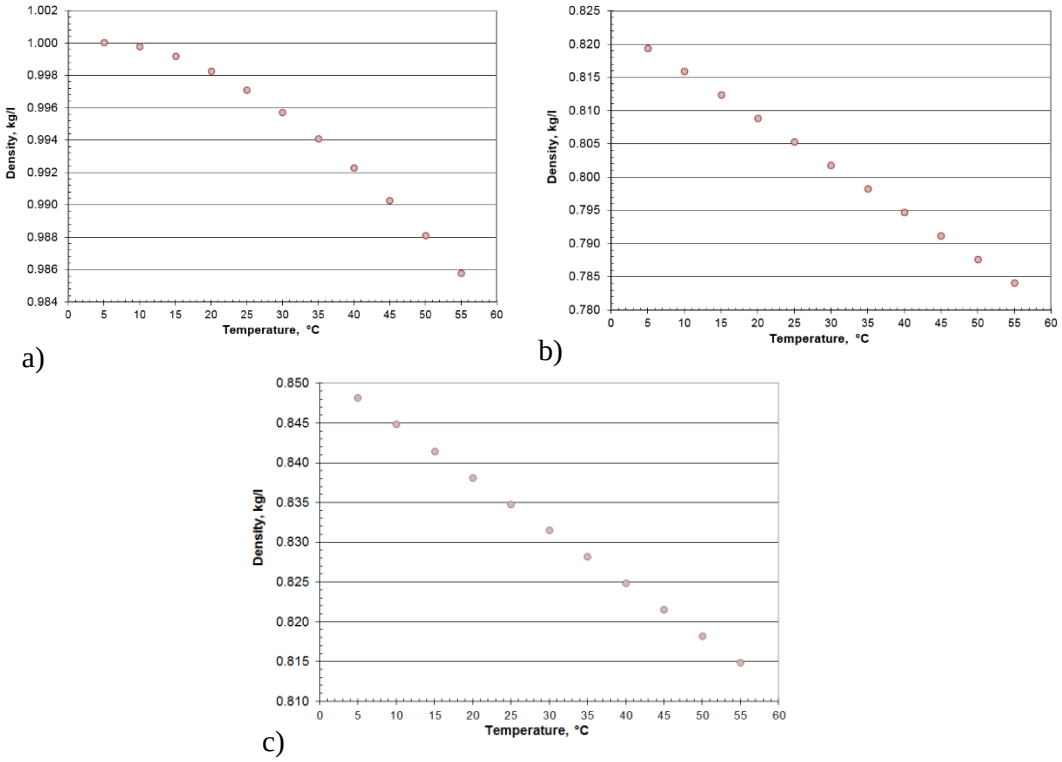

Figure 5-6 Fluid sample density response with respect to temperature a) Test 1 (Water) b) Test 2 (Kerosene) c) Test 3 (Gas Oil)

5.5.3 Live Fluid Properties

Figure 5-7 shows the live fluid trends which were calculated using the analysed sample response and the facility reference PRT individual scan cycle data throughout testing.

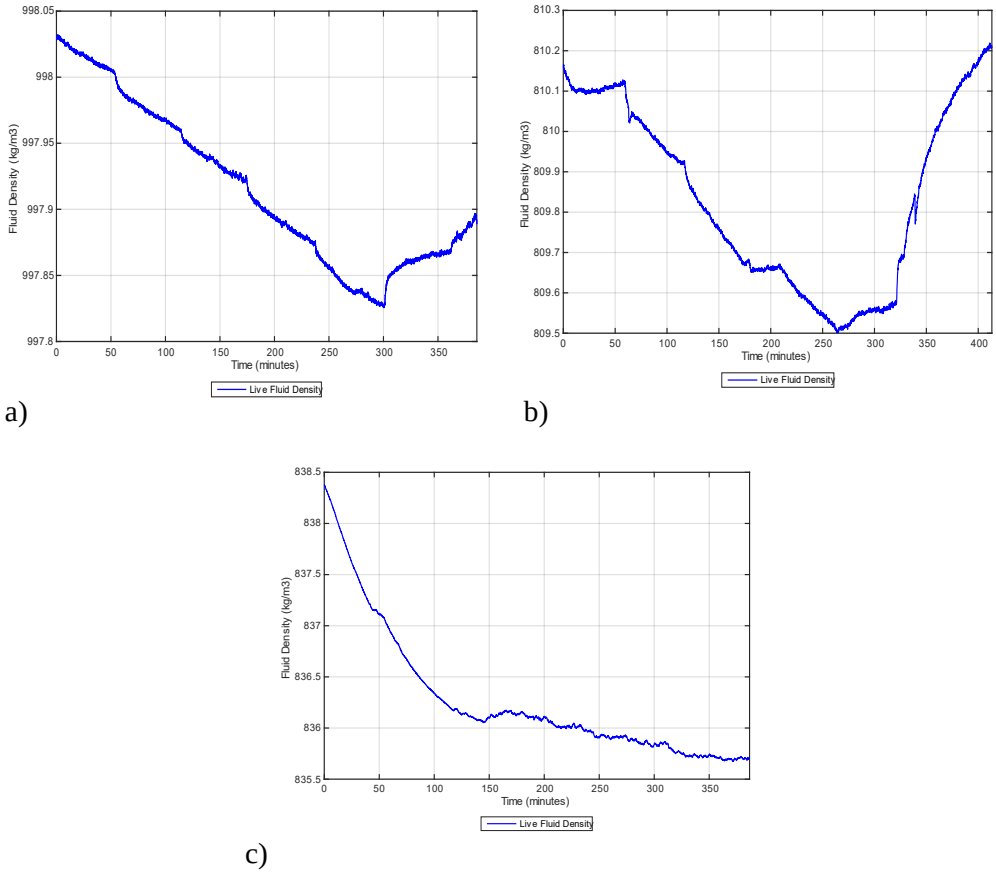

Figure 5-7 Transient fluid density calculation representative of live response during testing.
a) Test 1 (Water) b) Test 2 (Kerosene) c) Test 3 (Gas Oil)

5.5.4 Mass Flow

The facility commissioning tests (Appendix 3) demonstrated that varying the Mass flow while at elevated ambient temperatures did not produce errors in the calculated density error as described for manufacturers A and B in chapter 4. Therefore, no further fluid fluctuation trials are reported upon within this chapter.

The target mass flow rate was determined by the fluid viscosity and combined constraints inherent in the single speed pumps and small pipe bores associated with the facilities operating constraints. Each flow rate was determined to be the optimal flow for the respective fluids used.

5.5.5 Test Meter Temperature Sensor Error

Figure 5-8 shows the response of the two temperature sensors installed on the test meter body (Figure 5-2). As expected, there is a clear correlation with ambient air temperature increase on both sensors, with the Torsion Bar temperature sensor showing a higher sensitivity to the air temperature changes.

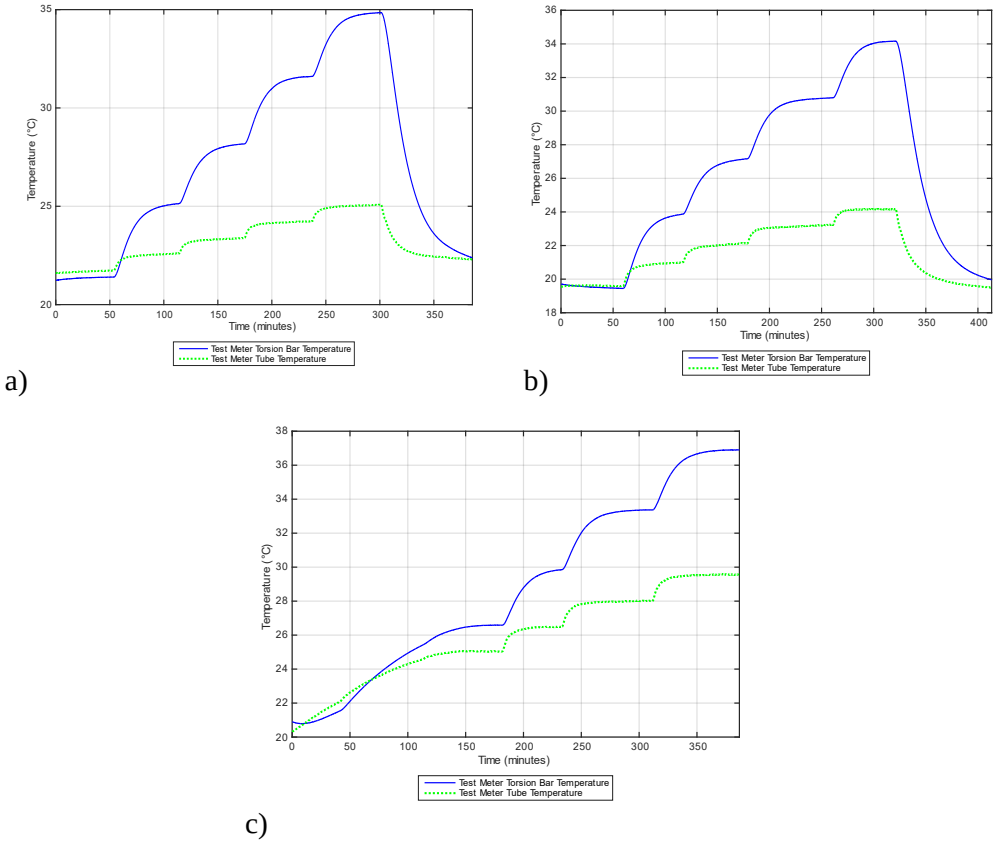

Figure 5-8 Test meter tube and torsion bar temperature sensor response during testing.
a) Test 1 (Water) b) Test 2 (Kerosene) c) Test 3 (Gas Oil)

The corresponding meter reported temperature errors with respect to the facility reference RTDs are shown in Figure 5-9. The data shows that the test meter Torsion bar contained absolute errors of 13°C, 14.5°C and 13°C for water, kerosene and gas oil respectively.

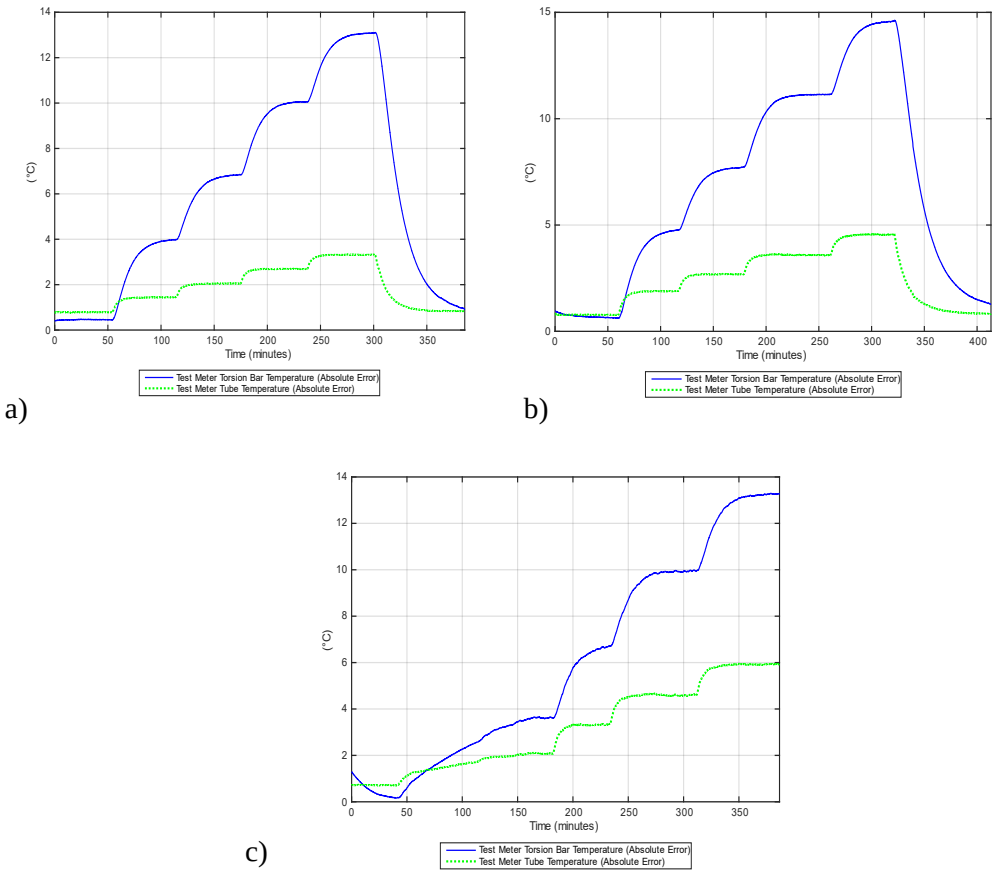

Figure 5-9 Test meter tube and torsion bar temperature sensor errors with respect to facility reference RTDs. a) Test 1 (Water) b) Test 2 (Kerosene) c) Test 3 (Gas Oil)

When one considers the location of the tube temperature sensor compared to the torsion bar (Figure 5-2), the trends observed here are comparable to those observed in the additional thermocouples fitted to Manufacturer A's in section 4.2.3.3. The tube sensor is effectively cooled by the fluid flowing through the tubes due to its location on the meter manifold, whereas the Torsion bar sensor is situated on the greatest mass of metal on the meter body. This therefore effectively damps the cooling effect of the fluid. The Torsion bar temperature sensor as a result drifts further from the actual fluid temperature due to the ambient air effects on the system.

5.5.6 Reference Meter Temperature Sensor Performance

Figure 5-10 shows the corresponding reference meter temperature sensor response. For all tests, the tube and torsion bar sensor are shown to follow comparable trends that correspond with the increase in fluid temperature.

Note that during test 3 (Gas Oil), the meter's modbus process values ceased updating at 300 minutes. As a result, all meter digital values post 300 minutes which were logged by the DAQ software appear to be constant (flatlined). The modbus connection to the OPC server remained uninterrupted, and was therefore not detected as a crash. The OPC server simply continued to log the last successfully calculated value output from the meter transmitter instead of flagging an error. Therefore, the data presented in Figures 5-10 (c), 5-12 (c), 5-13 (c) and 5-15 (c) each contain the "data freeze" beyond 300 minutes.

The test meter did not experience this problem, therefore given that the ambient key temperature setpoints for test 3 had already been successfully logged (20°C - 60°C) and the true reference for density is the live fluid property calculation (Figure 5-6 and 5-7) there was no need to repeat the test.

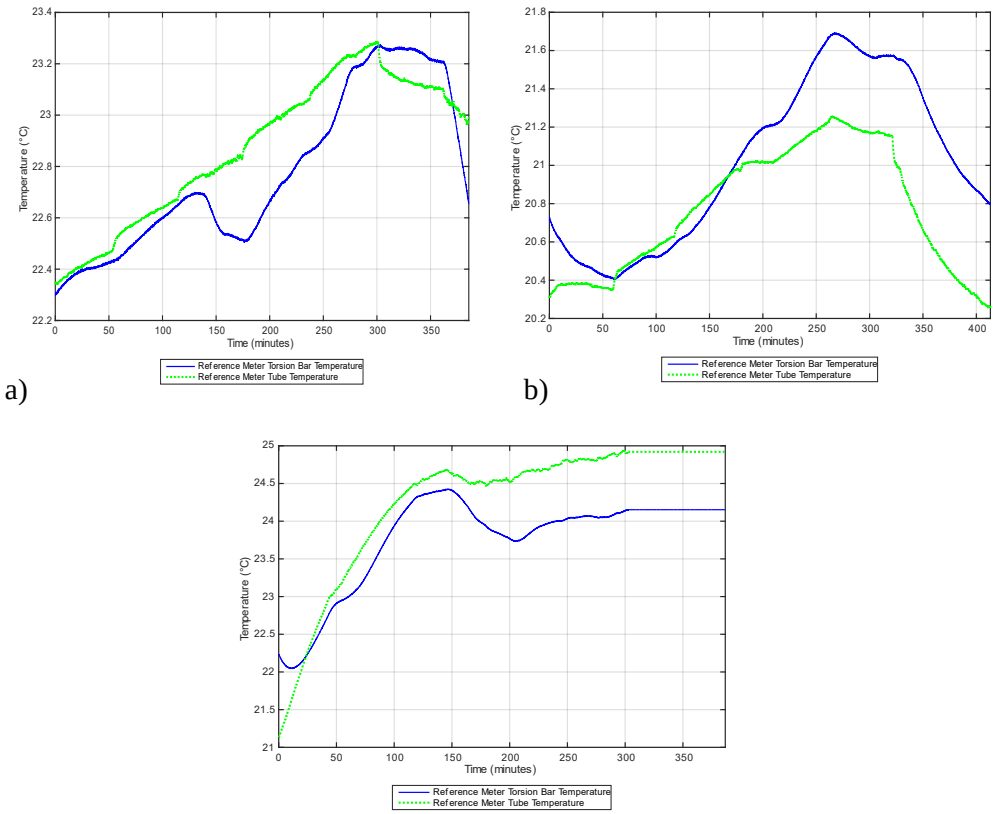

Figure 5-10 Reference meter tube and torsion bar temperature sensor response during testing.
a) Test 1 (Water) b) Test 2 (Kerosene) c) Test 3 (Gas Oil)

Figure 5-11 shows the corresponding absolute temperature error for both temperature sensors on the reference meter.

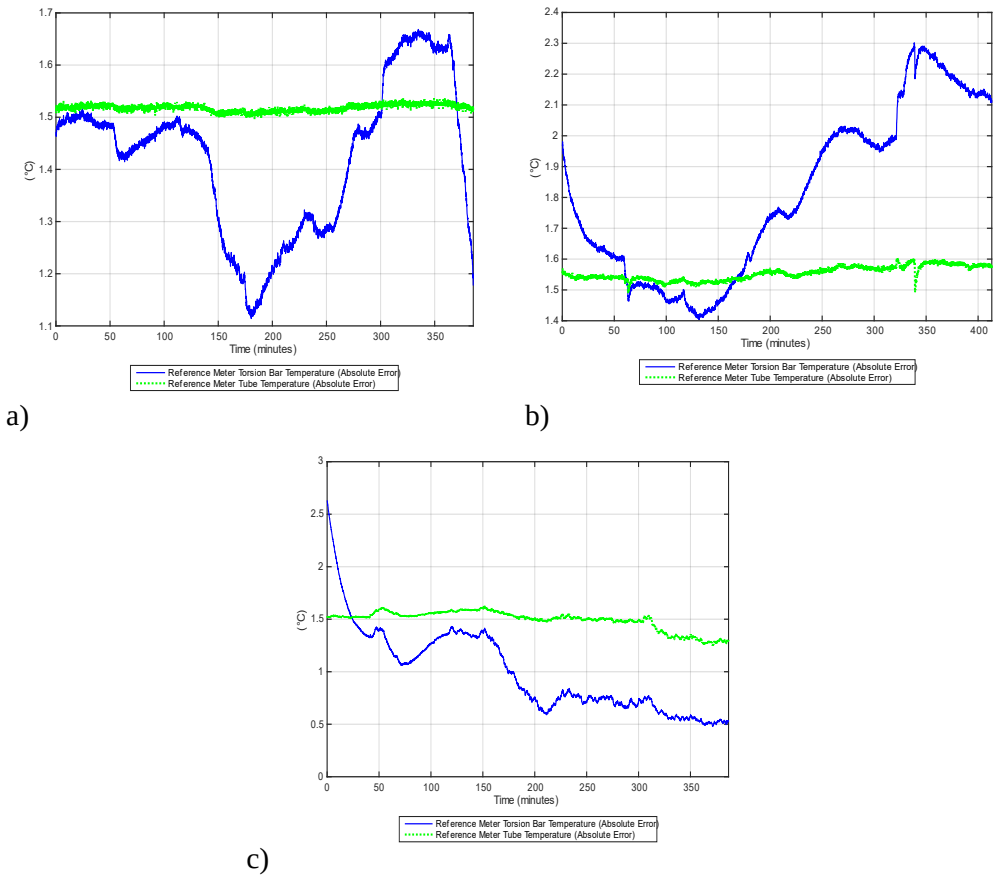

Figure 5-11 Reference meter tube and torsion bar temperature sensor errors with respect to facility reference RTDs. a) Test 1 (Water) b) Test 2 (Kerosene) c) Test 3 (Gas Oil)

It should also be noted that the values reported by both test and reference meter temperature sensors contained offset errors ranging from 1°C – 2.5°C across the differing fluid properties, highlighting minor temperature sensor calibration errors on both the tube and torsion bar sensors on both meters. However, since it is generally accepted in industry that fluid temperature should be measured by dedicated temperature probes (either thermocouple or RTD based depending on application), this offset would generally be acceptable if the values were to be used as a general indication.

5.5.7 Meter Calculated Fluid Density (Manufacturer Corrected)

The raw (uncorrected) process variables logged during tests 1-3 were post processed using the manufacturer's equations (Equations 24 and 25) to determine fluid density. The results are shown in Figure 5-12.

Despite the use of a temperature compensation algorithm that takes account of the two temperature sensors discussed in section 5.5.5, there is still a clear correlation with the fluid density output and the ambient air temperature changes that is comparable to the effects observed in chapter 4.

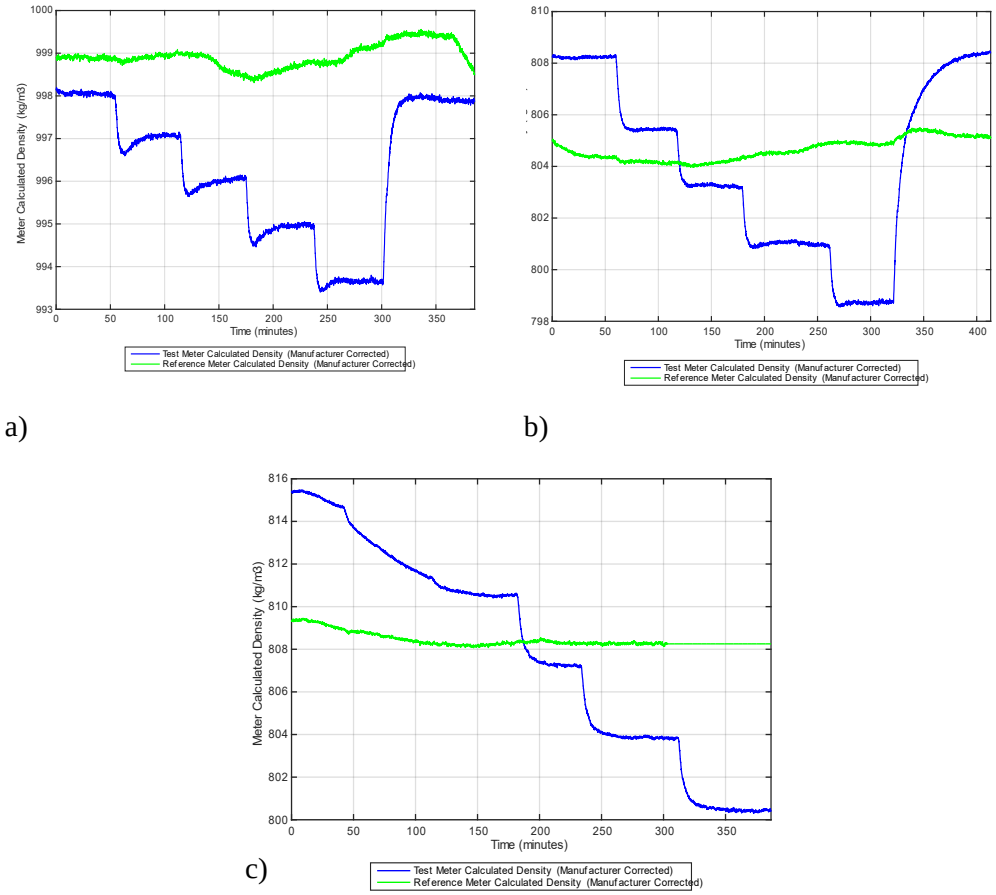

Figure 5-12 Test and reference meter calculated fluid density response. a) Test 1 (Water) b) Test 2 (Kerosene) c) Test 3 (Gas Oil)

While the data for test 1 (water) is within the manufacture's stated uncertainty (±5 kg/m^3), the data pertaining to the oils tested (kerosene and gas oil) demonstrates performance significantly out with this value.

Figure 5-13a shows that for water an error of -0.42% was calculated for the test meter density value at the maximum ambient air temperature. The reference meter corrected fluid density is shown to correlate to room ambient conditions and fluid temperatures. It should be noted that an offset of 0.08% is present for the reference meter when compared to both the test meter baseline value and fluid properties curve (Figure 5-6).

The corrected data for test 2 (Figure 5-12b and 5-13b) show similar trends to test 1 (Figure 5-12a and 5-13a). Here the test meter error reached a value of -1.3% at the maximum ambient temperature tested. For kerosene, the initial baseline value for the test meter was shown to contain a -0.2% error from the known fluid property value. It should also be noted that the baseline error between the reference and test meter also increased to a value of -0.4%, with the reference meter showing -0.6% error from known fluid properties. For test 3 the corrected density values during baseline conditions for the test and reference meter showed an initial error offset of -2% and -3.5% respectively when compared to the known fluid properties. At the maximum test meter air temperature, the test meter reported an error of -4.2%.

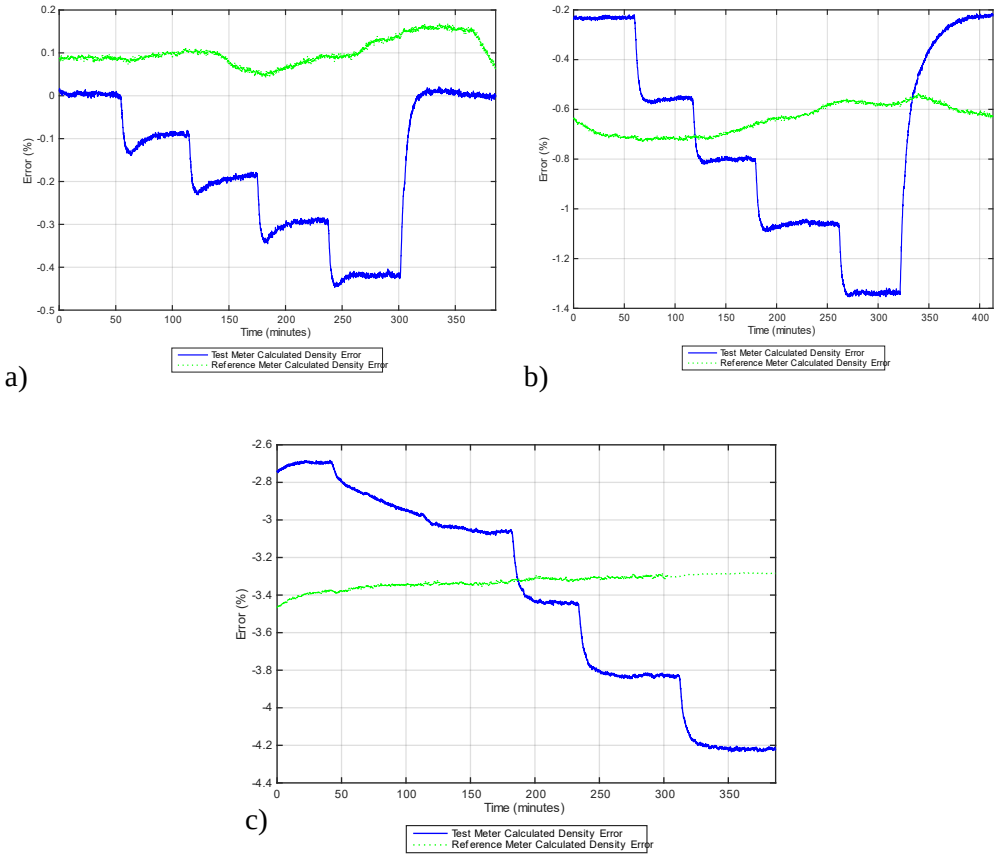

Figure 5-13 Test meter calculated fluid density error (resulting from manufacturers existing temperature compensation method. a) Test 1 (Water) b) Test 2 (Kerosene) c) Test 3 (Gas Oil)

The overall increase in errors when a fluid of lower density than water is present within the meter reinforces the observations in chapter 4. The fluid density calculation and temperature compensation techniques currently implemented by the manufacturers tested are sensitive to fluid property changes.

5.5.8 Meter Frequency

The change in raw frequency process values during test 1-3 are shown in Figure 5-14 and Figure 5-15 for both the test and reference meter respectively.

As expected, the baseline tube frequency is shown to change with the fluid properties used in tests 1-3. It is noteworthy that the baseline frequencies of the test meter compared to the reference meter have a consistent difference of 4.2Hz across the three fluids tested. This difference is representative of the individual meter characteristics, which are dependent on construction materials and techniques specific to the manufacturer. The coefficients derived and programmed into the meter at the point of manufacture account for said difference.

The test meter tube frequency is shown to respond to the stepped ambient temperature changes, with the reference meter showing a response to the overall fluid temperature increase as well as to the subtle variations in room temperature detected by the torsion bar temperature sensor.

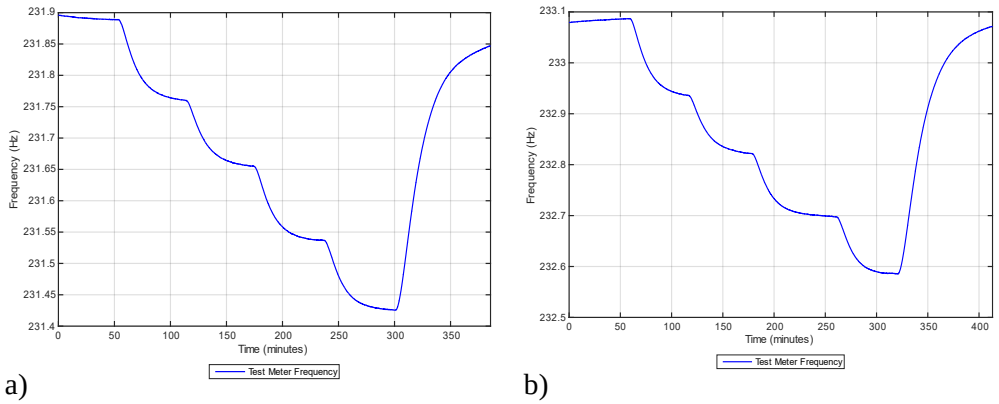

a)

b)

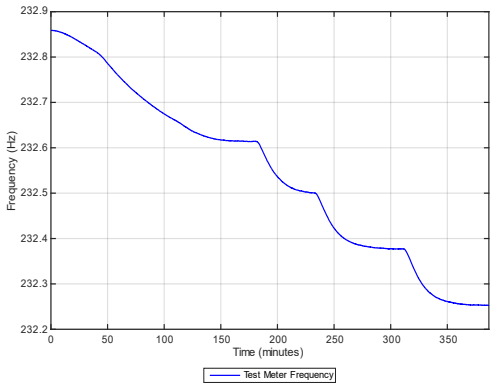

c)

Figure 5-14 Response of raw test meter tube frequency during testing. a) Test 1 (Water) b) Test 2 (Kerosene) c) Test 3 (Gas Oil)

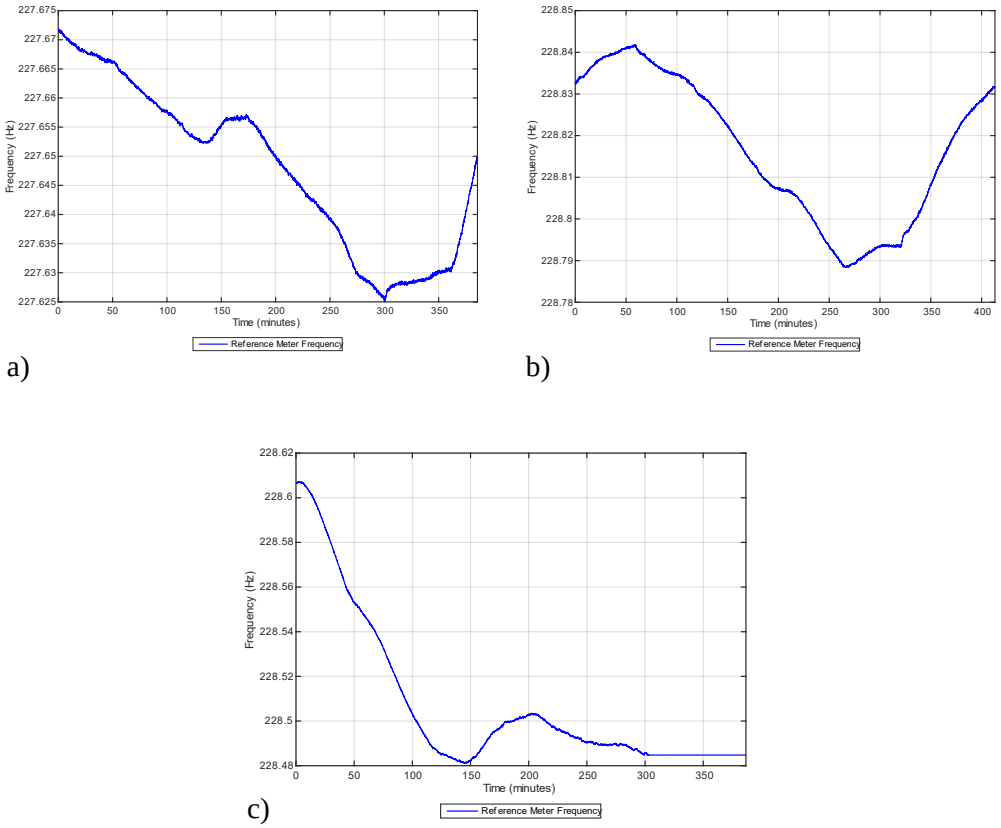

Figure 5-15 Reference meter raw tube frequency response during testing. a) Test 1 (Water) b) Test 2 (Kerosene) c) Test 3 (Gas Oil)

5.5.9 Mass Flow Error

The mass flow rate temperature compensation techniques (Equation 23) were applied to the raw data collected during tests 1-3. Figure 5-16 shows the resulting error plots with respect to the reference meter. The mass flow rate is shown to be stable, with an error of ~-0.4% present for Kerosene and -~0.2% for gas oil.

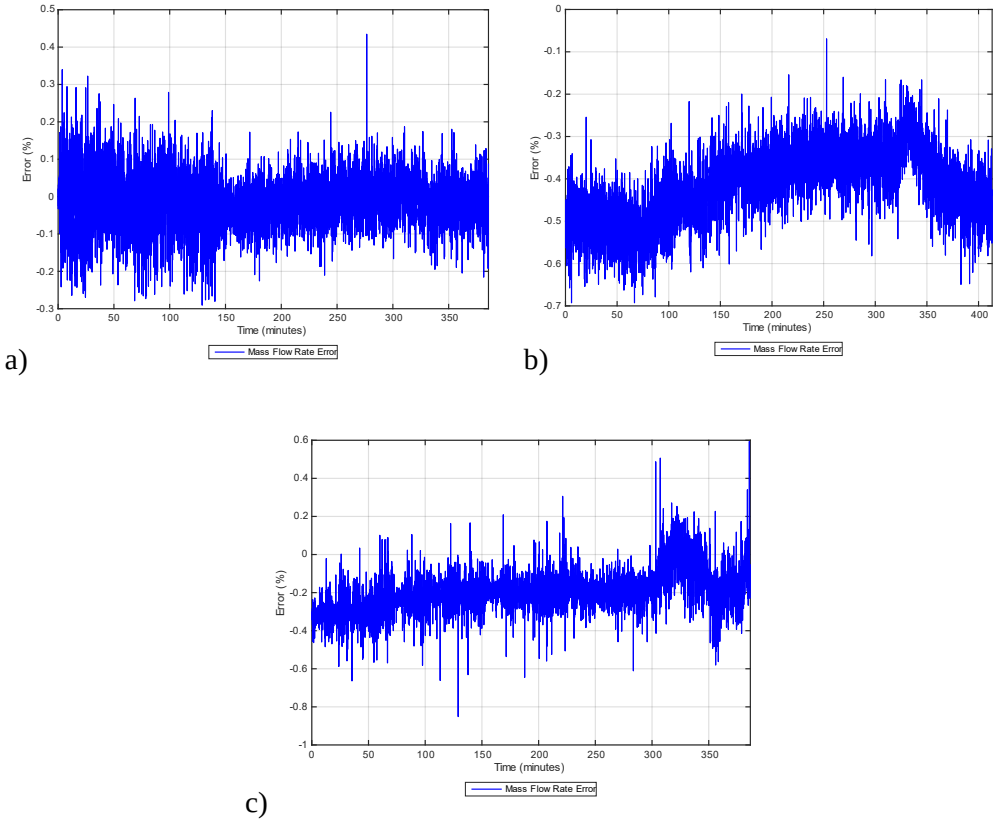

Figure 5-16 Test meter mass flow rate error with respect to reference meter during testing. a) Test 1 (Water) b) Test 2 (Kerosene) c) Test 3 (Gas Oil)

5.6 Manufacturer's Compensation Method Results Conclusions

The data presented in this section have demonstrated the advantage of undertaking experimentation with manufacturer support. Access to information relating to the calibration coefficients programmed into the meter at the point of manufacturer (Table 5-1) combined with the fluid dependent errors (section 5.5.7) has shown that the errors observed due to fluid properties are a result of the overall inflexibility inherent in the transmitter's data infrastructure. The differing response of both the tube and torsion bar temperature sensors (section 5.5.5) combined with the changes to tube frequency due to thermal effects (section 5.5.8) have highlighted that the correction methods implemented by the manufacturer are subject to error due to the reliance on maintaining conditions that are close to the initial factory setup parameters.
The current algorithm is not dynamic in nature and therefore lacks the intelligence to account for the additional factors of varying fluid properties and the fluid/air temperature differential effect on the efficiency of the tube and torsion bar temperature sensors.

In the next section, a new temperature compensation method for density calculation is described, the structure of which takes into account the results described herein and demonstrates how the errors observed can be live corrected within the meter transmitter during service.

5.7 Manufacturer Equation Performance

The manufacturer's existing density calculation relies on a temperature compensated harmonic period ($Pn - Comp$) to account for Young's modulus [20] effects on the flow tubes. The equation was derived by the manufacturer based on their knowledge of the manufacturing process and associated build materials that ultimately make up the physical mass flow meter.

Coefficients $U10$ and $U01$, are determined by the manufacturer during initial product testing and calibration of the device, making them unique to the physical properties and make up of each mass flow meter. Pn is a live process value, which is dependent on the fluid properties present within the flow tubes as well as the physical properties of

Coriolis sensing tube - both of which are dependent on the thermal interactions that can occur between the ambient air, meter body temperature and fluid temperature.

Since both ΔT_1 and ΔT_2 are values that are derived from reference parameters in the factory ($T_{x,Ref(Dens)}$), the relevance of said parameters are limited to scenarios which are directly comparable to the conditions of the factory during initial setup and calibration. Since $\left(\Delta T_x = T_x - T_{x,Ref(Dens)}\right)$ the effectiveness of the compensation equation will reduce when the difference between the sensor temperature (T_x) deviates significantly from either the reference temperature or value of the inverse sensor (T_x).

This effect has been repeatably demonstrated through tests 1 – 3. Since the values of $T_{1,Ref(Dens)}$ and $T_{2,Ref(Dens)}$ for the test meter are 22.27°C and 21.93°C respectively (Table 5-1), this limits the flexibility of the equation at the ambient temperatures, which were present during testing. As demonstrated in section 5.5.5, the torsion bar temperature sensor experienced greater drift due to ambient air temperature compared to that of the tube temperature sensor. This drift is effectively the meter's only process value that gives an indication of the differential between the ambient air temperature and the fluid temperature.

5.8 Statistical Validation

Further statistical analysis of the digital process values logged from the test meter during tests 1-3 was undertaken to provide further insight and validate the findings of section 5.5.

Figure 5-17 details the Pearson correlation coefficients for the test meter process values detailed in Table 5-3 below, across the three fluids used during testing. The correlation coefficients were generated with respect to oven air temperature.

Table 5-3 Definition of test facility and meter generated process values assessed for correlation/covariance with test variables

Process Variable	Description
Amplifier Efficiency	Meter generated 'diagnostic' value output over modbus. Indicator of meter transmitter amplifier efficiency.
Density	Fluid density determined and output by meter.
Density Error	Based on % error calculated from Meter Density value and true density determined from fluid sampling process.
Electronics Temperature	Meter generated 'diagnostic' value output over modbus. Indicator of meter electronics temperature.
Mass Flow Rate	Mass flow rate determined and output by meter.
Mass Flow Rate Error	Mass flow rate error. Determined by checking against reference meter value.
Period Stability	Meter generated 'diagnostic' value output over modbus. Indicator of sensor stability (comparison of raw and filtered period values)
Pressure U/S	Upstream pressure reported from test facility pressure transducer.
Pressure D/S	Downstream pressure reported from test facility pressure transducer.
Temperature U/S	Upstream fluid temperature determined from test facility PRT
Temperature D/S	Downstream fluid temperature determined from test facility PRT.

Process Variable	Description
Temperature Middle	Test and reference meter middle fluid temperature determined from test facility PRT
Torsion Temperature	Temperature reported from Torsion bar temperature sensor
Torsion Error	Based on absolute error calculated from Torsion Bar Temperature value and true fluid temperature determined from test facility 'Middle' PRT probe.
Tube Temperature	Temperature reported from Torsion bar temperature sensor
Tube Error	Based on absolute error calculated from Tube Temperature value and true fluid temperature determined from test facility 'Middle' PRT probe.

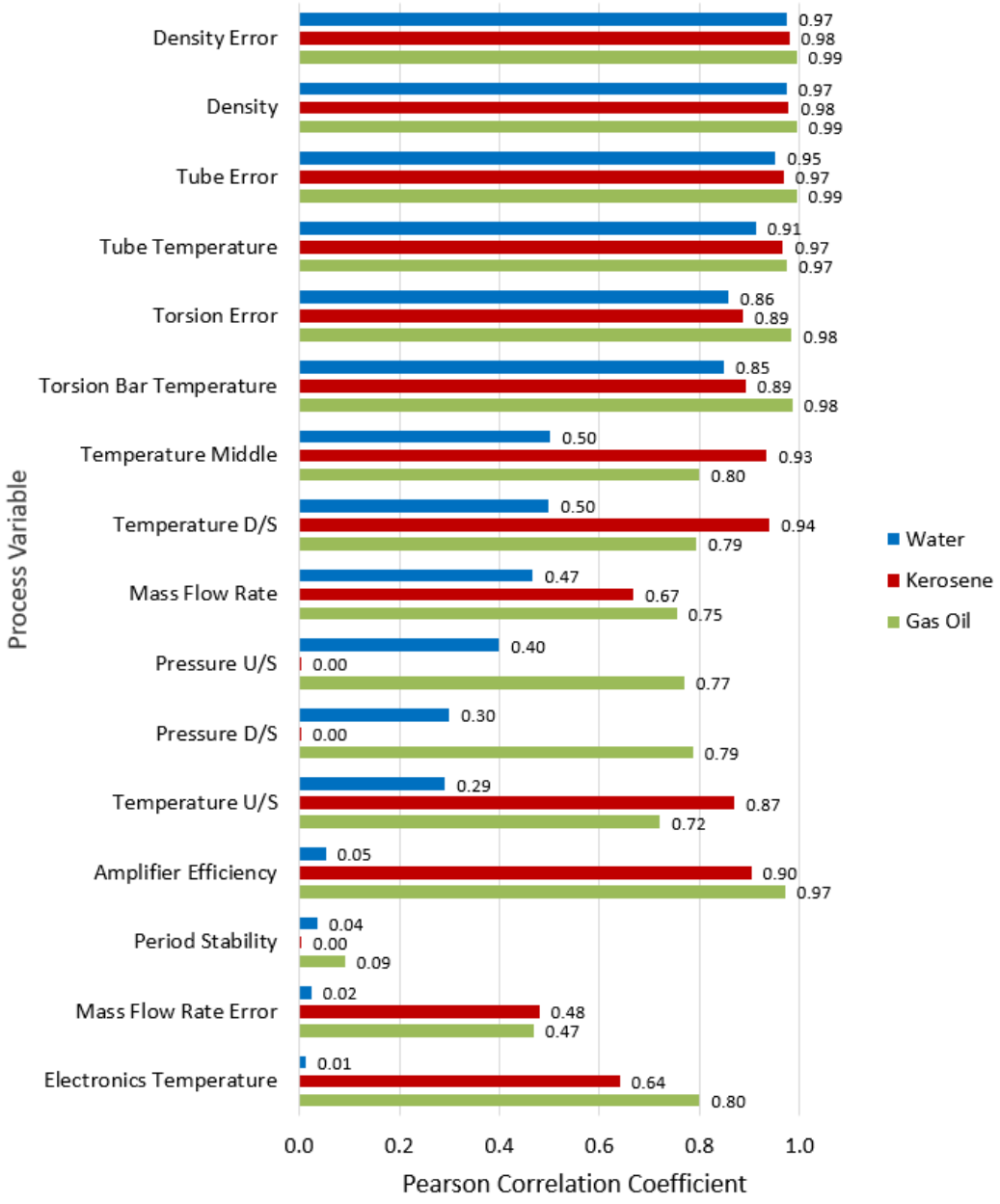

Figure 5-17 Tests 1 – 3 Pearson correlation coefficients for test meter diagnostic values and facility reference instrumentation values with respect to differing fluid properties and oven air temperature.

When the torsion and tube temperature sensor correlation coefficients were analysed with respect to the oven air temperature, the data did not fully validate the findings of sections 5.5 – 5.7. While both parameters were shown to be highly correlated with the air temperature, the tube sensor was in fact shown to be the parameter with the higher correlation across the three fluids compared to the torsion bar.

However, we know from the data presented in section 5.5 as well as an overall understanding of the experiment and algorithm structure that this is not a fully accurate depiction of the system's response to ambient air temperature. Therefore, while useful for showing an overall summary of parameter response, the Pearson correlation in this instance is misleading as the experimental data has highlighted there was not a true linear correlation between the values. The data suggested non-linear variable dependency in the individual parameters.

As demonstrated in chapter 4, analysing the individual covariance values for each parameter with respect to the primary variable (oven air temperature in this case) can yield more realistic dependency information. In the specific case of the torsion bar vs tube temperature sensor discrepancy, the key factor was the standard deviation of both values. For example, over the course of test 1, the standard deviations of the torsion bar temperature sensor, tube temperature sensor and oven temperature were 4.49°C, 1.094°C and 15.67°C respectively. Therefore, when applied to Equation 19 (Section 3.7) the resulting correlation coefficients for both sensors with respect to oven temperature becomes an incorrect representation of the real-world effects. Therefore, simply analysing the covariance values as shown in Figure 5-18 provides a superior representation of process value importance with respect to oven temperature.

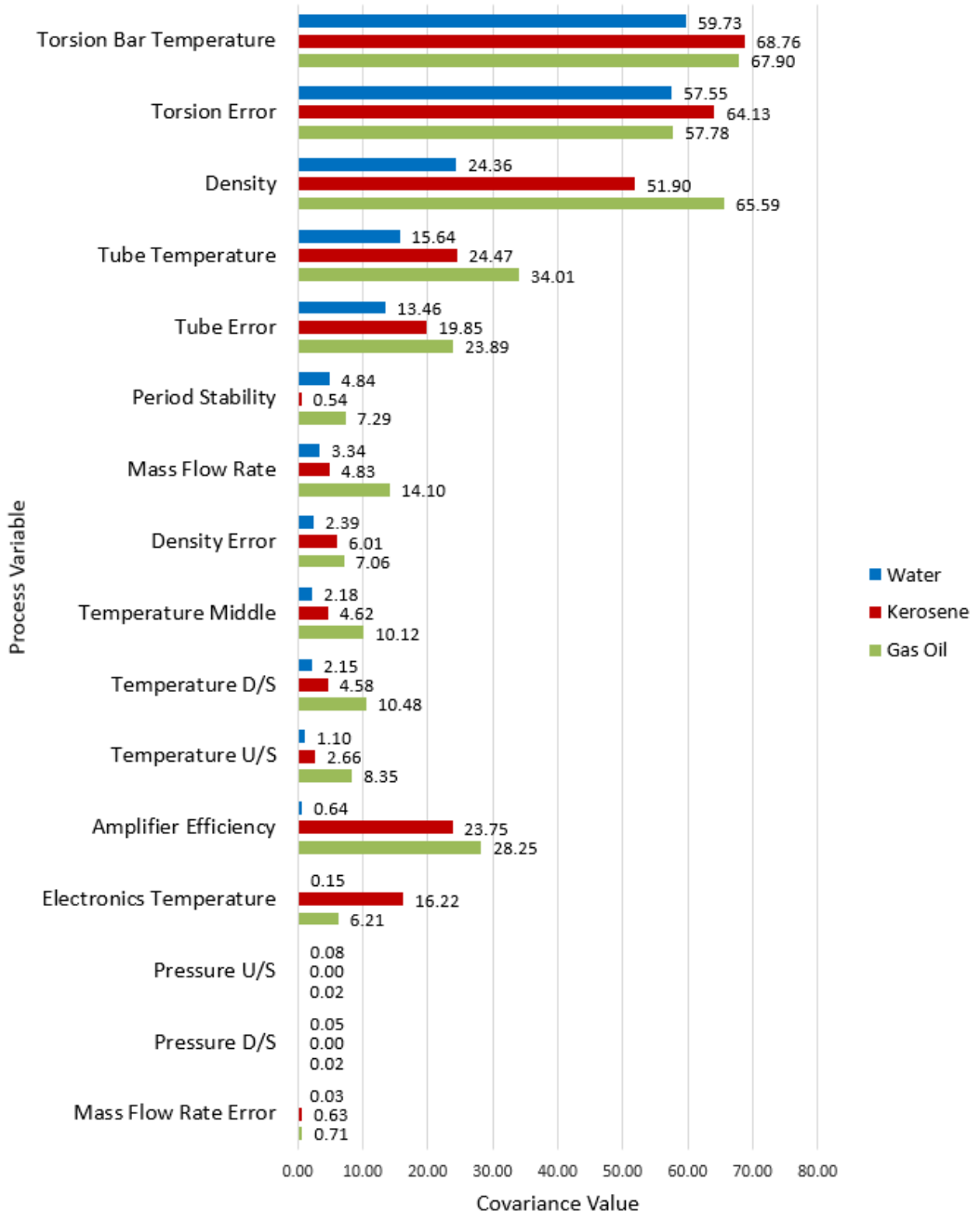

Figure 5-18 Tests 1- 3 covariance values for test meter diagnostic values and facility reference instrumentation values with respect to differing fluid properties and oven air temperature.

Figure 5-18 confirms the experimental observations of section 5.5 to 5.7. The torsion bar sensor is indeed the process value most affected by ambient air temperature.

The data also indicates that as the fluid properties deviated from water the dependency of the density and even mass flow rate meter calculated values increased, and thus confirmed that the algorithms reliance on coefficients generated in water (Table 5-1 and section 5.7) was a critical factor in resolving the errors observed.

5.9 New Temperature Compensation Method

5.9.1 Theory

To ensure that the solution to the temperature related errors detailed thus far could be realistically deployed by the manufacturer in real world scenarios, the following assumptions were taken into account during development:-

- The manufacturer would not be able to change their manufacturing process.
- The manufacturer would not be able to change their initial calibration conditions.
- The manufacturer would not be able to provide additional coefficients to accommodate fluid property changes (Table 5-1 remains unchanged).
- The solution should be applicable to existing devices in the field and new build devices.

The data discussed in Sections 5.5 to 5.8, provided an insight into meter operation and sensor performance during high ambient air temperature vs fluid temperature differentials.

To overcome the weakness of the existing method, with respect to the combined effects of ambient air temperature and fluid properties, Equation 25 was modified to include a check on the differential between the tube and torsion bar temperature sensor ($\Delta T_{1,2}$) with a new coefficient (X) serving as the denominator, relating to the specific heat capacities of the actual fluid properties within the meter.

$$\mathbf{p_{n-comp}^2} = \mathbf{p_n^2}\left(\mathbf{1} + \mathbf{u_{10}} * \Delta\mathbf{T_{1(Dens)}} + \mathbf{u_{01}} * \Delta\mathbf{T_{2(Dens)}} + \frac{\Delta\mathbf{T_{1,2}}}{\boldsymbol{X}}\right) \quad (26)$$

where

- T_1 is the tube temperature
- T_2 is the torsion bar temperature
- $T_{1,Ref(Dens)}$ is the tube temperature at the time of density calibration
- $T_{2,Ref(Dens)}$ is the torsion bar temperature at the time of density calibration

- $\Delta T_{x(Dens)}$ is the difference between T_x and $T_{x,Ref(Dens)}$ $\left(\Delta T_x = T_x - T_{x,Ref(Dens)}\right)$
- $\Delta T_{1,2}$ is the difference between the tube and torsion bar temperature sensors
- X is fluid specific correction term

The addition of a check on the differential between the two temperature sensors increases the robustness of the equation. In this form, should the live operating conditions deviate from the initial calibration conditions, to which Table 5-1 pertains, the equation is capable of augmenting these values per processor scan cycle to account for the deviation. In effect, the torsion bar temperature sensor has been re-purposed in this equation to act as an air temperature detector negating the need for additional temperature sensor placement and therefore adhering to the assumptions stated above.

The introduction of the fluid specific dimensionless X coefficient as the denominator with respect to $\Delta T_{1,2}$ affords the algorithm further awareness of the specific conditions for which it is being deployed. Specifically, the X value is fluid dependent and therefore enables configuration of the equation for use with fluids of differing properties and specific heat capacities.

The value of X can in theory be implemented via two differing mechanisms:-

Fixed Value – The manufacturer builds their devices to order. It is therefore feasible to establish the fluid which is intended to pass through the meter during service. The fluid specific X coefficient would be derived at the point of manufacturer and would be programmed into the meter transmitter firmware via Modus registers.

Dynamic selection – Based on the meter tube frequency, the limits of which are already defined by the manufacturer with respect to air and water densities, the firmware would automatically select the appropriate X value from a range of predefined values, applicable to fluid densities between 1 kg/m^3 and 1000 kg/m^3.

5.9.2 Validation of Fixed X Value Method

The new form of the equation was validated against the data obtained during tests 1-3 by feeding the appropriate raw values for each DAQ scan cycle through Equation 26. This allowed for a realistic simulation of the new method's performance under the exact conditions experienced by the manufacturer existing method. For water, kerosene and gas oil, an ideal X value was determined by incrementally tuning the data with respect to the response of the known fluid properties during testing. Fixed X values of 12.5, 5.5 and 3.5 were applied for water, kerosene and gas oil respectively.

Figures 5-19 shows the density trends for the test meter produced by the manufacturer's version of the formula for both the test and reference meter as well as a trend for density value calculated using Equation 26.

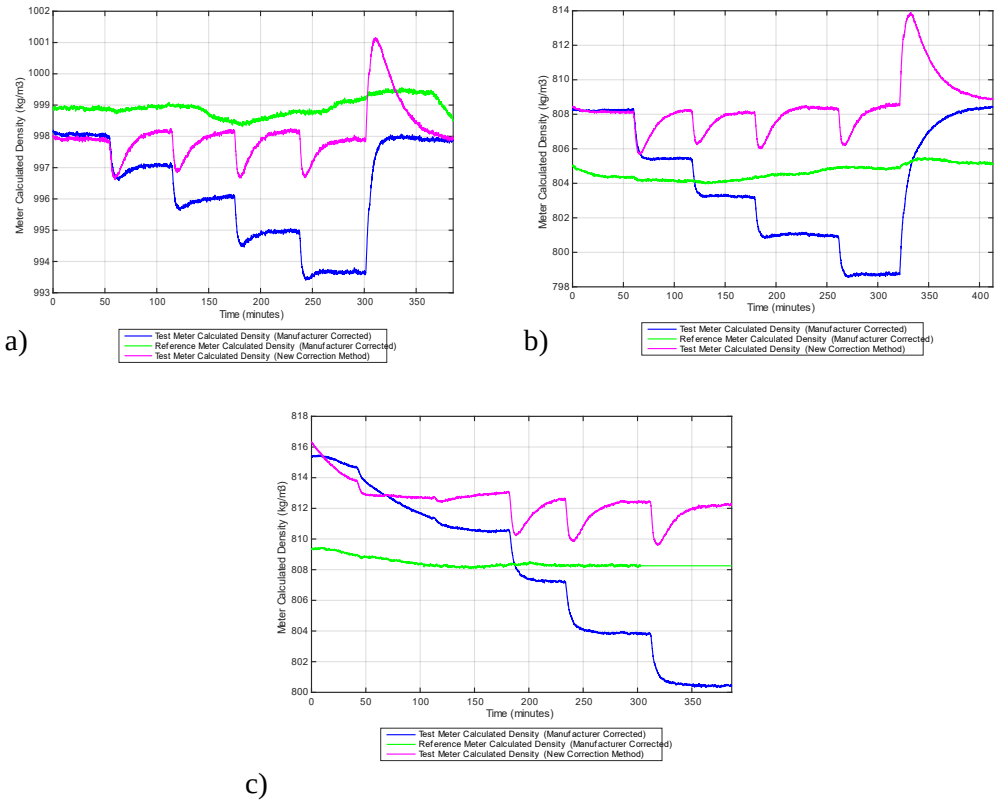

Figure 5-19 Comparison of new correction method response vs original manufacturer correction method. a) Test 1 (Water) b) Test 2 (Kerosene) c) Test 3 (Gas Oil)

For each 10°C air temperature increase, the new correction method is shown to correctly detect the fluid properties present in the system and applies the appropriate X coefficient. The deviation between the torsion and tube temperature sensor is also

detected and the new method is shown to reduce the drift caused by the stepped increases in ambient air temperature per 10°C as well as the overall 20°C – 60°C range. Once a thermal equilibrium has been achieved in the system after each temperature transition, the test meter density value is shown to be stable at the expected value.

The temporary errors observed during the periods of thermal instability after an air temperature change (referred to as transition region hereafter) are detailed below in Figure 5-20. Immediately after a 10°C air temperature increment, the errors observed were restricted to maximum values -0.12%, -0.25% and -3.13% for water, kerosene and gas oil respectively, before ultimately recovering after ~30 minutes. When the air temperature was rapidly cooled during tests 1 and 2 (300 to 375 minutes and 325 to 400 respectively), the new correction method is shown to temporarily contain an error, which reached a maximum value of +0.3% for water and kerosene before recovering to the expected value.

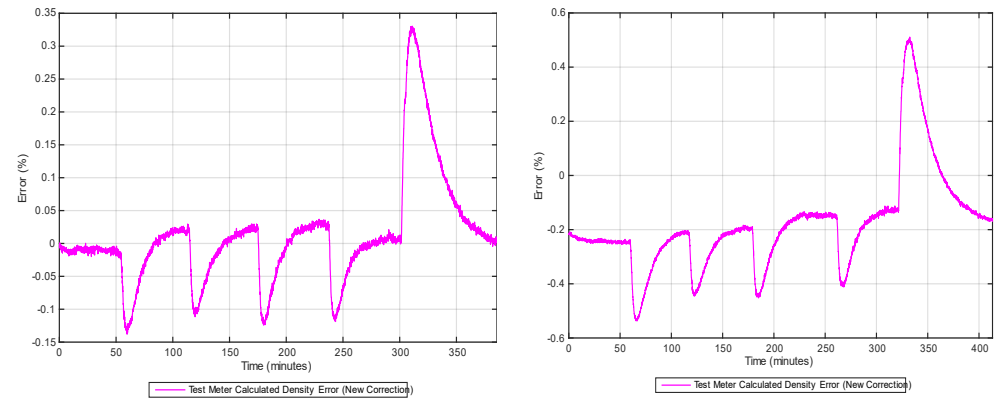

a) b)

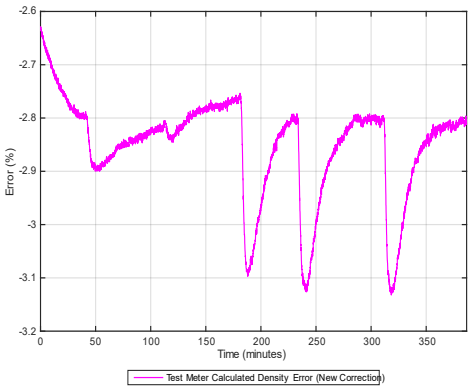

c)

Figure 5-20 New correction method errors with respect to the know fluid properties.

a) Test 1 (Water) b) Test 2 (Kerosene) c) Test 3 (Gas Oil)

Table 5-4 summarises the errors observed during tests 1 – 3. The new correction method ensured that the manufacturer's stated uncertainty was adhered to, and in fact significantly improved upon the margin of error.

Table 5-4 Summary of New correction method vs manufacturer correction method performance

Test No	New Correction Density Value at minimum air temperature (kg/m3)	New Correction Error at minimum air temperature (%)	Transition region error recorded at minimum air temperature (%)	New Correction Density Value at maximum air temperature (kg/m3)	New Correction Error at maximum air temperature (%)	Transition region error recorded at maximum air temperature (%)	Manufacturer Correction Density Value at minimum air temperature (kg/m3)	Manufacturer Correction Error at minimum air temperature (%)	Transition region error recorded at minimum air temperature (%)	Manufacturer Correction Density Value at maximum air temperature (kg/m3)	Manufacturer Correction Error at maximum air temperature (%)	Transition region error recorded at minimum air temperature (%)
1	997.8	-0.01	-0.13	997.8	+0.01	-0.11	997.9	+0.01	-0.13	993.6	-0.42	-0.45
2	808.0	-0.25	-0.54	808.6	-0.14	-0.41	808.2	-0.23	-0.58	798.7	-1.35	-1.35
3	816.2	-2.62	N/A	812.2	-2.81	--3.12	815.3	-2.73	N/A	800.4	-4.22	-4.22

5.9.3 Development and Validation of Dynamic X value method

Figure 5-21 summarises the observed effects on resonant frequency between the air temperature extremes of 20°C and 60°C and the three fluids (at ~20°C) tested in this chapter. Specifically it was shown that, despite the fluid temperature remaining nominally stable throughout testing, the tube frequency will reduce due to the air temperatures effect on the structure's elasticity.

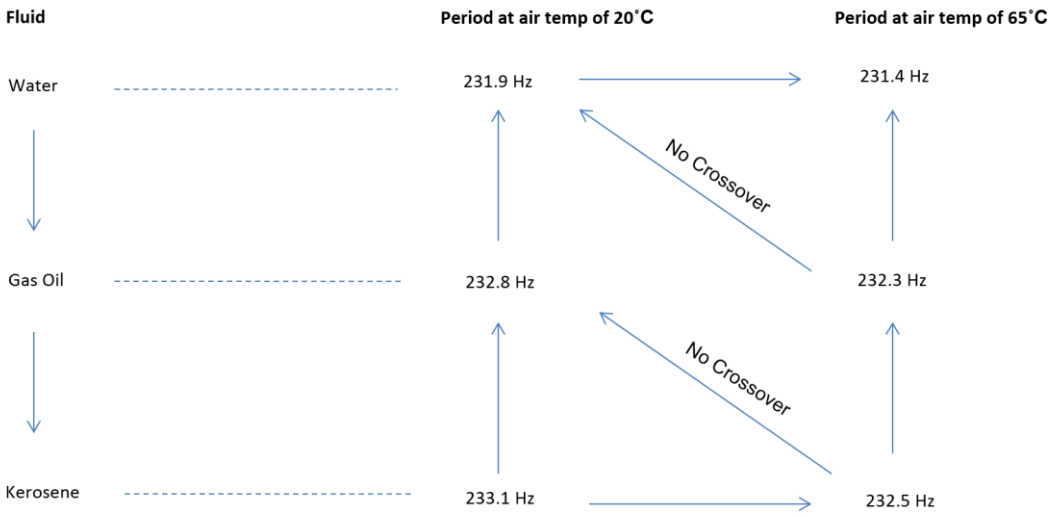

Figure 5-21 Summary of meter frequency changes with respect to air temperature.

To allow the value of X be automatically determined as suggested in 5.9.1, the new method must be able to distinguish between tube frequencies relating to low and high air/fluid temperature differentials. For example, it is possible that for conditions that deviate from those explored in this chapter, the new correction method would be capable of incorrectly identifying the fluid type, and therefore apply the wrong X coefficient to the algorithm. Therefore, an additional level of automation was added to the new method through logical range checking that in practice would be implemented in the meter firmware, with variables stored within the Modbus register.

The automation first assesses the value of $\Delta T_{1,2}$. Depending on the extent of deviation between the two sensors, a linear augmentation of the raw resonant frequency (f_{rf}) is performed to return the value to within the ideal factory value (f_{20}) (Table 5-1). The resolution, frequency of parameter checks and temperature differential value can be increased or decreased as appropriate to the installation scenario. It is likely that this

would form the basis of an initial on-site commissioning programme or meter requirements specification that the end-user would provide to Rheonik at the point of meter purchase. For illustration purposes, a simplified form of the underlying logic is summarised as follows.

If $\Delta T_{1,2}$ *< 2 then No change to frequency*

If $\Delta T_{1,2}$ *> 2 < 4 then f =* f_{20} *+ 0.1*

If $\Delta T_{1,2}$ *> 3 < 5 then f =* f_{20} *+ 0.15*

If $\Delta T_{1,2}$ *> 4 < 6 then f =* f_{20} *+ 0.2*

If $\Delta T_{1,2}$ *> 5 < 7 then f =* f_{20} *+ 0.25*

If $\Delta T_{1,2}$ *> 6 < 8 then f =* f_{20} *+ 0.3*

If $\Delta T_{1,2}$ *> 8 < 10 then f =* f_{20} *+ 0.35*

If $\Delta T_{1,2}$ *> 10 then f =* f_{20} *+ 0.4*

The resulting value is then evaluated to determine the appropriate X value to be used in the modified temperature compensation model (Equation 26). For example: -

If f_{20} *is < 232.0 and > 231.4 then X = 12.5 (Water)*

If f_{20} *is < 233.3 and > 232.8 then X = 5.5 (Kerosene)*

If f_{20} *is < 232.5 and > 232.1 then X = 3.5 (Gas Oil)*

The method described above was applied to the raw data sets and new correction method (Equation 26). It was found to produce identical results to the fixed value method (Figures 5-19 and 5-20, Table 5-4), by correctly interpreting the ranges and applying the appropriate augmentations and coefficients. Therefore, Table 5-4 summarises the results of both the fixed and dynamic methods.

5.9.4 Solution Refinement

The temporary errors summarised in Figure 5-20 and Table 5-4 were further investigated by observing the response of the individual parameters of Equation 26. The response of components (p_n^2) and ($1 + u_{10} * \Delta T_{1(Dens)} + u_{01} * \Delta T_{2(Dens)}$) during the first ambient air temperature increase of test 1 (20°C - 30°C) is shown in Figure 5-22b and 5-22c respectively.

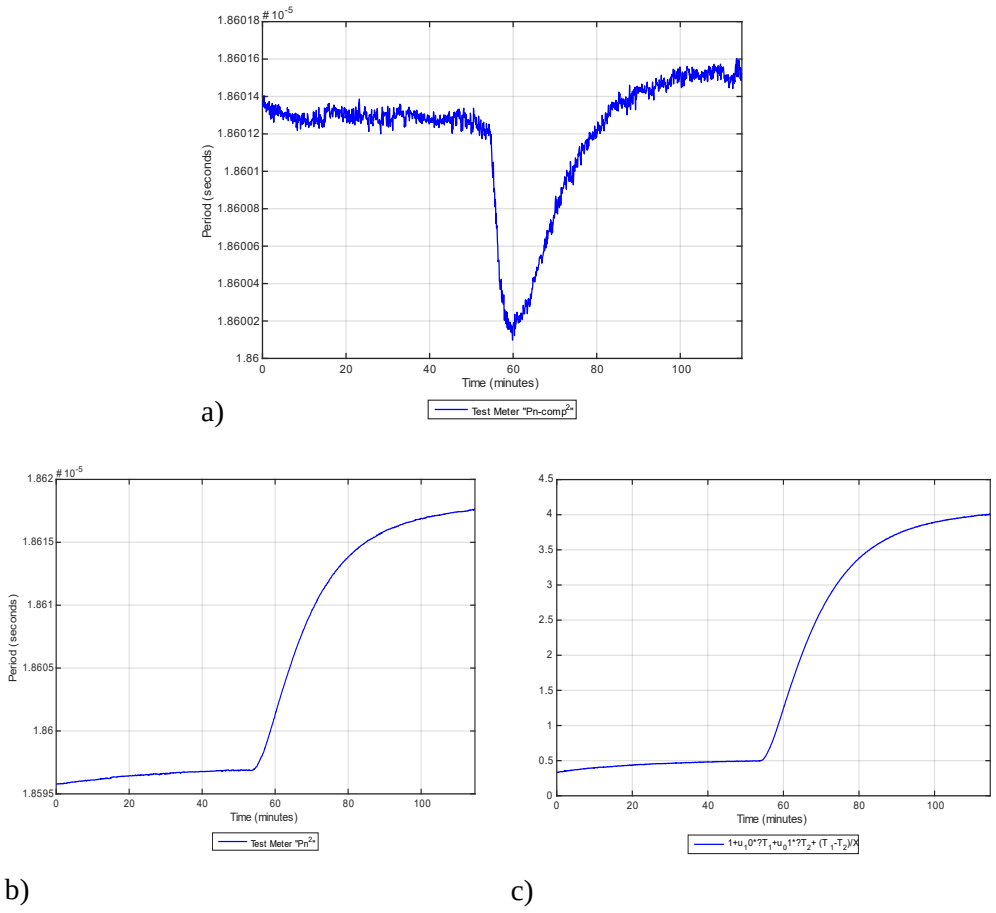

Figure 5-22 Breakdown of Equation 26 parameter response during first air temperature increase as part of test 1 (water). a) Temperature compensated period value (manufacturer's existing methods), b) Raw period value, c) Temperature sensor vs calibration coefficient parameter

By analysing the rate of change of both parameters from 55 to 100 minutes, it was observed that the rate of change in (p_n^2) was greater than that of ($1 + u_{10} * \Delta T_{1(Dens)} + u_{01} * \Delta T_{2(Dens)}$), thus highlighting that the response of the meter's PT100s, which feed $\Delta T_{1(Dens)}$and $\Delta T_{2(Dens)}$ are not suited to this resolution of live temperature compensation.

In lieu of replacing the physical sensors and in keeping with the ethos described in 5.9.1, Figure 5-23 demonstrates the response of an alternative solution, where the imbalance between the two terms, was compensated for with a damping term of 155 seconds to the (p_n) used in Equation 26.

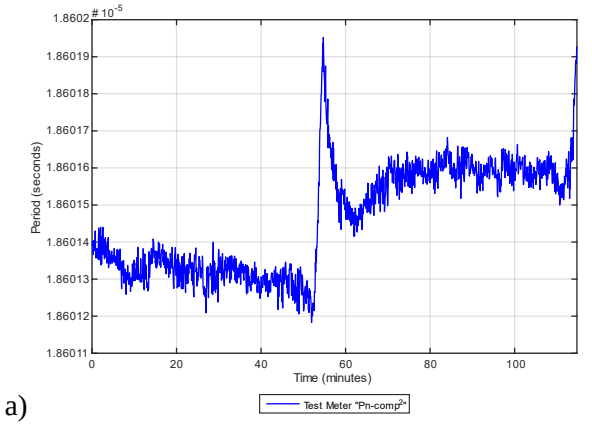

a)

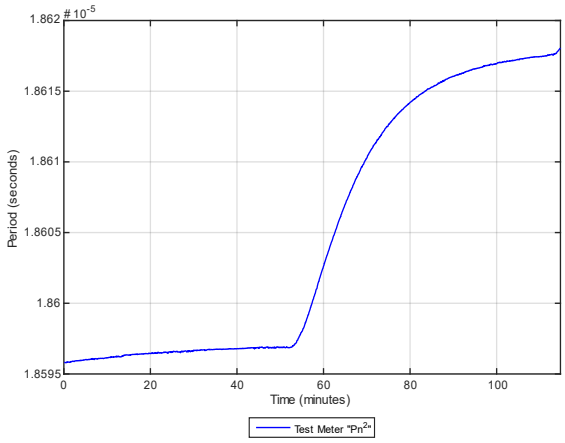

b)

Figure 5-23 Temperature compensated period (a) and raw period (b) response with damping term now active.

An 'ideal' damping term of 155 seconds, 132 seconds and 151 seconds were applied to tests 1, 2 and 3 respectively. The need for differing damping terms reinforces the fluid dependency observations of this thesis with respect to the thermal conductivity and overall response in the raw harmonic period value.

The effect on the data reported in section 5.9.2 is shown in Figure 5-24, with the drift originally observed during the temperature transition regions now reduced.

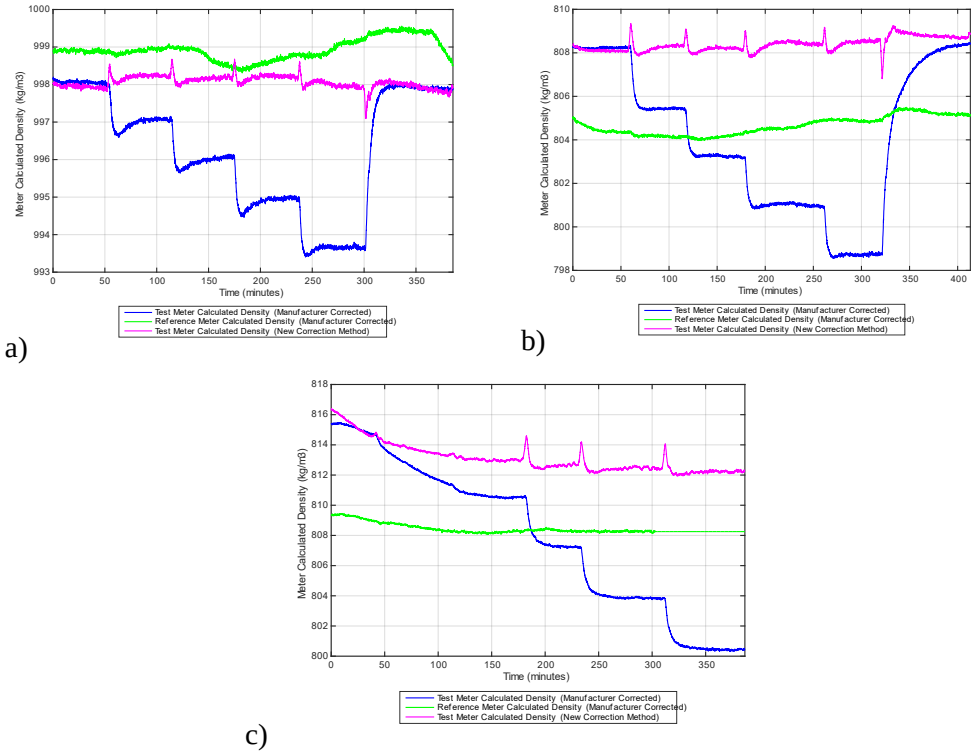

Figure 5-24 Comparison of new correction method response (damped) vs original manufacturer correction method. a) Test 1 (Water) b) Test 2 (Kerosene) c) Test 3 (Gas Oil)

The maximum error observed during a 10°C air temperature change was reduced to +0.08, +0.15 and +0.2 for water, kerosene and gas oil respectively as a result of implementing period damping as shown in Figure 5-25.

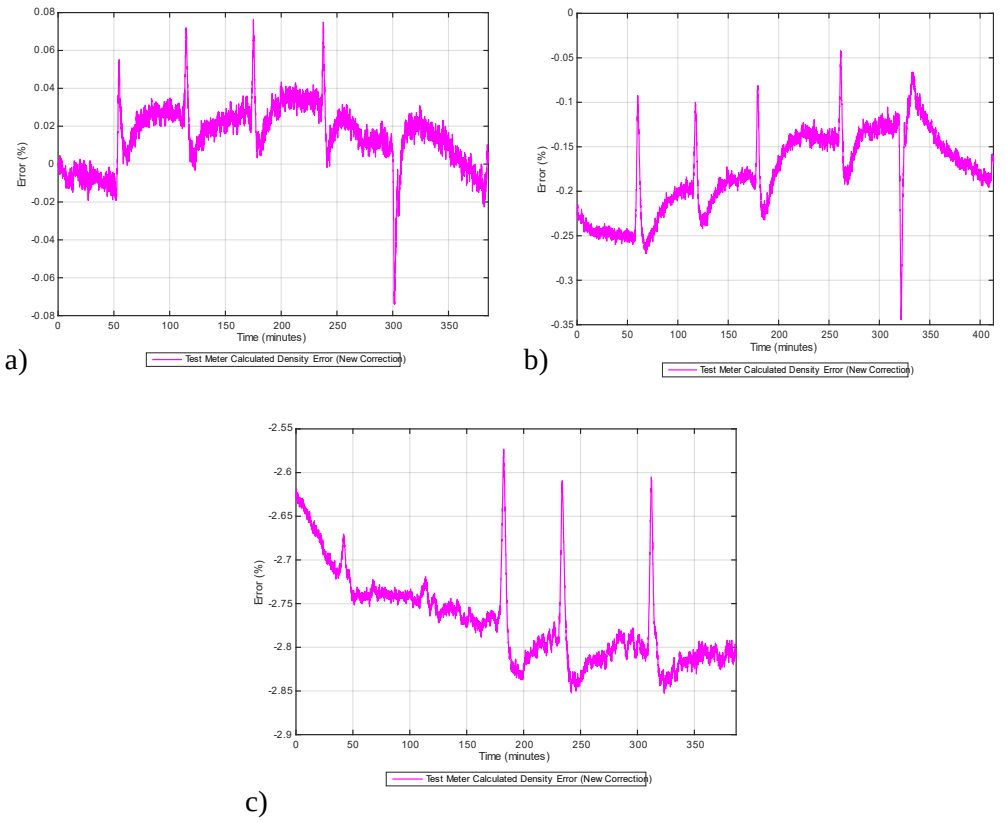

Figure 5-25 New correction method (damped) errors with respect to the know fluid properties. a) Test 1 (Water) b) Test 2 (Kerosene) c) Test 3 (Gas Oil)

Therefore, the X coefficient logic described in section 5.9.4 was further modified to include automatic selection of the fluid specific damping term.

If f_{20} is < 232.0 and > 231.4 then X = 12.5 and D = 155 seconds (Water)

If f_{20} is < 233.3 and > 232.8 then X = 5.5 and D = 132 seconds (Kerosene)

If f_{20} is < 232.5 and > 232.1 then X = 3.5 and D = 151 seconds (Gas Oil)

The results of tests 1 – 3 with the damping terms applied are summarised in Table 5-5.

Table 5-5 Summary of new correction (damped) and manufacturer correction method response

Test No	New Correction Density Value at minimum air temperature (kg/m3)	New Correction Error at minimum air temperature (%)	Transition region error recorded at minimum air temperature (%)	New Correction Density Value at maximum air temperature (kg/m3)	New Correction Error at maximum air temperature (%)	Transition region error recorded at maximum air temperature (%)	Manufacturer Correction Density Value at minimum air temperature (kg/m3)	Manufacturer Correction Error at minimum air temperature (%)	Transition region error recorded at minimum air temperature (%)	Manufacturer Correction Density Value at maximum air temperature (kg/m3)	Manufacturer Correction Error at maximum air temperature (%)	Transition region error recorded at minimum air temperature (%)
1	997.8	-0.01	-0.06	997.9	+0.01	+0.07	997.9	+0.01	-0.13	993.6	-0.42	-0.45
2	808.0	-0.25	-0.1	808.5	-0.125	-0.04	808.2	-0.23	-0.58	798.7	-1.35	-1.35
3	816.2	-2.62	N/A	812.2	-2.81	-2.60	815.3	-2.73	N/A	800.4	-4.22	-4.22

In practice, when fully implemented in the Coriolis meter firmware, the damped period values described above should be stored in a separate Modbus register so as to distinguish them from the “live” period values used elsewhere in process values calculations and tube oscillation control. It should also be noted that the selected damping terms and the associated results apply to the specific conditions and facility conditions tested as part of this research project. It is likely that in real world scenarios these terms would be tuned as part of a commissioning phase for a new meter installation, in a similar manner as suggested for determining the X coefficient value.

5.9.5 Statistical analysis of new method performance

Figure 5-26 shows the modified Pearson correlation, accounting for the response of the new correction method.

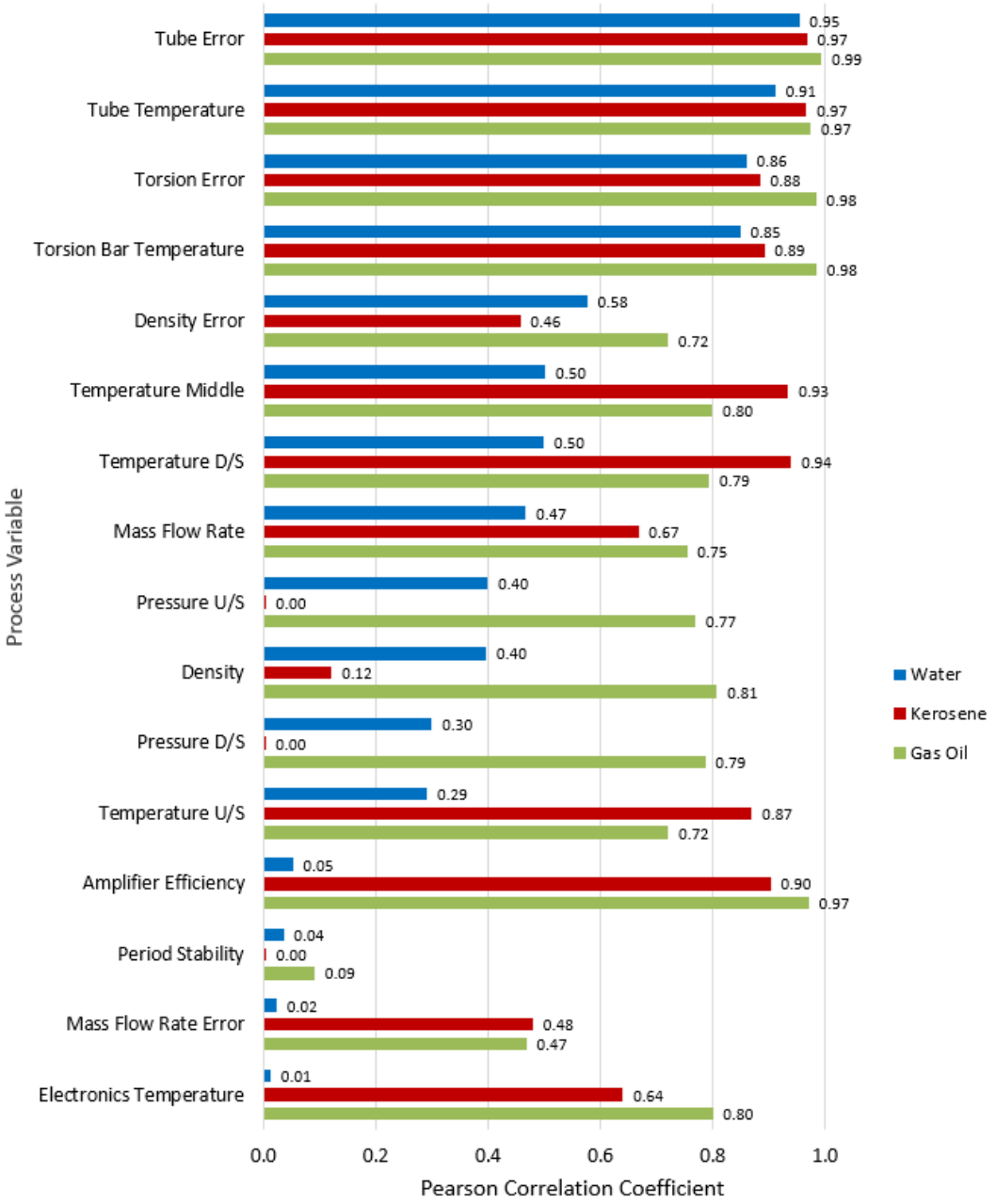

Figure 5-26 Tests 1 – 3 Pearson correlation coefficients for test meter diagnostic values based on new temperature correction algorithm and facility reference instrumentation values with respect to differing fluid properties and oven air temperature.

The coefficients confirm that although, the Pearson correlations relating to the physical temperature sensors remain unchanged and highly correlated with ambient air temperature, their impact on the new equation's structure and data output has significantly reduced the density and density error value coefficients across the three fluids.

The corresponding covariance values highlight the new correction method's density value and associated dependence, the results of which are shown in Figure 5-27.

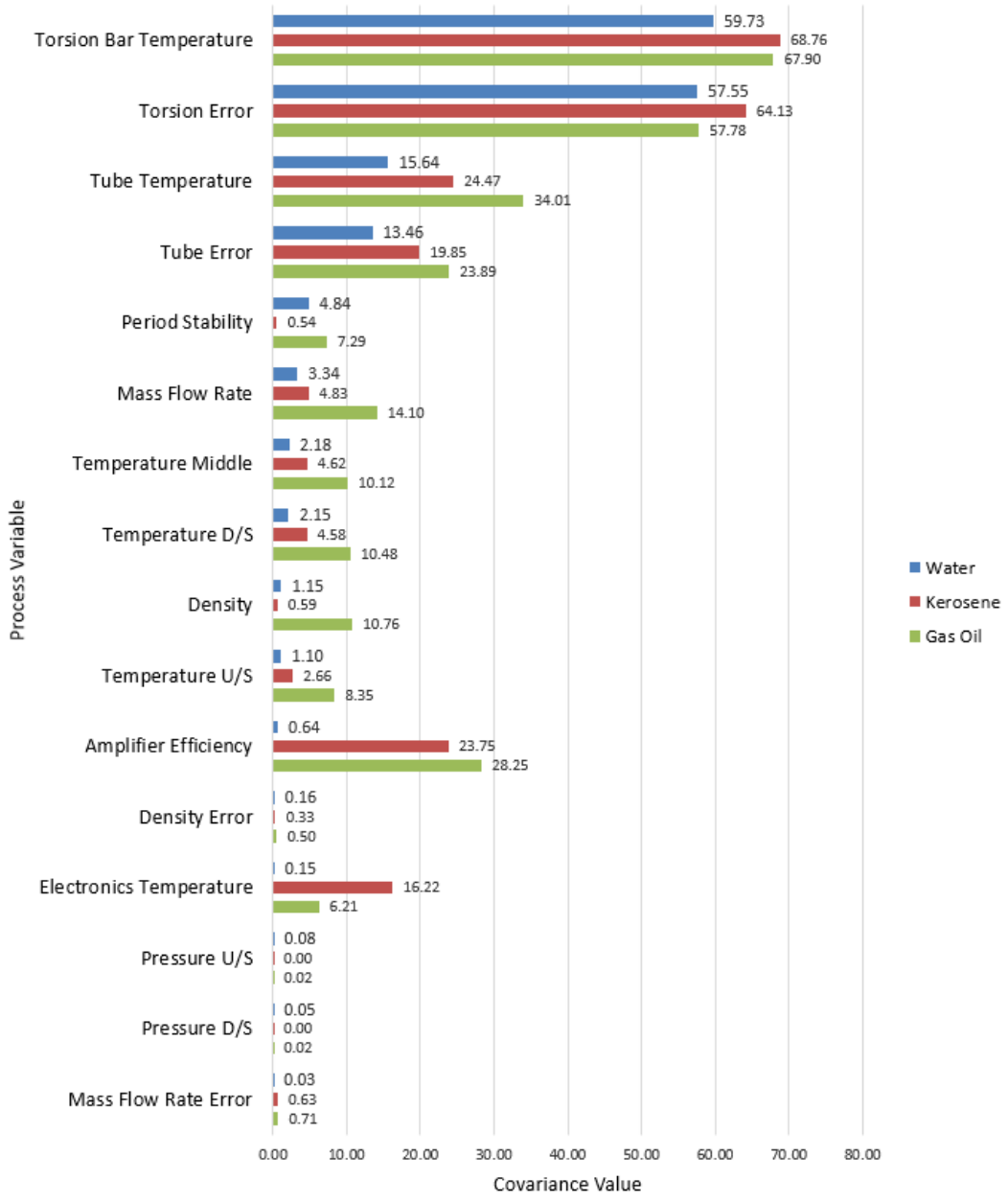

Figure 5-27 Tests 1- 3 covariance values demonstrating new temperature correction algorithm reducing density calculation dependency on oven air temperature for the three fluids tested.

The covariance data validates the effectiveness of the solution. The density covariance values with respect to oven air temperature have been reduced from values of 24.36 (water), 51.90 (kerosene) and 65.59 (gas oil) to 1.15 (water), 0.59 (kerosene) and 10.76 (gas oil).

5.10 **Conclusions**

The results described in this chapter have proposed that, with full access and understanding of meter design and operation, it is possible to correct for the effects observed in chapter 4. The specific process value importance and dependence on air temperature has been established by the experimental methods and results described, as well as the statistical analysis. The modified harmonic period temperature compensation equation (Equation 26) is able to provide repeatable and stable fluid density calculations while the air temperature surrounding the meter causes changes in the elasticity of the measuring tubes.

In addition, it has been shown that with enough data it is possible to implement automatic and fluid specific coefficient selection via frequency drift and temperature differential assessment within the transmitter. The results have shown that with this implementation the meters are now capable of calculating the correct value of fluid density for three distinct fluid properties at stable temperatures and flow rates without the need for manual reprocessing of the results.

In summary the proposed modifications would change the overall structure of Rheonik's fluid density calculation as shown in Figure 5-28.

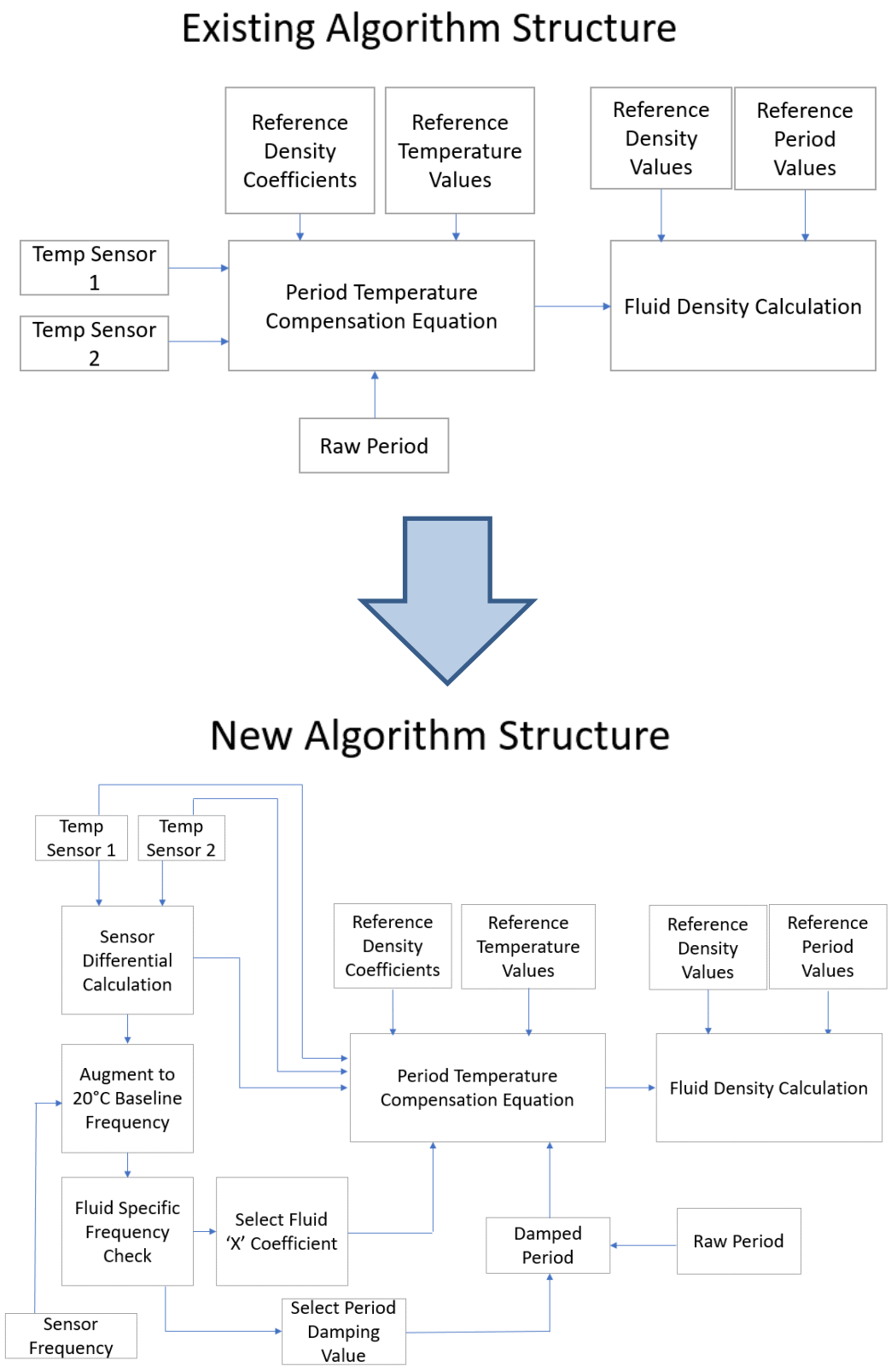

Figure 5-28 Block diagram comparison of Rheonik's existing harmonic period and density calculation with the proposed new model.

It is anticipated by the author that in practice, in order to generate a truly effective X value for specific operating conditions and fluids, one would be required to undertake an extended meter response profiling exercise that included the experimental and data analysis steps detailed in the preceding sections, where all anticipated flow rates and temperature differentials are simulated. For example, although in terms of Equation 26 X is a single parameter, the ideal value of said parameter was found to vary depending upon the temperature range for which it was applied.

The data sets and results described in this chapter represent a first step in this process. Once a complete data set is obtained covering all potential installation scenarios it could be implemented by Rheonik as an upgrade to existing products currently installed in the field or as an improvement to new product design by mapping specific field conditions to the reference data and generating a corresponding X coefficient.

Since this method does not require the manufacturer to add additional sensors, change the physical device structure or change their standard factory calibration and setup process, this outcome is therefore in line with the objectives outlined in Chapter 1.

The data contained within this chapter has answered the second research question of the thesis. It is possible to compensate for ambient temperature effects on Coriolis flow meters. The next chapter will address the final research question of the thesis, as well as provide further validation of the solutions performance, with non-incremental changes in ambient air temperature combined with fluctuating fluid flow and changes in fluid temperature.

Chapter 6

6 Validation of Solution Transferability and Extreme Environmental Testing

6.1 Overview

This chapter describes the experiments undertaken and associated results used to assess the transferability of the new correction method to a new design of meter developed by Rheonik. In addition, the experiments undertaken were designed to expose the test meter and new correction method to transient conditions representative of potential changes in ambient air temperature, fluid temperature and fluid viscosity that may be met in field service.

6.2 Experiment Setup

The flow facility, associated reference instrumentation and temperature control units were not altered from the design used in chapter 5, with the only change to the setup being the Coriolis meters themselves. Variables included fluid properties, air temperature heating pattern, repeat points at lower fluid temperatures and mass flow rate fluctuations. Table 6-1 details the individual tests.

Table 6-1 Test matrix

Test No	Fluid	Highest Fluid Flow Rate (kg/hr)	Lowest Fluid Flow Rate (kg/hr)	Description of Fluid Flow Change (kg/hr)	Test Meter Air Temp Setpoint Pattern (˚C)	Time Spent at Test Meter Air Temp (hrs:mins)	Reference Meter Air Temp (˚C)	Initial Fluid Setpoint Temp (˚C)	Final Fluid Setpoint Temp (˚C)	Test Duration (Hrs)	Comment
1	Water	100	100	N/A	40, 20, 60	2:00, 1:00, 1:00	20	20	30	3.5	Fluctuating test air temperature, increasing fluid temperature
2	Water	100	100	N/A	20, 30, 40, 50, 60	1:00, 1:00, 1:00, 1:00, 1:00	20	20	20	5	Increase in test air temperature (repeat of standardised phase 2 tests)

Test No	Fluid	Highest Fluid Flow Rate (kg/hr)	Lowest Fluid Flow Rate (kg/hr)	Description of Fluid Flow Change (kg/hr)	Test Meter Air Temp Setpoint Pattern (˚C)	Time Spent at Test Meter Air Temp (hrs:mins)	Reference Meter Air Temp (˚C)	Initial Fluid Setpoint Temp (˚C)	Final Fluid Setpoint Temp (˚C)	Test Duration (Hrs)	Comment
3	Kerosene	86	86	N/A	20, 30, 40, 50, 60	1:00, 1:00, 1:00, 1:00, 1:00	20	20	20	5	Increase in test air temperature (repeat of standardised phase 2 tests)
4	Kerosene	86	86	N/A	60, 20, 60, 20, 40, 20	0:15, 0:05, 0:30, 0:30, 0:30	20	20	20	2.5	Fluctuating test air temperature
5	Kerosene	82	82	N/A	20, 30, 40, 50, 60	1:00, 1:00, 1:00, 1:00, 1:00	20	13	15	5	Viscosity effects test – chilled fluid, increase in test air temperature
6	Kerosene	82	82	N/A	60, 20, 60, 20, 40, 20	0:15, 0:05, 0:30, 0:30, 0:30	20	15	15	2.5	Viscosity effects test – chilled fluid, fluctuating test air temperature
7	Kerosene	86	86	N/A	20, 40, 25	0:30, 1:00, 0:20	20	20	30	2	Fluid heating over two stable test air temperatures
8	Kerosene	88	50	Reduced to 50 for 20 mins then returned to 88	60	2:30	20	20	20	1.5	High test air temperature, fluctuating flow
9	Gas Oil	45	45	N/A	20, 40, 20, 60	0:05, 1:00, 0:30, 0:30	20	20	30	2.5	Fluid heating with test air temperature fluctuation
10	Gas Oil	40	40	N/A	20, 30, 40, 50, 60	1:00, 1:00, 1:00, 1:00, 1:00	20	14	18	3.5	Viscosity effects test – chilled fluid, increase in air temperature
11	Gas Oil	40	40	N/A	60, 20, 60, 20, 40, 20	0:15, 0:05, 0:30, 0:30, 0:30	20	17	17	2.5	Viscosity effects test – chilled fluid, fluctuating test air temperature
12	Gas Oil	47	47	N/A	20, 30, 40, 50, 60	1:00, 1:00, 1:00, 1:00, 1:00	20	20	20	5	Increase in test air temperature (repeat of standardised phase 2 tests)
13	Gas Oil	47	47	N/A	60, 20, 60, 20, 40, 20	0:15, 0:05, 0:30, 0:30, 0:30	20	20	20	2.5	Fluctuating test air temperature
14	Gas Oil	45	25	10 / 10 mins (returned to 45 at end)	40	2:00	20	20	20	2	Fluctuating flow, extended logging at end to observe settling time
15	Gas Oil	45	25	10 / 10 mins (returned to 45 at end)	60	3:00	20	20	20	3	Fluctuating flow, extended logging at end to observe settling time (higher test air temperature)

Rheonik provided two identical Coriolis meters that were, at the time of testing, in the prototype stage. The physical structure of the device represented the intended design of future products which will ultimately replace the devices tested in chapter 5.

The meter specification for this final phase of testing was as follows: -

Meter Type: -

- 2 of Omega shaped, dual tube Coriolis flow meter.
- Model RHM02S (Prototype design)

Sizing: -

- 0.25” Coriolis Meter
    - ±0.10% of flow rate
    - ±5 kg/m^3

Communications: -

- Transmitter Model RHE27
- Pulse Output
- 4-20mA Output
- RS485 Output

Custom Features: -

- Removable meter case to allow access to meter internals
- Ability to access correction factors and reference values stored on meter transmitter

Figures 6-1 to 6-3 show the mechanical and electrical internals of a prototype RHM02S Rheonik Coriolis meter. The key components of the device are highlighted noting the difference in structure compared to that of the RHM04. While the omega shaped sensor structure has been retained for the RHM02S, there are notable differences in the geometry when compared to the RHM04. For example, the torsion bar and excitation coil configuration structure has been reconfigured from a solid dual beam structure to suspended frame structure, in doing so reducing the mass of metal used in device construction. In doing so, the manufacturers hope to increase the overall device sensitivity. Both the tube and torsion bar temperature sensor locations remain unchanged.

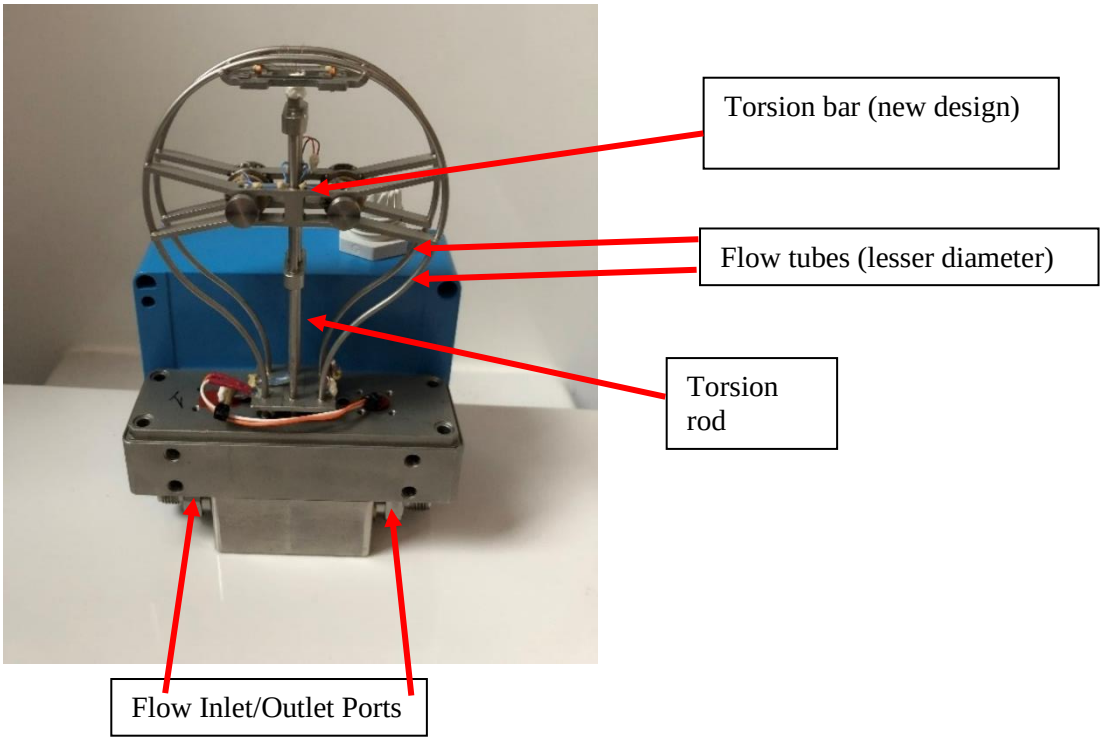

Figure 6-1 Rheonik RHM02S Prototype meters with key mechanical components highlighted

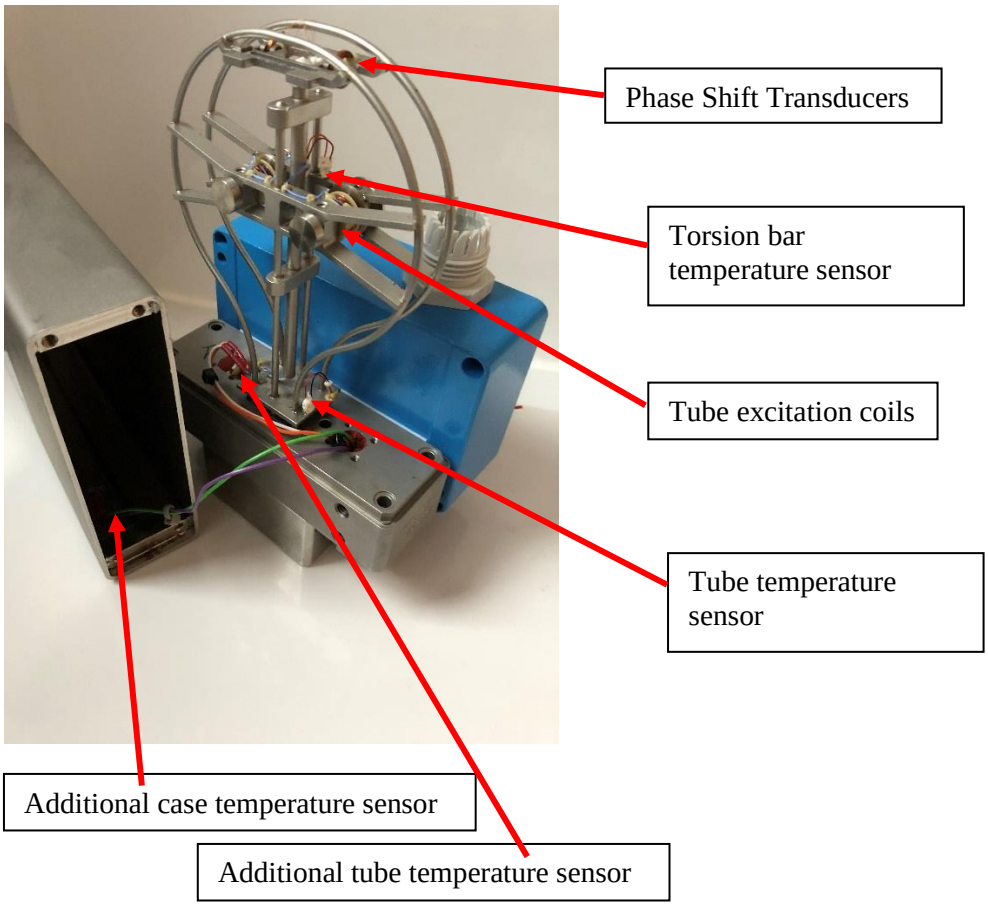

Figure 6-2 Rheonik RHM02S Prototype meters with sensor and drive components highlighted

Side by side comparison of RHM04 (left) and RHM02S with covers removed (above) and fitted (below).

Figure 6-3 Rheonik RHM02S Prototype meters with protective covers fitted.

Despite the physical modifications to the flow meter design, it should be noted that the mass flow and temperature correction algorithms (Equations 23, 24 and 25) deployed by the manufacturer remain unchanged. The coefficients derived by the manufacturer for the new test and reference meter are detailed in Table 6-2.

Table 6-2 Mass flow and density temperature compensation coefficients provided by the manufacturer for use with both the reference and test meters

	U_{00}	U_{10}	U_{01}	S_{01}	S_{10}	$T_{1\,Ref}$	T_{2Ref}	$\rho_{1\,(air)}$	$\rho_{2\,(water)}$	$P_{1\,(air)}$	$P_{2\,(water)}$	$T_{1Ref(Dens)}$	$T_{2Ref(Dens)}$
Ref	1	-0.000118627	-0.0003559	0.000119666	-0.000429637	20.0	20.0	1.2	998.16	1.99173E-05	2.05307E-05	20.32	20.48
Test	1	-0.000171914	-0.0002865	0.000194586	-0.000628976	20.0	20.0	1.2	998.16	1.93683E-05	1.99619E-05	20.34	20.28

6.3 **Results**

In this section the results from the setup detailed in section 6.2 are analysed. The results from key test conditions are detailed in 6.3.1 and 6.3.2 with appropriate figures to demonstrate transient response. The data was selected for presentation here as being representative of the distinct operating conditions tested and demonstrates the new correction method's response to said conditions.

6.3.1 Direct Comparison with RHM04 results

The data from tests 2, 3 and 12 are described in this section. The test conditions recreated those of the tests described in chapter 5 and were used as an assessment of the correction methods transferability between the RHM04 and RHM02S models.

The new correction method's logic pertaining to automatic X coefficient selection was modified to account for the new meters differing resonant frequency at 20°C (Table 6-2). In addition, the damping values were set to zero during initial data analysis.

6.3.1.1 Water

Figure 6-4 shows the calculated density values and associated errors with respect to the known fluid density using both the manufacturer's original method and the new correction method.

Undamped

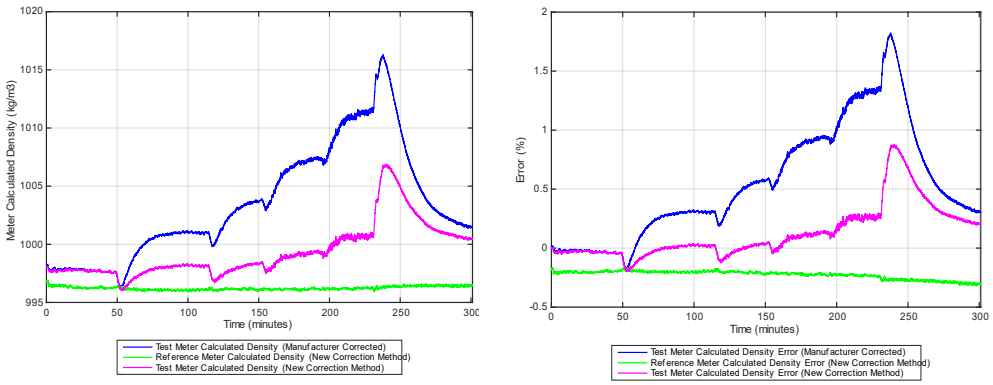

a) b)

Figure 6-4 Comparison of new correction method response (undamped) vs original manufacturer correction method in water. a) Density response, b) Errors with respect to known fluid properties

The new correction method was observed to perform more efficiently than the manufacturer's method with an error of +0.25% present at the maximum ambient air temperature of 65°C. At the same air temperature, the manufacturer's method reported a density value of 1012 kg/m^3, which was in error of +1.3%. It should be noted that due to the increased sensitivity of the new model, both the manufacturer error and new correction method errors have increased compared to those observed for the RHM04 meters tested in chapter 5 at the same conditions
(-0.42% and -0.12% for the manufacturer and new correction method respectively).

Figures 6-4b also showed that the temporary errors observed during the temperature transition regions were once again present in the meter output.

A value of 28 seconds was determined to be optimal (a reduction of 127 seconds compared to the RHM04 damping term for water) and the reduction in response and associated errors is shown in Figure 6-5.

Damped

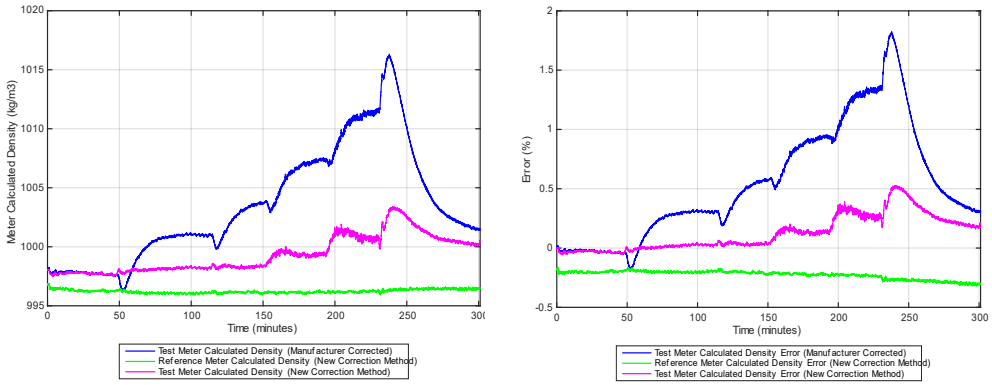

a) b)

Figure 6-5 Comparison of new correction method response (damped) vs original manufacturer correction method in water. a) Density response, b) Errors with respect to known fluid properties

The data shows that, with the damping term active, the maximum error observed on the new correction method (due to sudden cooling at 240 minutes) is reduced from 0.8% to 0.5%. The transition region errors pertaining to the first two ambient air temperature increases were effectively smoothed out at ~55 mins and ~120 mins. It should be noted that the transition errors (while reduced) are still present for the 40°C – 50°C, 50°C - 60°C and 60°C - 20°C air temperature regions, highlighting that for the RHM02S a single period value is not as effective for the temperature differentials tested compared to the RHM04s, which showed a consistent error reduction across all transition regions. It should also be noted that under the same conditions the RHM04 produced a density values with an error of +0.08% using the new correction method with a damping coefficient.

6.3.1.2 Kerosene

Figure 6-6 shows the calculated density values and associated errors with respect to the known fluid density of Kerosene using both the manufacturer's original method and the new correction method.

Undamped

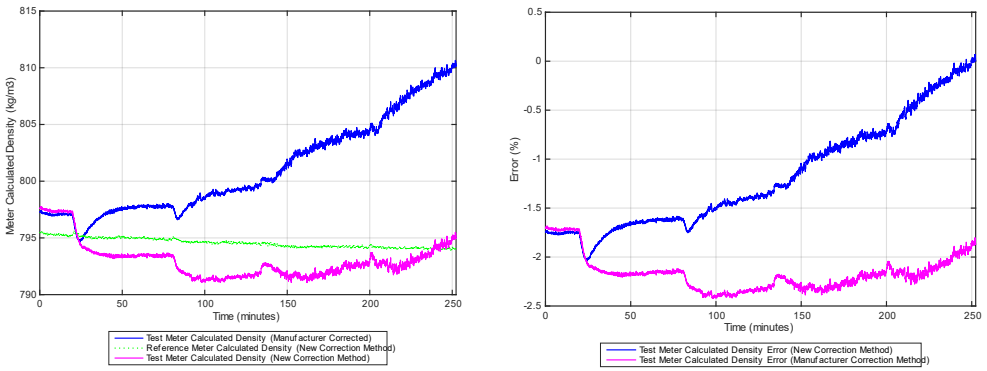

a) b)

Figure 6-6 Comparison of new correction method response (undamped) vs original manufacturer correction method in kerosene. a) Density response, b) Errors with respect to known fluid properties

The data revealed an offset in both the test and reference meters with respect to the true density at baseline conditions (20°C) with calculated density values containing a -1.7% error. This is a significant increase in meter baseline errors for kerosene when compared to the values obtained for the RHM04 meters (-0.22% for test meter and -0.62% for reference meter). This data further demonstrates the fluid dependency effects described in chapters 4 and 5 as well as highlighting that the difference in meter geometry, while effective for water, has potentially exaggerated the fluid property error potential inherent in the meter design and baseline calibration coefficients (Table 6-2).

The negative offset combined with the increasing density value drift with respect to ambient air temperature shown in Figure 6-6b is therefore misleading as it would appear that the error for both manufacturer and new correction methods decrease during the course of the test. For clarity, the data reported upon for kerosene in the remainder of this chapter has been tared with respect to the baseline conditions established between 0 – 20 minutes.

The tared error values for both the manufacturer and new correction methods are shown in Figure 6-7.

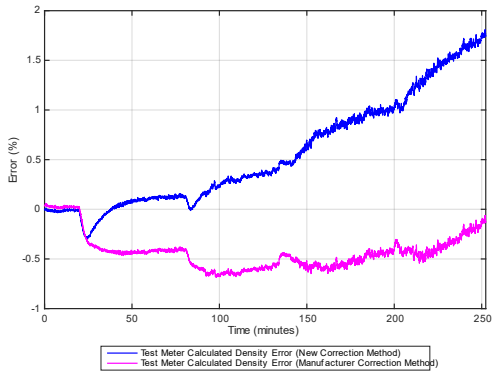

Figure 6-7 Resulting tared density calculation errors for kerosene with respect to baseline 20°C (air and fluid) conditions established in test 3

Figure 6-7 shows that by accounting for the initial offset, a maximum error value of -0.6% was observed using the new method compared to the maximum error of 1.75% in the manufacturer's correction algorithm. As noted in 6.3.1.1 these observed errors highlighted an increase from the values observed on the RHM04 meters under the same conditions (-0.25% using the new method and -1.3% using the manufacturers method).

A range of damping values were systematically applied to the data in an effort to establish an optimal reduction in transition errors (as done in 6.3.1.2), however it was found that no degree of damping could improve upon the undamped data. An optimal damping value of 28 seconds, was determined to maintain the overall errors observed for each air temperature transition, however the peak to peak transition region error was found to increase as shown in Figure 6-8.

Damped

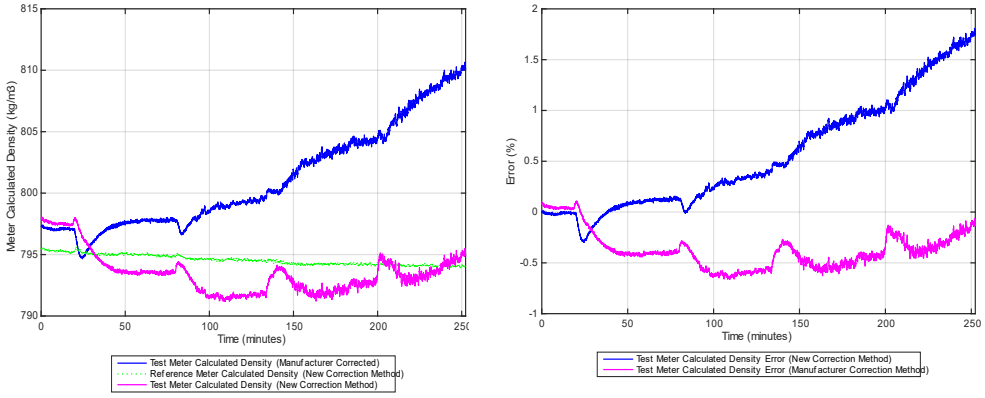

a) b)

Figure 6-8 Comparison of new correction method response (damped) vs original manufacturer correction method in kerosene. a) Density response, b) Errors with respect to baseline 20°C (air and fluid) conditions established in test 3

6.3.1.3 Gas Oil

Figure 6-9 shows the calculated density values and associated errors with respect to the known fluid density of Gas Oil using both the manufacturer's original method and the new correction method. During the 20°C baseline period (0 – 50 minutes) the error on both the manufacturer and new correction method is shown to deviate from an initial offset of -0.8% to a further -1.3%. This coincides with an increase in fluid temperature during this time, which was the result of pump/fluid heat transfer due to the increased work required to circulate a fluid of higher viscosity.

Undamped

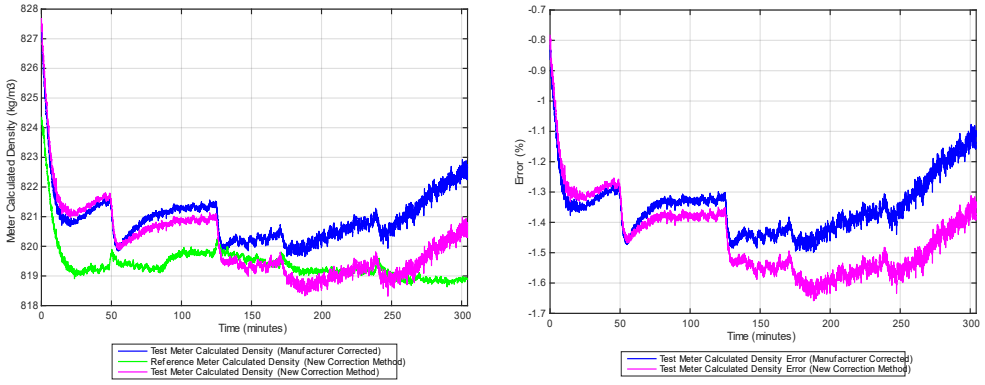

a) b)

Figure 6-9 Comparison of new correction method response (undamped) vs original manufacturer correction method in gas oil. a) Density response, b) Errors with respect to known fluid properties

As with the data described in 6.3.1.2, the errors were tared with respect to their 20°C baseline (fluid and air) values. The resulting data is shown in figure 6-10.

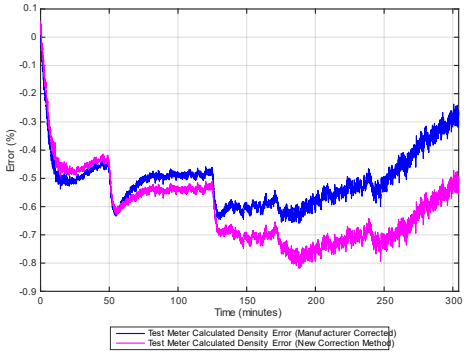

Figure 6-10 Resulting tared density calculation errors for gas oil with respect to baseline 20°C (air and fluid) conditions established in test 12

The data highlights that for Gas Oil, both the manufacturer and new correction method operate within narrower error margins compared to the observed performance in lower viscosity fluids (water and kerosene). In this instance, the new correction method is shown to perform with lesser efficiency than the manufacturer's method where maximum error values of -0.8% and -0.65% observed respectively. These values also represent the only reduction in fluid density errors over the older RHM04 designs (-3.13% and -4.2% using the new and manufacturer methods respectively).

A damping value of 18 seconds was applied to the period value to assess if either the overall performance or transition errors could be improved upon. The resulting data is shown in Figure 6-11.

Damped

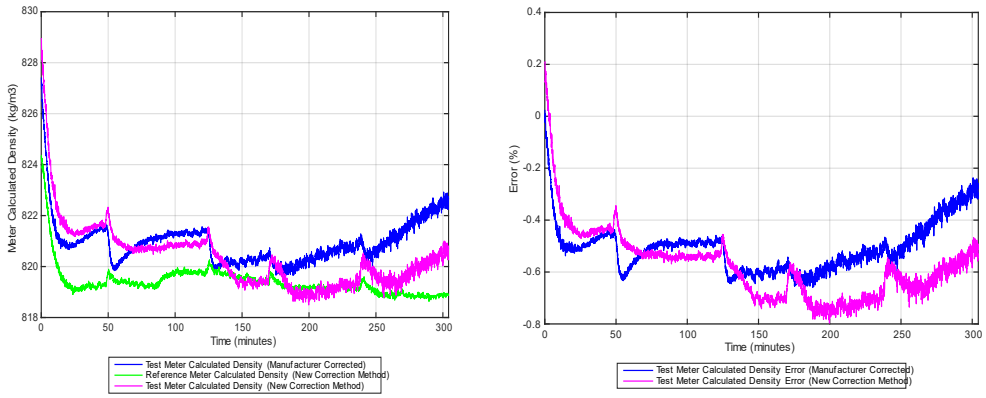

a) b)

Figure 6-11 Comparison of new correction method response (damped) vs original manufacturer correction method in gas oil. a) Density response, b) Errors with respect to baseline 20°C (air and fluid) conditions established in test 12

As observed with kerosene, the overall peak to peak error in the transition regions were shown to increase, with the overall errors due to each air temperature change ultimately unaltered once thermal equilibrium was achieved after each air temperature increase.

6.3.1.4 Conclusions

Summaries of the undamped and damped errors observed for the three fluids are detailed in Tables 6-3 and 6-4.

Table 6-3 Summary of test results (undamped)

Test No	New Correction Density Value at minimum air temperature (kg/m3)	New Correction Error at minimum air temperature (%)	Transition region error recorded at minimum air temperature (%)	New Correction Density Value at maximum air temperature (kg/m3)	New Correction Error at maximum air temperature (%)	Transition region error recorded at maximum air temperature (%)	Manufacturer Correction Density Value at minimum air temperature (kg/m3)	Manufacturer Correction Error at minimum air temperature (%)	Transition region error recorded at minimum air temperature (%)	Manufacturer Correction Density Value at maximum air temperature (kg/m3)	Manufacturer Correction Error at maximum air temperature (%)	Transition region error recorded at minimum air temperature (%)
1	997.5	-0.03	-0.19	1000.5	+0.24	+0.08	997.5	-0.03	-0.19	1011.6	+1.3	+0.88
2	797.6	+0.02	-0.42	795.4	-0.14	-0.30	796.9	-0.05	-0.30	810.17	+1.75	+1.00
3	821.6	-0.44	-0.62	820.4	-0.76	-0.57	821.64	-0.44	-0.63	822.36	-0.58	-4.22

Table 6-4 Summary of test results (damped)

Test No	New Correction Density Value at minimum air temperature (kg/m3)	New Correction Error at minimum air temperature (%)	Transition region error recorded at minimum air temperature (%)	New Correction Density Value at maximum air temperature (kg/m3)	New Correction Error at maximum air temperature (%)	Transition region error recorded at maximum air temperature (%)	Manufacturer Correction Density Value at minimum air temperature (kg/m3)	Manufacturer Correction Error at minimum air temperature (%)	Transition region error recorded at minimum air temperature (%)	Manufacturer Correction Density Value at maximum air temperature (kg/m3)	Manufacturer Correction Error at maximum air temperature (%)	Transition region error recorded at minimum air temperature (%)
1	997.5	-0.03	-0.03	1000.5	+0.24	+0.08	997.5	-0.03	-0.19	1011.6	+1.3	+0.88
2	797.6	+0.02	-0.42	795.4	-0.14	-0.18	796.9	-0.05	-0.30	810.17	+1.75	+1.00
3	821.64	-0.44	-0.36	820.4	-0.50	-0.72	821.64	-0.44	-0.63	822.36	-0.58	-4.22

The data has shown that the new correction method is able to correct the density value to account for the changes due to ambient air temperature on a differing design of meter when exposed to the replicated test conditions of chapter 5. However, while density calculation errors are reduced by using the new method over the existing manufacturer method, the remaining errors using the new method were found to greater on the RHM02 compared to the RHM04 (chapter 5) for both water and kerosene.

Despite the increase in errors observed between models, the data does demonstrate that the new correction method is transferable to the new design of meter which going forward is expected to be the manufacturer's replacement to the RHM04 design (tested in chapter 5).

Discussions with the manufacturer regarding the offsets observed for both Kerosene and Gas Oil confirmed that while the values observed are larger than expected, the manufacturer at the time of writing has not undertaken similar validation of the new meter designs in fluid densities which are comparable to Gas Oil and Kerosene. Therefore, the data sets described herein represent the only observations currently available of the RHM02S performance with fluid densities less than that of water and have enlightened the manufacturer as to the potential for error under such operating conditions.

While applying a damping term to the data collected for water was found to increase the efficiency of the new correction method, it was shown that for the lower density fluids the use of a damping term had a detrimental impact on the quality of the data.

The lesser performance of the new correction method in gas oil highlighted a potential viscosity limit with respect to the effectiveness of the new method on this design of meter that was not observed on the RHM04.

6.3.2 Non–Ideal Operating Conditions

Having established that the new temperature correction method is applicable to the RHM02S design, the data presented in the following sections pertains to non-ideal operating conditions. The data discussed in this section makes use of the new correction X coefficient values and damping terms established generated in 6.3.1.

6.3.2.1 Test 1 Increasing water temperature with sudden test meter air changes

The reference measurements for test 1 are shown in Figure 6-12.

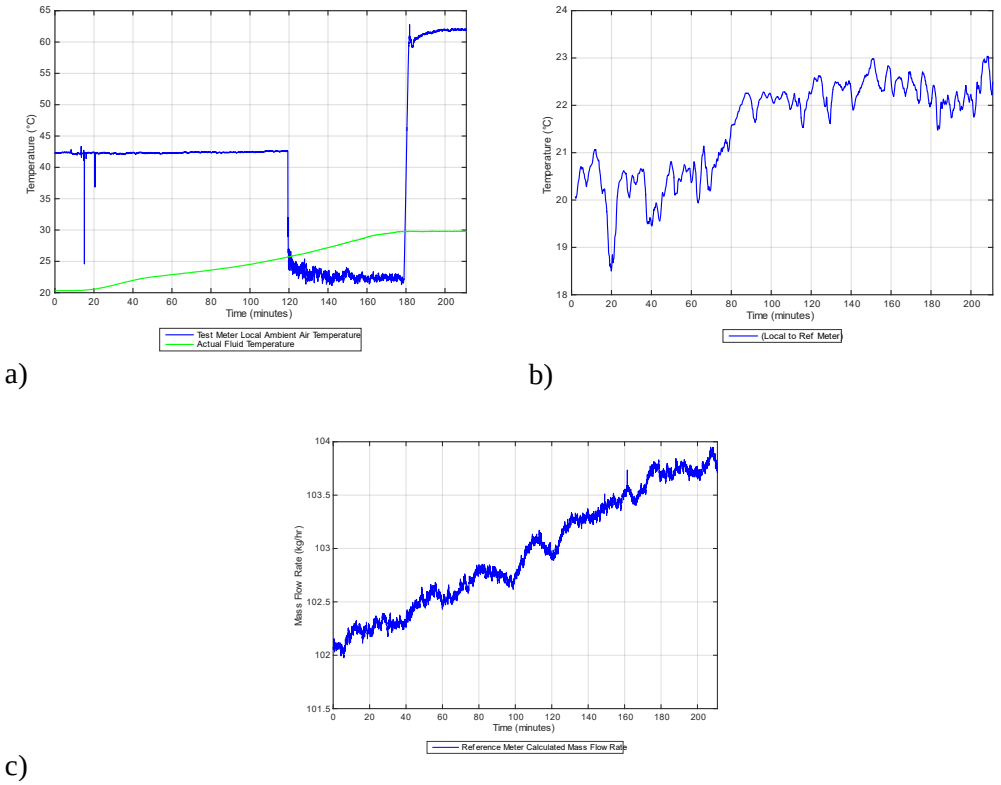

Figure 6-12 Reference measurements a) Test meter air temperature and actual fluid temperature, b) Reference meter air temperature, c) Mass flow rate

The performance of the new correction method is shown in Figure 6-13.

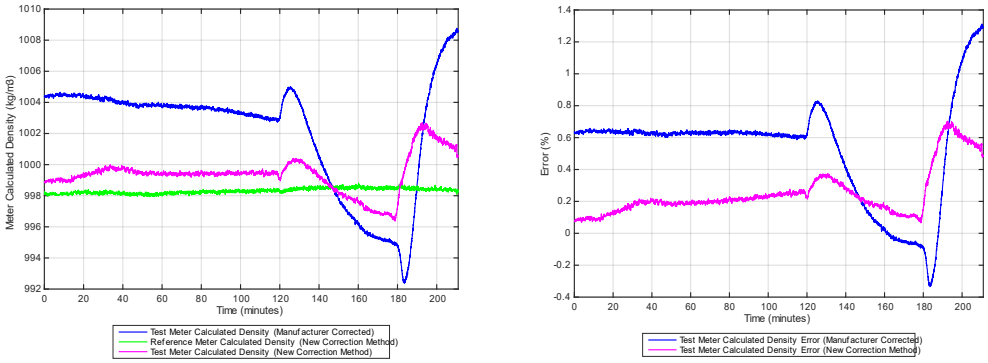

a) b)

Figure 6-13 Comparison of new correction method response (damped) vs original manufacturer correction method in water. a) Density response, b) Errors with respect to known fluid properties

The data between 0 and 120 mins shows that the new method corrected for the already elevated ambient air temperature (42.5°C) with errors minimised to a maximum value of +0.25% compared to the 0.65% error observed as per the manufacturers existing methods. When the test meter air temperature was rapidly cooled from 42.5°C to 22.5°C between 120 and 180 minutes, the error associated with new correction method is shown to temporarily increase to 0.35% before falling to within the initial baseline value. When the air temperature is increased to 62°C at 180 mins, the error increases to a temporary value of 0.7% before beginning to show a decrease. In comparison, the manufacturers correction method error is shown to increase to 1.3% and shows no sign of reduction before the test ends at 210 minutes.

6.3.2.2 Test 4 Kerosene - Sudden test meter air changes

The data from Test 4 shows the response of the new correction method in an environment where the surrounding air temperature is suddenly increasing and decreasing over a period of 2.5 hours (detailed in Table 6-1). The reference measurements for test 4 are shown in Figure 6-14.

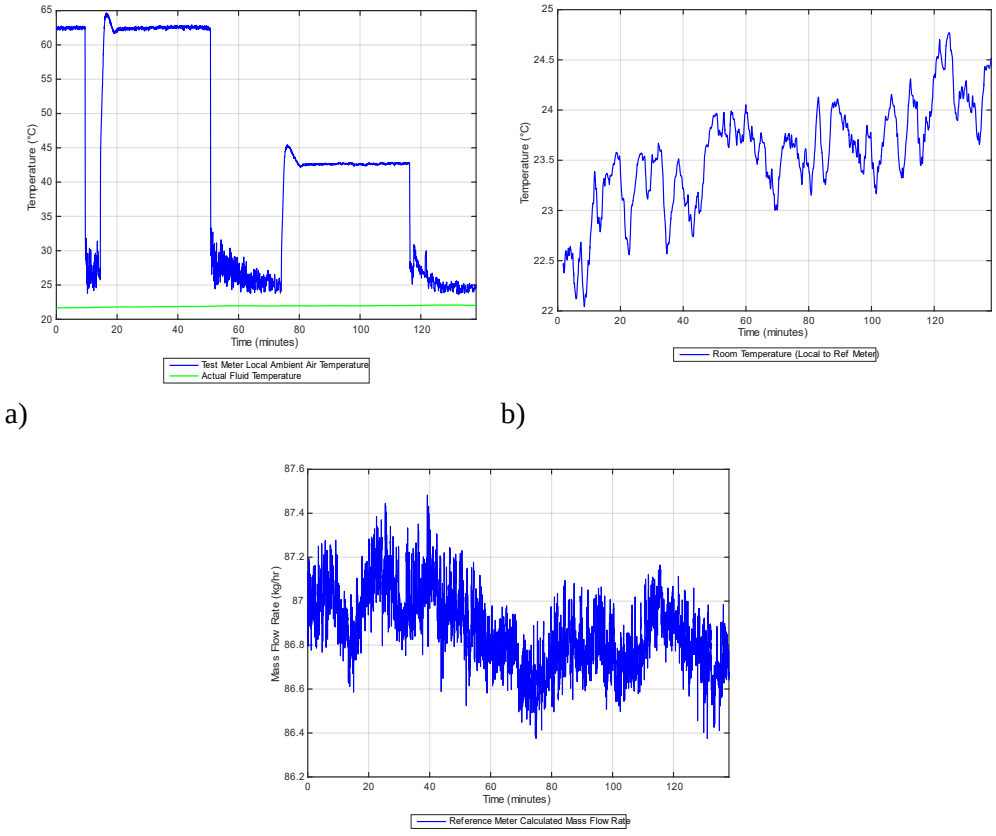

Figure 6-14 Reference measurements a) Test meter air temperature and actual fluid temperature, b) Reference meter air temperature, c) Mass flow rate

The response of the new correction method vs the manufacturer method is shown in Figure 6-15. With no damping term active, the new correction method was found to contain temporary errors of +1.45% during the 60°C – 20°C cool down period (50 – 75 minutes). Note that the test started (0 - 10 minutes) with an elevated ambient air temperature of 60°C and as such the new correction method is shown to have corrected the density value to within an error -0.1% with respect to the baseline offset. During the same time period, the manufacturer method is shown to contain a 1.80% error.

Undamped

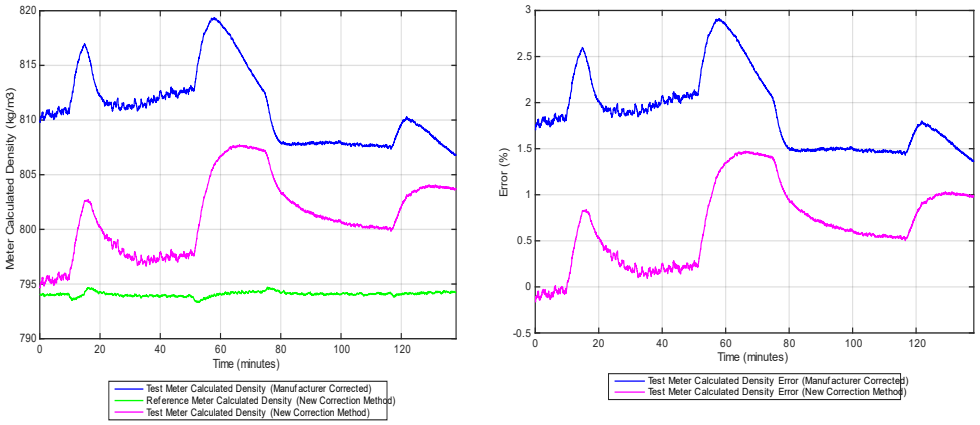

a) b)

Figure 6-15 Comparison of new correction method response (undamped) vs original manufacturer correction method in kerosene. a) Density response, b) Errors with respect to baseline 20°C (air and fluid) conditions established in test 3

By applying the damping term, a reduction in errors was observed during the transition regions. The maximum error observed during the test was reduced from +1.45% to +1.25%.

The improved response using the damping term contrasts with the data observed in test 3 (section 6.3.1) and highlights that for the RHM02S, a damping term is in fact still effective in improving the density calculation performance during more extreme air temperature fluctuations.

6.3.2.3 Test 8 Kerosene – Elevated test meter air temperature and sudden fluid flow changes

The data collected during test 8 shows the new correction method vs manufacturer correction method response to fluctuating flow rates at elevated ambient temperatures.

The reference conditions for test 8 are shown in Figures 6-16. Figure 6-16a shows that after an initial 20 ambient baselining between 0 and 12 minutes, the test meter air temperature was increase to 60, where it remained for the duration of the test. The facility was then allowed to reach thermal equilibrium over a period of 45 minutes, after which time the mass flow rate was reduced from 90 to 45 kg/hr (Figure 6-16c). At 77

minutes, the flow rate was then returned to 90 kg/hr where it remained until 105 minutes, at which point the flow was reduced to 0 kg/hr.

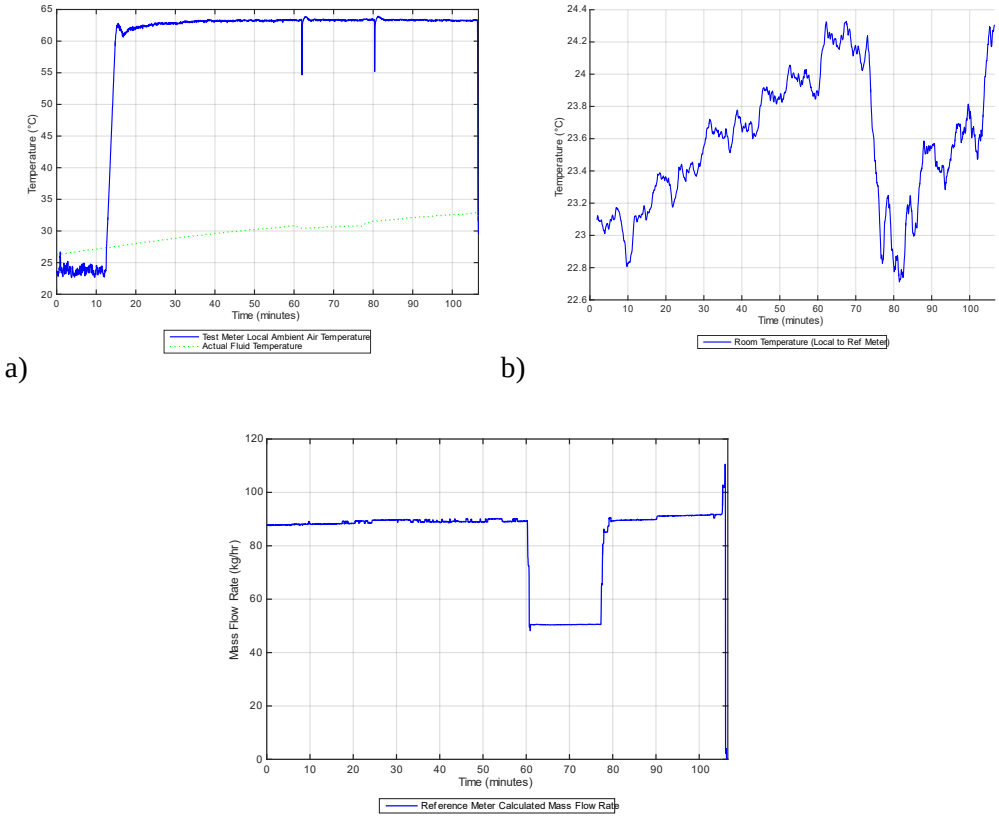

Figure 6-16 Reference measurements a) Test meter air temperature and actual fluid temperature, b) Reference meter air temperature, c) Mass flow rate

The undamped response of the new correction method vs the manufacturer method is shown in Figures 6-17. Note that at the start of the test, both the new and manufacturer correction methods contain errors with respect to the established 20°C offset. Given that the fluid temperature at the start of the test was measured to be 26°C by the facility reference RTDs, the increase in error indicated a potential fluid temperature dependency.

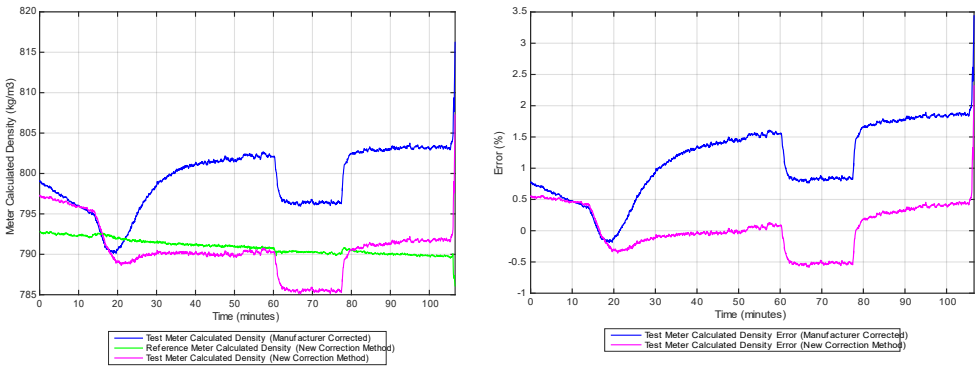

a) b)

Figure 6-17 Comparison of new correction method response (undamped) vs original manufacturer correction method in gas oil. a) Density response, b) Errors with respect to baseline 20°C (air and fluid) conditions established in test 12

The error on the new correction method after the initial air temperature increase is shown to reach -0.25% (-0.75% reduction from starting point) and settle at 0% (a -0.5% reduction from starting point). The manufacturer's calculated density is shown to be +1.5% in error (an increase of 0.8% from baseline of this test). When the flow rate was reduced by 50% at 60 minutes, an immediate negative bias is imparted on both the manufacturer and new correction method data. The new correction method's density value was shown to contain a further -0.6% error, while the manufacturer's calculated value contained a further -0.7%.

6.3.3 Results Summary

The tests and resulting data described in this section have shown that the new method is capable of calculating fluid density values containing reduced errors with respect to the know fluid properties when comparted to the existing methods used by the manufacturer. Specifically, the new method was shown to be effective for water and kerosene over a number of fluctuating ambient and flowing conditions. The new correction method was shown to be ineffective for gas oil during the direct chapter 5 comparison test (test 12).

Table 6-5 Summary of test results

Test No	New Correction Minimum Density Calculation Error Observed (%) Undamped	New Correction Maximum Density Calculation Error Observed (%) Undamped	New Correction Minimum Density Calculation Error Observed (%) Damped	New Correction Maximum Density Calculation Error Observed (%) Damped	Manufacturer Correction Minimum Density Calculation Error Observed (%)	Manufacturer Correction Maximum Density Calculation Error Observed (%)
1	-0.29	+0.52	+0.06	+0.70	-0.33	+1.31
4	-0.16	+1.74	-0.23	+1.74	+1.36	+2.91
5	-0.84	+0.27	-0.80	+0.33	-0.04	+2.07
6	-0.21	+1.65	-0.34	+1.71	+1.81	+3.24
7	-0.38	+0.60	-0.31	+0.57	-0.28	+1.16
8	-0.59	+2.33	-0.54	+3.41	-0.19	+3.44
9	-1.21	-0.04	-1.07	-0.02	-1.12	+0.13
10	-1.41	-0.29	-1.34	-0.21	-0.86	-0.23
11	-1.22	+0.50	-1.33	0.44	-0.54	+0.97
13	-0.89	+0.49	-0.95	+0.25	-0.30	+0.92
14	-1.25	-0.77	-1.30	-0.74	-0.98	-0.49
15	-1.61	-0.53	-1.70	-0.52	-1.07	+0.03

6.4 Summary

The results described in this chapter have demonstrated that the new correction method developed by this thesis can be transferred to a Coriolis meter of differing mechanical design. The new method was shown to contain lower error values across the temperature differentials tested than the manufacturer's method for water and kerosene. The tests conducted with gas oil highlighted that the efficiency of the new method on the new RHM02S sensor is limited, indicating a potential viscosity dependence.

The new correction method was also shown to contain lower error values than the manufacturer's method during extreme air temperature and mass flow fluctuations, as well as accounting for combinatory effects of increasing fluid temperatures.

This chapter has therefore answered the third and final research question posed by the thesis. The new methods developed can be transferred to a different design of Coriolis flow meter. In the next chapter, overall conclusions for the thesis are discussed. Potential future research topics that further the discoveries of this thesis are also proposed.

Chapter 7

7 Conclusions and Proposed Future work

7.1 **Conclusions**

Through the experimentation and analysis described in chapters 4, 5 and 6 an understanding has been developed with respect to the effects of air to fluid temperature differentials on the efficiency of fluid density calculation using Coriolis flow meters. The findings described in chapter 4 answered the first research question posed by this thesis. The air temperature surrounding a Coriolis flow meter can induce errors in the data output by the device. This statement was found to be true for the differing manufacturers and differing meter geometries investigated throughout the thesis. In total, three manufacturers and four distinct meter geometries were tested as part of this body of work. All meters tested demonstrated errors in the fluid density calculation when the air temperature surrounding the meter was increased beyond the fluid temperature present within the flow tubes.

With the support of Coriolis meter manufacturer Rheonik, access to proprietary information pertaining to the mechanical build, setup and compensation algorithms allowed for the second research question to be answered. This thesis has shown that it is indeed possible to isolate the source of fluid density calculation error and automatically correct for the air temperature effects. This thesis has demonstrated a method that not only accounts for air temperature variation but also accounts for additional variables such as the effects of fluid property variation. Specifically, the new method is capable of automatically selecting correction coefficients best suited to the fluid present within its internals. The new method is capable of repeatably calculating the correct fluid density despite fluctuations in ambient air temperature and the associated effect on the thermal balance of the system. By repurposing the torsion bar temperature sensor as an indicator of temperature differentials between the fluid and air surrounding the meter body, the Coriolis meter now has an additional ‘awareness’ of its surroundings. The thesis has shown that the addition of damping parameters to the

period value has allowed for temporary error spikes during the transition region to be smoothed out in the final calculated density value, making the process value a viable parameter to feed into fluid contamination automation routines in process control systems as well as transient condition monitoring systems. The automatic compensation for fluid properties is a step change in compensation methods currently implemented by the meter manufacturers tested in this programme. The only comparable method was provided by manufacturer B's transmitter (Density Mode 2), however it was still limited by the requirement for manual reprogramming to account for fluid property changes and expected fluid temperature ranges.

The new method of correction was successfully deployed on both Rheonik's legacy design of transmitter RHM04 (Chapter 5) and their new generation model RHM02S (Chapter 6) and in doing so answered the third research question posed by this thesis. The new temperature correction methods are transferable to a meter of differing design. However, it should be noted that due to the reliance of the specific temperature sensor placement and additional knowledge provided by Rheonik, it is unlikely that the solution in its current form could be directly transferred to a competing manufacturer's device. Given that the principle of Coriolis meter-based fluid density calculation adheres to the same physics of device operation regardless of manufacturer, the underlying principles of the new method's operation are certainly applicable to other manufacturer designs once access to the same level of proprietary information has been granted.

In addition, the raw data collected as well as the experimental techniques developed throughout this thesis are a unique contribution to the fields of fluid density measurement and Coriolis flow metering technology. As found in chapter 2, there are no existing publications that target ambient temperature effects on Coriolis flow meters, an area this thesis and the resulting publications have addressed.

7.2 Future Work Overview

The research detailed within this thesis has investigated the effectiveness of temperature compensation methods deployed by a range of Coriolis flow meter manufacturers. The sizes of said meters ranged from ¼" to 1" pipe bore. In its current form, the solution described in chapters 5 and 6 is only directly applicable to the specific geometry, sensor configurations and transmitters implemented by Rheonik. This chapter therefore proposes multiple research avenues that could be pursued to further our understanding of Coriolis meter performance in this field.

7.2.1 Meter Size

Regardless of meter geometries specific to any given manufacturer, increasing the pipe bore to accommodate larger fluid flows requires the use of greater masses of metal alloy in device construction. Therefore, the inherent resonant frequency and associated response with respect to varying fluid densities is subject to change. For example, Rheonik's 6" Coriolis flow meter variant (RHM80) [134], has a resonant frequency of ~70Hz with water present within its internals compared to the ~230Hz found in the ¼" meters used during testing in this thesis. By focussing on smaller bore meters, this thesis has targeted the most challenging aspects relating to meter size. Specifically, small bore Coriolis meters and their outputs are more sensitive to frequency changes than larger bore devices.

Further research on profiling the response of multiple meter manufacturers of increasing sizes could however be pursued. This thesis has demonstrated that, to effectively target the effects of ambient air temperature on meter response, the experimental methods described by this thesis is an efficient method of maintaining control and awareness of the key variables relevant to meter operation and response. However, as the meter size increases, the size of the associated test facility components such as upstream/downstream pipe work, temperature enclosure and fluid temperature conditioning requirement will also increase, as will the energy requirements for fluid circulation. The data acquisition system infrastructure would not be affected. The associated practicalities and cost associated with such an expansion of experimental scale should be fully considered.

7.2.2 Fluid Properties

The experiments described in chapters 4 to 6 made use of fluids that were available within the NEL laboratories and represent a range of fluid densities between 810 and 998 kg/m^3. Further research, which targets the effectiveness of multiple meter manufacturer correction algorithms as well as the new correction methods described in chapters 5 and 6 could be conducted using fluids of differing densities. In doing so, this would generate additional information to refine the resolution of the X coefficient generation. Chapter 6 highlighted that at higher viscosities (Gas Oil), the effectiveness of the new correction method compared to the manufacturer's existing method decreased. Further research with high viscosity fluids would be a recommended extension of this work, however as with 7.2.1, the energy and associated pipe size requirements to circulate high viscosity fluids increase and therefore the 'Very Low Flow' facility used for testing in this thesis becomes redundant.

7.2.3 Supporting Software

At present Rheonik support a software platform (RHMPro), which connects directly to the meter transmitter, providing a real-time data overview of all Modbus registers. In addition, the platform also has the functionality to simulate meter response over given flows and temperatures. Such a feature would benefit from the data sets developed as part of this thesis, offering realistic responses of all 25+ Modbus registers logged with respect to temperature.

7.2.4 Computational Fluid Dynamics (CFD)

By using modern CFD packages, the effects which were experimentally investigated in this thesis could be reproduced and validated via simulation. The challenge in developing a model which is representative of Coriolis meter operation however remains. The manufacturer specific nature of pipe geometry, sensor positioning, signal interpretation and oscillation control should be considered before attempting to simulate such a system.

8 References

[1] G. Lindsay, J. Hay, N. Glen, and S. Shariatipour, “Profiling and trending of coriolis meter secondary process value drift due to ambient temperature fluctuations,” *Flow Meas. Instrum.*, vol. 59, pp. 225–232, 2018.

[2] G. Lindsay, N. Glen, J. Hay, S. Shariatipour and M. P. Henry, “Coriolis Meter Density Errors Induced by Ambient Air and Fluid Temperarure Differentials,” *Flow Meas. Instrum.*, (Under Review)

[3] G. Lindsay, N. Glen, S. Shariatipour, and M. P. Henry, “Detecting and Correcting for Coriolis Meter Calculated Fluid Density Drift due to Ambient Temperature Variation,” in *North Sea Flow Measurement Workshop*, 2018.

[4] G. Lindsay, “Coriolis Density Error-Targeting Ambient Temperature Fluctuation and the Development of a New Temperature Compensation Model,” in *North Sea Flow Measurement Workshop*, 2019.

[5] Britannica.com, “Gustave-Gaspard Coriolis (French physicist),” *British online encyclopedia*, 2019. [Online]. Available: https://www.britannica.com/biography/Gustave-Gaspard-Coriolis. [Accessed: 02-Jul-2019].

[6] P. Kollsman, “Apparatus for Measuring Weight Flow of Fluids - US2602330,” 1952.

[7] J. Pearson, “Flowmeter - US2624198,” 1953.

[8] W. Wiley, “Oscillating Mass Flowmeter - US3080750,” 1963.

[9] A. Sipin, “Mass Flow Metering Means - US3329019,” 1967.

[10] A. Sipin, “Mass Flow Metering Means US3355944,” 1967.

[11] B. M. Cox and F. A. Gonzalez, “Coriolis Mass Flow Rate Metering Means - US4127028,” 1978.

[12] J. Smith, “Method and Structure for Flow Measurement - US4187721,” 1980.

[13] J. Smith and D. Cage, “Parallel Path Coriolis Mass Flow Rate Meter - US4491025,” 1985.

[14] R. C. Baker, “Coriolis flowmeters: industrial practice and published information,” *Flow Meas. Instrum.*, vol. 5, no. 4, pp. 229–246, 1994.

[15] T. Wang and R. Baker, “Coriolis flowmeters: A review of developments over the past 20 years, and an assessment of the state of the art and likely future directions,” *Flow Meas. Instrum.*, vol. 40, pp. 99–123, 2014.

[16] *ISO 10790:2015 - Measurement of fluid flow in closed condiots - Guidance to the selection, installation and use of Coriolis flowmeters (mass flow, density and volumen flow measurements)*. 2015.

[17] C. A. Wade and A. Dandridge, “An optical fiber flowmeter based on the Coriolis effect,” *Fiber Opt. Laser Sensors VI*, vol. 985, pp. 299–304, 1988.

[18] Y. Zhao, K. Chen, and J. Yang, “Novel target type flowmeter based on a differential fiber Bragg grating sensor,” *Meas. J. Int. Meas. Confed.*, vol. 38, no. 3, pp. 230–235, 2005.

[19] T. O’Banion, “Coriolis: The direct approach to mass flow measurement,” *Chem. Eng. Prog.*, vol. 109, no. 3, pp. 41–46, 2013.

[20] Britannica.com, “Young’s Modulus,” *British online encyclopedia*, 2019. [Online]. Available: https://www.britannica.com/science/Youngs-modulus. [Accessed: 10-Jul-2019].

[21] N. M. Keita, “Behaviour of straight pipe Coriolis mass flowmeters in the metering of gas: theoretical predictions with experimental verification,” *Flow Meas. Instrum.*, vol. 5, pp. 289–294, 1994.

[22] F. Cascetta, “Effect of fluid pressure on Coriolis mass flowmeter’s performance,” in *ISA Transactions*, 1996, vol. 35, pp. 365–370.

[23] R. Paton, “Calibration techniques for Coriolis mass flowmeters,” in *9th international conference for flow measurement (FLOMEKO ’98)*, 1998.

[24] F. Cascetta, “Experimental investigations upon the pressure effects on two Coriolis mass flowmeters of different generation,” *ISA Trans.*, vol. 38, no. 2, pp. 149–156, 1999.

[25] T. Wang and Y. Hussain, “Pressure effects on Coriolis mass flowmeters,” *Flow Meas. Instrum.*, vol. 21, no. 4, pp. 504–510, 2010.

[26] C. Mills, “Coriolis Flow Meter Good Practice Guide,” NEL Report, East Kilbride, 2019.

[27] P. Tschabold, V. Kumar, and M. Anklin, “Paper 6.3 Influence and Compensation of Process Parameters on Coriolis Meters with a View to Custody Transfer of Hydrocarbon Products,” in *SE Asia Hydrocarbon Flow Measurement Workshop*, 2010.

[28] C. Hardie, “Effect of Pressure on Coriolis Meters, JIP Report 2,” NEL Report, East Kilbride, 2014.

[29] C. Mills, “Calibrating and Operating Coriolis Flow Meters with Respect to Process Effects,” in *North Sea Flow Measurement Workshop*, 2018.

[30] C. Mills, “The Consistency of Pressure Effects Between DN80 Coriolis Flow Meters,” NEL Report, East Kilbride, 2019.

[31] D. Alveringh, R. J. Wiegerink, and J. C. Lotters, “Integrated Pressure Sensing Using Capacitive Coriolis Mass Flow Sensors,” *J. Microelectromechanical Syst.*, vol. 26, no. 3, pp. 653–661, 2017.

[32] D. Alveringh, T. V. P. Schut, R. J. Wiegerink, W. Sparreboom, and J. C. Lötters, “Resistive Pressure Sensors Integrated with a Coriolis Mass Flow Sensor,”Report - MESA+ Institute for Nanotechnology, University of Twente, Enschede, The Netherlands, 2017.

[33] T. V. P. Schut, D. Alveringh, W. Sparreboom, J. Groenesteijn, R. J. Wiegerink, and J. C. Lotters, “Fully integrated mass flow, pressure, density and viscosity sensor for both liquids and gases,” in *IEEE International Conference on Micro Electro Mechanical Systems (MEMS)*, 2018, pp. 218–221.

[34] P. Enoksson, G. Stemme, and E. Stemme, “Fluid density sensor based on resonance vibration,” *Sensors and Actuators*, vol. A, pp. 327–331, 1995.

[35] P. Enoksson, G. Stemme, and E. Stemme, “A silicon resonant sensor structure for coriolis mass-flow measurements,” *J. Microelectromechanical Syst.*, vol. 6, no. 2, pp. 119–125, 1997.

[36] R. Smith, D. R. Sparks, D. Riley, and N. Najafi, “A MEMS-based coriolis mass flow sensor for industrial applications,” in *IEEE Transactions on Industrial Electronics*, 2009, vol. 56, no. 4, pp. 1066–1071.

[37] J. Haneveld, T. S. J. Lammerink, M. Dijkstra, H. Droogendijk, M. J. De Boer, and R. J. Wiegerink, “Highly sensitive micro coriolis mass flow sensor,” *Proc. IEEE Int. Conf. Micro Electro Mech. Syst.*, no. 1, pp. 920–923, 2008.

[38] R. C. Baker, “Flow Measurement Handbook,” in *Flow Measurement Handbook*, Second Edi., 2000, pp. 560–601.

[39] A. Kenbar, Y. Hussain, and T. Wang, “Calibration of a Coriolis Mass Flowmeter for LNG at Cryogenic Temperatures,” in *Production and Upstream Flow Measurement Workshop*, 2008.

[40] T. Wang and Y. Hussain, “Coriolis mass flow measurement at cryogenic temperatures,” *Flow Meas. Instrum.*, vol. 20, no. 3, pp. 110–115, 2009.

[41] C. Hardie, “Effect of Temperature on Coriolid Meters,” NEL Report, East Kilbride, 2014.

[42] N. I. Heywood and K. B. Mehta, “The Performance of Commercially-Available Coriolis Mass Flowmeters Applied to Industrial Slurries,” in *Hydrotransport 12 Conference*, 1996.

[43] I. Fyrippi, I. Owen, and M. P. Escudier, “Flowmetering of non-Newtonian liquids,” *Flow Meas. Instrum.*, vol. 15, pp. 131–138, 2004.

[44] G. Miller and B. Belshaw, “An Investigation into the Performance of Coriolis and Ultrasonic Meters at Liquid Viscosities up to 300 cSt,” in *North Sea Flow Measurement Workshop*, 2008.

[45] A. F. Skea and A. R. W. Hall, “Effects of gas leaks in oil flow on single-phase flowmeters,” *Flow Meas. Instrum.*, vol. 10, pp. 145–150, 1999.

[46] A. F. Skea and A. W. R. Hall, “Effects of water in oil and oil in water on single-phase flowmeters,” *Flow Meas. Instrum.*, vol. 10, pp. 151–157, 1999.

[47] R. P. Liu, M. J. Fuent, M. P. Henry, and M. D. Duta, “A neural network to correct mass flow errors caused by two-phase flow in a digital coriolis mass flowmeter,” *Flow Meas. Instrum.*, vol. 12, pp. 53–63, 2001.

[48] M. Seeger, “Coriolis flow measurement in two phase flow,” *Comput. Control Eng.*, vol. 16, no. 3, pp. 10–16, 2005.

[49] D. L. Gysling, “An aeroelastic model of Coriolis mass and density meters operating on aerated mixtures,” *Flow Meas. Instrum.*, vol. 18, no. 2, pp. 69–77, 2007.

[50] H. Yeung, J. Hemp, M. Henry, and M. Tombs, “Coriolis Meter in Liquid/Liquid, Liquid/Gas and Liquid/Liquid/Gas Flows,” in *Hydrocarbon Flow Measurement Workshop*, 2004.

[51] M. P. Henry and M. J. De la Fuente, “Correcting for Two-Phase Flow in a Digital Flowmeter US6981424B2,” 2006.

[52] M. Henry, M. Duta, M. Tombs, H. Yeung, and W. Mattar, “How a Coriolis mass flow meter can operate in two-phase (gas/liquid) flow,” in *ISA EXPO*, 2004.

[53] M. Henry *et al.*, “Two-phase flow metering of heavy oil using a Coriolis mass flow meter: A case study,” *Flow Meas. Instrum.*, vol. 17, pp. 399–413, 2006.

[54] M. Henry, M. Tombs, M. Zamora, and F. Zhou, “Coriolis mass flow metering for three-phase flow: A case study,” *Flow Meas. Instrum.*, vol. 30, pp. 112–122, 2013.

[55] M. Henry, M. Tombs, and F. Zhou, “Field experience of well testing using multiphase Coriolis metering,” *Flow Meas. Instrum.*, vol. 52, pp. 121–136, 2016.

[56] N. T. Basse, “A review of the theory of Coriolis flowmeter measurement errors due to entrained particles,” *Flow Meas. Instrum.*, vol. 52, pp. 40–52, 2014.

[57] N. T. Basse, “Coriolis flowmeter damping for two-phase flow due to decoupling,” *Flow Meas. Instrum.*, vol. 52, no. September, pp. 40–52, 2016.

[58] T. O. Donnell and R. Harvey, “The Performance of Coriolis Meters in Multiphase Flow,” in *The Americas Flow Measurement Conference*, 2013.

[59] T. Leonard and R. Harvey, “The Performance of Coriolis Meters in Two-component Oil / Water Mixtures and Multiphase Flow,” in *South East Asia Flow Measurement Conference*, 2015.

[60] M. Tombs, F. Zhou, and M. Henry, “Two-phase coriolis mass flow metering with high viscosity oil,” *Flow Meas. Instrum.*, vol. 59, pp. 23–27, 2018.

[61] M. Li and M. Henry, “Complex signal processing for Coriolis mass flow metering in two-phase flow,” *Flow Meas. Instrum.*, vol. 64, pp. 104–115, 2018.

[62] J. W. Kunze, R. Storm, and T. Wang, “Coriolis Mass Flow Measurement with Entrained Gas,” Krohne Report, Duisburg, 2014.

[63] L. Wang, J. Liu, Y. Yan, X. Wang, and T. Wang, “Mass flow measurement of two-phase carbon dioxide using coriolis flowmeters,” in *I2MTC EEE International Instrumentation and Measurement Technology Conference, Proceedings*, 2017, pp. 1–5.

[64] N. M. Keita, “Contribution to the understanding of the zero shift effects in Coriolis mass flowmeters,” *Flow Meas. Instrum.*, vol. 1, pp. 39–43, 1989.

[65] R. Storm, K. Kolahi, and H. Röck, “Model-based correction of coriolis mass flowmeters,” *IEEE Trans. Instrum. Meas.*, vol. 51, no. 4, pp. 605–610, 2002.

[66] L.-J. Wang, L. Hu, X. Fu, and P. Ye, “Experimental Investigation on Zero Drift Effect in Coriolis Mass Flowmeters,” in *FLOMEKO*, 2010.

[67] F. Koschmieder and H. Röck, “Compensation Method Applied to Coriolis Mass Flow Metering,” in *FLOMEKO*, 2010.

[68] S. Enz, J. J. Thomsen, and S. Neumeyer, “Experimental investigation of zero phase shift effects for Coriolis flowmeters due to pipe imperfections,” *Flow Meas. Instrum.*, vol. 22, pp. 1–9, 2011.

[69] H. Röck and F. Koschmieder, “A new method to detect zero drift and sensitivity of a coriolis mass flow meter (CMFM) by using phasor control,” in *Proceedings of the 3rd International Conference on Sensing Technology, ICST 2008*, 2008.

[70] A. A. Yaushev, P. A. Taranenko, and V. A. Loginovskiy, “Analysis of influence of mechanical boundary conditions on zero point shift of Coriolis flowmeter,” in *Procedia Engineering*, 2017.

[71] R. C. Mottram, “Introduction. An overview of pulsating flow measurement,” *Flow Meas. Instrum.*, vol. 3, pp. 114–117, 1992.

[72] G. Vetter and S. Notzon, “Effect of pulsating flow on Coriolis mass flowmeters,” *Flow Meas. Instrum.*, vol. 5, no. 4, pp. 263–273, 1994.

[73] R. Cheesewright and C. Clark, “The Effect of Flow Pulsations on Coriolis Mass Flow Meters,” *J. Fluids Struct.*, vol. 12, pp. 1025–1039, 1998.

[74] R. Cheesewright, C. Clark, and D. Bisset, “Understanding the experimental response of Coriolis massflow meters to flow pulsations,” *Flow Meas. Instrum.*, vol. 10, no. 4, pp. 207–215, 1999.

[75] A. Belhadj, R. Cheesewright, and C. Clark, “The simulation of coriolis meter response to pulsating flow using a general purpose F.E. Code,” *J. Fluids Struct.*, vol. 14, pp. 613–634, 2000.

[76] R. Cheesewright, C. Clark, and Y. Y. Hou, “The response of Coriolis flowmeters to pulsating flows,” *Flow Meas. Instrum.*, vol. 15, pp. 59–67, 2004.

[77] S. Enz and J. J. Thomsen, “Predicting phase shift effects for vibrating fluid-conveying pipes due to Coriolis forces and fluid pulsation,” *J. Sound Vib.*, vol. 330, pp. 5096–5113, 2011.

[78] A. Svete, J. Kutin, G. Bobovnik, and I. Bajsić, “Theoretical and experimental investigations of flow pulsation effects in Coriolis mass flowmeters,” *J. Sound Vib.*, vol. 352, pp. 30–45, 2015.

[79] R. Cheesewright and S. Shaw, “Uncertainties associated with finite element modelling of Coriolis mass flow meters,” *Flow Meas. Instrum.*, vol. 17, no. 6, pp. 335–347, 2006.

[80] D. Cage and G. Dragnea, “System and Method for Fluid Compressibility Compensation in a Coriolis Mass Flow Meter - US6502466B1,” 2003.

[81] J. Hemp and J. Kutin, “Theory of errors in Coriolis flowmeter readings due to compressibility of the fluid being metered,” *Flow Meas. Instrum.*, vol. 17, pp. 335–347, 2006.

[82] P. Kalotay, “Density and viscosity monitoring systems using Coriolis flow meters,” in *ISA Transactions*, 1999.

[83] A. Mathews, “Theory and Operation of Vibrating Element Liquid and Gas Densitometers in the Hydrocarbon Industry,” in *National Engineering Laboratory Density Seminar*, 1994.

[84] L. N. Philp, “Hydrocarbon Density - The PMI’s Interest,” in *National Engineering Laboratory Density Seminar*, 1994.

[85] D. S. Geach, “Density Measurement in the Real World,” in *National Engineering Laboratory Density Seminar*, 1994.

[86] K. Kolahi, T. Schröder, and H. Röck, “High Precision Density Measurement with Coriolis Mass Owmeters,” in *Canada*, 2005.

[87] K. Kolahi, T. Schröder, and H. Röck, “Model-based density measurement with Coriolis flowmeter,” in *IEEE Transactions on Instrumentation and Measurement*, 2006, pp. 1258–1262.

[88] J. Ren, L. Zhang, P. Zhang, and Z. Yin, “Characteristic analysis of non-uniform mixed liquid density measurement based on Coriolis mass flowmeter,” *Proc. - IEEE 2011 10th Int. Conf. Electron. Meas. Instruments, ICEMI 2011*, vol. 4, no. 2, pp. 114–117, 2011.

[89] C. Huber, “MEMS-based Micro-Coriolis Density and Flow Measurement Technology,” *AMA Conf.*, pp. 286–291, 2015.

[90] K. Adefila, Y. Yan, L. Sun, and T. Wang, “Flow measurement of CO2 in a binary gaseous mixture using an averaging Pitot Tube and Coriolis mass flowmeters,” *Flow Meas. Instrum.*, vol. 54, pp. 265–272, 2017.

[91] N. Glen and L. Hunter, “Measurement challenges for carbon capture and storage,” in *Measurement and Control*, 2011, vol. 44, no. 3.

[92] C. Hardie, “Developing measurement facilities for Carbon Capture and Storage,” *Meas. Control*, vol. 46, no. 2, 2013.

[93] M. Nazeri, M. M. Maroto-Valer, and E. Jukes, “Performance of Coriolis flowmeters in CO2 pipelines with pre-combustion, post-combustion and oxyfuel gas mixtures in carbon capture and storage,” *Int. J. Greenh. Gas Control*, vol. 54, pp. 297–308, 2016.

[94] M. Nazeri, M. M. Maroto-Valer, and E. Jukes, “Density of carbon dioxide with impurities by Coriolis flow meter, oscillation-type densitometer and equations of state,” *Appl. Energy*, vol. 212, pp. 162–174, 2018.

[95] O. Seifert, “New Developments in Flow Sensors for Industrial Furnaces,” *Energy Procedia*, vol. 120, pp. 469–476, 2017.

[96] Endress+Hauser, “Technical Information - Proline Promass Q 300 Coriolis flow meter,” 2018.

[97] A. Rieder and P. Ceglia, “New Generation Vibrating Tube Sensor for Density Measurement under Process Conditions,” in North Sea Flow Measurement Workshop, 2017.

[98] A. Rieder and E. H. Doorenspleet, “Products Solutions Services Evaluating New Generation Vibrating Tube Sensor for Density Measurement under Process Conditions,” Endress + Hauser Report, Freising, 2018.

[99] N. Glen, “Calibration of Density Output of Proline Promass Q 500 Coriolis Flow Meter,”, NEL Report, East Kilbride, 2017.

[100] A. García-Berrocal, C. Montalvo, P. Carmona, and J. Blázquez, “The Coriolis mass flow meter as a volume meter for the custody transfer in liquid hydrocarbons logistics,” in *ISA Transactions*, 2019.

[101] K. Kolahi, T. Gast, and H. Röck, “Coriolis mass flow measurement of gas under normal conditions,” *Flow Meas. Instrum.*, vol. 5, pp. 275–283, 1994.

[102] D. W. Clarke, “Non-linear Control of the Oscillation Amplitude of a Coriolis Mass-Flow Meter,” *Eur. J. Control*, vol. 4, pp. 196–207, 1998.

[103] M. Henry and D. W. Clarke, “The Self-Validating Sensor: Rationale, Definitions and Examples,” 1993.

[104] M. P. Henry, “A Seva Sensor - The Coriolis Mass Flow Meter,” in *IFAC Proceedings Volumes*, 1994.

[105] M. P. Henry *et al.*, “A self-validating digital Coriolis mass-flow meter: An overview,” *Control Eng. Pract.*, vol. 8, pp. 487–506, 2000.

[106] M. Henry, “On-line compensation in a digital coriolis mass flow meter,” *Flow Meas. Instrum.*, vol. 12, pp. 147–161, 2001.

[107] *British Standard BS 7986:2005 Data quality metrics for industrial measurement and control systems-Specification*. 2005.

[108] “Process Instrumentation,” in *Powder Technology Handbook, Third Edition*, 2010.

[109] C. Clark, M. Zamora, R. Cheesewright, and M. Henry, “The dynamic performance of a new ultra-fast response Coriolis flow meter,” *Flow Meas. Instrum.*, vol. 17, no. 6, pp. 391–398, Dec. 2006.

[110] J. Ruoff, W. Gauchel, and H. Kück, “Advances in signal acquisition and signal processing of coriolis flow meters,” *Procedia Eng.*, vol. 87, pp. 1585–1588, 2014.

[111] Q.-L. Hou, K.-J. Xu, M. Fang, C. Liu, and W.-J. Xiong, “Development of Coriolis mass flowmeter with digital drive and signal processing technology,” in *ISA Transactions*, 2013.

[112] Q. L. Hou, K. J. Xu, M. Fang, W. J. Xiong, and C. Liu, “A DSP-based signal processing method and system for CMF,” *Meas. J. Int. Meas. Confed.*, vol. 46, pp. 2184–2192, 2013.

[113] J. G. Zhang, K. J. Xu, S. Dong, Z. Liu, Q. L. Hou, and Z. Y. Fang, “Mathematical model of time difference for Coriolis flow sensor output signals under gas-liquid two-phase flow,” *Meas. J. Int. Meas. Confed.*, vol. 95, pp. 345–354, 2017.

[114] F. Leach, S. Karout, F. Zhou, M. Tombs, M. Davy, and M. Henry, “Fast Coriolis mass flow metering for monitoring diesel fuel injection,” *Flow Meas. Instrum.*, vol. 58, pp. 1–5, 2017.

[115] M. P. Henry, “An Introduction to Prism Signal Processing Applied to Sensor Validation,” *Meas. Tech.*, vol. 60, no. 12, pp. 1233–1237, 2018.

[116] G. Lindsay, “Digital Data in Practice : Networks , Users and Benefits, NEL Report 2018_771,” East Kilbride, 2019.

[117] S. Enz, “Effect of asymmetric actuator and detector position on Coriolis flowmeter and measured phase shift,” *Flow Meas. Instrum.*, vol. 21, pp. 497–503, 2010.

[118] M. H. Ghayesh, M. Amabili, and M. P. Païdoussis, “Thermo-mechanical phase-shift determination in Coriolis mass-flowmeters with added masses,” *J. Fluids Struct.*, vol. 34, pp. 1–13, 2012.

[119] O. Oiestad, S. Fosse, S. Vervik, and L. Falnes, “Are Coriolis Mass meters suitable for Fiscal Liquid Applications?,” in *North Sea Flow Measurement Workshop*, 2010.

[120] R. Cheesewright, C. Clark, and D. Bisset, “The identification of external factors which influence the calibration of Coriolis massflow meters,” *Flow Meas. Instrum.*, vol. 11, no. 1, pp. 1–10, 2000.

[121] C. P. Stack, “Vibratory Flow Meter and Method for Determining a Fluid Temperature of a Flow Material - US8302491B2,” 2012.

[122] V. O. Apostolyuk, “Optimal filtering of temperature errors for coriolis vibratory gyroscopes,” *2013 IEEE 2nd Int. Conf. Actual Probl. Unmanned Air Veh. Dev. APUAVD 2013 - Proc.*, pp. 96–98, 2013.

[123] T. G. Nesterenko, A. N. Koleda, E. S. Barbin, and S. V. Uchaikin, “Temperature error compensation in two-component microelectromechanical gyroscope,” *IEEE Trans. Components, Packag. Manuf. Technol.*, vol. 4, no. 10, pp. 1598–1605, 2014.

[124] *Directive 2004/108/EC of the European Parliament and of the Council of 15 December 2004 on the approximation of the laws of the Member States relating to electromagnetic compatibility and repealing Directive 89/336/EEC*. 2004.

[125] P. Kalotay and L. Colo, “Coriolis Effect Using Optical Fiber Sensors - US5379649,” 1995.

[126] M. Anklin, W. Drahm, and A. Rieder, “Coriolis mass flowmeters: Overview of the current state of the art and latest research,” *Flow Meas. Instrum.*, vol. 17, pp. 317–323, 2006.

[127] L. van de Ridder, M. A. Beijen, W. B. J. Hakvoort, J. van Dijk, J. C. Lötters, and A. de Boer, “Active vibration isolation feedback control for Coriolis Mass-Flow Meters,” *Control Eng. Pract.*, vol. 33, pp. 76–83, 2014.

[128] L. van de Ridder, W. B. J. Hakvoort, D. M. Brouwer, J. van Dijk, J. C. Lötters, and A. de Boer, “Coriolis mass-flow meter with integrated multi-DOF active vibration isolation,” *Mechatronics*, vol. 36, pp. 167–179, 2016.

[129] C. Clark and R. Cheesewright, “The influence upon Coriolis mass flow meters of external vibrations at selected frequencies,” *Flow Meas. Instrum.*, vol. 14, pp. 33-42, 2003.

[130] N. F. Glen and A. I. Johns, “Determination of the density of toluene in the range from (293 to 373) K and from (0.1 to 30) MPa,” *J. Chem. Eng. Data*, vol. 54, no. 9, pp. 2538–2545, 2009.

[131] Keysight Technologies Inc., “Keysight 34970A Data Acquisition / Switch Unit Family technical Overview.” 2018.

[132] “National Instruments MXI-4 Series User Manual,” no. August. 2010.

[133] “Rheonik RHM Series Compact Low Flow Coriolis Flow Sensors Data Sheet.” 2018.

[134] “Rheonik RHM80 - High Flow Coriolis Mass Flow Meter Datasheet.” 2016.

9 Appendices

9.1 Appendix 1 – Further information on test facility operation

The ‘Very Low Flow’ test facility at NEL has two modes of operation - recirculatory or gravimetric.

Recirculatory:-
In this mode the fluid is simply drawn from the supply tanks by the pumps, discharged through the test section and returned directly to the supply tank. This mode of operation was used for the ambient temperature experimentation work described in chapters 4, 5 and 6.

Gravimetric:-
This mode is reserved for UKAS flow meter calibrations and is a method of comparing the mass or volume flow reported from a flow meter installed in the test section. Instead of returning the fluid directly to the supply tank after passing through the test section, the fluid is instead diverted to one of two containers of known volume, which are positioned on two calibrated scales.

Both scales are manufactured by Sartorius and can be used with either pump line. The scales have differing capacities and are selected depending on the flow rate expected of a given test.

A 25-litre aspirator bottle with a draining tap is used as a collection tank on the 16 kg scale. A customised 1 litre glass beaker with a glass drain valve serves as the collection tank for the 3.2 kg scale. Once data collection is complete, the fluid is returned to the supply tank. Both scales are tared before data collection to account for any remaining fluid that has not fully drained.

A calibration in this mode operates under a standing start principle. The pipe work leading to the inlet valve of both tanks are primed and held at pressure by the facility pumps in preparation for data collection.

This mode of operation was used to perform initial commissioning checks and calibrations of the Coriolis meters used in the research programme, however due to the aforementioned standing start principle of operation, it was not used for the ambient temperature experimentation. Doing so would have caused the fluid to remain static within the scientific oven, resulting in unwanted heat exchange.

9.2 Appendix 2 - Data Acquisition System Infrastructure

9.2.1 Analog signals

To ensure that the pulsed signals logged were representative of the signal generated by the devices under test, a low pass filter circuit was implemented per channel to remove the potential for electrical noise to distort the waveform. To provide electrical protection for both the device under test and the data acquisition hardware, an opto-isolator unit was also implemented per channel as detailed in Figure 9-1.

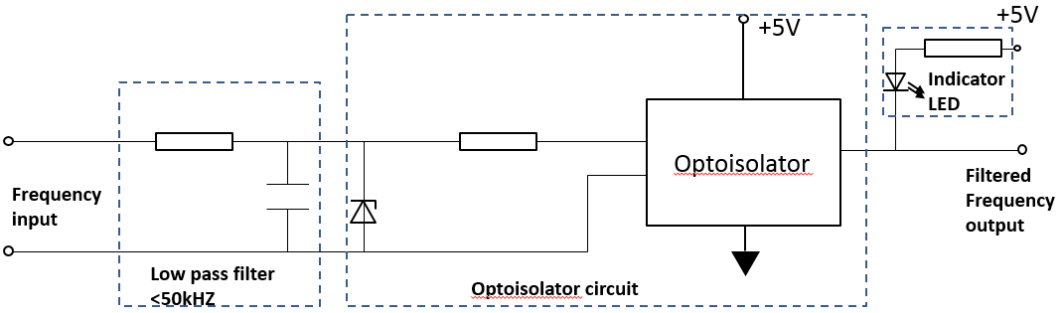

Figure 9-1 Circuit diagram of pulse conditioning circuit built for filtering electrical noise and amplification of Coriolis flow meter frequency output to Transistor-transistor logic (TTL) standards

Fluke 6669 units were used to log the pulse outputs from the flow meters and were interfaced with the DAQ PC over IEEE 488.2 (General Purpose Interface Bus).

The circuit shown in Figure 9-2 was built to provide additional flexibility on the multiplexed analog channels. Circuit allows selection between active or passive devices and provides additional surge protection for individual channel circuitry.

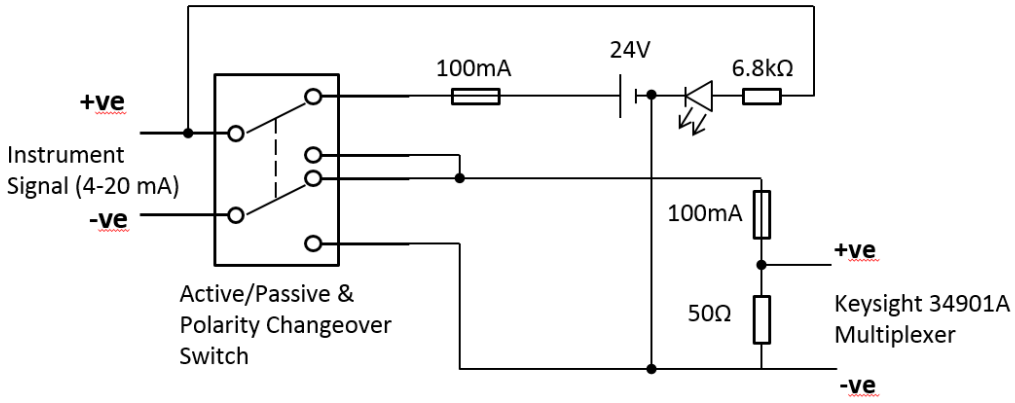

Figure 9-2 Diagram of loop power circuit built to accommodate both passive and active 4-20mA signals and protect Agilent multiplexer channels from electrical surges.

9.2.2 Data acquisition (DAQ) Software

The DAQ software developed for this thesis was coded to log data from both the hardware and digital servers as part of a sequential instrument scan cycle. For analog measurements, the software was designed to record raw electrical property measurements per instrument and apply appropriate calibration coefficient to produce the corresponding SI unit of measurement. To allow polling of the OPC server, Siemens Direct Access (DA) dynamic link libraries (DLL) were embedded within the software. Custom drivers for the Agilent 34970, National Instruments chassis and Fluke PM6669 were codded and embedded within the software. An overview of the software architecture is shown in Figure 9-3.

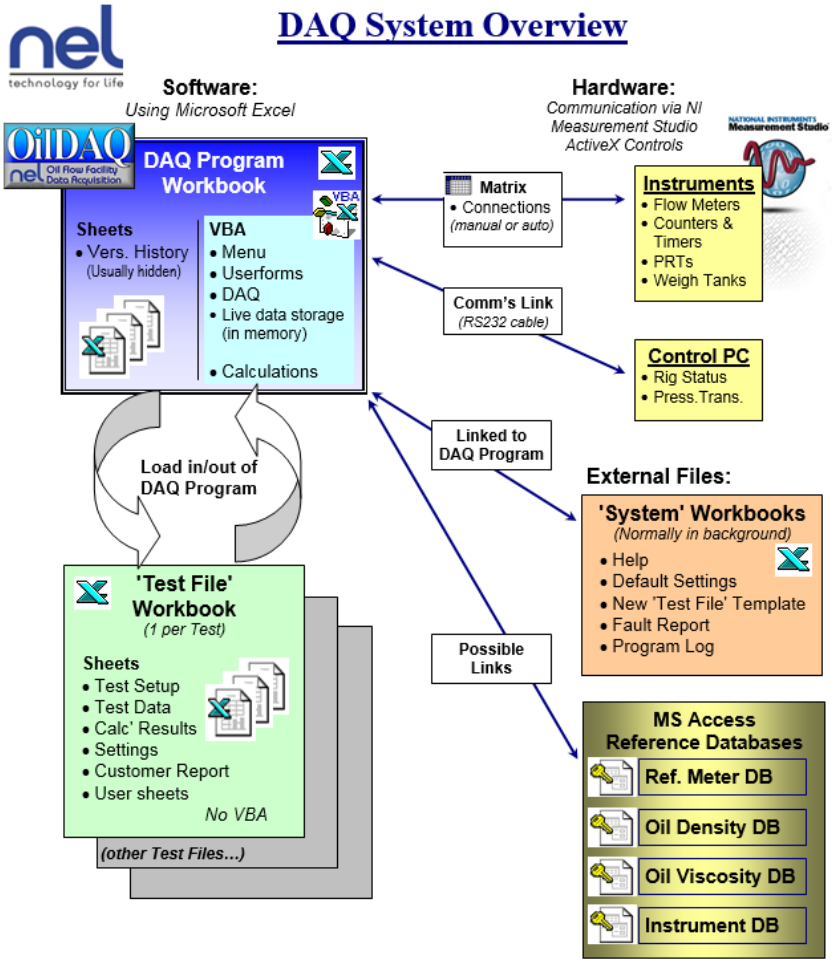

Figure 9-3 Data acquisition software suit architecture

9.2.3 Gating

To ensure that all logged pulsed and timed values were synchronised, the triggering of all logging hardware was performed by signals specific to the mode of rig operation. For gravimetric operations of the facility the trigger source was a 24VAC control signal, which was sent to the solenoid associated with the weigh tank isolation valve (Figure 9-4). This in turn toggled the position of the valve between open and closed. To satisfy the TTL requirements of the NI 6602 card this signal was routed to actuate a 24VAC non-latching relay, which in turn switched a 5V DC value, the source of which was a programmable DC power supply.

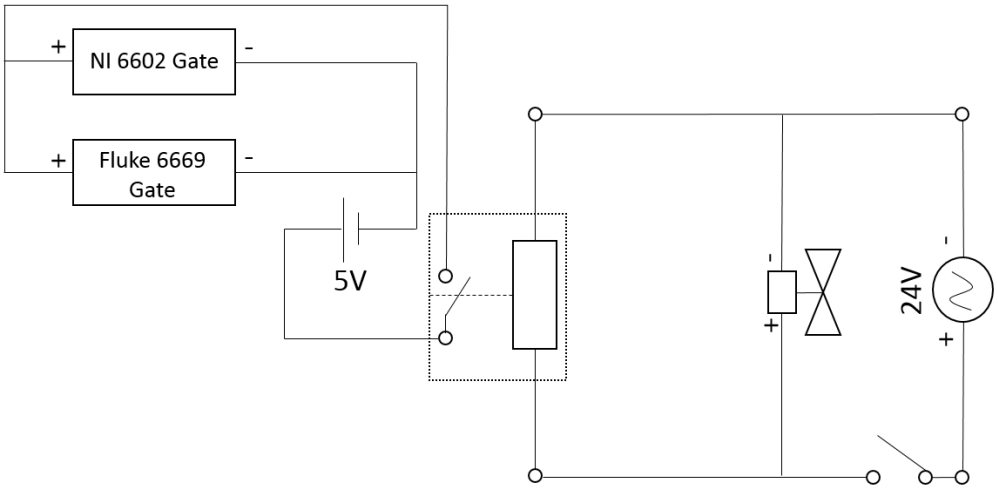

Figure 9-4 Schematic of pulse channel triggering (gating) from weighbridge isolation valve solenoid control signal

For recirculatory mode, the trigger was generated using the aforementioned Keysight 34901 mainframe, equipped with a Keysight 34907 DIO multifunction module. The 34907 is capable of outputting 2 bytes of binary values in the form of 5V DC per bit (Figure 9-5). This module was programmed remotely from the DAQ software. The gate signal was wired to bit 0 of byte 1 on the module. At the start of a test, bit 0 was set to hi, sending a 5V value to each of the pulse counter and timer gates terminals and therefore synchronising the triggering of all pulse counters and timer.

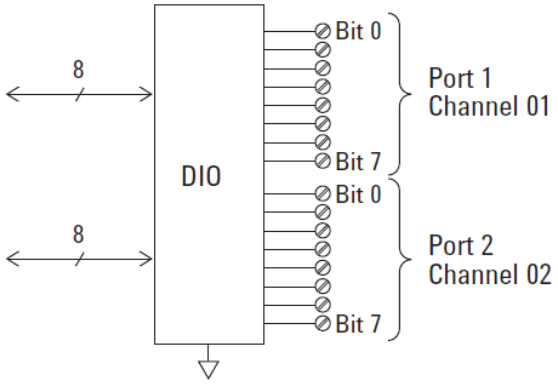

Figure 9-5 Diagram of DIO module installed in Keysight 34970 used to trigger (gate) pulse signal logging during recirculation experimentation [131]

9.3 **Appendix 3 - Facility Commissioning**

9.3.1 Overview

Once the facility build was complete, the system was put through a commissioning program to ensure that the flow and temperature conditions could be met, as well as ensuring that electrical and data acquisition components were performing to specification.

9.3.2 Facility Performance

Trials were conducted on the fluid conditioning capabilities of the facility to ensure that that fluid temperature setpoints could be achieved under standard conditions. Trials were also conducted on the fluid conditioning system efficiency while the temperature enclosure was set to provide an air temperature of 65°C. Liquid flow 'baseline trials' were also conducted on both the reference and test meters. During this period the thermal chamber was not active and the enclosure door was open to atmosphere to ensure that both reference and test meters were exposed to the same ambient conditions. Under these conditions the analog and digital process values output from both meters were logged by the data acquisition system to determine any offset in process values between the reference and test meter.
The zeroing guidelines specific to each Coriolis manufacturer were followed at the point of meter installation for all research phases. Full details of the conditions tested are detailed in Table 9-1.

9.3.3 Facility Commissioning Test Matrix

Table 9-1 Facility commissioning test matrix

Test No	Fluid	Highest Fluid Flow Rate (kg/hr)	Lowest Fluid Flow Rate (kg/hr)	Description of Fluid Flow Change (kg/hr)	Initial Test Meter Air Temp (˚C)	Final Test Meter Air Temp (˚C)	Rate of Test Meter Air Temp Change (˚C)	Reference Meter Air Temp (˚C)	Fluid Temp Setpoint (˚C)	Test Duration (Hrs)	Comment
1	Water	118	86	10 / 15 mins	60	60	N/A	20	20	1.5	High test temp, fluctuating flow
2	Water	118	118	N/A	20	60	Variable	20	20	3.5	Random test air temperature fluctuation
3	Water	118	118	N/A	20	60	Variable	20	20	6	Random test air temperature fluctuation
4	Water	128	160	10 / 15 mins	60	60	N/A	20	20	1	High test temp, fluctuating flow
5	Water	160	130	Single step change	20	60	Single step change	20	20	1.5	Sudden test air temperature increase, fluctuating flow
6	Water	160	130	30 / 15 mins	60	60	N/A	20	20	1.5	High test temp, fluctuating flow
7	Water	190	130	Single step at initial test meter air temperature	60	40	5 / 50 mins	20	20	3.5	Decrease in test air temperature, fluctuating flow
8	Water	130	130	N/A	20	60	10 / 50 mins	20	20	4	Increase in test air temperature
9	Water	130	170	20 / 15 mins	60	60	N/A	20	20	2	High test temp, fluctuating flow
10	Water	126	126	N/A	20	60	6 / 15 mins	20	20	2.5	Increase in test air temperature
11	Water	125	85	20 / 15 mins	60	60	N/A	20	20	1	High test temp, fluctuating flow (Modbus drop out end of test)
12	Water	125	125	N/A	20	60	4 / 60 mins	20	20	10	Increase in test air temperature
13	Water	125	260	4 x step changes; 125 – 148, 148 – 125, 125 – 170, 170 - 125	60	60	N/A	20	20	6	High test temp, fluctuating flow
14	Water	125	125	N/A	60	20	Natural cooling	20	20	7.5	Test air temperature allowed to cool from 60 ˚C to ambient
15	Water	260	260	N/A	60	20	Natural cooling	20	20	6.5	Test air temperature allowed to cool from 60 ˚C to ambient (higher flow rate)
16	Water	260	260	N/A	20	60	4 / 60 mins	20	20	8	Increase in test air temperature
17	Water	260	260	N/A	20	20	N/A	20	40	5	High fluid temperature
18	Water	260	260	N/A	40	60	Single step change	20	40	1	High fluid temperature, 2 x high test meter air temperature

Test No	Fluid	Highest Fluid Flow Rate (kg/hr)	Lowest Fluid Flow Rate (kg/hr)	Description of Fluid Flow Change (kg/hr)	Initial Test Meter Air Temp (˚C)	Final Test Meter Air Temp (˚C)	Rate of Test Meter Air Temp Change (˚C)	Reference Meter Air Temp (˚C)	Fluid Temp Setpoint (˚C)	Test Duration (Hrs)	Comment
19	Water	260	260	N/A	60	20	Natural cooling	20	40	6	High fluid temperature, 2 x high test meter air temperature, Test air temperature allowed to cool from 60 ˚C to ambient
20	Water	230	230	N/A	20	60	20 / 60 mins	25	20	3	Reference meter air temperature elevated above the norm, increase in test meter air temperature

9.4 Appendix 4 - Ethics Approval Details

Coventry University ETHICS

Low Risk Research Ethics Approval

Project Title

Compensating for air temperature effects on Coriolis Flow Meter Density Calculation

Record of Approval

Principal Investigator

I **request an ethics peer review** and confirm that I have answered all relevant questions in this checklist honestly.	X
I confirm that I will carry out the project in the ways described in this checklist. I will immediately suspend research and request new ethical approval if the project subsequently changes the information I have given in this checklist.	X
I confirm that I, and all members of my research team (if any), have read and agreed to abide by the Code of Research Ethics issued by the relevant national learned society.	X
I confirm that I, and all members of my research team (if any), have read and agreed to abide by the University's Research Ethics, Governance and Integrity Framework.	X

Name: Gordon Lindsay ....

Date: 26/08/2019 ....

Student's Supervisor (if applicable)

I have read this checklist and confirm that it covers all the ethical issues raised by this project fully and frankly. I also confirm that these issues have been discussed with the student and will continue to be reviewed in the course of supervision.

Name: James Brusey..... ....

Date: 27/08/2019 ....

Reviewer (if applicable)

Date of approval by anonymous reviewer: 27/08/2019

Low Risk Research Ethics Approval Checklist

Project Information

Project Ref	P93962
Full name	Gordon Lindsay
Faculty	Faculty of Engineering, Environment and Computing
Department	School of Mechanical, Aerospace and Automotive Engineering
Supervisor	James Brusey
Module Code	FCS
EFAAF Number	
Project title	Compensating for air temperature effects on Coriolis Flow Meter Density Calculation
Date(s)	24/09/2015 - 21/09/2019
Created	26/08/2019 13:53

Project Summary

This is a 4 year doctorate research project, where the performance of the fluid density calculation abilities of Coriolis meters in changing air temperature environments have been experimentally investigated. The results were used to create a new correction algorithm that can be implemented live within the device firmware.

All experimentation has been completed. This academic year is the write up year.

Names of Co-Investigators and their organisational affiliation (place of study/employer)	
Is the project self-funded?	NO
Who is funding the project?	
Has the funding been confirmed?	NO
Are you required to use a Professional Code of Ethical Practice appropriate to your discipline?	YES
Have you read the Code?	YES

Project Details

What is the purpose of the project?	To perform experimentation on flow metering technology and gain a unique perspective as to how said technology operates in extreme industrial environments
What are the planned or desired outcomes?	A new method for temperature correcting the fluid density value output by the technology, which is capable of accounting for the combined effects of process fluid density changes, fluid temperature changes and ambient air temperature changes.
Explain your research design	1. Through experimentation obtain high resolution data sets from Coriolis mass flow meters as their surrounding ambient temperature conditions are varied 2. Analysis of data sets to identify the digital process values used in the fluid density calculation which are effected by the changes in ambient temperature 3. Develop meter design improvements (sensor based/internal processing) that will eliminate process value drift due to ambient temperature effects. 4. Publish scientific papers detailing the potential for 'real world effects' as the technology currently stands as well as show how potential to improve based on experiments conducted as part of this project. 5. By the end of EngD project unique output and contribution to science and industry will consist of a. Profiling of Coriolis flow meter output error with respect to ambient temperature fluctuations

	b. Engineering and scientific solutions to reduce/eliminate drift in the form of unique correction model	
Outline the principal methods you will use	Practical Experimentation making use of UK national flow facilities Numerical Data Analysis	
Are you proposing to use an external research instrument, validated scale or follow a published research method?		NO
If yes, please give details of what you are using		
Will your research involve consulting individuals who support, or literature, websites or similar material which advocates, any of the following: terrorism, armed struggles, or political, religious or other forms of activism considered illegal under UK law?		NO
Are you dealing with Secondary Data? (e.g. sourcing info from websites, historical documents)		NO
Are you dealing with Primary Data involving people? (e.g. interviews, questionnaires, observations)		NO
Are you dealing with personal or sensitive data?		NO
Will the Personal or Sensitive data be shared with a third party?		
Will the Personal or Sensitive data be shared outside of the European Economic Area ("EEA")?		
Is the project solely desk based? (e.g. involving no laboratory, workshop or off-campus work or other activities which pose significant risks to researchers or participants)		NO
Are there any other ethical issues or risks of harm raised by the study that have not been covered by previous questions?		NO
If yes, please give further details		

Laboratory/Workshops

Question			Yes	No
1	Does any part of the project involve work in a laboratory or workshop which could pose risks to you, researchers or others?			X
	If YES: If you have risk assessments for laboratory or workshop activities you can refer to them here & upload them at the end, or explain in the text box how you will manage those risks			

Research with non-human vertebrates

	Question		Yes	No
1	Will any part of the project involve animal habitats or tissues or non-human vertebrates?			X
	If YES, please give details			
2	Does the project involve any procedure to the protected animal whilst it is still alive?			
3	Will any part of your project involve the study of animals in their natural habitat?			
	If YES, please give details			
4	Will the project involve the recording of behaviour of animals in a non-natural setting that is outside the control of the researcher?			
	If YES, please give details			
5	Will your field work involve any direct intervention other than recording the behaviour of the animals available for observation?			
	If YES, please give details			
6	Is the species you plan to research endangered, locally rare or part of a sensitive ecosystem protected by legislation?			
	If YES, please give details			
7	Is there any significant possibility that the welfare of the target species of those sharing the local environment/habitat will be detrimentally affected?			
	If YES, please give details			
8	Is there any significant possibility that the habitat of the animals will be damaged by the project, such that their health and survival will be endangered?			
	If YES, please give details			
9	Will project work involve intervention work in a non-natural setting in relation to invertebrate species other than Octopus vulgaris?			
	If YES, please give details			

Blood Sampling / Human Tissue Analysis

	Question		Yes	No
1	Does your study involve collecting or use of human tissues or fluids? (e.g. collecting urine, saliva, blood or use of cell lines, 'dead' blood)			X
	If YES, please give details			
2	If your study involves blood samples or body fluids (e.g. urine, saliva) have you clearly stated in your application that appropriate guidelines are to be followed (e.g. The British Association of Sport and Exercise Science Physiological Testing Guidelines (2007) or equivalent) and that they are in line with the level of risk?			
	If NO, please explain why not			
3	If your study involves human tissue other than blood and saliva, have you clearly stated in your application that appropriate guidelines are to be followed (e.g. The Human Tissues Act, or equivalent) and that they are in line with level of risk?			
	If NO, please explain why not			

Travel

	Question		Yes	No
1	Does any part of the project require data collection off campus? (e.g. work in the field or community)			X
	If YES: You must consider the potential hazards from off campus activities (e.g. working alone, time of data collection, unfamiliar or hazardous locations, using equipment, the terrain, violence or aggression from others). Outline the precautions that will be taken to manage these risks, AS A MINIMUM this must detail how researchers would summon assistance in an emergency when working off campus. For complex or high risk projects you may wish to complete and upload a separate risk assessment			
2	Does any part of the project involve the researcher travelling outside the UK (or to very remote UK locations)?			
	If YES: Please give details of where, when and how you will be travelling. For travel to high risk places you may wish to complete and upload a separate risk assessment			
3	Are all travellers aware of contact numbers for emergency assitance when away (e.g. local emergency assistance, ambulance/local hospital/police, insurance helpline [+44 (0) 2071 737797] and CU's 24/7 emergency line [+44 (0) 2476 888555])?			
4	Are there any travel warnings in place advising against all, or essential only travel to the destination? NOTE: Before travel to countries with 'against all travel', or 'essential only' travel warnings, staff must check with Finance to ensure insurance coverage is not affected. Undergraduate projects in high risk destinations will not be approved			
5	Are there increased risks to health and safety related to the destination? e.g. cultural differences, civil unrest, climate, crime, health outbreaks/concerns, and travel arrangements?			
	If YES, please specify			
6	Do all travelling members of the research team have adequate travel insurance?			
7	Please confirm all travelling researchers have been advised to seek medical advice regarding vaccinations, medical conditions etc, from their GP			